DOCTORAL THESIS

The white matter microstructure of the basal ganglia circuitry and its changes in Parkinson's disease

by

Jilu Princy Mole

A thesis submitted in partial fulfilment for the degree of Doctor of Philosophy

at

Cardiff University Brain Research Imaging Centre (CUBRIC), Cardiff University

Schools of Medicine and Psychology

Summary of thesis

Parkinson's disease (PD) is the second most prevalent neurodegenerative with an estimated prevalence of 1% in people older than 60 years and rising to 3% in people older than 80 years (Lee and Gilbert 2016). Currently, the exact aetiology of PD is not known, there is no cure and there are no therapeutic interventions that can possibly delay disease progression. The symptoms can be controlled or managed by treatment, physical therapy and/or surgical procedures however these cause side effects and complications. Therefore, there is an increasing need for understanding the underlying pathophysiology of the disease which will aid in developing therapeutic treatments that help alleviate symptoms without side effects while minimizing the requirement for medications.

The aim of this thesis was to explore selected white matter connections of the basal ganglia circuitry and investigate their changes in PD thereby potentially increasing our understanding of the underlying pathophysiology in PD. Results from my PhD show selective compensatory and neurodegenerative differences in selected motor and non-motor white matter pathways in PD patients compared to healthy controls. For the first time, I describe and develop an anatomical protocol for in vivo segmentation of two basal ganglia-cerebellar tracts and demonstrate their spatial independence and their cortical connections. Results from my investigation of the main cerebellar pathways and the two basal ganglia-cerebellar tracts show that the cerebellar input and output structures are involved in the pathophysiology of PD. My results pave way for future studies to further explore and delineate the specific compensatory and neurodegenerative processes of these white matter pathways in PD.

DECLARATION

This work has not been submitted in substance for any other degree or award at this or any other university or place of learning, nor is being submitted concurrently in candidature for any degree or other award.

Signed …… (candidate) Date ……..……..……

STATEMENT 1

This thesis is being submitted in partial fulfillment of the requirements for the degree of PhD

Signed…… (candidate) Date ……..……

STATEMENT 2

This thesis is the result of my own independent work/investigation, except where otherwise stated, and the thesis has not been edited by a third party beyond what is permitted by Cardiff University's Policy on the Use of Third Party Editors by Research Degree Students. Other sources are acknowledged by explicit references. The views expressed are my own.

Signed……(candidate) Date ……..……

STATEMENT 3

I hereby give consent for my thesis, if accepted, to be available online in the University's Open Access repository and for inter-library loan, and for the title and summary to be made available to outside organisations.

Signed……(candidate) Date ……

STATEMENT 4: PREVIOUSLY APPROVED BAR ON ACCESS

I hereby give consent for my thesis, if accepted, to be available online in the University's Open Access repository and for inter-library loans **after expiry of a bar on access previously approved by the Academic Standards & Quality Committee.**

Signed ……(candidate) Date ……..……

Acknowledgements

"Let us not become weary in doing good, for at the proper time we will reap a harvest if we do not give up." *Galatians 6:9 (The Bible, NIV)*

I would like to express my sincere gratitude to my PhD supervisors, Prof. David Linden and Dr. Claudia Metzler-Baddeley, and to Cardiff University for funding my PhD through the Cardiff University's Overseas Research Scholarship.

Thanks to…
… Prof. David Linden, for your encouraging support and guidance throughout my PhD. Thank you for the opportunity to learn and grow as a researcher, and for sharing your expertise.
… Dr. Claudia Metlzer-Baddeley, for your support and advice during my PhD. Thank you for sharing your expertise and your data, thereby making this work possible. Thank you also for the extra bit of financial cover via the part-time research assistant job.
… Dr. Leena Subramanian, for sharing your carefully collected data, without which this thesis would not have been possible.
… Dr. Tobias Bracht for your help with my first steps into diffusion tractography and analysis.
… Dr. Nils Muhlert for your help with the subcortical volumes analysis.
… Dr. Cyril Charron for taking the time to fix (most of) the IT, data and technical problems encountered during my PhD.
… Peter Hobden, for clarifying MRI basics through your book MRI Gold Publications 'Introduction to Brain Research MRI'.
… Dr. Ilona Lipp, my favourite collaborator, for the delicious cakes, hot chocolate motivation breaks and for scripting the spatial overlap measures and tract probability maps.
… Naomi Warne, my BFF, for cheering me on since the beginning of this PhD journey. Thank you also for proof reading my thesis on short notice.
… to all my friends and colleagues, for your support.

Finally, I'm eternally indebted and grateful to my supportive mum and dad. My heartfelt thanks to you both, I could not have done this without your constant love, prayers, encouragement and understanding. Thanks to my wonderful sisters, who have (patiently) listened to my long hours of ranting on the phone. Thank you for being there for me, even though you were all (literally) 8483 kilometres away from me. Special thanks to my church family at City Church Cardiff, for being a home away from home.

"Now to Him who is able to do immeasurably more than all we ask or imagine, according to His power that is at work within us, to Him be glory in the church and in Christ Jesus throughout all generations, for ever and ever! Amen."

Ephesians 3:20-21(The Bible, NIV)

Data collection and Funding

I was supported by funding from Cardiff University's Overseas Research Scholarship (2014-2017).

The Parkinson's disease patient data were collected as part of the study "Real-time fMRI Neurofeedback for Treatment of Parkinson's Disease" (NCT01867827). These data were collected by Dr. Leena Subramanian and Prof. David Linden. Thanks to Prof. Huw Morris, Dr Alistair Church, Dr Biju Mohammed, Dr Chris Thomas and Mrs Debbie Davies for their help with patient recruitment.

The matched healthy controls data were from an aging study which was supported by funding from the Medical Research Council, UK, via a Clinician Scientist Fellowship to Dr. Michael J. O'Sullivan. (G0701912). These data were collected by Dr. Claudia Metzler- Baddeley.

The young healthy participants were from a working memory study which was funded by Wellcome Trust New Investigator Award to Prof. Derek Jones (Grant number 502341). This data was collected by Dr. Claudia Metzler- Baddeley.

Many thanks to all patients, carers and control participants for their participation.

10 middle aged healthy participants' data were collected by me within my free PhD scanning allowances under Ethics number EC.14.09.09.3843R2 (08/09/2015). These participants' data were collected as part of larger study into midlife risk of Alzheimer's disease and were not included within this thesis. Prof. David Linden and I acquired permission to analyse data from the Parkinson's Progressive Markers Initiative (PPMI) database to perform a replication analysis. I downloaded and partially pre-processed a sub-sample of patients and healthy control data from the PPMI database. However, due to several technical and data storage difficulties the processing and analysis of this data was not completed within the time frame of the PhD and was therefore not included within this thesis.

Thesis Impact

Chapter 3 has been published as a journal article

Mole, J.P., Subramanian, L., Bracht, T., Morris, H., Metzler-Baddeley, C. and Linden, D.E.J. (2016). Increased fractional anisotropy in the motor tracts of Parkinson's disease suggests compensatory neuroplasticity or selective neurodegeneration. European Radiology 26:3327–3335.

Chapter 4 has been submitted as a journal article and is currently under review

Mole, J.P., Lipp, I., Subramanian, L., Metzler-Baddeley, C. and Linden, D.E.J. (2017). Anatomy of the dentato-rubro-thalamic tract (DRTT) and the subthalamo-ponto-cerebellar tract (SPCT): A diffusion tractography approach. Brain Structure and Function. *Under review*

Chapter 5 is currently in preparation for submission as journal article

Mole, J.P., Subramanian, L., and Linden, D.E.J., Metzler-Baddeley, C (2017). White matter alterations of the cerebellar pathways in Parkinson's disease. Neuroimage Clinical.

Conference publications

Mole, JP; Subramanian, L; Morris, H; Metzler-Baddeley, C; Linden, D. (2016) White matter of the cerebellar pathways in Parkinson's disease: A deterministic tractography study. Organisation for Human Brain Mapping (OHBM) Abstract, 2043 [https://ww5.aievolution.com/hbm1601/index.cfm?do=abs.viewAbs&abs=2000]

Mole, JP; Subramanian, L; Bracht, T; Morris, H; Metzler-Baddeley, C; Linden, D. (2015) Structural connectivity of motor pathways in Parkinson's disease. British Neurosci. Assoc. Abstr., Vol. 23: Page 344 ISSN 1345-8301 2015 [https://www.bna.org.uk/media/resources/files/BNA2015-Abstract-Book.pdf]

Abbreviations

PD: Parkinson's disease

MHC: Matched Healthy Controls

YHP: Young Healthy Participants

BG: Basal ganglia

CST: Corticospinal tract

SMA-PUT: Supplementary motor area-putamen tract

THAL-MC: Thalamus-motor cortex tract

UNF: Uncinate Fasiculus

slMFB: supero-lateral medial forebrain bundle

FA: Fractional anisotropy

MD: Mean diffusivity

RD: Radial diffusivity

AD: Axial diffusivity

dRL: damped Richardson-Lucy

HMOA: Hindrance modulated orientational anisotropy

DRTT: Dentato-rubro-thalamic tract

SPCT: Subthalamo-ponto-cerebellar tract

MCP: Middle cerebellar peduncle

SCP: Superior cerebellar peduncle

ICP: Inferior cerebellar peduncle

List of Figures and Tables

Figure 1.1 Sub-structures of the basal ganglia 7
Figure 1.2 Normal basal ganglia input and output pathways 8
Figure 1.3 Five parallel circuits of the basal ganglia 11
Figure 1.4 Somatotopic organisation of the BG motor circuitry 13
Figure 1.5 Basal ganglia-thalamo-cortical pathway in normal and Parkinson's disease 15
Figure 1.6 Braak staging of PD pathology 16
Figure 1.7 Unfolded view of the cerebellar cortex showing the fissures, lobules, lobes and its somatotopy 21
Figure 1.8 Overview of cerebellar anatomy and function 22

Figure 2.1 Protons aligned along the magnetic field B0 28
Figure 2.2 T1 and T2 signal 29
Figure 2.3 T1 and T2 contrasted images of a representative human brain in the axial view 30
Figure 2.4 Diffusion weighted spin echo sequence 31
Figure 2.5 T1, FA, DWI and FA colour coded images of a single slice axial view of a representative subject 32
Figure 2.6 The diffusion tensor and its quantitative measures 33
Figure 2.7 Tractography based on Diffusion Tensor Imaging 35
Figure 2.8 Fiber ODFs reconstructed from the in vivo data for adjacent voxels in the pons..... 37
Table 2.1 Demographics of the Young healthy participants (YHP), Parkinson's disease (PD) patients and Matched healthy controls (MHC) 39

Table 3.1 Demographics of the PD patients and MHCs 50
Figure 3.1 Reconstructed motor tracts 51
Figure 3.2 Anatomical landmarks for CST 52
Figure 3.3 Anatomical landmarks for THAL-MC tract 53
Figure 3.4 Mask accuracy for THAL-MC tracts 54
Figure 3.5 Anatomical landmarks for SMA-PUT tract 55
Figure 3.6 Mask accuracy for SMA-PUT tract 56
Figure 3.7 Reconstructed non-motor tracts 57
Figure 3.8 Anatomical landmarks for UNF 58
Figure 3.9 Anatomical landmarks for the slMFB 59
Table 3.2 Inter-rater reliability tests 61

Table 3.3 Multivariate effects 62
Table 3.4 Univariate group effects 63
Table 3.5 Subcortical volumes analysis results 64

Figure 4.1 The DRTT tract along with the ROIs in axial, sagittal and coronal views of T1 anatomical scan of a representative participant 77
Figure 4.2 Regions of interest and reconstruction of the SPCT for a representative participant in coronal view 78
Figure 4.3 Alternative ROIs used for reconstruction of DRTT and SPCT 79
Table 4.1 Number of successful reconstructions of the DRTT and SPCT tracts 82
Figure 4.4 DRTT and SPCT anatomical connections shown as probability maps in axial slices in the YHC group 83
Figure 4.5 The probability maps in axial slices, showing the probability (in percent) of the DRTT, SPCT, CST, ICP, SCP and MCP tracts in the YHC group 84
Figure 4.6 Circuits interconnecting the cerebellum and the basal ganglia including the cerebral cortex connections 85
Table 4.2 Spatial overlap 86
Figure 4.7 Matrix plots representing the overlaps as group-averaged dice scores between the tracts in each group 87

Table 5.1 Demographics of the PD patients and MHCs for the cerebellar analyses 100
Figure 5.1 Reconstruction of the Middle Cerebellar Peduncle (MCP) 101
Figure 5.2 Reconstruction of the Superior Cerebellar Peduncle (SCP) 102
Figure 5.3 Reconstruction of the Inferior Cerebellar Peduncle (ICP) 103
Figure 5.4 Reconstructed full and segmented DRTT and SPCT 104
Table 5.2 Results from the MANCOVAs for the main cerebellar tracts 106
Table 5.4 Post-hoc ANCOVAs for the main cerebellar tracts 107

Table of Contents

Summary of Thesis ii

Declaration iii

Acknowledgements iv

Data collection and Funding v

Thesis Impact vi

Abbreviations vii

List of Figures and Tables viii

Table of Contents 1

Chapter 1 General Introduction 4

1.1 Basal ganglia 7

1.1.1 Sub-structures of BG 7

1.1.2 Input and Output nuclei 8

1.2 BG circuitry 10

1.2.1 Foundational research on the BG loops 10

1.2.2 Motor circuit 12

1.3 Parkinson's disease 15

1.3.1 BG circuitry in PD 15

1.3.2 Braak's staging of PD pathology 16

1.3.3 PD symptoms and the BG model 17

1.4 Cerebellum 21

1.4.1 Anatomy 21

1.4.2 Cerebellar circuitry 23

1.4.3 Cerebellum in PD 24

1.5 Main white matter connections for investigation 26

Chapter 2 General Methods 27

2.1 Magnetic Resonance Imaging 28

2.2 Diffusion MRI Imaging and Tractography 31

2.2.1 Background 31

2.2.2 Tractography 35

2.3 MRI data acquisition and processing 39

2.3.1 Data cohorts 39

2.3.2 Structural MRI scanning 40

2.3.3 Diffusion MRI scanning 40

2.3.4 Diffusion MRI pre-processing 40
2.3.5 Tractography 41
2.3.6 Anatomical methods 42
2.3.7 Clinical and behavioural measures from the PD cohort 42
Chapter 3 Comparison of selective motor and non-motor pathways in Parkinson's disease 44
3.1 Abstract 45
3.2 Background and Rationale 47
3.3 Aims 49
3.4 Materials and Methods 50
3.4.1 Participants 50
3.4.2 Tractography 50
3.4.3 Subcortical volumes analysis 59
3.4.4 Statistical Analysis 60
3.5 Results 61
3.5.1 Inter-rater reliability 61
3.5.2 Multivariate effects 62
3.5.3 Univariate group effects 63
3.5.4 Subcortical volumes analysis 64
3.6 Discussion 66
3.6.1 Neurodegenerative models 66
3.6.2 Neuroplastic models 67
3.6.3 Subcortical volumes 67
3.6.4 Methodological considerations 68
3.7 Conclusion 69
Chapter 4 Anatomy of the dentato-rubro-thalamic tract (DRTT) and the subthalamo-ponto-cerebellar tract (SPCT) 70
4.1 Abstract 71
4.2 Background and Rationale 73
4.3 Aims 75
4.4 Materials and Methods 76
4.4.1 Data cohorts, MRI acquisition and processing 76
4.4.2 Tractography protocols 76
4.4.3 Statistical Analysis 80
4.5 Results 82
4.5.1 Tract probability maps 82
4.5.2 Spatial overlap between tracts 85
4.5.3 Inter-rater reliability of tract reconstruction 87
4.6 Discussion 88

4.6.1 Tract probability maps 88
4.6.2 Spatial overlap 89
4.6.3 Inter-rater reliability 90
4.6.4 Consistent reconstruction across data sets 91
4.6.5 Limitations 91
4.7 Conclusion 92
Chapter 5 Investigating microstructural differences in the white matter of the main cerebellar and basal ganglia-cerebellar pathways in Parkinson's disease 93
5.1 Abstract 94
5.2 Background and Rationale 96
5.3 Aims 99
5.4 Materials and Methods 100
5.4.1 Data cohorts, MR acquisition and processing 100
5.4.2 Reconstruction of the major cerebellar pathways 100
5.4.3 Statistical Analysis 104
5.5 Results 106
5.5.1 Microstructural differences 106
5.6 Discussion 109
5.6.1 Increased FA in the Right SCP and Right ICP 109
5.6.2 Increased HMOA in the right SCP 110
5.6.3 DRTT and SPCT 111
5.6.4 Limitations and future directions 113
5.7 Conclusion 114
Chapter 6 General discussion 115
6.1 Summary of findings 116
6.2 Limitations and future research in PD 118
6.3 Wider clinical relevance of investigated BG white matter connections 120
6.4 Conclusion 121
Chapter 7 References 122
Chapter 8 Supplementary material 157
8.1 Chapter 3 Supplementary material 157
8.2 Chapter 4 Supplementary material 162
8.3 Chapter 5 supplementary material 171

Chapter 1 General Introduction

Parkinson's disease (PD) is the second most prevalent neurodegenerative disease with an estimated prevalence of 1% in people older than 60 years, rising to 3% in people older than 80 years (Lee and Gilbert 2016). PD is named after James Parkinson who gave the first description of the disease in '*An essay of the Shaking Palsy'* in 1817 (Goetz 2011). The four main symptoms of PD are tremor, bradykinesia (slowness of movement), rigidity and postural instability (Jankovic 2008; Andalib *et al.* 2014). Currently, the exact aetiology of PD is not known, there is no cure and there are no therapeutic interventions that have been shown to delay disease progression. The symptoms can be managed by drug treatment and/or surgical procedures. Medications cause adverse side effects such as nausea, hallucinations, delusions, impulse control disorders, dyskinesia (Fernandez 2012) and other complications with their long term usage, which affect the quality of daily life. Surgical procedures such as Deep Brain Stimulation (DBS) can cause intracranial haemorrhage, infection and seizures (Kleiner-Fisman *et al.* 2006). It is therefore important to gain further understanding of the underlying pathophysiology of the disease, so that therapeutic treatments that help alleviate symptoms with minimal side effects can be developed.

The main pathophysiological feature associated with the motor symptoms of PD is the loss of substantia nigra dopaminergic neurons of the basal ganglia (Fearnley and Lees 1991). This loss affects structures of the basal ganglia circuitry such as the putamen and the thalamus which are connected to regions of the cortex such as the supplementary motor area and the motor cortex (Wichmann and Dostrovsky 2011). There is increasing evidence that the cerebellum is also involved in motor and non-motor symptoms of PD (Wu and Hallett 2013) and studies have also revealed direct anatomical connections between the basal ganglia and the cerebellum in non-human primates (Hoshi *et al.* 2005; Bostan and Strick 2010). However, the roles of these structures and their white matter connections have not yet been researched in PD.

Therefore, the aim of this thesis was to explore selected white matter connections of the basal ganglia circuitry and investigate their changes in PD using advanced diffusion MRI methods, thereby increasing our understanding of the underlying pathophysiology in PD. The current chapter provides an introduction to the basal ganglia circuitry and Parkinson's disease. Chapter 2 gives an introduction to diffusion MRI, and an overview of methodology used in this thesis. Chapter 3 explores the differences in diffusion metrics in selected motor and non-motor tracts in Parkinson's disease. Chapter 4 provides an anatomical protocol for the reconstruction of the anatomical connections between the basal ganglia and the cerebellum using diffusion tractography and assesses their spatial overlap with the main cerebellar tracts (the middle, inferior and superior cerebellar peduncles) and the corticospinal tract. Chapter 5 investigates the differences in the microstructural diffusion metrics in the main cerebellar tracts and basal ganglia-cerebellum connections in Parkinson's disease. Finally, Chapter 6 presents a summary and integration of the findings set out in this thesis. The wider clinical relevance of the studied white matter connections and future directions of current work are also discussed in Chapter 6.

1.1 Basal ganglia

The basal ganglia (BG) are a collection of deep grey matter nuclei that are located within the white matter of the cerebral hemispheres. The BG consists of the caudate nucleus, putamen, globus pallidus, nucleus accumbens, substantia nigra and the subthalamic nuclei (Blumenfeld 2010). The thalamus is an oval shaped structure located behind the BG just above the brain stem on either side of the third ventricle. Parts of it serves as a relay station for sensory pathways, and the motor portion of the thalamus is functionally related to the BG and sometimes subsumed under the BG. The subthalamic nucleus of the ventral thalamus and the substantia nigra of the mesencephalon are also functionally related to the BG.

1.1.1 Sub-structures of BG

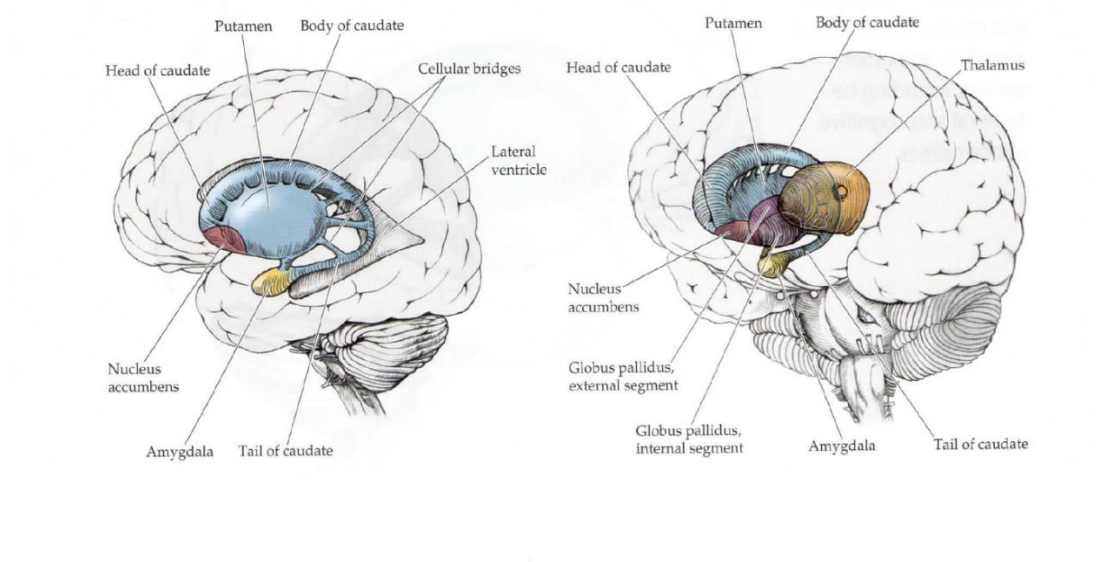

Figure 1.1 Sub-structures of the basal ganglia (Blumenfeld 2010)

The caudate nucleus is an elongated C-shaped curved cell mass that is in direct contact with the lateral ventricle throughout its extent. The putamen is a large nucleus forming the lateral portion of the BG and it is anteriorly and ventrally connected to the caudate forming the striatum (Figure 1.1). The caudate and the putamen have similar histological and embryological profiles. Their histological structure is characterised by medium-sized neurons with 75% of these being medium spiny projection neurons (Blumenfeld 2010). The caudate and putamen are interconnected by cell bridges distributed among bundles of the internal capsule, giving rise to the term “striatum”.

The globus pallidus lies medial to the putamen and means “pale globe” because of the myelinated fibres that pass through this region, which appear paler than the caudate and putamen on sections of the post mortem brain. The putamen and globus pallidus together form the lenticular or lentiform nucleus (lentil-shaped) with the putamen forming the outer part and the globus pallidus forming the inner part.

The nucleus accumbens includes the ventral parts of the head portion of the caudate and the putamen. The nucleus accumbens and the medium sized cells of the olfactory tubercle together form the ventral striatum (Nieuwenhuys *et al.* 2008). The subthalamic nucleus is an oval shaped component of the subthalamus, which lies lateral to the hypothalamus and medial to the internal capsule. The substantia nigra, is latin for “black substance” because of its darker appearance on post mortem slices due to high levels of neuromelanin in dopaminergic neurons (Rabey and Hefti 1990). It is composed of two parts; the ventral, pars reticulata and the dorsal, pars compacta.

1.1.2 Input and Output nuclei

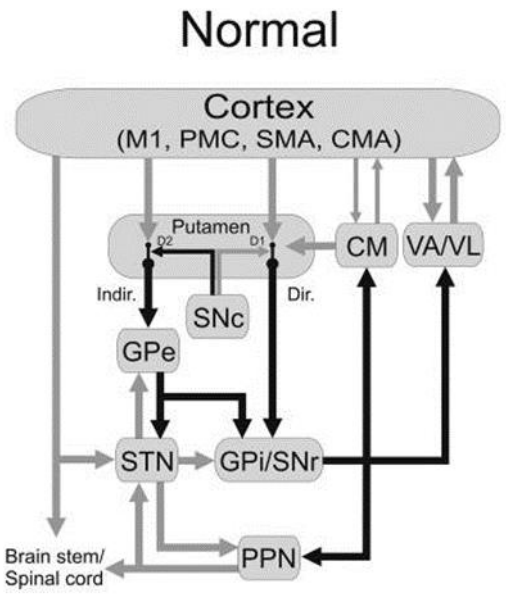

Figure 1.2 Normal basal ganglia input and output pathways

M1- Motor cortex, PMC- Primary motor cortex, SMA – Supplementary motor area, CMA – Cingulate motor area, CM – Centromedian nucleus of thalamus, VA/VL – Ventro anterior and ventro lateral nuclei of thalamus, GPe – Globus pallidus external, GPi - Globus pallidus internal, SNc – Substantia nigra pars compacta, SNr – Substantia nigra pars reticulata, STN – Subthalamic nucleus, PPN – Pedunculopontine nucleus, D1, D2 - Dopamine receptor subtypes, Indir – Indirect pathway, Dir – Direct pathways. Black arrows are inhibitory connections and grey arrows are excitatory connections. Arrow thickness indicates the strength of the activity. Taken from (Wichmann and Dostrovsky 2011).

The input structures of the BG are the caudate, putamen, and nucleus accumbens. They receive input from the cerebral cortex (Figure 1.2), and from the thalamus, subthalamic

nucleus and other brain stem structures. Most of these cortical inputs to the striatum are excitatory and use glutamate as their neurotransmitter. The output structures are the internal segment of the globus pallidus, substantia nigra pars reticulata, and ventral pallidum, and they project back to the cerebral cortex via the thalamus (Middleton and Strick 2000). The outputs leave from the substantia nigra pars reticulata and the internal segment of the globus pallidus to the ventro anterior and ventro lateral nuclei of thalamus. The thalamic nuclei then relay these outputs to parts of the cerebral cortex (Figure 1.2). These output pathways are inhibitory and use the neurotransmitter gamma aminobutyric acid (GABA). The intrinsic nuclei within the BG comprise the lateral position of the globus pallidus, subthalamic nucleus and the substantia nigra pars compacta, which are interconnected by local circuit projections and are also connected to the input and output nuclei (Figure 1.2).

1.2 BG circuitry

Anatomical knowledge of the basal ganglia circuitry has been based on animal tracing studies and human post mortem work. Since invasive fibre tracking techniques are not possible in humans, anatomical studies exploring the presence of the parallel circuitry of the BG loops in humans have been largely based on primate-human extrapolations suggested by Alexander and colleagues (Alexander *et al.* 1986). It should be noted that the BG circuitry is highly complex with sub-structures within the BG having projections to and from other BG nuclei. Hence, the focus of this literature review is a brief overview of the topographical evidence of segregated and overlapping connections to and from the sub-structures of the BG, and the frontal and cortical regions, with specific focus on the motor circuitry for the purposes of this thesis.

1.2.1 Foundational research on the BG loops

The anatomical models of the organisation of BG circuits have undergone major revisions since their initial descriptions; it was primarily thought that the BG served as a "funnel", integrating and channelling information from the cerebral cortex to the thalamus and back to the motor cortex (Allen and Tsukahara 1974). Evidence for anatomical and functional segregation of influences from the cortex to the BG-thalamo-cortical circuits from anatomical and physiological findings has challenged and changed these initial views. DeLong and colleagues suggested that there were two loops; (i) a 'motor loop' that receives inputs from the sensory and motor areas that pass through the putamen and project back to the premotor areas; and (ii) an 'association loop' receiving input from the association areas passing through the caudate and returning back to the prefrontal areas (DeLong *et al.* 1984). Further evidence reinforced the principle that inputs from the BG are transmitted to segregated topographic portions of the frontal lobe. Alexander and colleagues proposed the organisation of the cortico-BG-thalamo-cortical (CBTC) circuits as a model of five parallel circuits; where, in addition to the motor circuit, there are four other circuits designated as 'oculomotor', 'dorsolateral prefrontal', 'lateral orbitofrontal' and 'anterior cingulate' circuits. (Alexander *et al.* 1986) as shown in Figure 1.3.

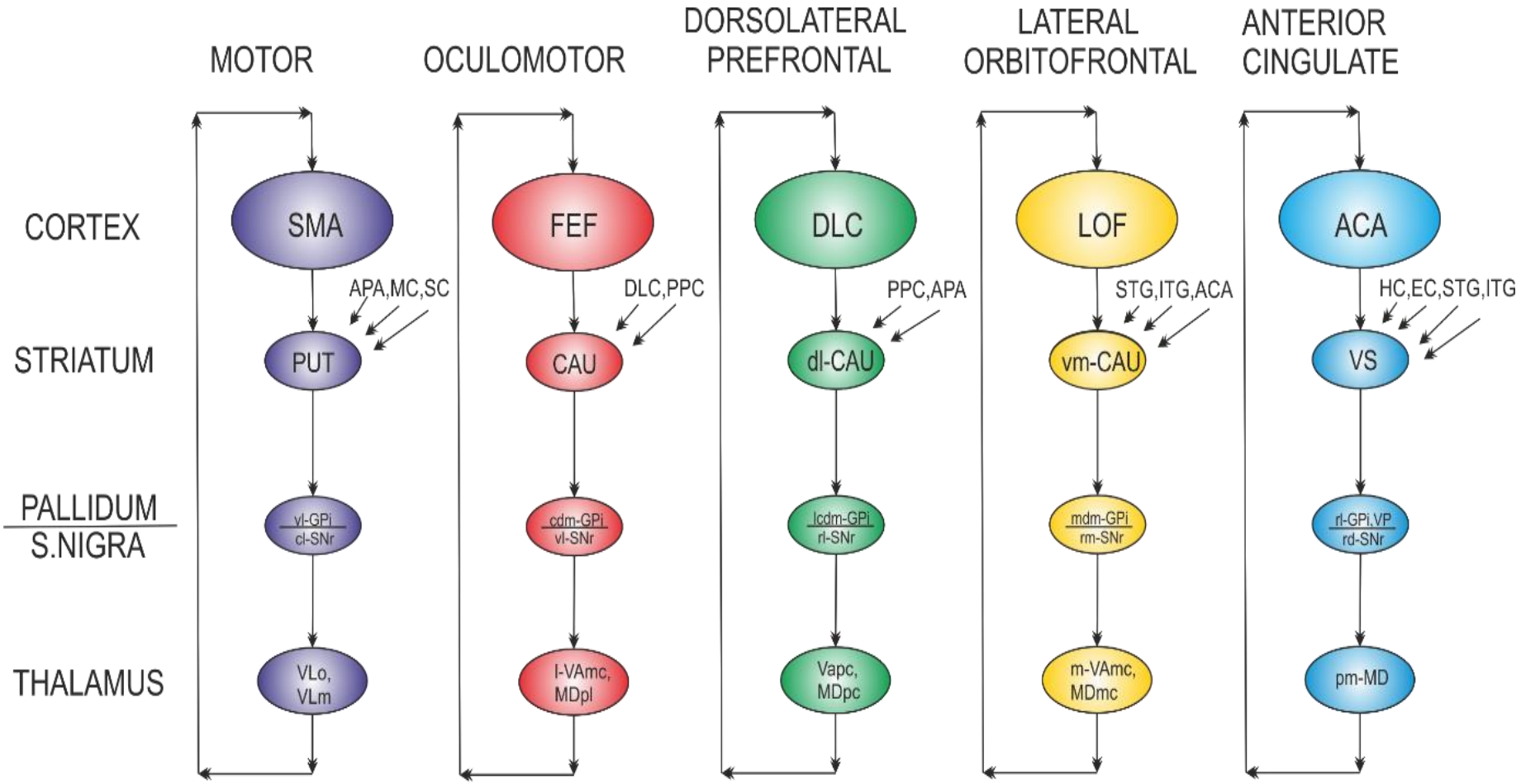

Figure 1.3 Five parallel circuits of the basal ganglia – modified and adapted from (Alexander *et al.* 1986)

Abbreviations: SMA: supplementary motor area, FEF: frontal eye fields, DLC: dorsolateral prefrontal cortex, LOF: lateral orbitofrontal cortex, ACA: anterior cingulate cortex, APA: arcuate premotor area, MC: motor cortex, SC: somatosensory cortex, PPC: posterior parietal cortex, STG: superior temporal gyrus, ITG: inferior temporal gyrus, HC: hippocampal cortex, EC: entorhinal cortex, PUT: putamen, CAU: caudate (b) body (h) head, VS: ventral striatum, GPi: globus pallidus internal, VP: ventral pallidum, SNr: substantia nigra pars reticulata, VLo: ventralis laterlis pars oralis, VLm: ventralis lateralis pars medialis, VAmc: ventralis anterior pars magnocellularis, VApc: ventralis anterior pars parvocellularis, MDpl: medialis dorsalis pars paralamellaris, MDmc: medialis dorsalis pars magnocellularis, MDpc: medialis dorsalis pars parvocellularis, cl-caudolateral, dl-dorsolateral, l-lateral, ldm-lateral

The basic design for each pathway is thought to be similar; each circuit contains non-overlapping parts of the striatum, globus pallidus, thalamus, substantia nigra and cortex. Each circuit receives multiple and partially overlapping cortical inputs, which are integrated to pass through pallidum and substantia nigra, then to a specific portion of the thalamus, and then back to a separate/single cortical area. The initial description of funnelling inputs into the BG has been retained, however, here this would be the funnelling of inputs from functionally related and anatomically interconnected regions within the segregated circuits. The term circuit in this context does not refer to a closed pathway without any other substantial inputs or outputs, but refers to a closed loop within each circuit despite the presence of other inputs and outputs. Anatomical evidence to support the circuits primarily came from primate studies and post mortem human tissue work (Alexander *et al.* 1986; Alexander and DeLong 1985; Vitek *et al.* 1994). For the purposes of this thesis, this will be discussed in relation to the motor circuitry of the BG.

1.2.2 Motor circuit

In the motor circuit, the putamen mostly receives substantial projections from the motor (Künzle 1975) and somatosensory cortices (Kunzle 1977). The motor and somatosensory 'leg' areas of the cortex are monosynaptically connected to the dorsolateral putamen while the 'face' area projects to the ventromedial region of the putamen and the 'arm' regions project to a region in between (Figure 1.4). The putamen also receives topographically organised projections from area 5 and lateral area 6 including the arcuate premotor area (APA) and from the supplementary motor area (SMA) in a model derived from non-human primate data (Jones *et al.* 1977; Selemon and Goldman-Rakic 1985). Striatal projections from the SMA were traced by anterograde label injections into the rostral 'face' region with the resulting terminals ending in the ventromedial putamen (Brinkman and Porter 1979; Muakkassa and Strick 1979). Therefore, as shown in Figures 1.3 and 1.4, the motor circuit has a combination of 'open' and 'closed loops' in which somatotopically organised influences from the SMA, APA, motor cortex (MC) and somatosensory cortex (SC) travel through the circuits and are then ultimately project back to the SMA.

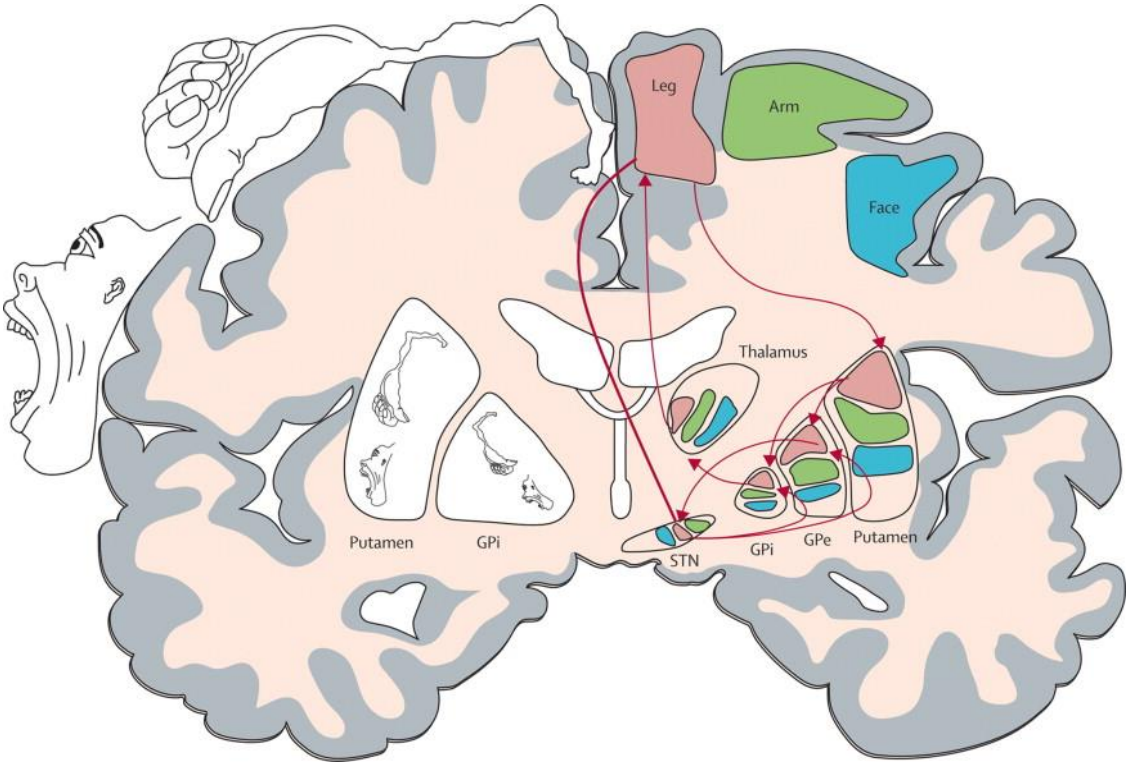

Figure 1.4 Somatotopic organisation of the BG motor circuitry

Here, the motor circuit is indicated by red arrows connecting the regions that modulate leg movements. It is somatotopically organised throughout the loop, with the regions representing leg movements lying dorsal and medial, those representing face movements lying ventral and lateral, and those representing arm movements lying in-between. The somatotopic arrangement of the primary motor cortex is generally maintained in the striatopallidal and subthalamic nuclei. GPe=globus pallidus pars externa. GPi=globus pallidus pars interna. STN=subthalamic nucleus. Figure from Obeso and colleagues and Rodriguez-Oroz and colleagues (Rodriguez-Oroz *et al.* 2009)

The cortical terminal of the motor circuit, the SMA, has an important role in the programming and the control of movements. In primates, it projects not only to the APA and MC (Muakkassa and Strick 1979; Schell and Strick 1984) but also directly to the spinal cord (Biber *et al.* 1978; Murray and Coulter 1981; Palmer *et al.* 1981; Macpherson *et al.* 1982). Micro-stimulation of the SMA in the monkey has been shown to produce limb movements (Macpherson *et al.* 1982) and single cell studies in behaving primates have shown discharge in relation to limb movements (Brinkman and Porter 1979; Tanji and Kurata 1979) and during the preparation of these movements (Tanji *et al.* 1980). However, there is also evidence that the BG and the putamen are directly involved in preparation and planning of limb movements (Alexander 1987).

Several studies in awake behaving primates confirmed the somatotopic organisation of putamen as suggested by the topographical organisation of corticostriatal projections (Crutcher and DeLong 1984; Alexander *et al.* 1985; Liles 1985). Ordered somatotopic distribution of the motor inputs within areas of the BG and the thalamus has been consistently described in primates (Wichmann *et al.* 1994; Vitek *et al.* 1994; Takada *et al.* 2001; Takada *et al.* 1998; DeLong *et al.* 1983; Nambu *et al.* 1996). Segregated somatotopy of movement related neurons was shown in sensorimotor areas of the monkey striatum (Takada *et al.* 1998), GPi and GPe (DeLong 1971; DeLong *et al.* 1985) and the thalamus (Vitek *et al.* 1994). A segregated loop that connects the primary motor cortex (M1), SMA, the premotor cortex (PMC), and cingulate motor areas (CMA) with the motor areas of the thalamus and the BG facilitates the processing of motor information (Alexander and Crutcher 1990; Alexander *et al.* 1986; Takada *et al.* 2001; Smith *et al.* 1998; Romanelli *et al.* 2005).

1.3 Parkinson's disease

Parkinson's disease (PD) is characterised by the irreversible depletion of dopaminergic neurons in the substantia nigra pars compacta (SNc) a structure located in the mid brain (Fearnley and Lees 1991) with projections that are relayed in the putamen and lead to the thalamus and motor cortex as shown in (Figure 1.5).

1.3.1 BG circuitry in PD

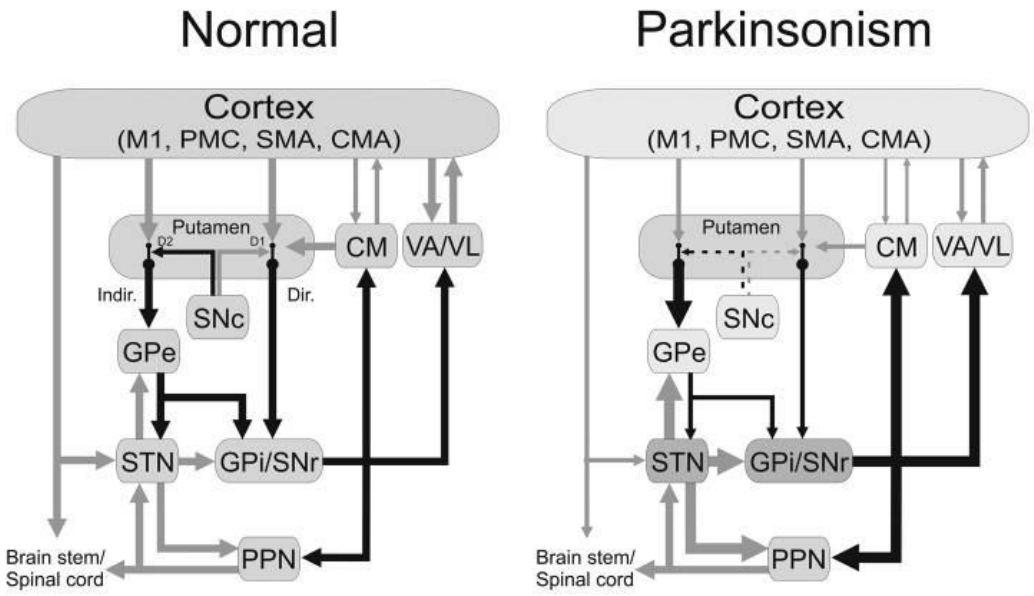

Figure 1.5 Basal ganglia-thalamo-cortical pathway in normal and Parkinson's disease.

M1- Motor cortex, PMC- Primary motor cortex, SMA – Supplementary motor area, CMA – Cingulate motor area, CM – Centromedian nucleus of thalamus, VA/VL – Ventro-anterior and ventro-lateral nuclei of thalamus, GPe – Globus pallidus external, GPi - Globus pallidus internal, SNc – Substantia nigra pars compacta, SNr – Substantia nigra pars reticulata, STN – Subthalamic nucleus, PPN – Pedunculopontine nucleus, D1, D2 - Dopamine receptor subtypes, Indir – Indirect pathway, Dir – Direct pathways. Black arrows are inhibitory connections and grey arrows are excitatory connections. Arrow thickness indicates the strength of the activity. Taken from (Wichmann and Dostrovsky 2011).

Disturbance in the BG circuitry occurs after the loss of around 80% of the nigral dopaminergic neurons that have projections to the striatum (Bernheimer *et al.* 1973). According to the most prevalent model of BG dysfunction in PD (Bergman *et al.* 1990), this leads to a decrease in the activation of the cortex and causes the motor symptoms of the disease to arise. In the normal circuitry, as shown in the black arrows (Figure 1.5), inhibitory signals are sent when the D1 receptors are activated in the direct output pathway from the putamen to the globus pallidus internus (GPi) and the substantia nigra pars reticula (SNr) (Wichmann and Dostrovsky 2011). The D2 receptors activate the indirect pathway and send inhibitory signals from the putamen to the globus pallidus externus (GPe) which in turn causes inhibitory signals to be sent to the subthalamic

nucleus (STN), which sends excitatory signals to the globus pallidus internus (GPi). The direct and indirect pathways to the GPi and SNr therefore help to modulate the transmission of signals to the ventro-anterior and ventro-lateral nuclei of the thalamus which in turn have excitatory connections to the cortex (Figure 1.5) (Alexander and Crutcher 1990; Albin *et al.* 1989). In PD, due to the reduced dopaminergic projections from the SNc, the activation of the D1 and D2 receptors in the putamen is reduced, causing reduction in the inhibitory signals to the GPi via the direct pathway. The GPi now also receives increased excitatory signals via the indirect pathway, causing increased inhibitory signals to the thalamus which in turn causes reduced excitatory signals to the cortex (Figure 1.4). After the description of this classic model of BG disruption in the 1990s, there has been a tremendous increase in clinical and experimental studies in PD.

1.3.2 Braak's staging of PD pathology

Though the crucial pathology of PD is loss of SNc dopaminergic neurons, from the neuroanatomical work by Braak it has become clear that PD is not just a neurodegenerative disease of the BG system, as there are stages in which other regions of the brain undergo PD-related changes as well (Figure 1.4) (Braak *et al.* 2003).

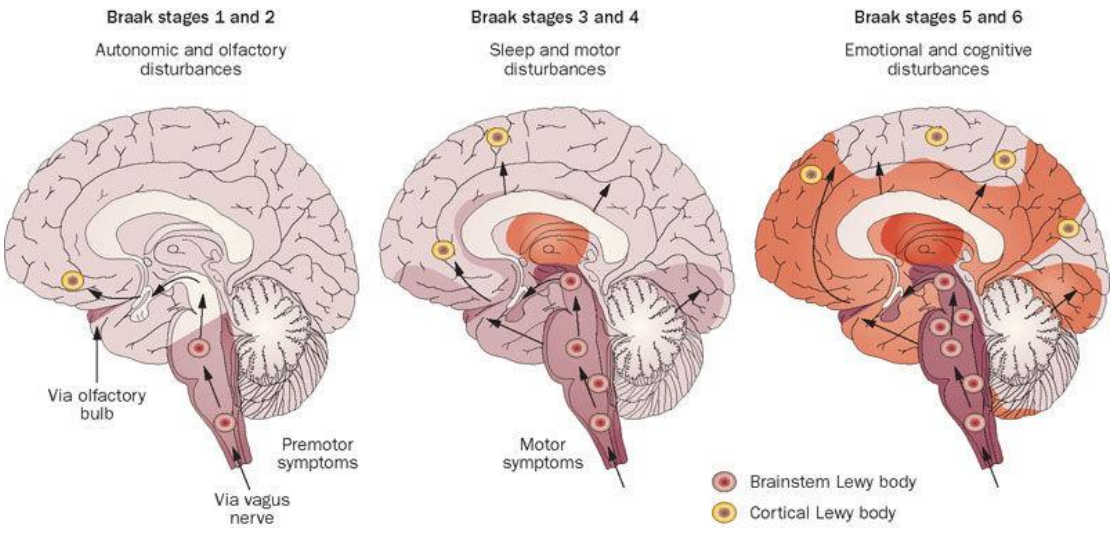

Figure 1.6 Braak staging of PD pathology.

Pathogens come into contact with olfactory and/or enteric nervous system (ENS) neurons, which trigger the α-Synuclein aggregation (Stages 1 and 2). The aggregated α-Synuclein spreads toward the central nervous system (CNS) via the olfactory bulb and the vagus nerve, eventually, arriving at the substantia nigra (Stages 3 and 4). And then spreads to the neocortex and the prefrontal cortical regions (Stages 5 and 6) (Halliday *et al.* 2011).

A consistent feature of PD pathology is the appearance of intercellular protein aggregates known as Lewy bodies in the dorsal motor nucleus of the vagus (DMV) within the medulla oblongata in post mortem analysis (Rietdijk *et al.* 2017). Baark's staging postulates that α-synuclein (a major component of the Lewy body pathology) in the olfactory tract (Beach, White, *et al.* 2009; Hubbard *et al.* 2007) and the enteric nervous system (ENS) (Wakabayashi *et al.* 1988; Heiko Braak, De Vos, *et al.* 2006; Shannon *et al.* 2012) cause gastrointestinal and olfactory problems (Doty 2012). There is clinical evidence that these occur during the earlier stages of PD before the onset of motor symptoms and disease diagnosis creating the pre-motor symptoms of the disease (Bloch *et al.* 2006; Abbott *et al.* 2007; Ross *et al.* 2008a; Braak *et al.* 2003; Shannon *et al.* 2012). This has also been substantiated in animal models where α-synuclein aggregates were found in gastrointestinal tracts of animal models (Hallett *et al.* 2012; Natale *et al.* 2010; Wang *et al.* 2012; Drolet *et al.* 2009; Kelly *et al.* 2014). The α-synuclein pathology spreads from the ENS to the central nervous system (CNS) via the vagal nerve (Tredici *et al.* 2010; Del Tredici and Braak 2008) and the DMV in the medulla oblongata (Takeda *et al.* 1993; Del Tredici *et al.* 2002; Jellinger 2004; Hely *et al.* 2008; Del Tredici and Braak 2008). This then spreads within the CNS from the lower brain stem regions towards the SN and eventually the neocortex and prefrontal cortex (Halliday *et al.* 2008; Del Tredici *et al.* 2002; Bloch *et al.* 2006; Braak *et al.* 2003) (Figure 1.6).

Despite evidence from in vitro, in vivo and clinical studies, not all PD patients adhere to the proposed pattern of α-synuclein spread within the Braak's stages such as those with young onset and long disease duration (Jellinger 2008; Kalaitzakis *et al.* 2009; Halliday *et al.* 2008). Recent studies have also suggested that neuronal loss and glial cell activation should be added to pathological studies in PD progression, as SNc neuronal loss shows linear relationship with motor symptoms (Greffard *et al.* 2006), while Lewy body aggregation only shows a trend towards a positive correlation with the motor symptoms (Beach, Adler, *et al.* 2009).

1.3.3 PD symptoms and the BG model

The cardinal symptoms of PD are resting tremor (shaking hands at rest), bradykinesia (slowness of movement), and rigidity (unnatural stiffness of the muscles) (Jankovic 2008). All the main symptoms of PD are known to be directly related to SNc

dopaminergic loss, and are mainly associated with the disruption of the BG motor circuitry. The onset of motor features correlates with loss of dopamine in the posterior putamen which is the motor region of the striatum (Rodriguez-Oroz *et al.* 2009).

Bradykinesia is characterised by reduction in the speed and amplitude of initiation and execution of movements up to a complete cessation (Jankovic 2008; Rodriguez-Oroz *et al.* 2009). Bradykinesia is a defect of the BG motor circuitry involving the structures of STN, GPi and GPe (Nambu *et al.* 1998; Kita 2005). It also involves the recruitment of cortical neurons and BG connections with the SMA and prefrontal cortices known for their involvement in time processing in animals and humans (Meck 2006; Jahanshahi *et al.* 2006) for adjusting initiated movement (Escola *et al.* 2003; Mink and Thach 1991; Boraud *et al.* 2000). In PD, there is increased difficulty in self-initiated movements than externally triggered movements and this fits in well with the BG model of PD which modulates areas such as SMA which is involved in self-initiated actions (Redgrave *et al.* 1999; Escola *et al.* 2003). Rigidity is caused by increased slow and sustained muscle stretching in PD patients (Andrews *et al.* 1972) and it is mediated through the primary motor cortex suggested by increased primary cortex excitability in humans (Lefaucheur 2005; Mir *et al.* 2005) and animals (Goldberg *et al.* 2002). However, the relationship between dopamine deficiency, increased BG output and its relation to primary motor cortex excitability and rigidity is not fully understood. Tremor is characterised by 4-6Hz activity at rest in the limbs. STN and GPi rhythmic and synchronous neuronal firing rates correlate with tremor in monkeys and in PD patients (Rodriguez *et al.* 1998; Bevan *et al.* 2002). The ventral intermediate nucleus (Vim) and cerebellar activation is also known to associated with tremor (Rodriguez-Oroz *et al.* 2009).

However, the BG model does not fully and clearly explain PD symptoms. Increased neuronal activity in the STN/GPi-SNr and the subsequent inhibition of thalamocortical projections does not explain the origin of tremor and rigidity (Rodriguez-Oroz *et al.* 2009). Levodopa-induced dyskinesia are eliminated by GPi lesions (pallidotomy), which is not compatible with a model that relates excessive GPi/SNr inhibition and reduced BG output activity with dyskinesia (Obeso, Rodríguez-Oroz, *et al.* 2008; Obeso, Marin, *et al.* 2008). Similarly thalamic lesions (thalamotomy) which causes disruption of the motor circuitry does not aggravate bradykinesia nor produces new

motor symptoms (Magrinelli *et al.* 2016). Therefore, the manifestation of the motor symptoms of PD suggests a more complex pathophysiological origin.

Dopamine levels can be adjusted temporarily by the administration of levodopa, a precursor of dopamine that crosses the blood brain barrier and can be metabolised to dopamine in the brain (Fahn 2015). Levodopa treatment, which is the current therapeutic standard in PD, targets the BG temporarily by increasing the amount of dopamine in the BG (caudate and putamen) and improving movement related functions (Mirdamadi 2016). Surgical treatment options available are DBS (Williams 2015), thalamotomy (Linhares and Tasker 2000) and pallidotomy (Lozano and Lang 1998), these are typically given when medications are not adequate in controlling the symptoms of the disease or have caused unacceptable side effects; however, recent research suggest that DBS may be specially effective in treatment in the earlier course of the disease (Hacker *et al.* 2015). The ventral intermediate nucleus (VIM) found at the centre of the thalamus is implicated as being the part of the circuit that generates tremor, it is therefore a target for thalamotomy and DBS (Rodriguez-Oroz *et al.* 2009).

Although PD is predominantly described and clinically classified as a motor disorder, there are a number of non-motor symptoms that occur during the progression of the disease including deficits in smell, mood, sleep, cognition and autonomic function (Goldman and Postuma 2014; van Rooden *et al.* 2009). Cognitive dysfunction is present in 20-40% of PD patients even in early PD but are often overshadowed by the motor symptoms (Foltynie *et al.* 2004; Muslimović *et al.* 2005; Elgh *et al.* 2009).

The specific neuroanatomical basis for the non-motor symptoms of Parkinson's disease remain unknown. Studies that explored olfactory disturbances in PD support that these symptoms are associated with Braak stage 1, where degeneration of neurons in the olfactory bulb and anterior olfactory nucleus occurs (Montgomery *et al.* 1999; Ross *et al.* 2008b). And within the Braak staging 1 and 2, the pathological changes in the lower brainstem, the pedunculopontine nucleus and the thalamocortical pathways are thought to mediate the sleep disturbances associated with PD (Rye 2004; Saper *et al.* 2001). Pallidosubthalamic projections within the basal ganglia circuitry have been regarded as anatomical base for most of the non-motor functions within PD in deep brain stimulation studies of the subthalamic nucleus (Karachi *et al.* 2005; Chaudhuri *et al.* 2006).

Non-motor symptoms such as anxiety, apathy and anhedonia in PD are associated with neuronal degeneration and decreased reward processing in projections between the ventral tegmentum and nucleus accumbens and in frontal-subcortical areas (Brown and Pluck 2000; Robbins and Everitt 1996; Kunig *et al.* 2000). The prefrontal cortex and the limbic loop are implicated in the cognitive symptoms of PD (Heiko Braak, Rub, *et al.* 2006), with decline in cognitive symptoms correlating with neuropathological stage of PD (Braak *et al.* 2005).

Resting state functional connectivity studies have shown that certain brain regions such as the ipsilateral orbito-frontal area was negatively correlated with the severity of non-motor symptoms (Yoo *et al.* 2015). Dysfunction in PD resting state extends beyond the sensorimotor network to include fronto-parietal and visual areas as well (Prodoehl *et al.* 2014). Cognitive deficits in PD also correlated with decreased functional connectivity of medial frontal area, temporal lobe, inferior parietal cortex and posterior cingulate areas (A Tessitore *et al.* 2012; Disbrow *et al.* 2014).

Due to the specific involvement of the above mentioned grey matter areas, two white matter tracts of interest; the uncinate fasiculus and the medial forebrain bundle were chosen for the purposes within this thesis. The uncinate fasiculus connects the orbitofrontal cortex with the anterior temporal lobes (Von Der Heide *et al.* 2013; Highley *et al.* 2002) and these brain regions as shown above are known to influence non-motor and cognitive symptoms in PD (Yoo *et al.* 2015; Alessandro Tessitore *et al.* 2012; A Tessitore *et al.* 2012; Disbrow *et al.* 2014; Papagno *et al.* 2011). The medial forebrain bundle connects the ventral tegmental area to the forebrain and the frontal lobe, and these brain areas as shown above as well as the bundle itself has been shown to be involved in reward processing alterations such as anhedonia and depression in PD (Coenen *et al.* 2012; Bracht *et al.* 2015; Brown and Pluck 2000; Robbins and Everitt 1996; Kunig *et al.* 2000).

PD is therefore a complex disorder with a wide range of motor and non-motor symptoms which may include various regions and pathways of the brain even though the main pathological feature is the degeneration of the BG system.

1.4 Cerebellum

1.4.1 Anatomy

The cerebellum is located below the cerebrum, behind the brainstem and is connected to both of these structures (Nieuwenhuys *et al.* 2008). It has two lateral cerebellar hemispheres and the medial vermis, and is classically divided into three lobes; an anterior lobe, a larger posterior lobe and a smaller flocculonodular lobe. The three cerebellar lobes are anatomically separated by 2 transverse fissures, the primary fissure separating the anterior and the posterior lobe and the posterolateral fissure between the posterior and flocculonodular lobe. The cerebellum has 10 further subdivisions or transverse lobules labelled by Roman numerals (lobules I-X) as shown in Figure 1.7 where the unfolded view of the cerebellar cortex also shows the fissures, lobules, lobes and its somatotopy (Roostaei *et al.* 2016). The cerebellum consists of highly convoluted outer layer of grey matter also known as the cerebellar cortex, that surrounds the branches of white matter which in turn surround the deep cerebellar nuclei (Nieuwenhuys *et al.* 2008; Ramnani and Owen 2004).

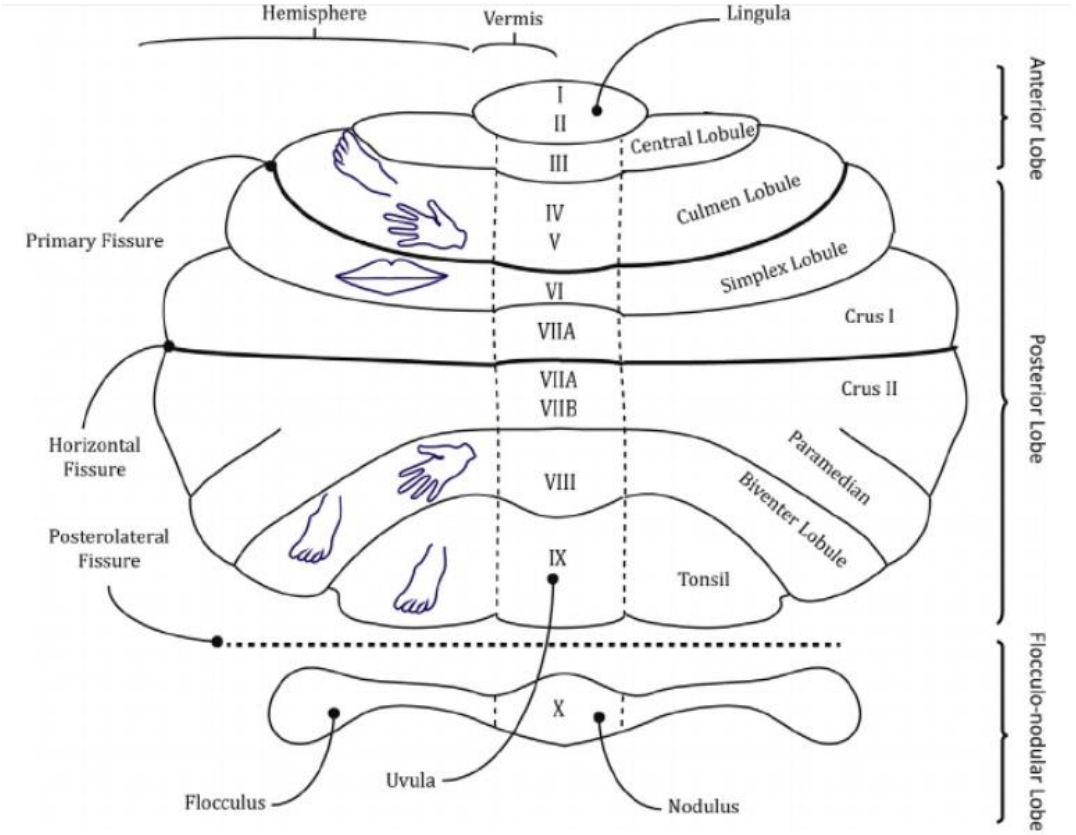

Figure 1.7 Unfolded view of the cerebellar cortex showing the fissures, lobules, lobes and its somatotopy (Roostaei *et al.* 2016).

The deep cerebellar nuclei are the dentate, interposed and the fastigial nuclei, with the dentate nucleus being the largest of them. The cerebellar cortex and the deep cerebellar nuclei are interconnected to extra cerebellar structures through the superior, inferior and middle cerebellar peduncles (Catani *et al.* 2008). All input and output connections from and to the cerebellum pass through these peduncles. An overview of cerebellar anatomy and function is shown in Figure 1.8.

The cerebellum has diverse and varied functions ranging from motor planning and execution to higher-order cognitive and emotional functions such as time perception, working memory, language, executive functioning and emotional processing (Ramnani 2006; Schmahmann 1996; O'Callaghan *et al.* 2016; Buckner *et al.* 2013; Balsters and Ramnani 2011; Koziol *et al.* 2014; Roostaei *et al.* 2016). It is also known to regulate balance, posture, motor coordination and cognitive functions (Nieuwenhuys *et al.* 2008; Ramnani 2006).

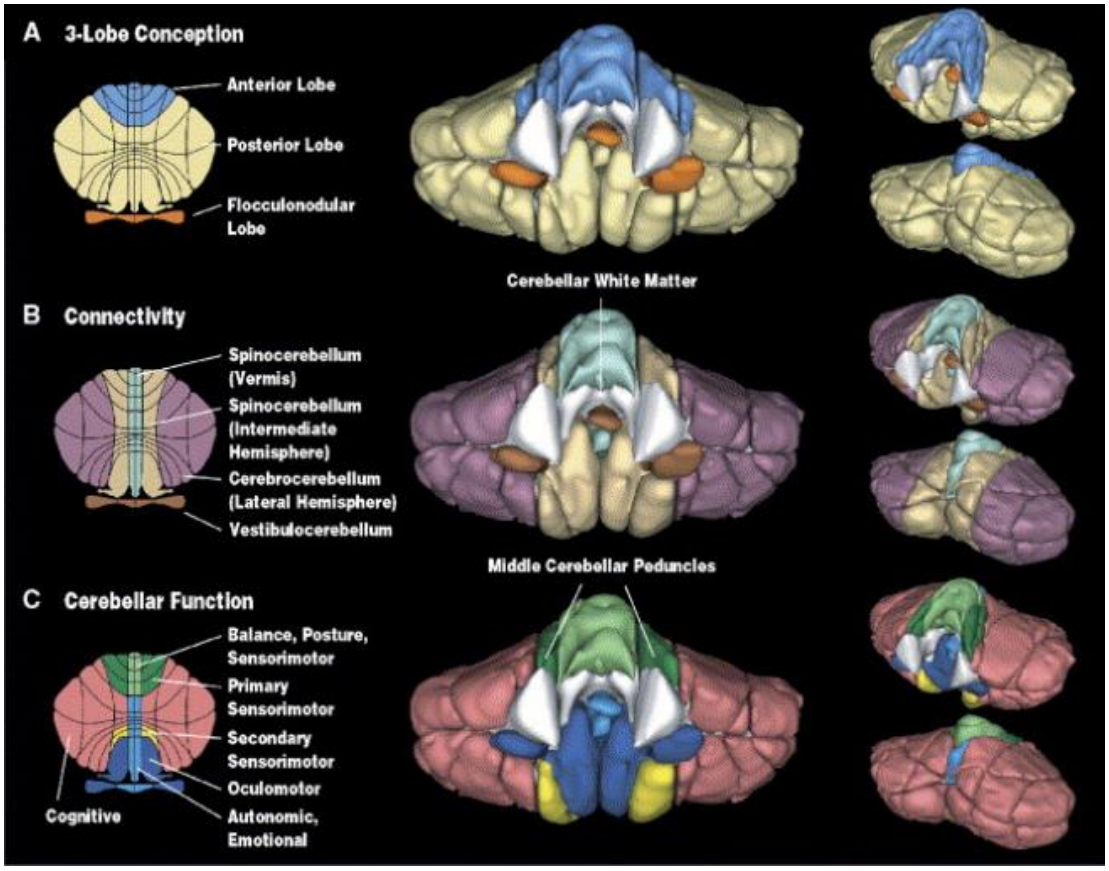

Figure 1.8 Overview of cerebellar anatomy and function

A shows the classical lobular divisions, B shows the classic connectivity patterns and C shows anatomical clusters with their putative functions (Makris *et al.* 2005).

1.4.2 Cerebellar circuitry

The cerebellum has direct and indirect connections to various brain regions including the brain stem, the spinal cord and various cerebral subcortical and cortical regions. The cerebellar circuitry is also organised similar to the BG circuitry in parallel and partially overlapping circuits. This circuitry originates from the motor, association and paralimbic regions of the cerebral cortex, with organised projections towards the pontine nuclei as fibres from the frontal, temporal, parietal and occipital regions (Schmahmann 1996; Stoodley and Schmahmann 2009; Glickstein *et al.* 1985; Ramnani and Owen 2004; Ramnani 2012).

The pontine nuclei project to distinct cerebellar input nuclei which are in turn connected to cerebellar output nuclei that project back to the contralateral cortical regions via the ventrolateral nucleus of the thalamus (Middleton and Strick 2001; Middleton and Strick 2000; Ramnani 2006). These cortico-cerebellar loops have functional distinctions with the 'motor' cerebellum comprising lobules V, VI, VIIb and VIII which project to pre and post central gyrus (cortical motor regions), and the 'cognitive' cerebellum containing Crus I and II which project to prefrontal and parietal cortices (Kelly and Strick 2003; Hoover and Strick 1999; O'Reilly *et al.* 2010; Balsters *et al.* 2014; Balsters and Ramnani 2011).

It is now known that both the BG and the cerebellum modulate the activity of largely overlapping cerebral cortical areas through multisynaptic loops, which were previously assumed to be anatomically and functionally separate (Wu and Hallett 2013). Studies show direct and distinct interconnections between the BG and the cerebellum in animals (Bostan *et al.* 2010; Hoshi *et al.* 2005) and similar connections have been described in humans (Jeong *et al.* 2012; Mollink *et al.* 2016; Fenoy *et al.* 2017; Calabrese *et al.* 2015).

The motor and cognitive regions output to distinct topographical regions in the sensorimotor and associative striatum via the dentate nucleus through projections towards the thalamus after decussating at the red nucleus (Meola *et al.* 2016; Mollink *et al.* 2016; Jeong *et al.* 2012; Jang and Kwon 2015; Calabrese *et al.* 2015; Kwon *et al.* 2011; Anthofer *et al.* 2017). And the STN has projections towards the contralateral cerebellar cortex via the pontine nuclei (Sweet *et al.* 2014; Bostan *et al.* 2010). Projections from the associative, limbic and motor territories of the STN terminate in

the motor and non-motor regions of the cerebellum (Bostan *et al.* 2013). These pathways that show BG and cerebellum interconnections show integration of a range of BG and cerebellum functions.

1.4.3 Cerebellum in PD

Increasing evidence suggests that the cerebellum may play certain roles in the PD pathophysiology. Cerebellar atrophy and volumetric changes have been reported in PD with these changes being attributed to motor and non-motor functions. Reduced cerebellar volume in the left cerebellum of PD patients compared to healthy controls and in patients with tremor at the quadrangular lobe was reported suggesting a role of cerebellum in tremor (Borghammer *et al.* 2010; Benninger *et al.* 2009). PD cerebellar atrophy has been associated with cognitive deficits and markers of disease severity (Pereira *et al.* 2009; Nishio *et al.* 2010; Yoo *et al.* 2015).

Another recent resting state functional connectivity study also found that cerebellar atrophy can cause pathological loss of connectivity with large-scale cortical networks and contribute to motor and cognitive changes in PD (O'Callaghan *et al.* 2016). Cerebellar grey matter changes correlated with reduced connectivity between the cerebellum and sensorimotor, dorsal attention and default networks while showing increased connectivity with the frontoparietal network (O'Callaghan *et al.* 2016).

Additionally, olfactory (K. Y. Zhang *et al.* 2011) and cognitive (Camicioli *et al.* 2009; Nishio *et al.* 2010; Pereira *et al.* 2009) related structural changes have also been reported in PD cerebellum. Dopaminergic degeneration has been reported to produce pathological changes in the cerebellum in PD patients and in animal models. In rat and monkey lesion models, degeneration of nigrostriatal dopaminergic neurons causes dysfunction of both the basal ganglia-thalamic and cerebello-thalamic pathways (Rolland *et al.* 2007). Post mortem brain tissue from PD patients showed reduced dopamine receptors in the cerebellum (Hurley *et al.* 2003).

Cerebellum has also been shown to play a role in PD symptoms such as gait disturbances (Schweder *et al.* 2010), tremor (Helmich *et al.* 2012), dyskinesia (Koch *et al.* 2009) and non-motor symptoms (Wu and Hallett 2013). PD resting tremor has been linked to changes in the BG and the cerebello-thalamo-cortical motor loop, and a recent functional MRI studied showed that the BG influences the tremor amplitude and the cerebello-thalamo-cortical loop is effectively influenced through the motor cortex and

not the cerebellum, suggesting that PD tremor arises in the BG and it's propagated via the cerebello-thalamo-cortical loop (Dirkx *et al.* 2016).

Furthermore, functional MRI studies reveal hyperactivity of the cerebellum in PD (Magrinelli *et al.* 2016; Jahanshahi *et al.* 2010; Yu *et al.* 2007a; Koch *et al.* 2009; Gao *et al.* 2017; Wu *et al.* 2009). In hypokinetic PD patients, the hyperactivity of the cerebello-thalamo-cortical circuit has been proposed to compensate for the hypoactivation of striato-thalamo-cortical circuit, while in PD tremor subtype, cerebello-thalamo-cortical circuit dysfunction is thought as a physiopathologic mechanism for rest tremor (Dirkx *et al.* 2016). Studies have also shown decreased α-synuclein levels in the cerebellum in PD (Westerlund *et al.* 2008; Fuchs *et al.* 2008; Solano *et al.* 2000). Therefore, converging evidence suggests the importance of the cerebellum and the cerebellar interconnections with the BG in PD.

1.5 Main white matter connections for investigation

In summary, from the literature above it is clear that the BG and the cerebellum form networks with the cortical areas and the thalamus and these are affected by the PD pathology. It is known that the motor symptoms of PD only arises after 80% of dopamine in the striatum is depleted and compensatory process have been suggested to occur within and outside the BG which should be reflected in the architecture of the fibre tracts connecting motor cortex, basal ganglia and thalamus (Bezard *et al.* 2003). The study of the white matter architecture of BG interconnections have been omitted in research into PD which provides the novelty and rationale for studying the white matter connections between the SMA and the putamen, and the thalamus and the premotor cortex in relation to BG circuitry in PD (Chapter 3). The corticospinal tract is the major motor tract and it is the pyramidal pathway from the primary motor cortex travelling through the cerebral hemispheres including the posterior internal capsule, which lies between the globus pallidus and the thalamus, the brain stem (crossing at the bottom of the medulla) and the lateral part of the spinal cord (Jang 2014). Therefore, the corticospinal tract was also added as the motor tract of interest for investigation in Chapter 3. Non-motor symptoms and their related white matter connections have also been overlooked in PD, which provides the rationale for including the uncinate fasiculus and the medial forebrain bundle for additional investigation in Chapter 3.

Despite converging evidence that the cerebellum plays a role in PD pathogenesis and the evidence showing direct connections between the BG and the cerebellum, no studies have looked at the white matter connections of the cerebellum and its interactions with the BG in PD. Therefore in Chapter 4, these connections were mapped out in healthy participants to provide an anatomical investigation and protocol for delineate the BG-cerebellum interconnections. And in Chapter 5, these connections and the main cerebellar pathways were investigated in the first diffusion tractography study of their alteration in PD. The work within this thesis closes the gaps in knowledge in PD were previous neuroimaging studies have overlooked the white matter connections of the BG and also the interconnections between the BG and the cerebellum while also provide an anatomical protocol for future studies in PD and other brain disorder to reconstruct and study these white matter connections.

Chapter 2 General Methods

2.1 Magnetic Resonance Imaging

Magnetic Resonance Imaging (MRI) uses the principle of applying radio frequency (RF) pulses to excite hydrogen nuclei (protons) within a tissue of interest and recording the energy released while they return back to their relaxed state. Hydrogen nuclei possess a magnetic dipole with a corresponding north and south pole, these dipoles also referred to as spins, align themselves to an externally applied magnetic field. Therefore, when a magnetic field is applied on a tissue, the protons within that tissue align themselves parallel to the direction of the magnetic field as shown in (Figure 2.1). This net magnetic field direction is referred to as B_0 and the net alignment of all the protons along this direction as M_0.

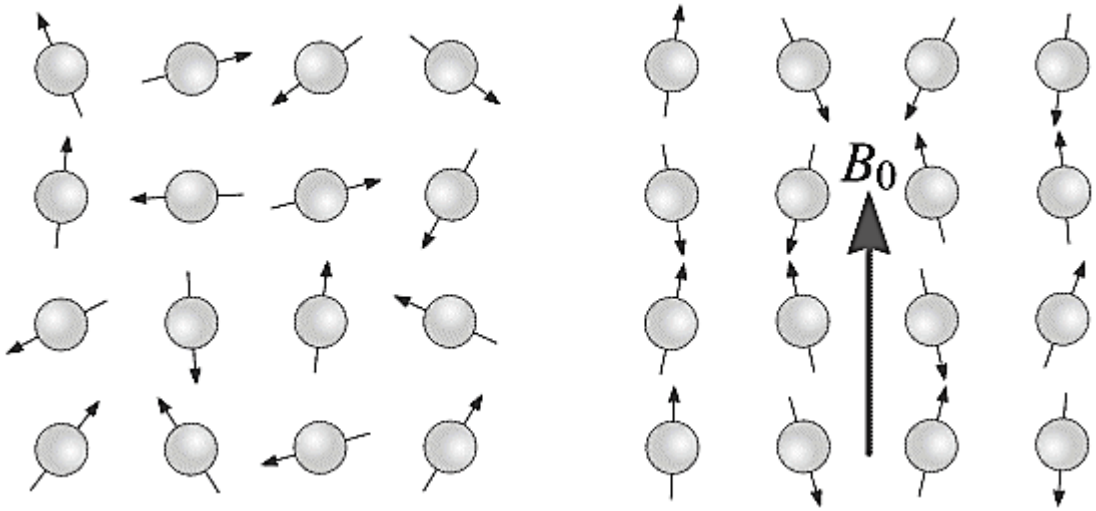

Figure 2.1 Protons aligned along the magnetic field B_0.

The excited protons spin around their axis and higher magnetic fields cause faster spins and *vice versa*. When an RF pulse that matches the frequency of the spin hits the protons, the protons absorb the energy and deflect or fall out of alignment with the magnetic field into a higher energy state (Figure 2.2a). The protons then recover back into alignment along B_0 while releasing the absorbed energy. This process is called as magnetic recovery, the time taken to recover is called T1 and the MR signal measured as the T1 signal (Figure 2.2b). RF pulses also help coordinate the protons magnetic fields so that they wobble in time together (in phase) and as they begin to relax, the wobble becomes uncoordinated (out of phase). This process of returning back to

uncoordinated wobbling is called as magnetic relaxation, the time taken to relax is called T2 and the MR signal is measured as T2 signal (Figure 2.2c).

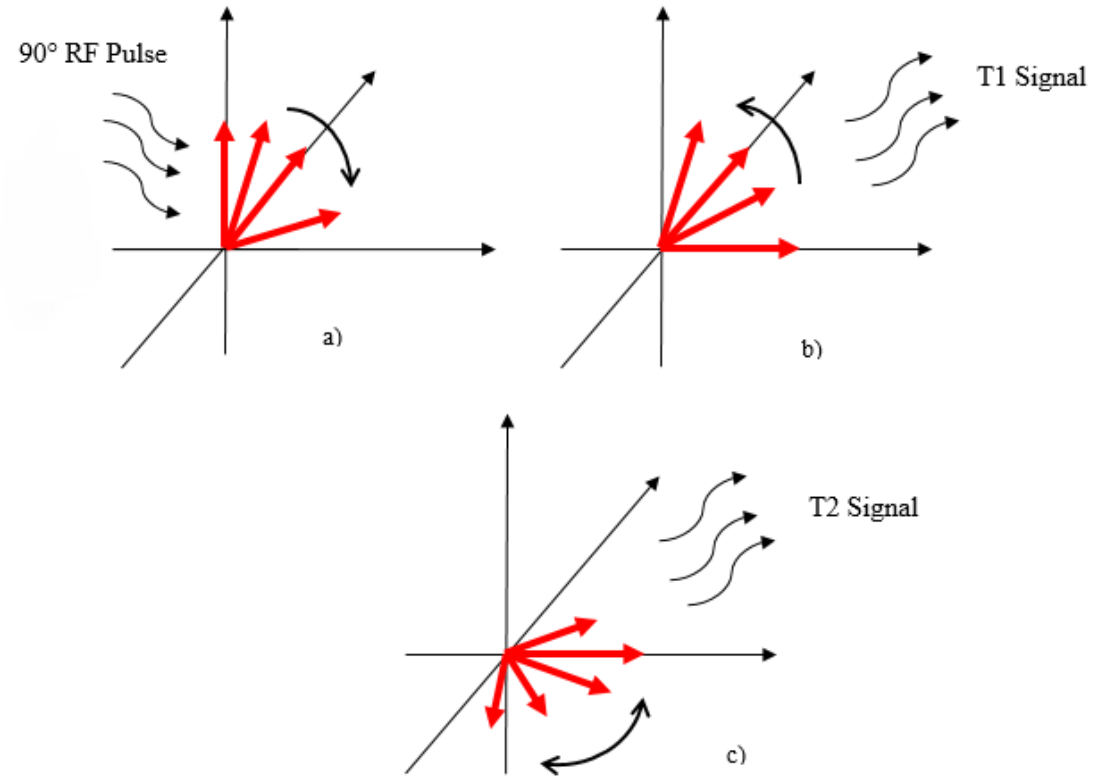

Figure 2.2 T1 and T2 signal

a) 90° RF pulse hits a proton causing it to fall in alignment with magnetic field. b) Proton gets back to low energy state by releasing energy as the T1 signal. c) Proton falls out of phase and give rise to the T2 signal.

In practice, the MR scanner produces a series of short RF pulses followed by longer periods of waiting to measure the MR signal that comes back. The signal that come backs is called the magnetic echo, the time between the RF pulse and the resulting magnetic echo is called as the echo time (TE). When double RF pulses are used, the image obtained is called a spin echo MRI image. The time between consecutive RF pulses is called as repetition time (TR). When extra magnets in the scanner called as the magnetic gradient systems, are rapidly switched ‘on’ and ‘off’, the image formed is called a gradient echo MRI image. MRI images are made up of pixels usually represented as a matrix, and the more pixels, the higher the resolution which gives more structural detail in the MRI image.

By manipulating the TE and the TR, different contrasts of MR images can be obtained. T1 and T2 times vary within different tissue in the brain (grey matter, white matter and cerebrospinal fluid) this causes different contrasts to the MR images as shown in Figure 2.3.

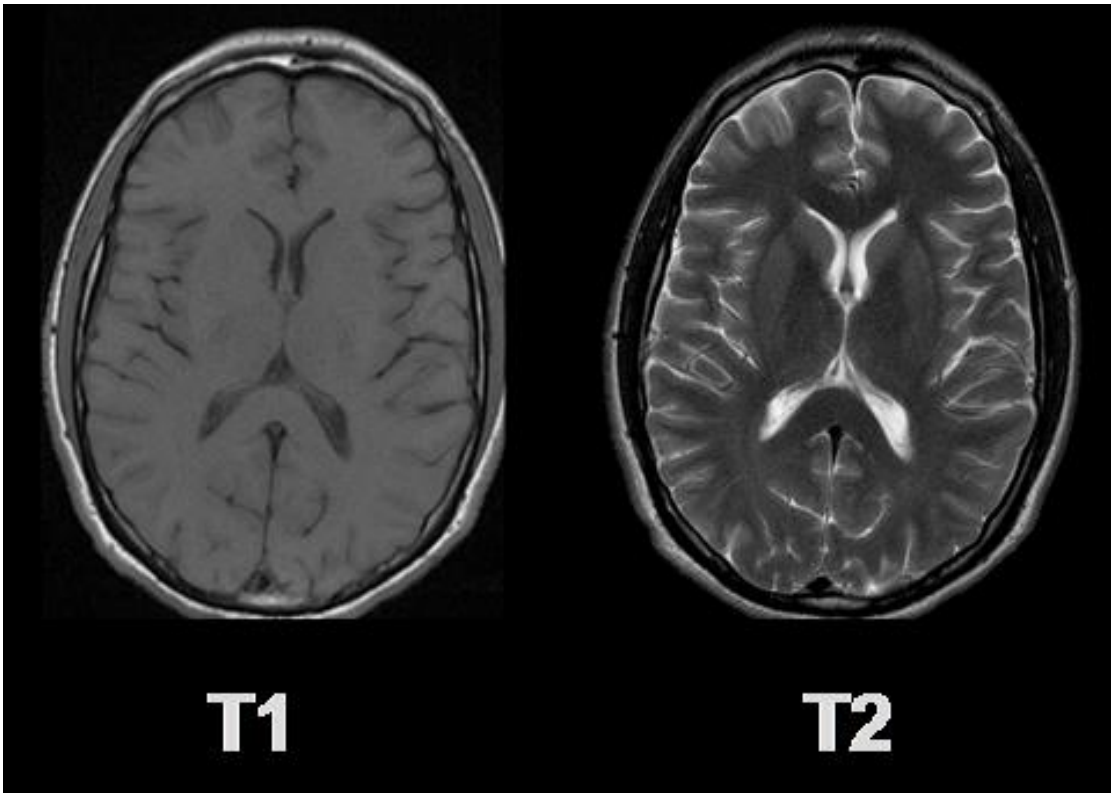

Figure 2.3 T1 and T2 contrasted images of a representative human brain in the axial view.

2.2 Diffusion MRI Imaging and Tractography

2.2.1 Background

Diffusion is the process of transporting matter by the random motion of molecules, also called as Brownian motion. And about 30 years ago, Le Bihan and colleagues made it possible to image the apparent diffusion of water molecules in the human brain (Le Bihan *et al.* 1986). Since then diffusion MRI has become a standard for understanding various brain diseases such as multiple sclerosis, dementia, traumatic brain injury, stroke, schizophrenia etc. (Oppenheim *et al.* 2004; Assaf and Pasternak 2008; Ciccarelli *et al.* 2008; Le Bihan and Johansen-Berg 2012; Dijkhuizen *et al.* 2012). Diffusion weighted imaging (DWI) uses the property of Brownian motion of water molecules (Le Bihan *et al.* 2001) to provide image contrasts based on the rate of diffusion (differences in magnitude of water diffusion) within the brain. The degree/rate of MR signal loss is dependent upon the degree/rate of diffusion (diffusivity), with higher diffusivity areas (E.g.: CSF) resulting in more MR signal loss and lower diffusivity areas (E.g.: white and grey matter areas) resulting in lower MR signal loss. This degree of the MR signal loss can be enhanced by increasing the strength and duration of the diffusion-encoding gradients which are characterised by the *b* value (s/mm^2).

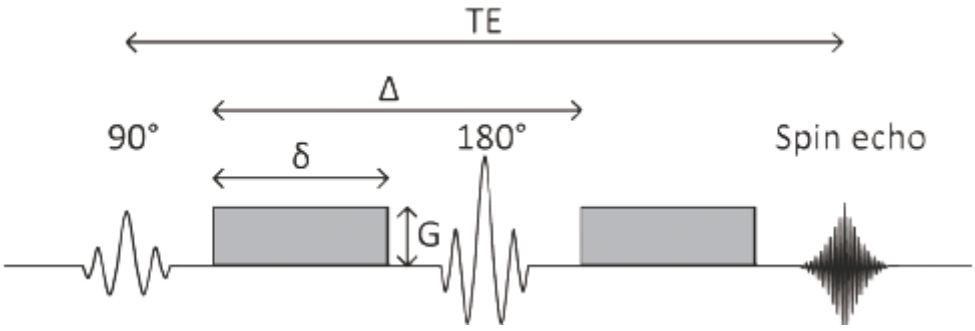

Figure 2.4 Diffusion weighted spin echo sequence (Winston 2012a)

The *b* value is defined by the Stejskal-Tanner equation:

$$b = \gamma^2 G^2 \delta^2 (\Delta - \delta/3)$$

Where, γ is the gyromagnetic ratio, G, δ, Δ correspond to the amplitude, duration and interval of the diffusion gradient, respectively (Figure 2.4). Two dimensional DWI images/maps of the diffusion rates are generated by calculations from a combined analysis of the two images acquired with different *b* values ($b = 0$ and $b = 1000$ s/mm^2) (Huisman 2010). A representative participant's T1 and DWI images are shown in

(Figure 2.5 A, B), respectively. The apparent diffusion coefficient (ADC) is the measure of the rate of diffusion, a representative ADC map can be seen in (Figure 2.5 B), where high diffusivity areas appear hyperintense and low diffusivity areas are hypointense.

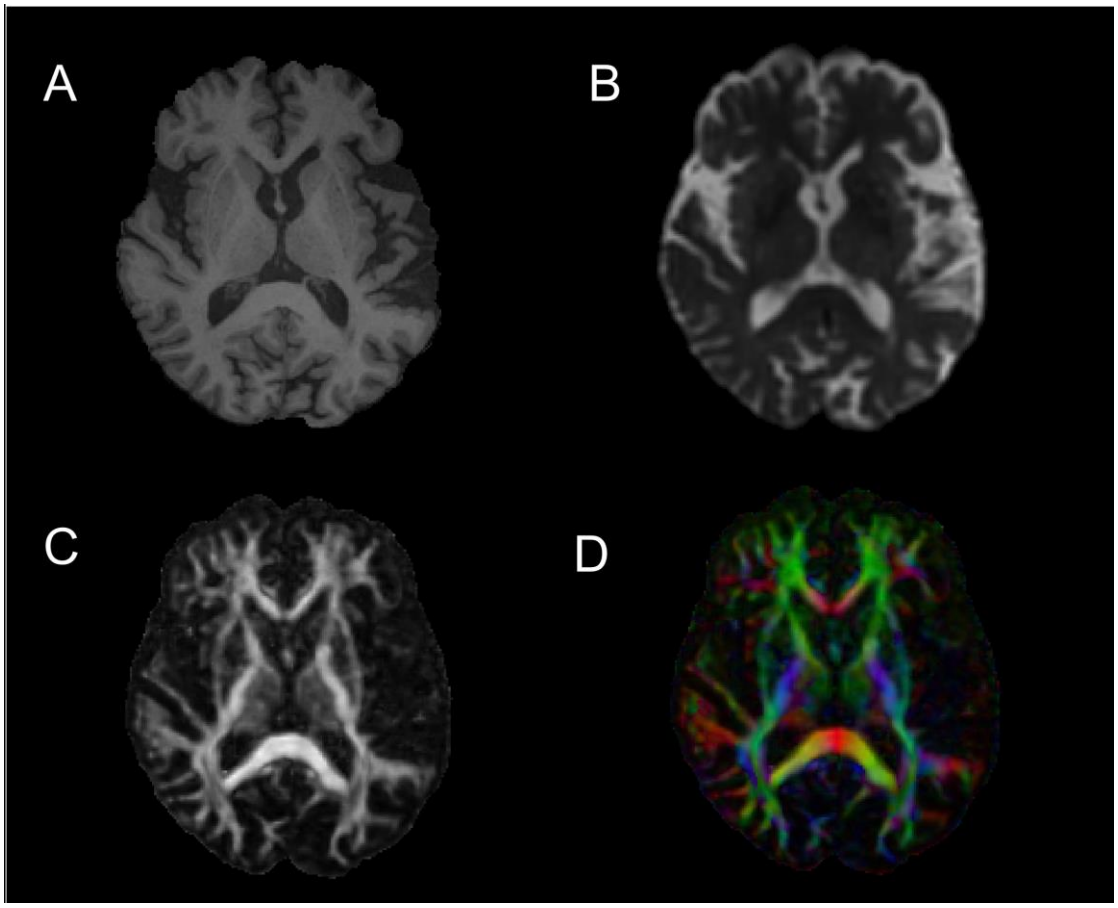

Figure 2.5 T1, DWI, FA and FA colour coded images of a single slice axial view of a representative subject.

A tensor is a mathematical vector which describes both direction and magnitude, therefore in diffusion tensor imaging (DTI), the DWIs are acquired in many orientations/directions to calculate the overall dominant direction and magnitude of water molecule diffusion within each voxel. DTI allows the calculation of the shape and orientation of the diffusion in space, which is the tensor graphically represented as the ellipsoid in Figure 2.6.

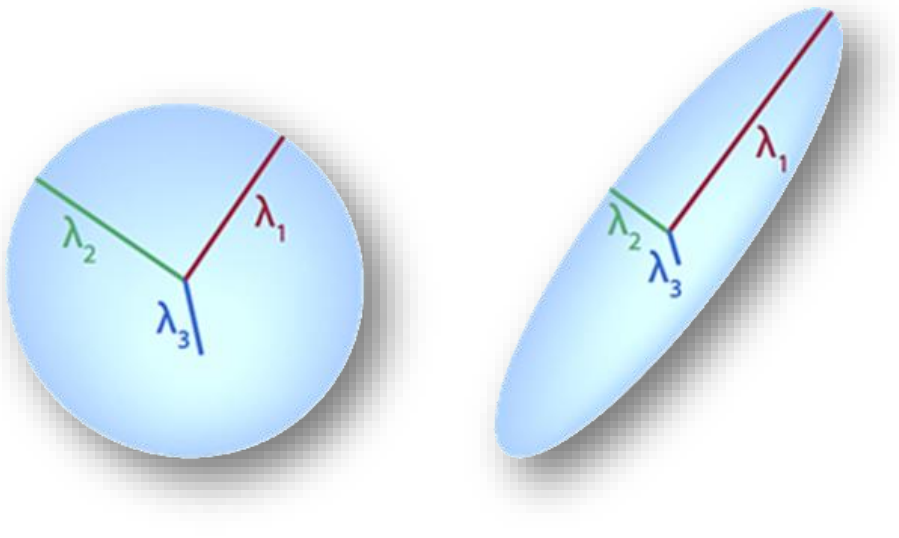

Figure 2.6 The diffusion tensor and its quantitative measures

Normalized (λ_1, λ_2, λ_3) = Fractional Anisotropy (FA)

λ_1 = longitudinal (axial) diffusivity (L1/AD)

(λ_2+λ_3)/2 = Radial diffusivity (RD)

(λ_1 + λ_2 + λ_3)/3 = Mean diffusivity (MD)

Therefore, DTI gives a 3D measurements with three principal diffusivities (eigenvalues, λ_1, λ_2, λ_3 in Figure 2.6) which are associated with the three mutually perpendicular principal directions (eigenvectors, Dxx, Dyy, Dzz). The tensor has three degrees of freedom and is represented by a 3×3 symmetric matrix (Dxx, Dxy, Dxz, Dyx, Dyy, Dyz, Dzx, Dzy, Dzz). The sampling of the tensor is performed by repeating diffusion-weighted sequence along different directions and one measurement is usually a low b-value or a zero b value.

However, diffusion is a three-dimensional property differing between brain areas and influenced by the various microstructural architecture as well as physiological factors with the various brain structures. When the movement of the water molecules is completely unhindered and they can move freely and equally in all three directions, the diffusion is isotropic and the 3D shape is represented by a sphere (E.g.: in the CSF). When the movement of the molecules is hindered, the diffusion becomes anisotropic (E.g.: in the white matter tracts) and this 3D shape is graphically represented as an ellipsoid (Figure 2.6). In the white matter tracts, diffusion happens predominantly along

the direction parallel to the long axis of the tracts (axonal bundles) and is more restricted along the directions perpendicular to the direction.

Various quantitative measurements can be extracted using the information from the directional restriction of diffusion along the three axes. The main quantitative measures extracted from this information are Fractional Anisotropy (FA), Axial Diffusivity (AD), Radial Diffusivity (RD) and Mean Diffusivity (MD) as shown in (Figure 2.6). Fractional anisotropy (FA) is a scalar measure of the degree of anisotropy and its value ranges from 0 to 1, with values approaching 0 reflecting isotropic tissue and values approaching 1 reflecting anisotropic tissue. It is a normalised measure of diffusion along all the three directions derived by the following formula (Pierpaoli and Basser 1996)

$$\mathrm{FA} = \sqrt{\frac{3}{2}} \frac{\sqrt{(\lambda_1 - \langle \mathrm{D} \rangle)^2 + (\lambda_2 - \langle \mathrm{D} \rangle)^2 + (\lambda_3 - \langle \mathrm{D} \rangle)^2}}{\sqrt{\lambda_1^2 + \lambda_2^2 + \lambda_3^2}}$$

$$\langle \mathrm{D} \rangle = \frac{1}{3}(\lambda_1 + \lambda_2 + \lambda_3)$$

FA values can also represented as degree of anisotropy maps and (Figure 2.4 C) shows high FA values as bright (e.g.: corpus callosum, internal capsule) and low FA value regions e.g.: CSF or grey matter. Mean diffusivity (MD) is a measure of the average diffusion along all three directions. Axial or Longitudinal diffusivity (AD/L1) is a measure of diffusion along the axial direction or direction of the largest eigenvector along the axonal bundle. Radial Diffusivity (RD) is measure of diffusion perpendicular to the axial direction or axonal bundle. (Pierpaoli *et al.* 1996; Song *et al.* 2002; Hagmann *et al.* 2006).

As DTI also gives the principal direction of the diffusion, colour-coded FA images depicting the direction of largest eigenvector can be derived where the red, green, and blue colours are assigned to the right-left, anterior-posterior, and superior-inferior directions of the fibre orientations, respectively (Pierpaoli *et al.* 1996) (Figure 2.4 D). MRI measurement of water diffusion in brain tissue provides information about the composition, microstructure, architectural organisation and physical properties of the constituents of the tissue in a non-invasive manner without the use of contrasting agents. Therefore, DTI has made it possible to visualise in vivo white matter

connections in the human brain and to investigate their white matter properties. The importance of white matter microstructure and it's organisation in unravelling the mysteries of cognition and disease is now widely recognised, particularly how white matter is vulnerable to neuropathological defects and neurodegenerative diseases.

2.2.2 Tractography

Using the information from the diffusion tensors or ellipsoids, the principal direction of the apparent diffusion can be determined for each voxel. With the development of mathematical algorithms that allow the connection of ellipsoids one voxel after another along their principal directions, it is possible to depict the trajectory of the apparent diffusion along white matter fibre tracts as shown in Figure 2.7. Mathematical methods were developed to extract and visualise coherently ordered fibre tract trajectories within each voxel followed in discrete steps to form tracts. In this way, diffusion tensor based tracking allows the visual representation of diffusion directions along white matter pathways (Derek K Jones *et al.* 1999; Pierpaoli *et al.* 1996; Mori *et al.* 1999; Catani *et al.* 2002).

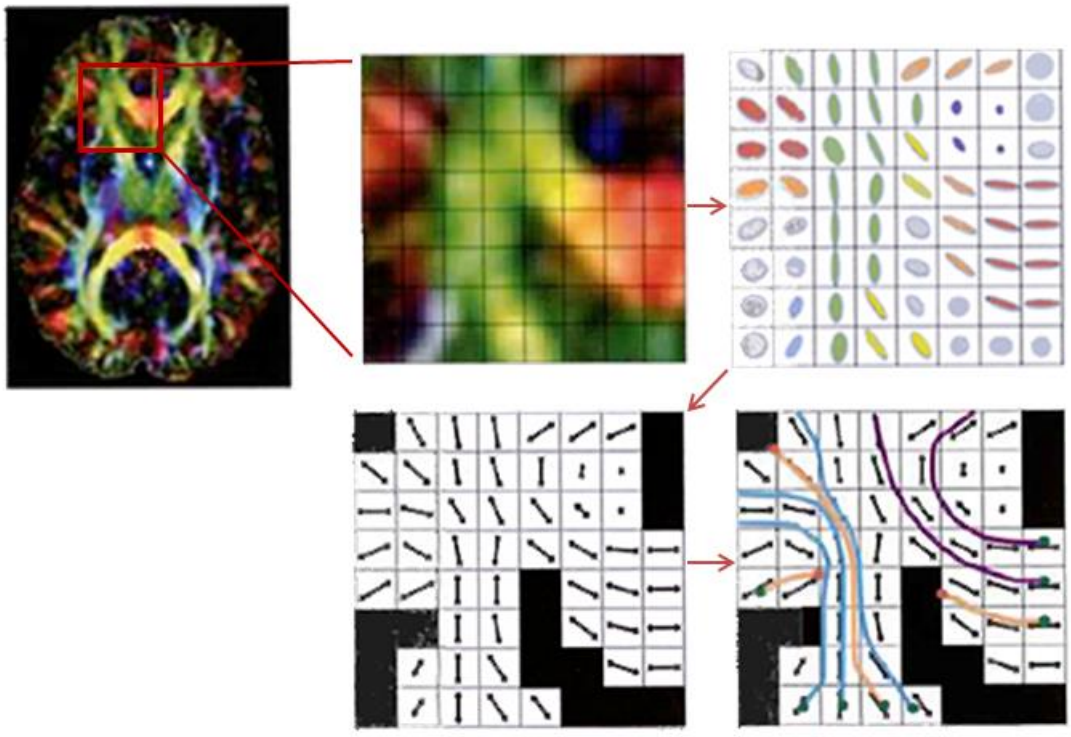

Figure 2.7 Tractography based on Diffusion Tensor Imaging [modified from book (Jones 2010)]

However, DTI based tractography has limitations; in particular, it is unable to resolve multiple fibre orientations within voxels (Alexander 2013; Von Dem Hagen and

Henkelman 2002). Therefore, several alternative methods to overcome the challenges posed by DTI have been developed, such as Diffusion Spectral Imaging (Wedeen *et al.* 2005), Q-ball imaging (Tuch 2004), persistent angular structure MRI (PAS-MRI) (Jansons and Alexander 2003) and spherical deconvolution (SD) (Anderson 2005; Tournier *et al.* 2004) methods. The data acquisition time for DSI is quite restrictive producing partially acquired data which don't provide sufficient data to reconstruct the full diffusion propagator. Q-ball imaging is a variant of DSI, which allows fibre orientation peaks to be derived from data acquired at a single b-value however these peaks are not very sharp. The PAS-MRI and the SD methods both attempt to sharpen the fibre orientation peaks however the PAS-MRI methods have longer computation time due to non-linear estimation requirements. Among these methods, the SD based tractography has been shown to resolve the DTI problem of crossing fibres with a good angular resolution, it also has a relatively short acquisition time similar to standard DTI clinical protocols and have reasonable computational analysis times (Huisman 2010; Jones 2004). Given that there are crossing fibres in about 90% of the voxels of the brain, allocation of voxel-based findings to specific tracts can be highly speculative (Jeurissen *et al.* 2013). The SD method is based on the assumption that the diffusion signals within a voxel can be modelled as a spherical convolution between the fibre orientation distributions (FOD) and the fibre orientation density function (fODF) which describes the common signal profile from the white matter fibres within a voxel (Tournier *et al.* 2004). Therefore the FOD is said to provide a better estimation of fibre bundles within each voxel as it does not require modelling of the diffusion process itself and does not require prior information about the likely number of different fibre populations present within each voxel. An example of SD based fODFs reconstructed in the pons is shown in Figure 2.8.

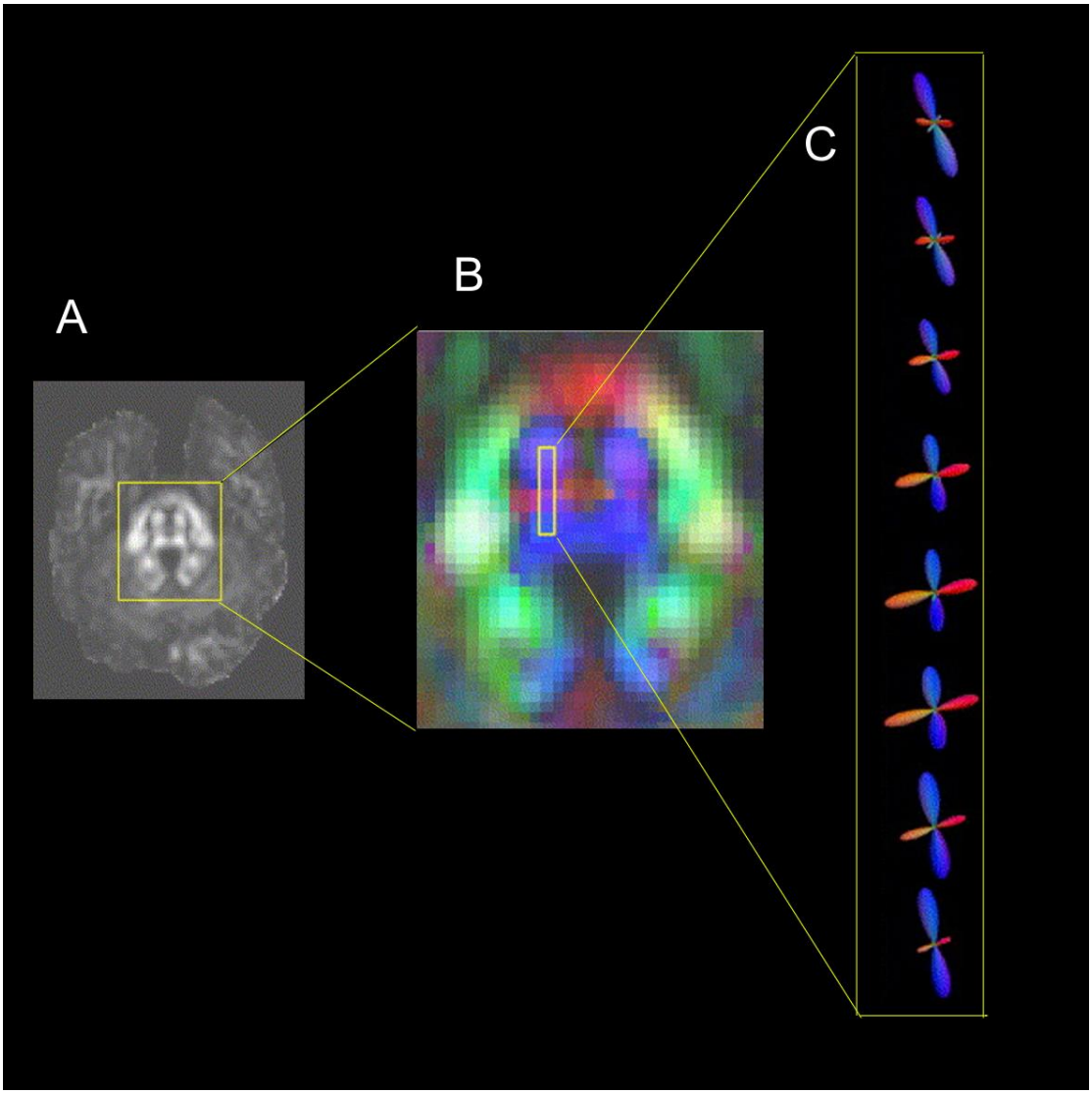

Figure 2.8 Fibre ODFs reconstructed from the in vivo data for adjacent voxels in the pons. A shows an axial FA map at the level of the pons. B shows a magnified section of the FA map, coloured according to the anatomic direction of the major eigenvector of the diffusion tensor (red: left–right, green: anterior–posterior, blue: inferior–superior). C shows the fibre ODFs reconstructed from the voxels highlighted in the direction map, also coloured according to orientation. [modified from (Tournier *et al.* 2004)]

Tractography done using only the tensor information from the DTI method is unsuitable due to problems with the crossing fibres, however the SD based methods can resolve up to 3 peaks reliably which is very important as most of the voxels within the brain are known to have crossing fibres (Jeurissen *et al.* 2013). Even though the SD method overcomes these limitations of the DTI method, it is known to be affected by isotropic partial volume effects which is likely to produce artefactual tractography results (Ciccarelli *et al.* 2008; Schonberg *et al.* 2006). The modified damped Richardson-Lucy (dRL) algorithm was developed to overcome these challenges of false positives, partial

volume effects, crossing fibres and spurious tracking (Dell'acqua *et al.* 2010). The dRL algorithm has been shown to reduce false positive fibre orientations while preserving angular resolution therefore making it robust in estimating the fibre orientations of white matter tracts are close to the cortex, thereby providing accurate description of white matter organization (Dell'acqua *et al.* 2010).

There are two main types of tractography methods: Deterministic and Probabilistic. In probabilistic tracking, a seed point (a chosen voxel) is assumed to have connections across all points but only those connections that have some minimal cost function are taken as most probable connections and pursued to create the fibre tract (Behrens *et al.* 2003; Jones and Pierpaoli 2005). The disadvantage of this method is that the frequently travelled connection ultimately becomes the most probable one and the cost function restricting the direction or coherence of the nerve fibre may not be useful in giving an actual representation of a fibre tract. In deterministic tracking, the fibres are launched from a defined region of interest in all directions until specified termination conditions are met (Mori *et al.* 1999; Basser *et al.* 2000). All ellipsoids or spherical convolutions that pass those conditions create the continuous trajectories that form a fibre tract, making it computationally less expensive than probabilistic tracking. The disadvantage of this strategy is that one cannot be sure whether the fibre tract may represent an actual or even a probable white matter pathway, therefore caution needs to be taken when performing deterministic tracking without prior knowledge of anatomical pathways.

Tractography has been shown to be able to generate tracts that are anatomically plausible when compared with post mortem sectioning results (Jellison *et al.* 2004).Tractography is not only non-invasive and time saving, but it helps to visualise white matter tracts in the brain, segment specific tracts for studying and understanding them better. Tractography elucidates the white matter anatomy to inform neurosurgery of brain tumours and other lesions (Ulmer *et al.* 2014) or deep brain stimulation (Torres *et al.* 2014) and also enables to find the differences between healthy and diseased white matter microstructure (Ciccarelli *et al.* 2008) thereby helping to understand the underlying neuropathology and disease mechanisms.

For the purposes of this thesis, a whole brain deterministic tractography based on the dRL algorithm was employed for the tractography analyses of the chosen white matter

pathways of interest guided by previous post mortem, animal tracing and/or human diffusion imaging studies.

2.3 MRI data acquisition and processing

2.3.1 Data cohorts

Previously collected data from three different studies were utilised for the analyses within this thesis. The first cohort was a group of 26 patients with Parkinson's disease (PD) who took part in a trial that compared functional magnetic resonance imaging (fMRI)-based neurofeedback and exercise intervention with a gaming console over 12 weeks (Subramanian *et al.* 2016). Here the data used for the analyses here is from the baseline scan, which were unaffected by the intervention. Two PD patients' scans had to be excluded from the final analysis due to corrupted data files. The second cohort used in this thesis was from a study that looked at the effects of ageing on white matter microstructure (Metzler-Baddeley *et al.* 2011). This study used the same diffusion imaging protocol as the PD intervention study and were included to provide 26 age and gender matched healthy control (MHC) individuals. The third cohort is a group of 20 young healthy participants (YHP), acquired as part of a study into white matter plasticity following working memory training (Metzler-Baddeley *et al.* 2016; Metzler-Baddeley *et al.* 2017). These studies were approved by the local NHS research ethics committee for the patient study and the ethics committee of the School of Psychology for the healthy aging and cognitive training studies. All patients and participants provided written informed consent. The demographics information of all three groups is shown in Table 2.1.

Table 2.1 Demographics of the Young healthy participants (YHP), Parkinson's disease (PD) patients and Matched healthy controls (MHC)

	YHP (n=20)	PD (n=24)	MHC (n=26)	Differences between PD and MHC
Age	25.4 ± 4.84	63.42 ± 10.82	64.88 ± 8.06	P = 0.5918, Two sample t-test
Sex (M:F)	12:8	22:2	17:9	P = 0.06, Chi squared test
No of diffusion directions	60	30	30	-
H & Y Stage	NA	1.75 ± 0.47	NA	-
MOCA	NA	26.54 ± 2.01	NA	-
LEDD (mg)	NA	537.64 ± 340.69	NA	-

Abbreviations: MOCA –The Montreal Cognitive Assessment; H & Y - Hoehn & Yahr Stage; LEDD – Levodopa Equivalent Daily Dose; YHP- Young Healthy Participants; PD- Parkinson's disease patients; HC – Healthy Controls; M - Male; F - Female; R – Right; L - Left

2.3.2 Structural MRI scanning

All data were collected at the Cardiff University Brain Research Imaging Centre (CUBRIC) on a 3T GE Signa HDx system (General Electric Healthcare) with eight head coils. T1-weighted structural scans were acquired using an oblique-axial, 3D fast spoiled gradient recalled sequence (FSPGR) with the following parameters: 178 slices; TE = 3 ms, TR = 7.9 ms, voxel size 1.0×1.0×1.0 mm^3, 256×256 Field of view (FOV), acquisition time of 6 minutes. These T1 structural images were acquired for correcting geometrical echo planar imaging (EPI) distortion by co-registration with the diffusion MRI data, for grey matter anatomical landmarks for localization of regions of interest for the tractography and for the subcortical volume analyses.

2.3.3 Diffusion MRI scanning

Diffusion weighted MRI data were acquired using a peripherally gated twice-refocused pulse-gradient spin-echo echo-planar imaging sequence providing whole oblique axial (parallel to the commissural plane) brain coverage. Data were acquired from 60 slices of 2.4 mm thickness, with a field of view 23 cm, and an acquisition matrix of 96 x 96 (yielding isotropic voxels of 2.4 x 2.4 x 2.4 mm, reconstructed to a resolution of 1.9 x 1.9 x 2.4 mm). Echo time (TE) was 87 ms and parallel imaging (ASSET factor = 2) was used. Diffusion encoding gradients (b = 1,200 s/mm^2) were applied as the optimal b-value for deriving good estimates of fractional anisotropy, mean diffusivity and fibre orientation is 750-1300 s/mm^2 (D K Jones *et al.* 1999). The gradients were applied along 30 isotropically-distributed directions for the PD group and MHC group and 60 isotropically-distributed directions for YHP group using an optimized gradient vector scheme (Jones *et al.* 2002; D K Jones *et al.* 1999). Three or six non-diffusion weighted images were acquired for the 30 or 60 directions respectively. The 60 direction scan was cardiac gated and took approximately 30 minutes while the 30 directions scan took a total acquisition time of 15 minutes.

2.3.4 Diffusion MRI pre-processing

Echo planar imaging (EPI) which is the technique used to acquire the images of the brain plane by plane can be affected by inhomogeneity in the magnetic field and this causes distortions in the intensity of each image obtained, and the strong gradients that

are used for diffusion encoding create eddy currents (EC) that causes geometric distortions to the images, particularly in areas adjacent to the sinuses i.e. frontal and anterior temporal lobe regions (Jezzard *et al.* 1998; Irfanoglu *et al.* 2012).

The data were corrected for these EC and EPI distortions by registering each image volume to the high resolution T1 weighted anatomical images (Irfanoglu *et al.* 2012). DWI data were also corrected for non-linear distortions induced by the diffusion-weighted gradients and artefacts due to head and subject motion with appropriate re-orienting of the encoding vectors (Leemans and Jones 2009). A single diffusion tensor model was fitted (Basser *et al.* 1994) to the data in order to compute quantitative parameters such as FA, MD, RD, AD. The Damped Richardson-Lucy Algorithm (dRL) was used to estimate the fibre orientation density function (fODF) in each voxel for whole brain tractography (Dell'acqua *et al.* 2010). Correction for free water contamination of the diffusion tensor based estimates was applied, before extracting the diffusion properties (FA, RD, AD and MD) along the tracts (Pasternak *et al.* 2009; Metzler-Baddeley *et al.* 2012). This was done because aging and neurodegeneration are associated with grey and white matter tissue loss which produces partial volume effects (PVE) which in turn causes artificial decreases in FA and increase in MD due to the contamination from cerebrospinal fluid (CSF) (Metzler-Baddeley *et al.* 2012).. Hence all the diffusion parameters extracted from the tracts in this study were corrected for the PVE using the Free Water Elimination (FWE) method (Vos *et al.* 2011).

2.3.5 Tractography

Whole brain deterministic tractography was performed in ExploreDTIv4.8.3 (Leemans, Jeurissen, Sijbers, *et al.* 2009) using the spherical deconvolution based dRL algorithm following peaks in the fODF reconstructed from dRL (Dell'acqua *et al.* 2010; Jeurissen *et al.* 2013). For each voxel in the data set, streamlines were initiated along any peak in the fODF that exceeded amplitude of 0.05. This enables multiple fibre pathways to be generated from any voxel. Each streamline was continued in 0.5 mm steps following the peak in the ODF that subtended the smallest angle to the incoming trajectory. The termination criterion was set to an angle threshold greater than 45 degrees; thereby streamlines that had angles above this threshold were excluded from the final tracts. Three-dimensional fibre reconstructions of the specific tracts were then obtained by applying waypoint region of interest (ROI) gates ("AND", "OR" and "NOT" gates

following Boolean logic) to isolate specific tracts from the whole brain tractography data. ROIs were drawn manually on either the T1 anatomical images or colour-coded fibre orientation maps in native space guided by known anatomical landmarks.

All white matter pathways reported in this thesis were reconstructed using this methodology. These were: the corticospinal tract, the uncinate fasiculus, the supero-lateral medial forebrain bundle, the white matter connection between the supplementary motor area and putamen and the white matter connection between the thalamus and motor cortex reported in Chapter 3, the dentato-rubro-thalamic tract and the subthalamo-ponto-cerebellar in Chapter 4 and the middle, inferior, and superior cerebellar peduncles in Chapter 5.

2.3.6 Anatomical methods

Anatomical landmarks were identified on either the T1 anatomical images or colour-coded fibre orientation maps in native space depending on the tract of interest with ExploreDTIv4.8.3 (Leemans, Jeurissen, Sijbers, *et al.* 2009). The identification of these anatomical landmarks were not reliant on any one specific anatomical atlas or piece of literature but rather a combination of animal tracing studies, human post mortem and human diffusion imaging based studies. Therefore the anatomical landmarks and accuracy of tract reconstruction for each tract within this thesis is provided in detail in their respective chapters. The special case for reconstruction of the white matter connection between the supplementary motor area and putamen and the white matter connection between the thalamus and motor cortex reported in Chapter 3, was the use of the Anatomical Automatic Labelling (AAL) atlas in the Montreal Neurological Institute (MNI) space with FSL (Jenkinson *et al.* 2012; Smith *et al.* 2004). The AAL atlas was used to create masks for the regions of thalamus, motor cortex, supplementary motor area and the putamen which were then used for the segmentation of the individual tracts were derived by reconstructing the connections between the chosen masks.

2.3.7 Clinical and behavioural measures from the PD cohort

The following clinical and behavioural measures from the PD cohort were also utilised within this thesis to explore their potential correlations with the extracted diffusion metrics:

(i) The Movement Disorder Society-Unified Parkinson's Disease Rating Scale (MDS-UPDRS) (Goetz *et al.* 2008) was performed when patients were in their

"off medication" state where they were requested not to take their medication for 12 hours before the assessment. The MDS-UPDRS full scale measured non-motor experiences of daily living, motor experiences of daily living and motor complications in addition to the motor examination (which was videotaped for later evaluation). Here the baseline off-medication MDS-UPDRS scores were utilised.

(ii) PD disease duration has been shown to correlate negatively with the uptake of dopamine transporters in the bilateral striatum, caudate and putamen (Benamer *et al.* 2000; Hsiao *et al.* 2014). PD patients with longer disease duration also presented with reduced cerebral blood flow to the bilateral motor cortex, the thalamus, subthalamic nucleus and the basal ganglia (Kapitan *et al.* 2009). As these structures are involved in investigated tracts of interest, duration since PD diagnosis (in months) was also added.

In patients with PD, well executed and skilled hand movements that are crucial for daily life are affected. Bradykinesia, one of the main symptoms of PD, is characterised by the slowness of initiation and progressive reduction on speed and amplitude of a repetitive action (Gibb and Lees 1988). Resting tremor of the hands during voluntary movements may also contribute to the difficulty in performing such a task (Dovzhenok and Rubchinsky 2012; Abdo *et al.* 2010). The SMA known to be involved in motor preparation and motor tasks (Picard and Strick 2003) was activated when participants imagined performing a complex sequence of finger movements (Samuel *et al.* 2001; Roland *et al.* 1980) while the primary motor cortex was activated when subjects actually performed the sequence (Inuggi *et al.* 2011). This provides the rationale for exploring correlations between the motor white matter connections of interest with the following two behavioural tasks:

(iii) The correct number of finger sequence responses and reaction time scores from a motor sequence task adapted and modified from a previous study (Tamas Kincses *et al.* 2008).

(iv) The total number of finger taps per minute for each hand were calculated. The finger tapping was measured using a wooden board with an electronic counter attached for counting the number of taps (Subramanian *et al.* 2011).

Chapter 3 Comparison of selective motor and non-motor pathways in Parkinson's disease

3.1 Abstract

Objective

To determine the differences in the white matter microstructure of selected motor pathways and non-motor pathways and of volumetric measures of the subcortical structures in Parkinson's disease (PD) compared to age-matched healthy controls (MHC).

Methods

Diffusion weighted imaging data of 24 PD patients and 26 MHCs were analysed and deterministic tractography analysis using the spherical deconvolution-based damped Richardson-Lucy algorithm was performed. Additionally, subcortical volume analyses was also performed.

Results

There was significantly increased fractional anisotropy (FA) in the motor pathways of PD patients: the bilateral corticospinal tract (right; corrected $p=0.0003$, left; corrected $p=0.03$), bilateral thalamus-motor cortex tract (right; corrected $p=0.02$, left; corrected $p=0.004$) and the right supplementary area-putamen tract (corrected $p=0.001$) compared to MHCs. There was also significantly decreased FA in the right uncinate fasiculus (corrected $p=0.01$) and no differences of FA in the bilateral supero-lateral medial forebrain bundles ($p>0.05$) of PD patients compared to MHCs. There were no subcortical volume differences ($p>0.05$) between the PD patients and MHCs.

Conclusion

Increased FA values in the motor tracts in PD may reflect neurodegeneration or compensatory reorganisation of neural circuits indicative of adaptive or extended neuroplasticity. These results can inform biological models of neurodegeneration and neuroplasticity in PD.

Key points

1. Fractional anisotropy was higher in motor pathways of PD patients compared to healthy controls.

2. Fractional anisotropy was lower in the uncinate fasciculus while there was no change in the fractional anisotropy of PD patients compared to healthy controls.

3. Increased fractional anisotropy could suggest adaptive neuroplasticity or selective neurodegeneration.

3.2 Background and Rationale

The motor symptoms in PD only arise after approximately 80% depletion of striatal dopamine and it has long been thought that compensatory plasticity must occur both within and outside the basal ganglia as the pathology progresses (Bezard *et al.* 2003). Such compensatory processes, as well as any long-range deficits arising from degeneration of the basal ganglia pathways, are expected to ultimately be reflected in the architecture of the fibre tracts connecting motor cortex, basal ganglia and thalamus.

To date most diffusion MRI based studies on PD have only considered changes within defined regions of interest (ROI) in grey matter (Meijer *et al.* 2013) or have conducted whole-brain analysis of white matter microstructure using tract based spatial statistics (TBSS) (Rae *et al.* 2012). These approaches are prone to partial volume effects and entail difficulties of spatial alignment across participants. Given that there are crossing fibres in about 90% of the voxels of the brain, allocation of voxel-based findings to specific tracts can be highly speculative (Jeurissen *et al.* 2013). The dRL based SD algorithm improves fibre tracking in areas of complex fibre architecture and regions affected by partial volume (Dell'acqua *et al.* 2010). Therefore, deterministic tractography using the dRL algorithm which is more sensitive to detect group differences than whole brain and group-wise voxel-based approaches and produces anatomically plausible white matter tracts (Jeurissen *et al.* 2013) was chosen for analysis.

The following motor pathways were reconstructed to investigate motor related changes in PD; (i) the corticospinal tract (ii) fibre connections between the thalamus and the motor cortex (iii) fibre connections between the SMA and the putamen. The corticospinal tract (CST) is crucial for self-initiated movements and thus putatively involved in bradykinesia in PD (Phillips *et al.* 2014; Jang 2014). Post mortem and diffusion MRI studies show direct white matter fibre connections from the SMA to the striatum (Vergani *et al.* 2014). The thalamus, a relay centre for sensory and motor information, conveys motor inputs from the basal ganglia to the cortex and decreased dopaminergic innervation to the thalamus is assumed to contribute to the pathophysiology of PD (Lindenbach and Bishop 2013). These structures and their connections are not only part of the BG motor circuitry affected in PD (Bergman *et al.* 1990), but also known to be mediating effective treatments options in PD (Mirdamadi

2016; Williams 2015; Rodriguez-Oroz *et al.* 2009; Sweet *et al.* 2014; Calabrese *et al.* 2015; Linhares and Tasker 2000). It has been proposed that these connections are relevant for motor performance in PD (Mink 1996) and thus are closely related to PD pathophysiology, symptoms, and potentially also their remediation.

The following non-motor pathways were also reconstructed to investigate any potential changes as PD is a diverse disease with motor and non-motor symptoms; (iv) the uncinate fasiculus and (v) the supero-lateral medial forebrain bundle.

The uncinate fasiculus connects the orbitofrontal cortex with the anterior temporal lobes and is assumed to be involved in language, emotional processing and episodic memory (Von Der Heide *et al.* 2013; Highley *et al.* 2002). These connecting brain regions are known to influence non-motor and cognitive symptoms in PD (Yoo *et al.* 2015; Alessandro Tessitore *et al.* 2012; A Tessitore *et al.* 2012; Disbrow *et al.* 2014; Papagno *et al.* 2011). The medial forebrain bundle connects the ventral tegmental area to the forebrain and the frontal lobe, and these brain areas as well as the bundle itself has been shown to be involved in reward processing alterations such as anhedonia and depression in PD (Coenen *et al.* 2012; Bracht *et al.* 2015; Brown and Pluck 2000; Robbins and Everitt 1996; Kunig *et al.* 2000). Due to their involvement in PD, these non-motor tracts were included as comparison tracts to examine specific changes in motor compared to non-motor pathways known to be involved in PD.

Additionally, studies have detected subcortical volume differences in PD patients compared to healthy controls (Rosenberg-Katz *et al.* 2016; Gerrits *et al.* 2016; Lee *et al.* 2011; Nemmi *et al.* 2015; Geng *et al.* 2006; Menke *et al.* 2014; Lisanby *et al.* 1993). Therefore, subcortical volume analysis was included to study any potential grey matter subcortical volumes changes that may also help in understanding their contribution to the disease pathology in addition to any white matter microstructure changes.

3.3 Aims

The primary aim was to determine the differences in selected motor pathways and non-motor pathways of the basal ganglia in PD patients compared to healthy controls. The second aim was to investigate any potential group differences in the subcortical volumes.

3.4 Materials and Methods

3.4.1 Participants

Table 3.1 Demographics of the PD patients and MHCs

	PD (n=24)	**MHC (n=26)**	**Analyses**
Age	63.42 ± 10.82	64.88 ± 8.06	P = 0.5918, Two sample t-test
Sex (M:F)	22:2	17:9	P = 0.06, Chi squared test
Handedness (R:L)	20:4	24:2	P = 0.3293, Chi squared test
H & Y Stage	1.75 ± 0.47	NA	-
UPDRS score	25.04 ± 11.01	NA	-
MOCA	26.54 ± 2.01	NA	-
LEDD (mg)	537.64 ± 340.69	NA	-

PD – Parkinson's disease; MHC - Healthy controls; MOCA – The Montreal Cognitive Assessment; H & Y - Hoehn & Yahr Stage; UPDRS – Unified Parkinson's Disease Rating Scale (pre-intervention and off medication); LEDD – Levodopa Equivalent Daily Dose; M - Male; F - Female; R – Right; L - Left

Please refer to the Chapter 2 General Methodology for full details of the MR data acquisition, diffusion MR pre-processing and the deterministic tractography algorithms used. The tracts of interest were reconstructed in the PD patient group and the MHC group, see Table 3.1 for demographics.

3.4.2 Tractography

3.4.2.1 Corticospinal tract (CST)

For the segmentation of the CST, the primary motor cortex was identified in the axial slice of a T1-weighted anatomical image using a "SEED" region (in blue) (Figure 3.1 A. (i)). Further, an "AND" region (in green) was drawn in the brain stem (identified as the blue colour of the pons in the anterior part of the brain stem) in the axial slice of an FA image (Figure 3.1 A. (ii)). The CST of a representative subject on a sagittal slice of a T1 image is shown in (Figure 3.1 A (iii)).

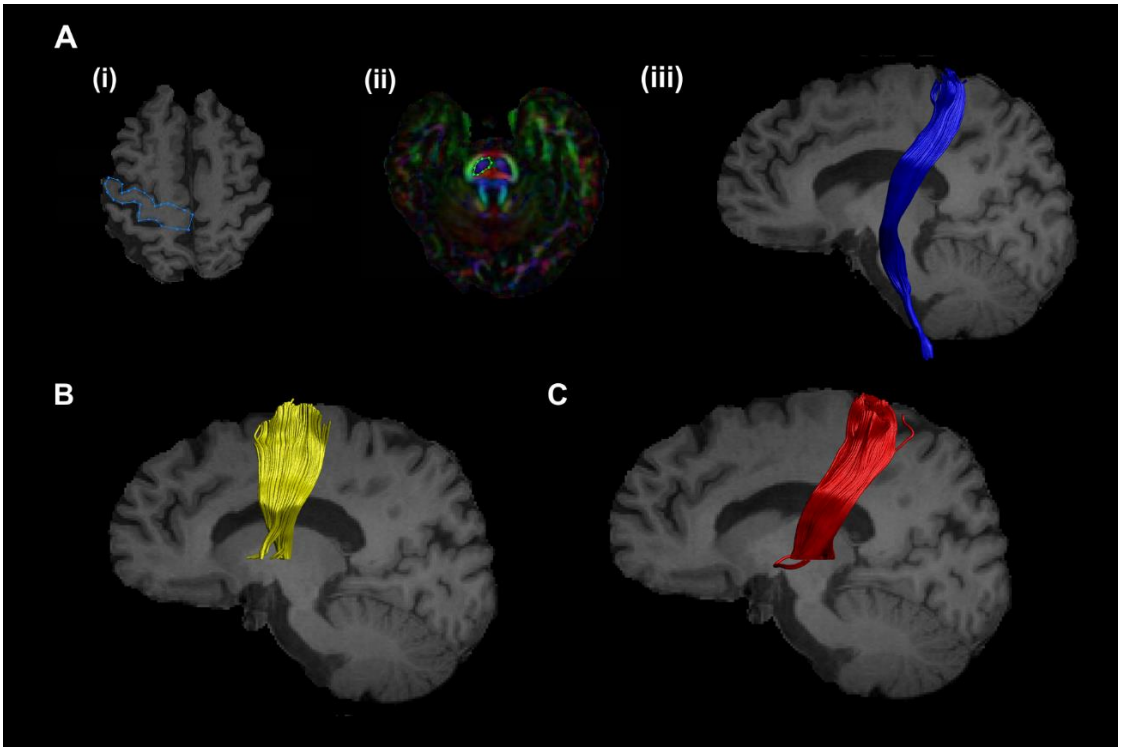

Figure 3.1 Reconstructed motor tracts

A. Corticospinal tract. A. (i) Axial slice of T1 image showing "SEED" region. A. (ii) Axial slice of FA image showing "AND" region. A. (iii) Sagittal slice of T1 image showing the reconstructed CST. B. Reconstructed supplementary area-putamen tract and C. Thalamus-motor cortex tract on sagittal slices of T1 image.

Anatomical landmarks and tract accuracy were quality assessed by manually checking through each CST on both hemispheres for each participant in all groups. The anatomical landmarks for the CST were the primary motor cortex identified by the inverted omega Ω symbol in the axial slice of a T1 image (Figures 3.1A (i) and 3.2 A), the pons identified by the blue colour of the pons in the anterior part of the brain stem in an axial slice of an colour coded FA image and FA image (Figures 3.1A (ii) 3.2 B) and the CST passing through the internal capsule identified below the thalamus in a coronal slice of T1 image (Figure 3.2 C and D), showing the front and reverse views respectively.

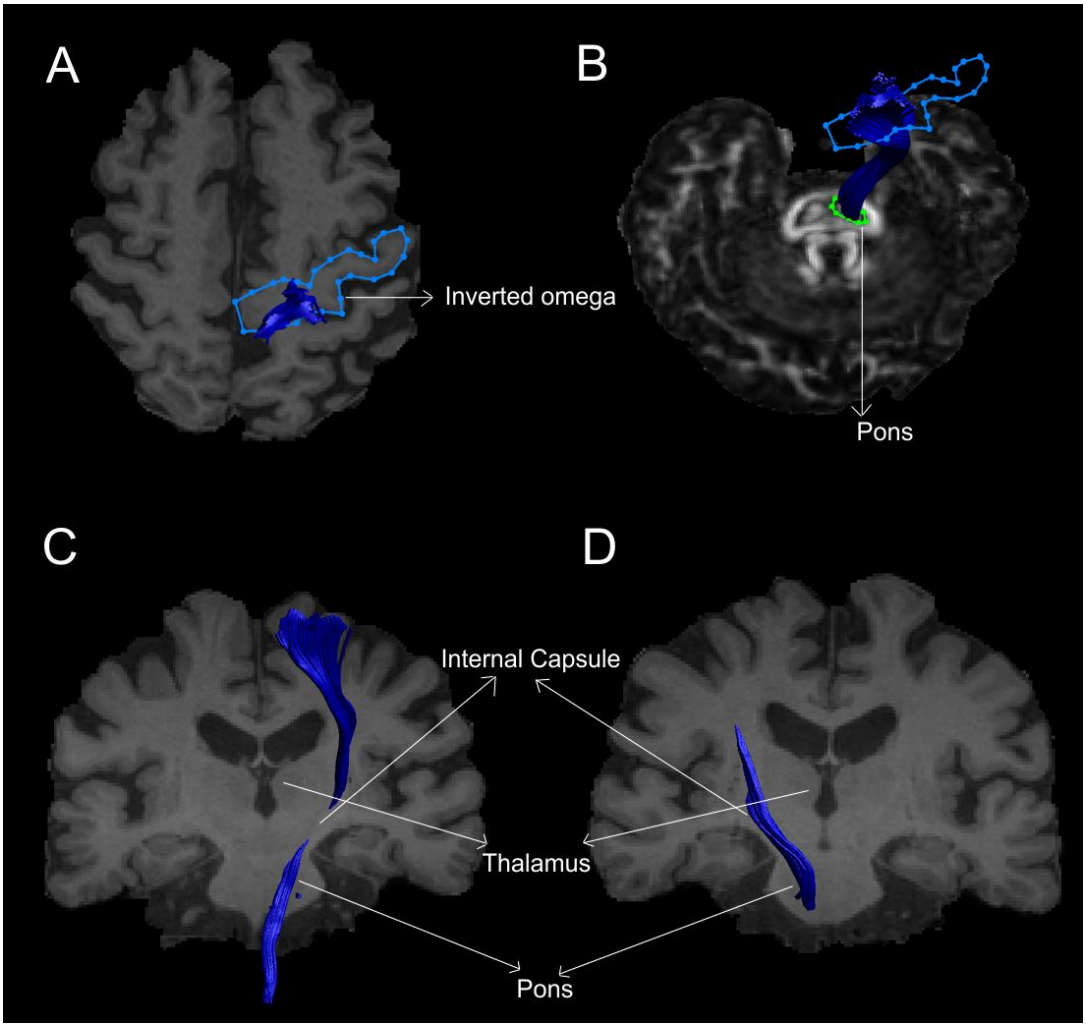

Figure 3.2 Anatomical landmarks for CST

A. Axial slice of T1 image showing the inverted omega (Ω) landmark. B. Axial slice of FA image showing the pons regions in the brain stem. C. Coronal slice showing the front view of the CST passing through the internal capsule just below the thalamus, going towards the primary motor cortex. D. Coronal slice showing the reverse view of the CST passing through the pons and the internal capsule.

3.4.2.2 Thalamus-motor cortex (THAL-MC) and Supplementary area-putamen (SMA-PUT) tracts

The ROIs for segmentation of THAL-MC and SMA-PUT tracts were derived by creating masks chosen from the Anatomical Automatic Labelling (AAL) atlas in the Montreal Neurological Institute (MNI) space. These masks were warped to the individual native space of each subject using inverse parameters derived from warping the T1 image to the AAL template using FSL FLIRT (Jenkinson *et al.* 2012; Smith *et al.* 2004). These masks were then used as "SEED" and "AND" regions in ExploreDTIv4.8.3 (Leemans, Jeurissen, Siibers, *et al.* 2009) for segmenting out the

respective tracts. The reconstructed THAL-MC and SMA-PUT tracts also included their connections towards the brain stem beyond the thalamus and putamen, respectively. These were then segmented using the Splitter tracts tool within ExploreDTI4.8.3. The splitter tracts tool is used to segment portions of a reconstructed tract by drawing SEED and AND ROIs to specify the location of segmentation. This was used here to include only the portion of the THAL-MC at the level of the thalamus towards the motor cortex, and portion of the SMA-PUT at the level of the putamen towards the SMA for extracting the diffusion metrics from these tracts. The final SMA-PUT and THAL-MC tracts in a sagittal slice of a T1 image of a representative subject are shown in (Figure 3.1 B) and (Figure 3.1 C), respectively.

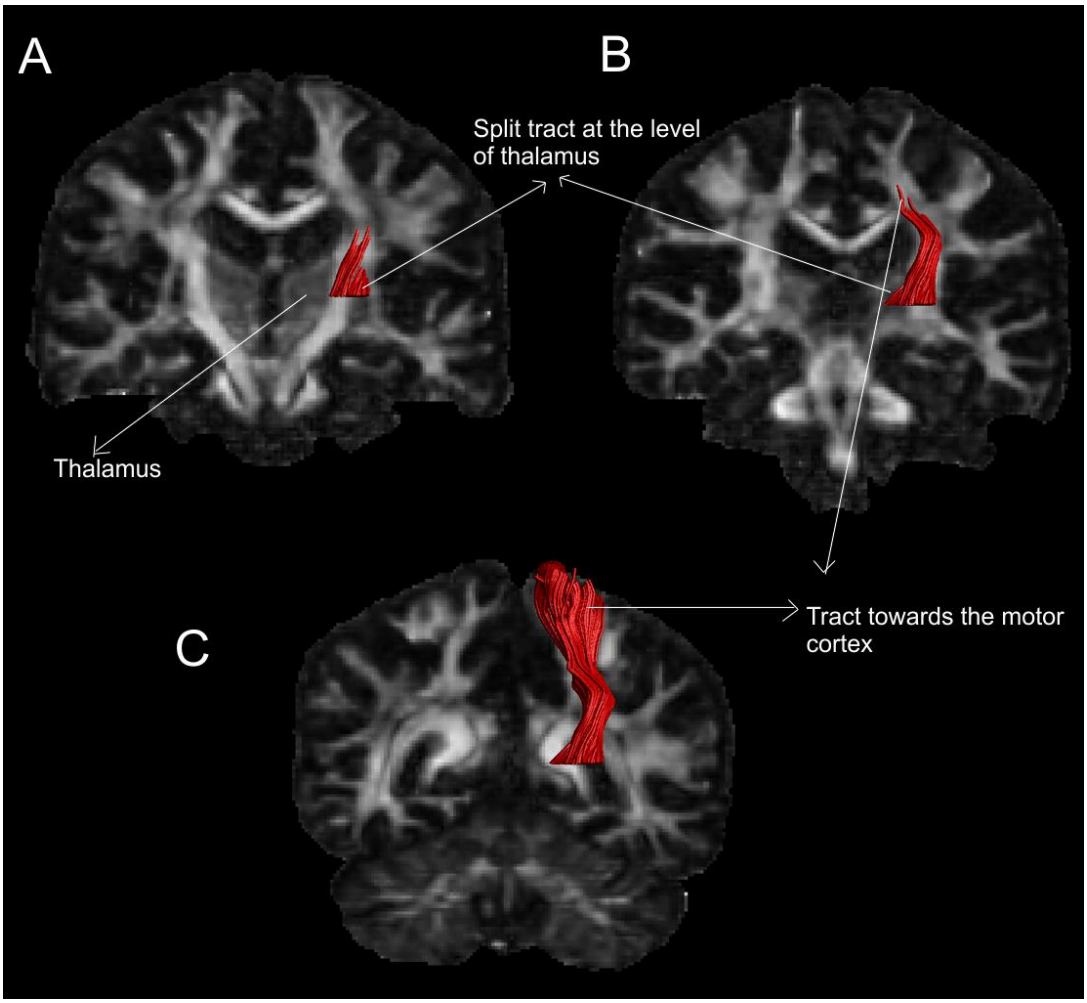

Figure 3.3 Anatomical landmarks for THAL-MC tract

A. Coronal slice T1 image showing THAL-MC tract split at the level of the thalamus. B. Coronal slice of T1 image showing THAL-MC tract split at the level of the thalamus with tract moving towards the motor cortex. C. Coronal slice of T1 image showing full THAL-MC tract between thalamus and the motor cortex.

Anatomical accuracy of the THAL-MC tract was verified by checking that the tract after the splitting began at the level of the thalamus (Figure 3.3 A) and then moved towards the motor cortex (Figure 3.3 B, C). The accuracy of the ROI masks were checked by overlaying them with the tract and the colour coded FA image to verify that they covered the thalamus and the motor cortex regions and that the tracts themselves passed originate or terminate in these ROI masks. (Figure 3.4)

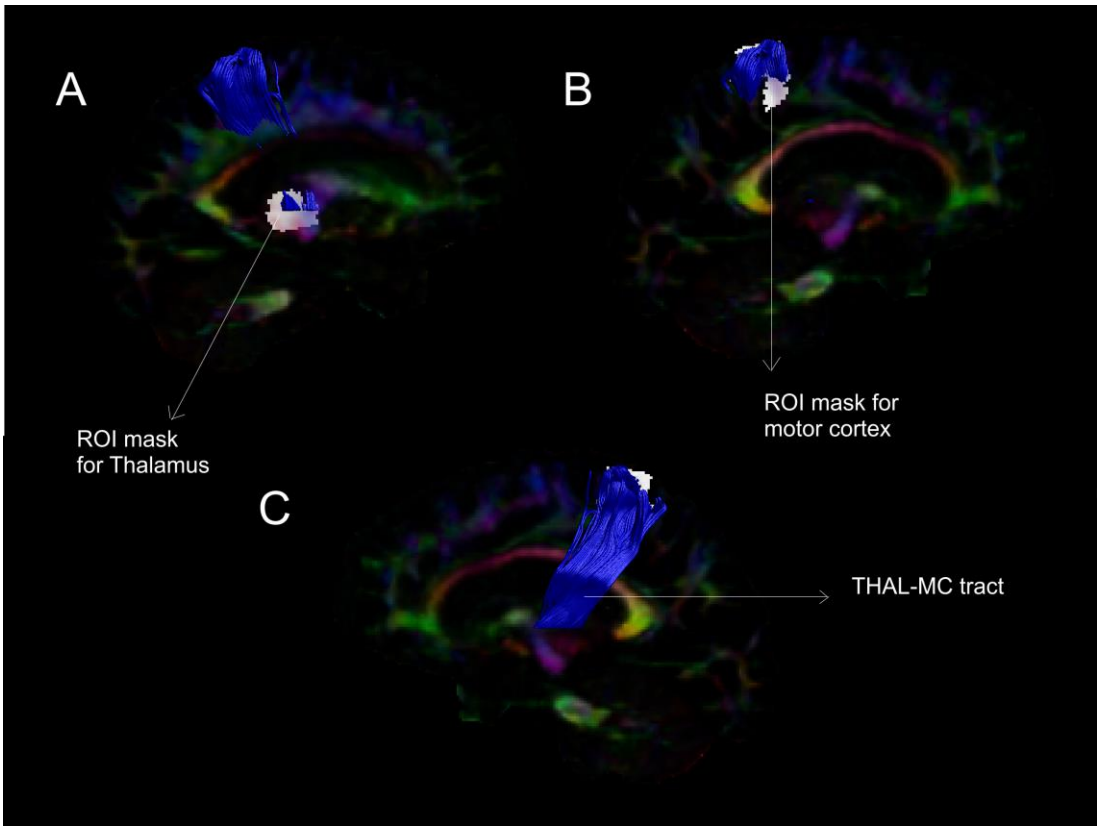

Figure 3.4 Mask accuracy for THAL-MC tracts

A. Sagittal slice of colour coded FA image with ROI mask for thalamus and THAL-MC tract overlaid on the ROI mask. B. Sagittal slice of colour coded FA image with ROI mask for motor cortex and THAL-MC tract overlaid on the ROI mask. C. Sagittal slice of colour coded FA image with ROI mask of motor cortex and full THAL-MC tract overlaid on it.

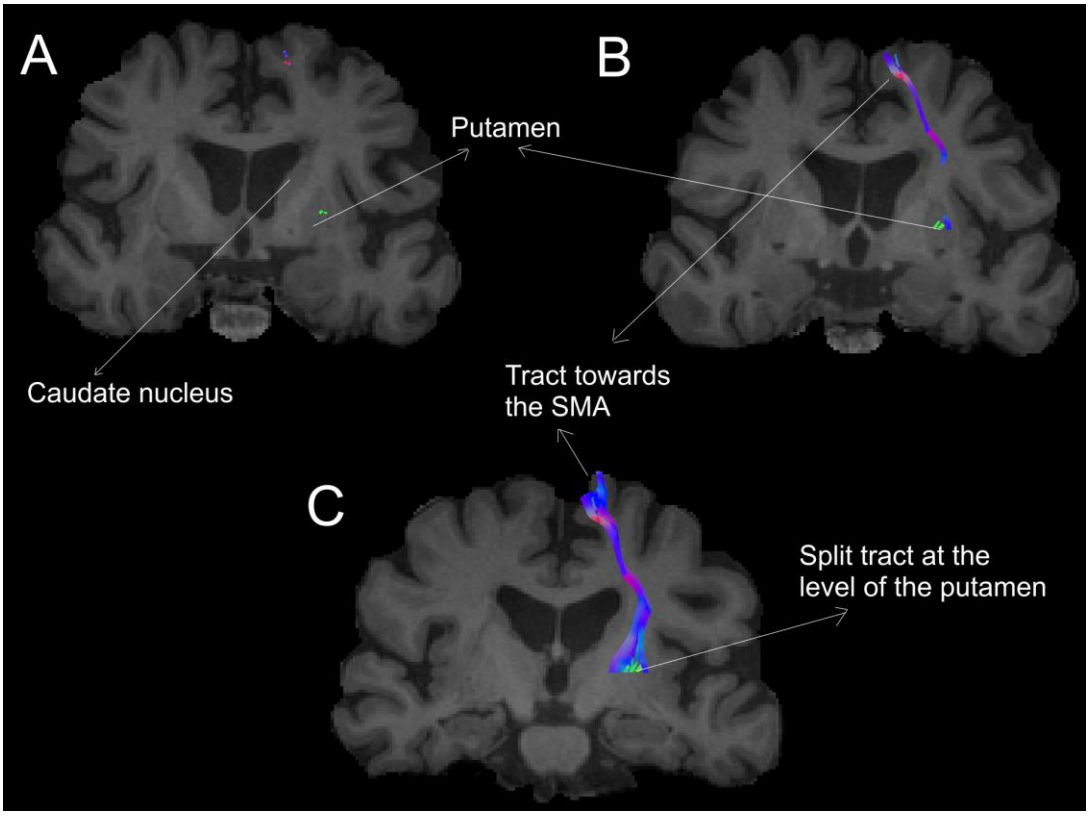

Figure 3.5 Anatomical landmarks for SMA-PUT tract

A. Coronal slice of T1 image showing the putamen and caudate nucleus. B. Coronal slice of T1 image showing Putamen and SMA-PUT tract split at this level as well a portion of the tract going towards the SMA. C. Coronal slice of T1 image showing full SMA-PUT tract split at the level of the putamen and going towards the SMA.

Anatomical accuracy for the SMA-PUT tracts was verified by checking that the tract after splitting began at the level of the putamen and then moved towards the SMA (Figure 3.5). The accuracy of the ROI masks were checked by overlaying them with the tract and the colour coded FA image to verify that they covered putamen and SMA regions and that the tracts themselves originated or terminated in these ROI masks (Figure 3.6).

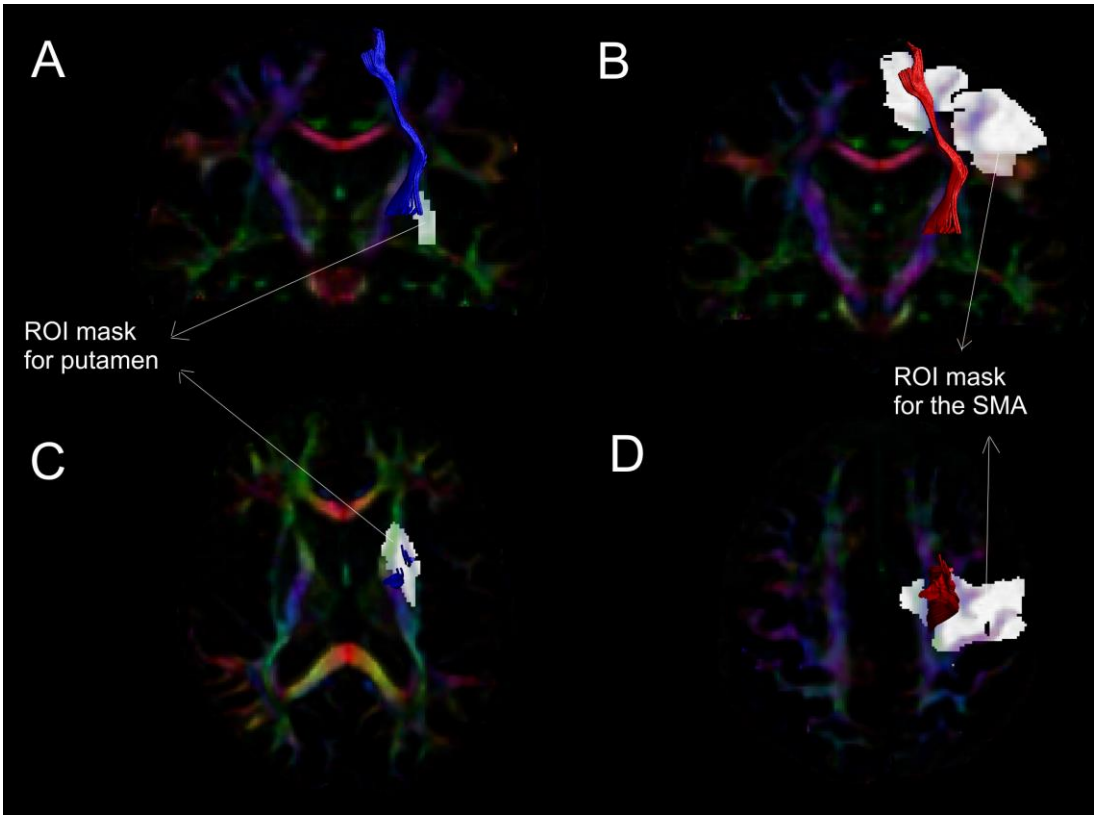

Figure 3.6 Mask accuracy for SMA-PUT tract

A. Coronal slice of colour coded FA image with ROI mask for putamen and the SMA-PUT tract overlaid on it. B. Coronal slice of colour coded FA image with ROI mask for SMA and the SMA-PUT tract overlaid on it. C. Axial slice of colour coded FA image with ROI mask for putamen and the SMA-PUT tract overlaid on it. D. Axial slice of colour coded FA image with ROI mask for SMA with the SMA-PUT tract overlaid on it.

3.4.2.3 Uncinate Fasiculus (UNF)

For segmentation of the UNF, the most posterior slice in the coronal view of a T1 image where the frontal and the temporal lobes are separated was chosen which is approximately at the height of the nucleus accumbens. The "SEED" region (in blue) was drawn around the temporal lobe (Figure 3.7 D. (i)) and the "AND" region (in green) was drawn around the region lateral to the caudate and the putamen (Figure 3.7 D. (ii)). The UNF tract of a representative subject on a sagittal slice of a T1 image is shown in (Figure 3.7 D (iii)). Anatomical accuracy for the uncinate was verified by checking if the tracts pass through the ROIs and that the spurious and unwanted fibres were removed from them (Figure 3.8).

3.4.2.4 Supero-lateral medial forebrain bundle (slMFB)

For reconstruction of the slMFB one horizontal "AND" region was placed surrounding the ventral tegmental area. The anatomical borders for this AND region were laterally the substantia nigra, anteriorly the mammillary bodies and posteriorly the red nucleus (Figure 3.7 E. (i)). Another "AND" region was drawn surrounding caudate and putamen on a coronal section at the height of the nucleus accumbens (Figure 3.7 E. (ii)) (Bracht *et al.* 2015). The slMFB tract of a representative subject on a sagittal slice of a T1 image is shown in (Figure 3.7 E. (iii)). Anatomical accuracy for the slMFB was verified by checking if the tracts pass through the ROIs and that the spurious and unwanted fibres were removed from them (Figure 3.9).

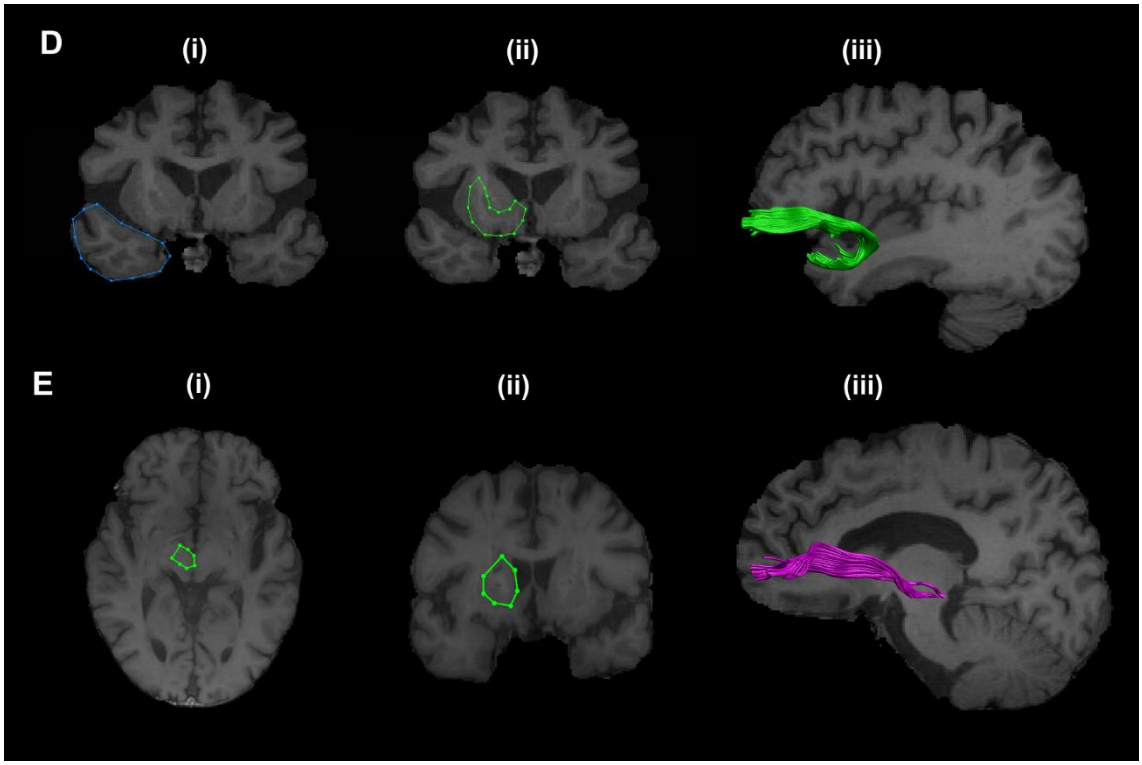

Figure 3.7 Reconstructed non-motor tracts

D. Uncinate fasiculus tract. D. (i) Coronal slice of T1 image showing "SEED" region for uncinate fasiculus segmentation. D. (ii) Coronal slice of T1 image showing "AND" region. D. (iii) Sagittal slice of T1 image showing reconstructed uncinate fasiculus tract. E. Supero-lateral medial forebrain bundle. E. (i) Axial slice of T1 image showing "AND" region. C. (ii) Coronal slice of T1 image showing "AND" region. E. (iii) Sagittal slice of T1 image showing reconstructed supero-lateral medial forebrain bundle.

Each reconstructed tract was visually inspected and any obvious outlier streamlines that were not consistent with their known anatomy were excluded by drawing "NOT" regions and the entire procedure was performed separately for both hemispheres.

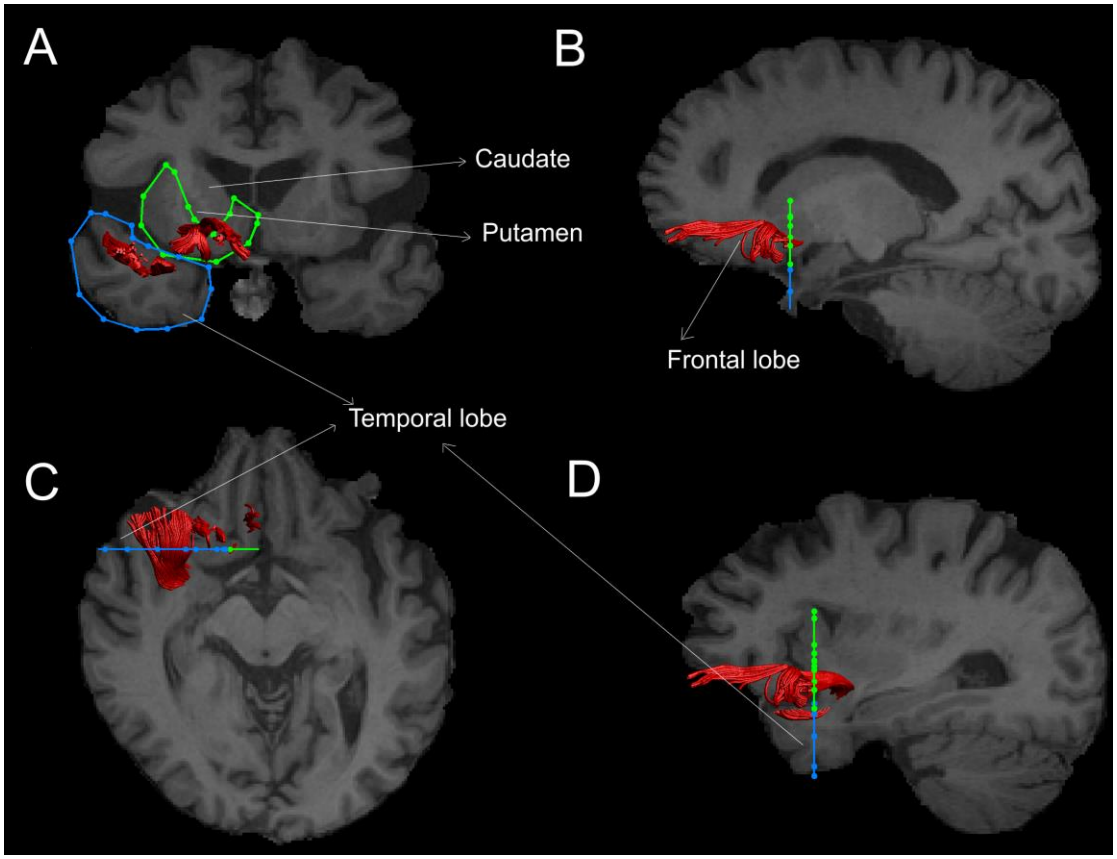

Figure 3.8 Anatomical landmarks for UNF

A. Coronal slice of T1 image showing anatomical landmarks of caudate and putamen for the AND region, and the frontal lobe for the SEED region with the UNF passing through them. B. Sagittal slice of T1 image showing frontal part of the UNF passing through the AND region in the frontal lobe. C. Axial slice of T1 image showing temporal part of UNF passing through the SEED region in the temporal lobe. D. Sagittal slice of T1 image showing temporal part of the UNF passing through the SEEN region in the temporal lobe.

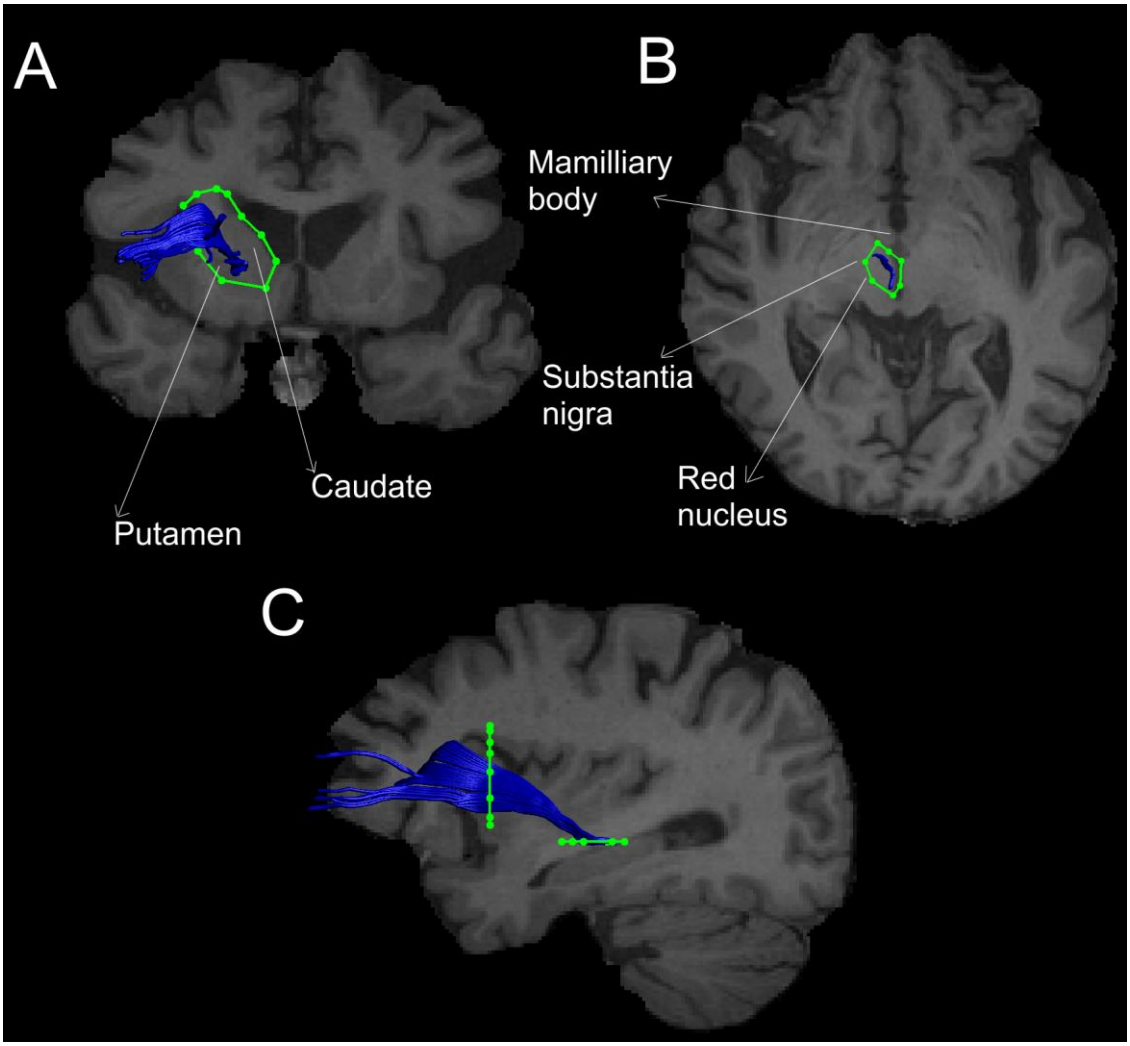

Figure 3.9 Anatomical landmarks for the slMFB

A. Coronal slice of T1 image showing the caudate and putamen surrounded by the AND region and the frontal part of the slMFB passing through it. B. Axial slice of T1 image showing AND region drawn laterally to the substantia nigra, anteriorly to the mammillary bodies and posteriorly to the red nucleus. C. Sagittal slice of T1 image showing the full slMFB passing through both the AND regions.

3.4.3 Subcortical volumes analysis

The volumes of subcortical brain structures were measured using FSL's FIRST software (FMRIB Image Registration and Segmentation Tool) (Patenaude *et al.* 2011; Jenkinson *et al.* 2012). The structures of the thalamus, caudate, putamen, pallidum, hippocampus, amygdala, nucleus accumbens and ventricles were extracted for both the hemispheres and their volumes measured for all T1-weighted MR images of the PD patients and MHCs. The extracted volumes were normalised using the scaling factor obtained from brain tissue normalization for subject head size, using SIENAX (Structural Image Evaluation using Normalization of Atrophy) (Smith *et al.* 2004).

3.4.4 Statistical Analysis

All the statistical analyses were carried out in the R statistical software v2.15.3 (R Core Team 2014). Before data analysis, all variables were checked for Gaussian distribution using Shapiro-Wilk test ($p<0.05$) and were transformed using appropriate transformations if necessary.

A multivariate analysis of covariance (MANCOVA) was performed in each hemisphere for each of the five tracts separately with FA, MD, AD and RD as dependent variables and group (PD and MHC) as independent variable, along with age and gender as covariates. These analyses were corrected for multiple comparisons using False Discovery Rate (FDR) correction ($p<0.01$). Significant results were further analysed using post-hoc univariate ANOVAs also corrected for multiple comparisons using FDR correction ($p<0.05$). The inter-rater reliability of diffusion metrics derived from the manually reconstructed tracts was investigated using the inter class correlation coefficient (ICC).

For the subcortical volumes analysis, two sample t-tests were carried out comparing the corrected subcortical volumes of the PD patients and MHCs.

Post hoc correlations were also performed in the PD group between metrics in tracts that showed significant group differences and the following clinical and behavioural measures: off medication baseline Unified Parkinson's Disease Rating Scale (UPDRS) scores, duration since diagnosis (in months), scores from a standard finger tapping task and a four button finger sequence task measuring the correct number of responses and reaction time.

3.5 Results

For all PD patients and MHCs, reliable reconstruction results of all investigated fibre tracts was obtained.

3.5.1 Inter-rater reliability

For inter-rater reliability testing, a subset of four subjects from the PD group and MHC group were randomly selected by two researchers (T.B and C.M.B) experienced in tractography. FA values were extracted and tests were performed independently and separately using the IRR package in the R statistical software. Inter-rater correlations coefficients (ICC) for the tracts are presented in Table 3.2.

Table 3.2 Inter-rater reliability tests

JPM and TB	ICC	p-value
L-CST	0.998	3.07e-21
R-CST	0.999	3.25e-22
L-UNF	1	9.6e-27
R-UNF	1	9.6e-27
JPM and CMB		
L-CST	1	5.99e-26
R-CST	1	2.44e-29
L-UNF	0.998	3.67e-20
R-UNF	0.998	3.67e-20

L-CST- Left corticospinal tract, R-CST-Right corticospinal tract, L-UNF- Left uncinate fasiculus, R-UNF- Right uncinate fasiculus, ICC – Inter-rater correlation coefficients

3.5.2 Multivariate effects

The MANCOVAs demonstrated a significant effect of group (PD and MHC) on the multivariate diffusion metrics (FA, MD, AD and RD) in the CST, SMA-PUT, THAL-MC and UNF, but not in the slMFB (Table 3.3).

Table 3.3 Multivariate effects

Tract		F statistic	Pillai's trace	P-value
Right CST	Group	F(4,43)=4.6907	0.3	0.003132 ***
	Age	F(4,43)=3.3356	0.23	0.018252
	Gender	F(4,43)=3.1088	0.22	0.024736
Left CST	Group	F(4,43)=8.5394	0.44	3.66E-05 ***
	Age	F(4,43)=2.7190	0.2	0.04189
	Gender	F(4,43)=2.5850	0.19	0.05026
Right SMA-PUT	Group	F(4,43)= 6.4230	0.38	0.000363 ***
	Age	F(4,43)=10.5065	0.48	1.00E-05 ***
	Gender	F(4,43)=0.5654	0.04	0.730037
Left SMA-PUT	Group	F(4,43)=4.8551	0.31	0.002546 ***
	Age	F(4,43)=5.5182	0.34	0.001123 ***
	Gender	F(4,43)= 0.3259	0.02	0.859045
Right THAL-MC	Group	F(4,43)=4.7410	0.31	0.002939 ***
	Age	F(4,43)=4.4941	0.29	0.00402 ***
	Gender	F(4,43)=0.6916	0.06	0.601839
Left THAL-MC	Group	F(4,43)=5.5699	0.34	0.001054 ***
	Age	F(4,43)=4.4365	0.29	0.004326 ***
	Gender	F(4,43)=1.4269	0.11	0.241373
Right UNF	Group	F(4,43)=5.7824	0.28	0.002011 ***
	Age	F(4,43)=2.5327	0.15	0.069178
	Gender	F(4,43)=3.2413	0.18	0.030894
Left UNF	Group	F(4,43)=5.0908	0.32	0.001898 ***
	Age	F(4,43)=3.8483	0.26	0.009263
	Gender	F(4,43)=2.6825	0.19	0.044023
Right slMFB	Group	F(4,43)=1.2095	0.1	0.320719
	Age	F(4,43)=5.1433	0.32	0.001778 ***
	Gender	F(4,43)=1.9735	0.15	0.115659
Left slMFB	Group	F(4,43)=1.1442	0.09	0.348703

	Age	F(4,43)=4.3186	0.28	0.005032 ***
	Gender	F(4,43)=3.2387	0.23	0.020777

CST - Corticospinal tract, SMA-PUT - Supplementary motor area-putamen tract, THAL-MC - Thalamus-motor cortex tract, UNF - Uncinate fasiculus, slMFB - supero-lateral medial forebrain bundle. *** = FDR corrected $p < 0.01$

3.5.3 Univariate group effects

Post hoc analyses showed significantly increased FA and AD in right CST, and significantly increased FA in the left CST of the PD patients compared to MHC (Table 3.4). In PD patients, there was significantly increased FA and AD in the right SMA-PUT tracts and significantly increased AD in the left SMA-PUT tracts. Similarly, there was significantly increased FA in both right and left THAL-MC tracts and increased AD in the left THAL-MC tracts of the PD patients compared to MHCs (Table 3.4). Conversely, in the UNF of PD patients, there was significantly decreased FA and significantly increased RD in the right UNF, and significantly increased MD and significantly increased RD in the left UNF (Table 3.4).

Table 3.4 Univariate group effects

Tract	Metric	HC (n=26) mean ± SD	PD (n=24) mean ± SD	F statistic	FDR Corrected p-value
Right CST	FA	0.54 ± 0.025	0.58 ± 0.024	F(1,48)=24.32	0.0003264 ***
	MD (10^{-3})	0.71 ± 0.018	0.72 ± 0.032	F(1,48)=2.601	0.134
	RD (10^{-3})	0.46 ± 0.022	0.45 ± 0.028	F(1,48)=4.068	0.0751
	AD (10^{-3})	1.21 ± 0.048	1.25 ± 0.072	F(1,48)=16.24	0.0012672 ***
Left CST	FA	0.53 ± 0.027	0.56 ± 0.030	F(1,48)=12.25	0.0032544 ***
	MD (10^{-3})	0.72 ± 0.023	0.73 ± 0.024	F(1,48)=2.098	0.1699
	RD (10^{-3})	0.48 ± 0.025	0.47 ± 0.025	F(1,48)=3.138	0.106
	AD (10^{-3})	1.20 ± 0.045	1.26 ± 0.058	F(1,48)=7.556	0.0179328
Right SMA-PUT	FA	0.42 ± 0.041	0.47 ± 0.029	F(1,48)=20.63	0.0006016 ***
	MD (10^{-3})	0.71 ± 0.024	0.73 ± 0.034	F(1,48)=4.459	0.06392
	RD (10^{-3})	0.53 ± 0.027	0.52 ± 0.026	F(1,48)=2.486	0.138742857
	AD (10^{-3})	1.07 ± 0.06	1.15 ± 0.071	F(1,48)=16.47	0.0012672 ***
Left SMA-PUT	FA	0.44 ± 0.041	0.46 ± 0.036	F(1,48)=3.695	0.084201739
	MD (10^{-3})	0.72 ± 0.024	0.74 ± 0.033	F(1,48)=6.4	0.027764706
	RD (10^{-3})	0.54 ± 0.033	0.54 ± 0.028	F(1,48)=0.08	0.7775

	AD (10^{-3})	1.10 ± 0.045	1.16 ± 0.075	F(1,48)=10.32	0.006258667 ***
Right THAL -MC	FA	0.49 ± 0.031	0.52 ± 0.036	F(1,48)=13.96	0.0017984 ***
	MD (10^{-3})	0.69 ± 0.018	0.70 ± 0.027	F(1,48)=1.353	0.2672
	RD (10^{-3})	0.48 ± 0.024	0.46 ± 0.025	F(1,48)=6.618	0.0264
	AD (10^{-3})	1.10 ± 0.044	1.16 ± 0.071	F(1,48)=8.312	0.01344
Left THAL -MC	FA	0.47 ± 0.030	0.51 ± 0.036	F(1,48)=17.4	0.0012672 ***
	MD (10^{-3})	0.71 ± 0.022	0.71 ± 0.027	F(1,48)=0.721	0.412
	RD (10^{-3})	0.51 ± 0.027	0.49 ± 0.027	F(1,48)=6.13	0.029
	AD (10^{-3})	1.11 ± 0.042	1.16 ± 0.076	F(1,48)=10.64	0.00593 ***
Right UNF	FA	0.43 ± 0.024	0.41 ± 0.019	F(1,48)=14.36	0.0017984 ***
	MD (10^{-3})	0.77 ± 0.018	0.78 ± 0.024	F(1,48)=3.56	0.0869
	RD (10^{-3})	0.57 ± 0.018	0.59 ± 0.022	F(1,48)=13.91	0.001798 ***
	AD (10^{-3})	1.11 ± 0.048	1.14 ± 0.049	F(1,48)=2.934	0.1147
Left UNF	FA	0.42 ± 0.039	0.40 ± 0.024	F(1,48)=3.973	0.0755
	MD (10^{-3})	0.75 ± 0.017	0.77 ± 0.021	F(1,48)=15.13	0.0016 ***
	RD (10^{-3})	0.57 ± 0.028	0.59 ± 0.024	F(1,48)=10.11	0.00634 ***
	AD (10^{-3})	1.18 ± 0.043	1.15 ± 0.051	F(1,48)=4.512	0.06392

PD- Parkinson's disease patients, MHC-Healthy Controls. CST - Corticospinal tract, SMA-PUT - Supplementary motor area-putamen tract, THAL-MC - Thalamus-motor cortex tract, UNF - Uncinate Fasiculus. FA – Fractional Anisotropy, MD – Mean Diffusivity, RD – Radial diffusivity and AD – Axial diffusivity. *** = FDR corrected ($p < 0.01$), SD - Standard deviation.

3.5.4 Subcortical volumes analysis

There were no significant volume differences between PD patients and MHCs in the FSL FIRST analysis of subcortical and ventricular volumes (Table 3.5).

Table 3.5 Subcortical volumes analysis results

Sub-cortical structures	PD (mean ± SD)	MHC (mean ± SD)	t-value	df	P-value
L-Amygdala	1812.24 ± 235.03	1759.77 ± 242.49	0.1275	48.89	0.8991
L-Caudate	4700.76 ± 504.54	4583.12 ± 458.61	-0.008	45.85	0.9931
L-Globus pallidus	1912.32 ± 183.76	1861.65 ± 206.15	0.2403	39.58	0.8113
L-Hippocampus	4901.72 ± 635.04	4872.85 ± 759.49	-0.532	47.25	0.5969

L-Nucleus accumbens	663.48 ± 188.68	624.12 ± 121.88	0.6446	37.98	0.523
L-Putamen	5073.24 ± 515.06	5154.19 ± 558.31	-1.33	47.65	0.1899
L-Thalamus	7919.24 ± 734.17	7865.15 ± 743.50	-0.556	36.35	0.5812
L-Ventricles	10996.24 ± 3795.60	13036.96 ± 4124.85	-1.924	48.95	0.0602
Brain stem	27039.76 ± 2420.41	25368.85 ± 2447.38	1.5628	45.16	0.1251
R-Amygdala	1778.8 ± 295.89	1737.65 ± 303.74	0.0859	45.95	0.9319
R-Caudate	5024.16 ± 645.34	4845.38 ± 536.10	0.3984	40.29	0.6924
R-Globus pallidus	1875.92 ± 236.54	1865.81 ± 227.78	-0.408	38.18	0.6855
R-Hippocampus	5044.4 ± 518.01	5001.35 ± 672.08	-0.382	48.03	0.7037
R-Nucleus accumbens	504.44 ± 145.58	519.15 ± 105.40	-0.529	40.78	0.5996
R-Putamen	4915.4 ± 809.16	4968.69 ± 643.96	-1.017	41.88	0.3148
R-Thalamus	7706.88 ± 686.55	7650.62 ± 700.39	-0.524	39.15	0.603
R-Ventricles	10087.52 ± 4117.54	11598.62 ± 4338.02	-1.370	48.86	0.1767

R – Right, L – Left, SD - Standard Deviation

There were no significant results from the correlation analyses as well (see supplementary table 3.3 and supplementary table 3.4).

3.6 Discussion

This is the first comprehensive deterministic tractography study of motor and non-motor tracts in PD. I found increased FA in the cortico-basal ganglia and CSTs, which may indicate compensatory mechanisms or structural changes related to altered pallido-thalamic activity in PD. Patients with early stage PD relative to age-matched controls demonstrated a specific increase in FA and AD in the white matter of motor tracts which was not present for two non-motor comparison tracts.

In the previous literature, neurodegenerative disorders have generally been associated with decreased FA in the major pathways, which has been attributed to primary white matter degeneration, demyelination, reduced gliosis or axonal damage as a result of grey matter loss (Concha *et al.* 2006; Assaf 2008; Lebel *et al.* 2008). Diffusion tensor based ROI and whole brain analyses in PD have shown reduced FA or increased MD in *a priori* regions such as the substantia nigra and putamen (Rae *et al.* 2012; Meijer *et al.* 2013; Schwarz *et al.* 2013). Thus only the finding of decreased FA and increased RD in the UNF, but not the findings of increased FA and AD in the CST and cortico-basal ganglia tracts, would be compatible with a general neurodegenerative process.

3.6.1 Neurodegenerative models

These findings may reflect selective neurodegeneration. AD, which is the measure of diffusion in the principal fibre direction is sensitive to the number of axons and their coherence (Takahashi *et al.* 2000) while RD, the measure of diffusion perpendicular to the principal diffusion direction is thought to reflect decreased myelination (Song *et al.* 2002). Therefore, in the current data the results of elevated FA in combination with elevated AD could suggest selective neurodegeneration causing lower neural branching, decreases of axonal diameter and thus higher coherence along the principal orientation. Increased FA in theses tracts may also occur as a primary pathogenic consequence of altered pallido-thalamic activity in PD. A combined diffusion tensor and histology based study of rat model of traumatic brain injury showed that increase in FA in the cortical regions was correlated with gliosis (Budde *et al.* 2011). It has been suggested that FA is more related to axonal package density and less to myelination (Winston 2012b). Along these lines, the results from the current data could suggest a higher axonal package density of motor pathways as there was no significant differences in RD in the current study.

3.6.2 Neuroplastic models

Alternatively, these findings might reflect early compensatory mechanisms associated with increases in axonal density in pathways of the cortico-basal-ganglia-thalamo-cortical loop. Such compensatory changes might preserve neural functions despite loss of the dopaminergic input (Bezard *et al.* 2003). A recent study in PD showed increase in striato-cortical connectivity mediated by levodopa intake (Herz *et al.* 2015), hence it could also be suggested that increased FA in the SMA-PUT and THAL-MC tracts may be an adaptive response to abnormal dopaminergic modulation and levodopa intake.

The results are consistent with the suggested compensation stages of PD where structures outside the basal ganglia, especially the SMA, would undergo changes to counterbalance the putative abnormal activity in the thalamus and basal ganglia (Bezard *et al.* 2003). Considering the long time-course from the onset of PD-related pathology to the onset of clinical symptoms (H Braak *et al.* 2006), the subcortical and cortical motor pathways may well have undergone compensatory and adaptive structural and functional reorganisation long before PD patients have been diagnosed clinically. Such a model would be supported by the observation (Supplementary Table 3.1) that changes in the diffusion metrics were not confined to the hemisphere contralateral to the side of dominant symptoms.

Recent evidence from PD rodent models showed axonal sprouting as compensatory mechanism (Arkadir *et al.* 2014), but this has not be studied in detail outside the nigrostriatal system. Based on the present findings, there may be compensatory sprouting in motor tracts in response to decreased input from thalamus and striatum as a consequence of PD pathology. The results could also suggest that sprouting should also be assessed in corticospinal and thalamo-cortical motor tracts, both in animal models and in human brains post-mortem.

3.6.3 Subcortical volumes

There were no differences in the subcortical volumes between the PD patients and the MHCs. This finding is inconsistent with previous studies that had similar sample sizes and PD patients' disease stages to our current cohort but reported smaller volumes of the subcortical structures in PD compared to healthy controls (Rosenberg-Katz *et al.*

2016; Lisanby *et al.* 1993; Gerrits *et al.* 2016; Lee *et al.* 2011; Nemmi *et al.* 2015; Geng *et al.* 2006; Menke *et al.* 2014).

3.6.4 Methodological considerations

Diffusion metrics are highly sensitive to white matter microstructural changes, however, they are non-specific indices with complex measures; hence one has to be cautious when inferring any specific biological mechanisms underlying changes in these measures (Jones *et al.* 2013). Before interpreting the current findings in terms of putatively increased structural connections in PD the possibility that they are influenced by methodological artefacts should be eliminated. The dRL algorithm was used, and this reduces the number of spurious fibre orientations that can produce artefactual reconstructions of tracts and is robust in mapping cortical connectivity (Dell'acqua *et al.* 2010). In patient and clinical studies, presence of degeneration makes the estimated tract reconstructions prone to isotropic partial volume effects (Ciccarelli *et al.* 2008) but the spherical deconvolution methods makes it possible to obtain accurate white matter fibres that are corrected for partial volume effects and crossing fibres. Additionally, there was higher number of reconstructed streamlines in PD patients than in MHCs in the motor tracts and the UNF (Supplementary Table 3.2) even though only the motor tracts showed increased FA whereas the UNF showed decreased FA. Thus it can be excluded that higher FA values were driven by the increase in number of reconstructed streamlines or number of occupied voxels or tract volume.

Because FA is a normalised measure it can be affected by changes in any of the compartments of white matter. For a better understanding of the specific contributions of axonal microstructural changes and myelination to changes in the white matter architecture in PD, future studies can apply complex diffusion microstructural models such as Composite Hindered and Restricted Model of Diffusion (CHARMED) or AxCaliber (Assaf 2008). However, their clinical application in patients with movement disorders is limited by the long duration of scanning protocols. Recently developed myelin water fraction mapping and quantitative magnetization transfer techniques could also be used in future studies to better quantify myelination (Levesque *et al.* 2010).

3.7 Conclusion

This first comprehensive deterministic tractography study of motor and non-motor tracts in PD revealed increased FA in the cortico-basal ganglia and CSTs, which may indicate compensatory mechanisms or structural changes related to altered pallido-thalamic activity in PD. Tractography analysis should be incorporated in future longitudinal imaging studies of PD in order to evaluate the role of white matter changes in neurodegenerative and neuroplastic processes.

Chapter 4 Anatomy of the dentato-rubro-thalamic tract (DRTT) and the subthalamo-ponto-cerebellar tract (SPCT)

4.1 Abstract

Objective

Evidence from animal tracing studies shows direct anatomical connections between the basal ganglia and the cerebellum. Although the presence of similar connections in humans have been reported in a few studies using diffusion MRI, the anatomy of these pathways and their reliable reconstruction has not been demonstrated yet.

Methods

Anatomical protocols were developed to delineate the two white matter tracts that connect the basal ganglia and the cerebellum: the dentato-rubro-thalamic tract (DRTT) and the subthalamo-ponto-cerebellar tract (SPCT), in young healthy adults with high angular resolution diffusion data using deterministic diffusion MRI tractography. The feasibility of transferring this protocol to clinical studies of diffusion MRI data from a cohort of Parkinson's disease patients and their matched healthy controls was also demonstrated.

Results

In all groups, the two tracts were reliably reconstructed using the developed anatomical protocols. The tracts obtained closely correspond to the previously described anatomical pathways of the DRTT and the SPCT. The cortical connections of the reconstructed tracts and their spatial overlap with the major cerebellar pathways and the corticospinal tract were also derived.

Conclusion

The findings from this study are thus consistent with the presence of direct anatomical connections between the basal ganglia and the cerebellum. Furthermore, the spatial independence and cerebellar-cortical connections of these tracts were demonstrated for the first time. These tracts have clinical research application and will help to understand the role of the cerebellum in neuropsychiatric and neurodegenerative disorders.

Key points

1. An anatomically guided tractography protocol was developed to reconstruct the DRTT and the SPCT using deterministic diffusion MRI tractography.

2. Successfully demonstrated feasibility of transferring the developed tractography protocol to standard diffusion imaging protocols in a cohort of PD patients and their matched healthy controls.

3. The spatial independence of the DRTT and the SPCT was assessed and the cortical connections were also described.

4.2 Background and Rationale

The loops that connect the basal ganglia and the cerebellum have long been thought to be anatomically and functionally distinct while interacting with each other only at the level of the cerebral cortex (Doya 2000). In primates, there are efferent connections from cerebellar nuclei to subdivisions of the thalamus which in turn project to motor, premotor and basal ganglia areas (Percheron *et al.* 1996; Sakai *et al.* 1996). However, recent neuronal tracing studies in non-human primates have found direct projections from the dentate nucleus not only to the thalamus but also to the dorsal striatum (Hoshi *et al.* 2005). Reciprocal inter-connections between the basal ganglia and the cerebellum, notably between the sub-thalamic nucleus and the cerebellar cortices have also been demonstrated (Bostan *et al.* 2010). These studies reveal direct anatomical connections between the basal ganglia and the cerebellum, suggesting close interactions that may influence aspects of motor, affective and cognitive functions known to be mediated by these structures (Wu and Hallett 2013).

There are two anatomical connections that are crucially implicated in the cerebellar output to the basal ganglia and the basal ganglia output to the cerebellum. The cerebellar output to the basal ganglia through the dentato-rubro-thalamic-tract (DRTT) was delineated through rabies virus injection into the sensorimotor area of the putamen of macaque monkeys and retrograde transneuronal transport (Hoshi *et al.* 2005). Their findings showed clear pathways (disynaptic projections) connecting the striatum, which is the input region of the basal ganglia, and the dentate nucleus, which is the output nucleus of the cerebellum, through the thalamus. In humans, the DRTT has been described as an ascending tract carrying the main efferent pathway from the cerebellum (Parraga *et al.* 2016). It ascends from the dentate nucleus through the superior cerebellar peduncle towards the red nucleus (with axon collaterals to this nucleus) (Surova *et al.* 2015) and decussates in the midbrain to reach the thalamus.

The basal ganglia output to the cerebellum, also known as subthalamo-ponto-cerebellar tract (SPCT), was described in a follow-up study in 2010 (Bostan and Strick 2010) by injecting rabies virus into the cerebellar cortex of non-human primates. From the injection site, retrograde transport was observed to first-order neurons that innervate the injection from the pontine nuclei, then to second-order neurons in the subthalamic nucleus (STN) that make synaptic connections with the first order neurons (Bostan *et*

al. 2010). In humans, the SPCT has so far been described in one study as a tract originating in the sub-thalamic nucleus and travelling through the pons into the contralateral cerebellar cortex (Sweet *et al.* 2014).

It has been a challenge to translate these tracing studies in non-human primates to human anatomy. Diffusion MRI tractography is presently the only technique that allows for *in vivo* and non-invasive investigation of white matter connections in humans. The importance of tractography is increasingly being recognised in neurology and neurosurgery and particularly important for the characterisation of the anatomical position of such white matter connections (Sweet *et al.* 2014; Coenen *et al.* 2015; Hana *et al.* 2016; Anthofer *et al.* 2017; Fenoy *et al.* 2017). Whilst some of these pathways, such as the main cerebellar peduncles, have been fairly well characterized in the literature (Stieltjes *et al.* 2001; Leitner *et al.* 2015; Rodriguez-Mena *et al.* 2017), research into the DRTT and SPCT has been scarce.

Some recent diffusion MRI studies have considered these two tracts (Kwon *et al.* 2011; Sweet *et al.* 2014; Calabrese *et al.* 2015; Surova *et al.* 2015; Hana *et al.* 2016; Meola *et al.* 2016), but so far, a comprehensive characterization of their anatomy with regards to cortical connections and relation to other cerebellar tracts, has not been conducted yet. One reason for this is, that these tracts are thin, long and multi-synaptic, and cross over to the contra-lateral hemisphere, making them prone to crossing fibres especially at the decussating regions and are therefore not straightforward to reconstruct using tractography. The dRL algorithm as described in Chapter 2 accounts for this problem. However, this issue was further resolved by first reconstructing the tracts in a high angular resolution diffusion imaging (HARDI) (Tuch *et al.* 2002) sample with 60 gradient directions, as the increase in number of directions for diffusion data acquisition may resolve the problem of crossing fibres (Behrens *et al.* 2003; Chung *et al.* 2011).

4.3 Aims

The primary aim of this study was to describe and develop an anatomically guided tractography protocol to reconstruct and delineate the DRTT and the SPCT using deterministic diffusion MRI tractography in HARDI (60 directions) dataset from a cohort of young healthy participants. The second aim of the study was to demonstrate feasibility of transferring this tractography protocol to diffusion imaging protocols commonly acquired in clinical studies (scans acquiring 30 directions), by reconstructing the DRTT and SPCT in a dataset from patients with Parkinson's disease and their matched healthy controls.

4.4 Materials and Methods

4.4.1 Data cohorts, MRI acquisition and processing

All three data cohorts previously described in Table 1 of Chapter 2 – General methodology were used. Also please refer to Chapter 2 – General methodology for detailed MRI acquisition and processing protocols.

4.4.2 Tractography protocols

4.4.2.1 DRTT

The dentate nucleus was identified in the axial view of the brain infero-lateral to the fourth ventricle, where the temporal lobe is still visible and the slice cuts through the middle of the basilar pons and an ROI was drawn as shown in Figure 4.1 (A). The thalamus was identified in the axial view and a second ROI was drawn contralateral to the AND region of the dentate nucleus as shown in Figure 4.1 (C). The red nucleus is located in the midbrain, infero-medial to the thalamus, infero-lateral to the 3rd ventricle and posterior to the cerebral peduncle. The decussation point of the DRTT was identified along with the red nucleus and the substantia nigra in the diffusion principal direction colour coded image, and another ROI was drawn (Figure 4.1 (B)). This procedure was repeated for the other hemisphere and for all participants. The full DRTT of a representative participant is shown in (Figure 4.1 (D & E)) and the right and left DRTTs are shown in (Supplementary Figure 4.1).

Anatomical landmarks to check the accuracy of tract reconstruction was the dentate nucleus, the decussation point in the midbrain at the level of the red nucleus and the thalamus (Figure 4.1). These landmarks were chosen as the ROIs based on animal tracing studies (Hoshi *et al.* 2005; Wu and Hallett 2013) and human diffusion tractography studies (Parraga *et al.* 2016; Surova *et al.* 2015) described in the introduction section.

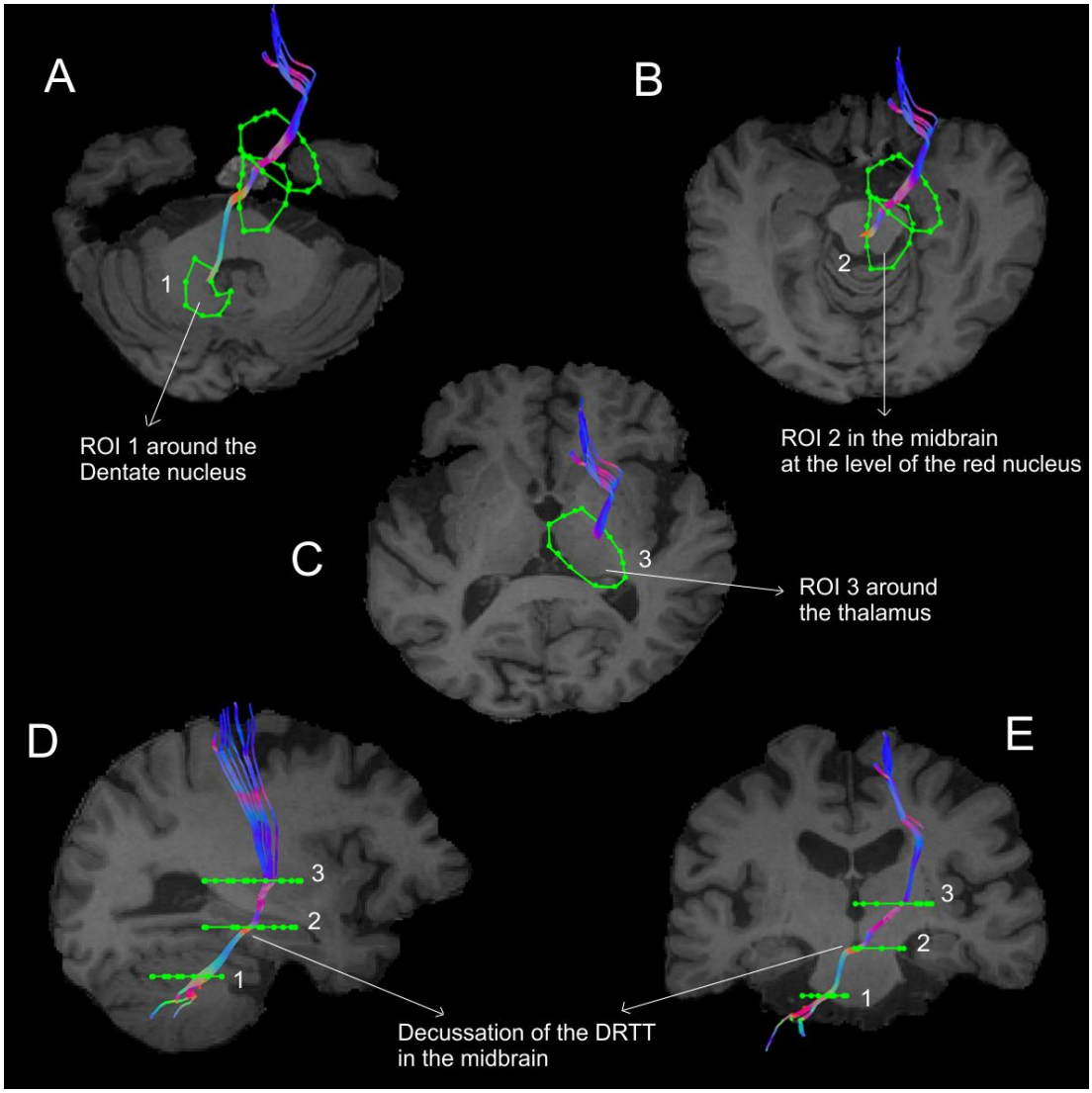

Figure 4.1 The DRTT tract along with the ROIs in axial, sagittal and coronal views of T1 anatomical scan of a representative participant.

A shows the DRTT tract from the dentate nucleus, B shows the DRTT decussating in the mid brain and C shows the DRTT passing through the thalamus in the axial view. D shows the entire DRTT with its cortical projections on a sagittal slice and E shows the entire DRTT with its cortical projections on a coronal slice.

4.4.2.2 SPCT

The subthalamic nucleus is small biconvex-shaped nucleus modulating the basal ganglia output and is located inferior to the thalamus and superior to the substantia nigra, and lateral to the internal capsule (Hamani *et al.* 2004). For the reconstruction of the SPCT, the subthalamic nucleus was identified in the coronal view and a ROI was drawn as shown in (Figure 4.2 (A)). The second ROI was drawn around the contralateral pons region surrounding the decussation of the SPCT into the cerebellar

hemispheres (Figure 4.2 (B)). This procedure was repeated for the other hemisphere and for all participants.

Anatomical landmarks to check for accuracy of tract reconstruction was the SPCT passing through both the ROIs and also the decussation at the level of the pons.

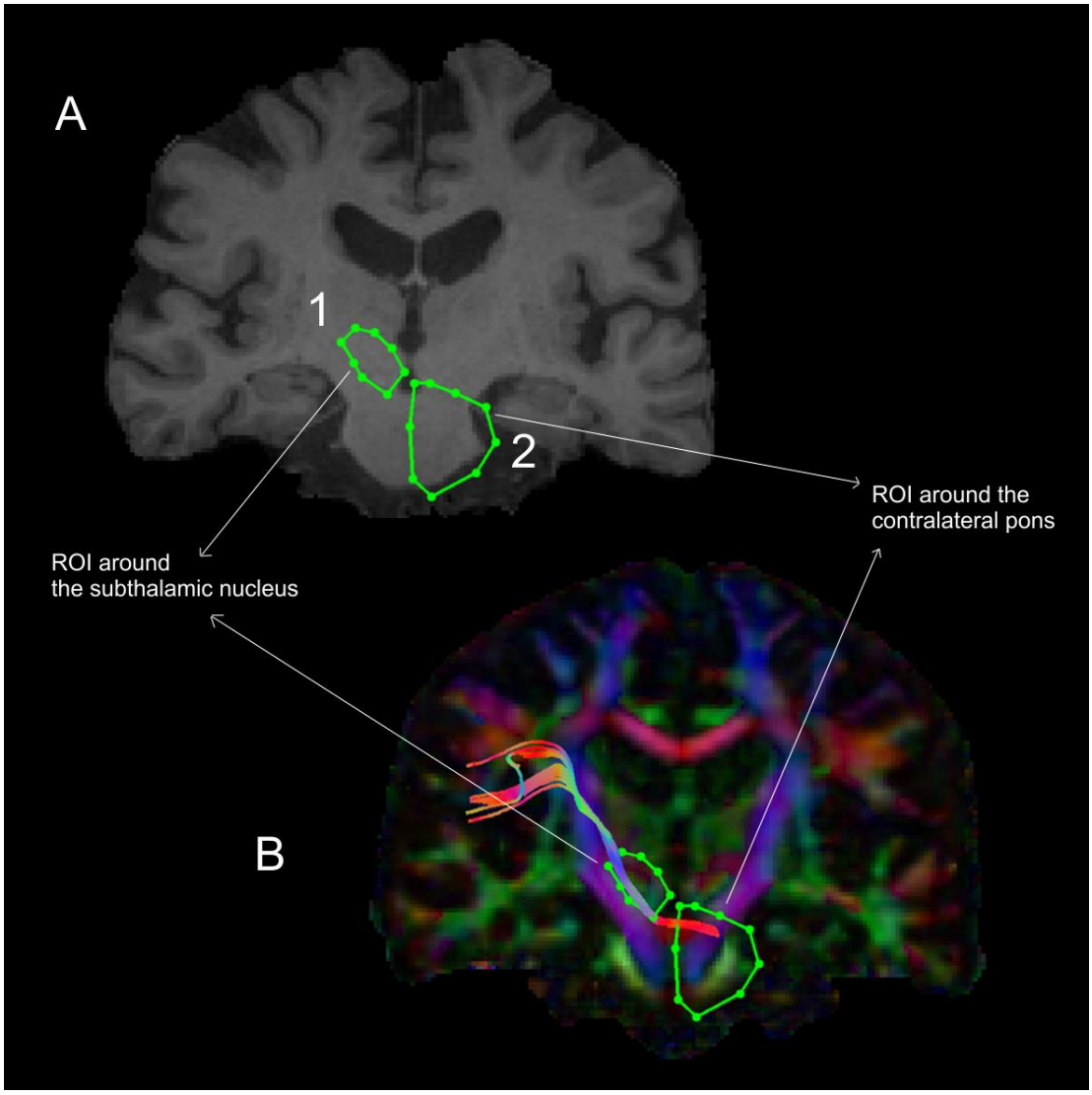

Figure 4.2 Regions of interest and reconstruction of the SPCT for a representative participant in coronal view.

The first ROI is drawn around the subthalamic nucleus in T1 anatomical (A) and the second ROI is drawn around the contralateral pons region in a diffusion colour coded image (B).

In some cases, where the methods described above were unsuccessful in delineating the SPCT or the DRTT, a different approach was taken: an ROI was drawn around the thalamus covering the posterior limb of the internal capsule in an axial view of the brain (Figure 4.3 (A)) and a second ROI around the contralateral cerebellar hemisphere at the

level of the pons was drawn also in the axial view of the brain as shown in (Figure 4.3 (B & C)). Appropriate NOT ROIs were drawn to delineate the DRTT and the SPCT separately. A representative SPCT obtained using this alternative method is shown in (Figure 4.3 (D)). The right and left SPCTs are also shown in (Supplementary Figure 4.2).

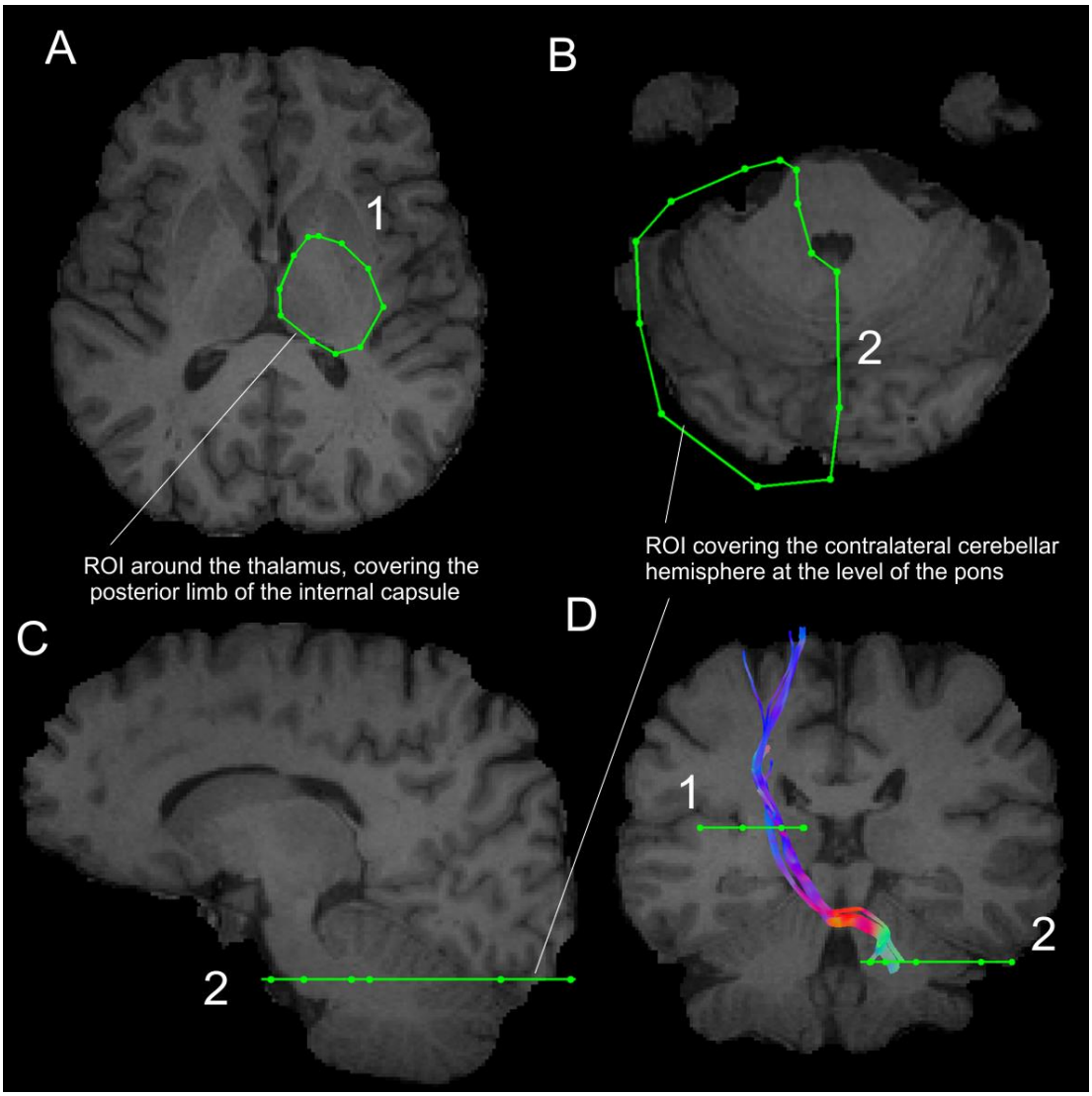

Figure 4.3 Alternative ROIs used for reconstruction of DRTT and SPCT.

The ROI around the thalamus covering the internal capsule is shown in (A), the ROI covering the contralateral cerebellar peduncle (B) & (C). An example of the SPCT obtained using this alternative method is shown in (D).

Additionally, the main cerebellar tracts (middle, inferior and superior cerebellar peduncles: MCP, ICP and SCP) and the corticospinal tracts (CST) were reconstructed in order to investigate the tract overlap and to compare reliability indices. The

procedure for the reconstruction of the CST has been described previously in Chapter 3 (Mole *et al.* 2016) and reconstruction of the cerebellar tracts were performed using descriptions from (Stieltjes *et al.* 2001; Oishi *et al.* 2011) and their reconstruction protocols are described in Chapter 5.

4.4.3 Statistical Analysis

4.4.3.1 Tract probability maps

The probability maps of connections of the various tracts (DRTT, SPCT, CST, MCP, SCP and ICP) within the brain were mapped out using group-based probability maps for each tract. To create these maps, the NIfTI-exported (Neuroimaging Informatics Technology Initiative) tracts of each participant were registered to MNI space. This was done by first registering each participant's structural high-resolution T1-weighted image to MNI space, using FSL FNIRT (FSL version 5.0.9, warp resolution: 10 mm, 10mm, 10mm) (Andersson *et al.* 2010; Jenkinson *et al.* 2012), and then applying the warp to the tract NIfTI file (which had already been registered to the high resolution structural scan as part of the pre-processing pipeline in ExploreDTIv4.8.3).

4.4.3.2 Spatial overlap between tracts

As the DRTT and SPCT lie in close proximity to other cerebellar tracts, I aimed to assess their spatial independence by looking at their spatial overlap with the MCP, SCP, ICP and CST. Spatial overlap was assessed by calculating overlap dice coefficient scores [see also (Zijdenbos *et al.* 1994)]. First the tracts were exported to binary NIfTI files, then the number of voxels for each tract and the number of voxels overlapping in two tracts were counted using the AFNI function 3DOverlap (Cox 1996). Finally, dice coefficients were calculated using the formula:

$$(2 \times \text{number of overlapping voxels}) \,/\, (\text{number of voxels in tract 1} + \text{number of voxels in tract 2})$$

And these were subsequently converted to percentage. This was performed in both directions to quantify what percentage of voxels in tract 1 were occupied by tract 2, and vice versa. Then the overlap dice coefficients were averaged across participants within each group.

4.4.3.3 Inter-operator reliability of tract reconstruction

I reconstructed all tracts (DRTT, SPCT, MCP, ICP, SCP and CST) for all participants in all groups. A second operator (IL) independently reconstructed tracts for a subset of randomly selected participants (5 from each group) to assess reliability and reproducibility of reconstructions. Similar to the procedure for assessing spatial overlap, reliability was assessed by calculating overlap dice coefficient scores using the formula:

$$(2 \times \text{number of overlapping voxels}) \,/\, (\text{number of voxels in tract by operator 1} + \text{number of voxels in tract by operator 2})$$

And these were converted to percentage as before.

4.5 Results

The DRTT and the SPCT was successfully reconstructed across all the three groups as shown in Table 4.1.

Table 4.1 Number of successful reconstructions of the DRTT and SPCT tracts

Tract	Young Healthy Controls	Parkinson's Disease	Matched Healthy Controls
Number of participants	20	24	26
Number of directions	60	30	30
Mean age ± SD	25.4 ± 4.84	63.42 ± 10.82	64.88 ± 8.06
Number of L DRTT (%)	16 (80%)	17 (71%)	18 (69%)
Number of R DRTT (%)	15 (75%)	16 (67%)	14 (54%)
Number of L SPCT (%)	11 (55%)	19 (79%)	22 (85%)
Number of R SPCT (%)	16 (80%)	19 (79%)	23 (89%)

SD – Standard deviation, L - Left, R - Right, DRTT – Dentato-Rubro-Thalamic Tract, SPCT – Subthalamo-Ponto-Cerebellar Tract

4.5.1 Tract probability maps

The probability maps depicting the anatomical connections for all tracts across the whole brain for the YHC group are shown in Figure 4.4 and Figure 4.5, for the PD group and the MHC group in Supplementary Figure 4.3 and Supplementary Figure 4.4. The tract projection maps of the DRTT and the SPCT in the YHC group were visually assessed using atlases (Juelich Histological atlas, Harvard-Oxford Subcortical Structural Atlas, MNI Structural Atlas) in both hemispheres.

The DRTT originates from the dentate nucleus and travels superiorly and medially through the SCP (Kwon *et al.* 2011; Surova *et al.* 2015; Meola *et al.* 2016) towards the midbrain. The DRTT showed extensive projections to the frontal lobe through the internal capsule. The DRTT also showed projections to the premotor cortex and the supplementary motor cortex, close but not overlapping with the corticospinal tract, with projections also towards the precentral, inferior and superior frontal gyri (Figure 4.4, Figure 4.5). There were no identifiable projections of the DRTT towards the occipital, parietal and temporal lobes. The DRTT is located medio-posteriorly to the CST in the internal capsule and then its cortical projections travel laterally anterior and posterior

to the CST (Figure 4.4, Figure 4.5). The current findings are in line with a previous study that found the DRTT projections are located medio-posteriorly to the CST (Hana *et al.* 2016). It was found that the DRTT also projects to the caudate and the putamen, which is again in line with the animal literature that reports projections into the motor regions of the putamen (Hoshi *et al.* 2005).

The SPCT showed connections with the frontal lobe, primary motor cortex, primary somatosensory cortex, premotor cortex, and precentral cortex, inferior and superior frontal gyri. While there were no connections between the SPCT and the occipital and temporal lobes, there were connections with the superior parietal lobe (Figure 4.4, Figure 4.5). A diagrammatic representation of the connections of the reconstructed DRTT and the SPCT including their cortical connections is depicted in (Figure 4.6). The connections of the reconstructed DRTT and the SPCTs appear consistent across the groups in both hemispheres (Figure 4.4, Figure 4.5, Supplementary Figure 4.3 and Supplementary Figure 4.4). The key anatomical landmarks that the DRTT and the SPCT pass through, shown here in serial axial slices of the brain are also depicted in Figure 4.4. For the DRTT, the tract at the level of the dentate nucleus and decussation at the level of the red nucleus, and for the SPCT the tract decussation at the level of the pons. Other key features for both the DRTT and the SPCT was passage through the internal capsule and connections towards the various cortical regions.

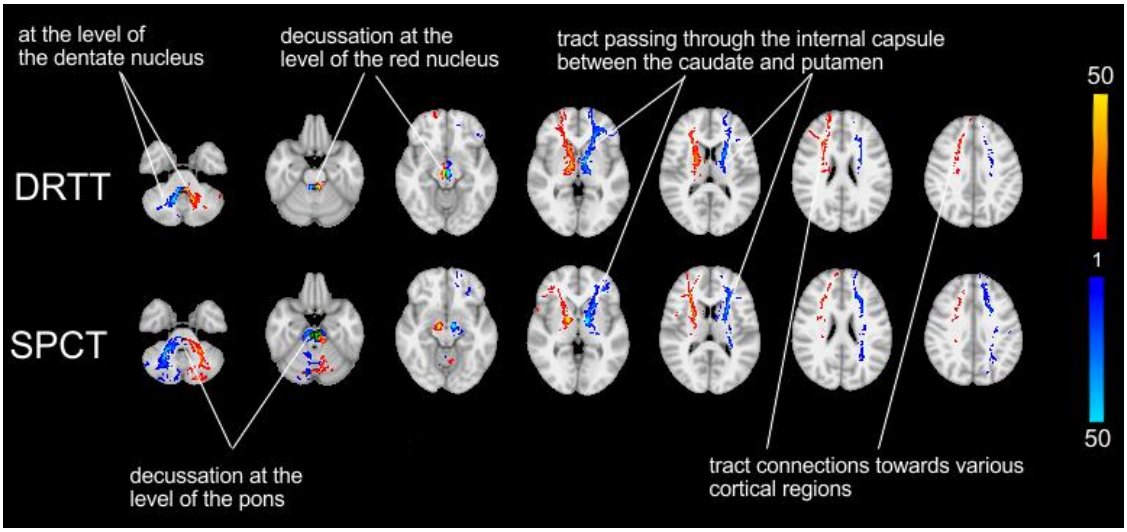

Figure 4.4 DRTT and SPCT anatomical connections shown as probability maps in axial slices in the YHC group. The range is from 1-50, hence areas of the brain showing yellow and light blue colours have at least 50% of participants' tracts passing through those voxels.

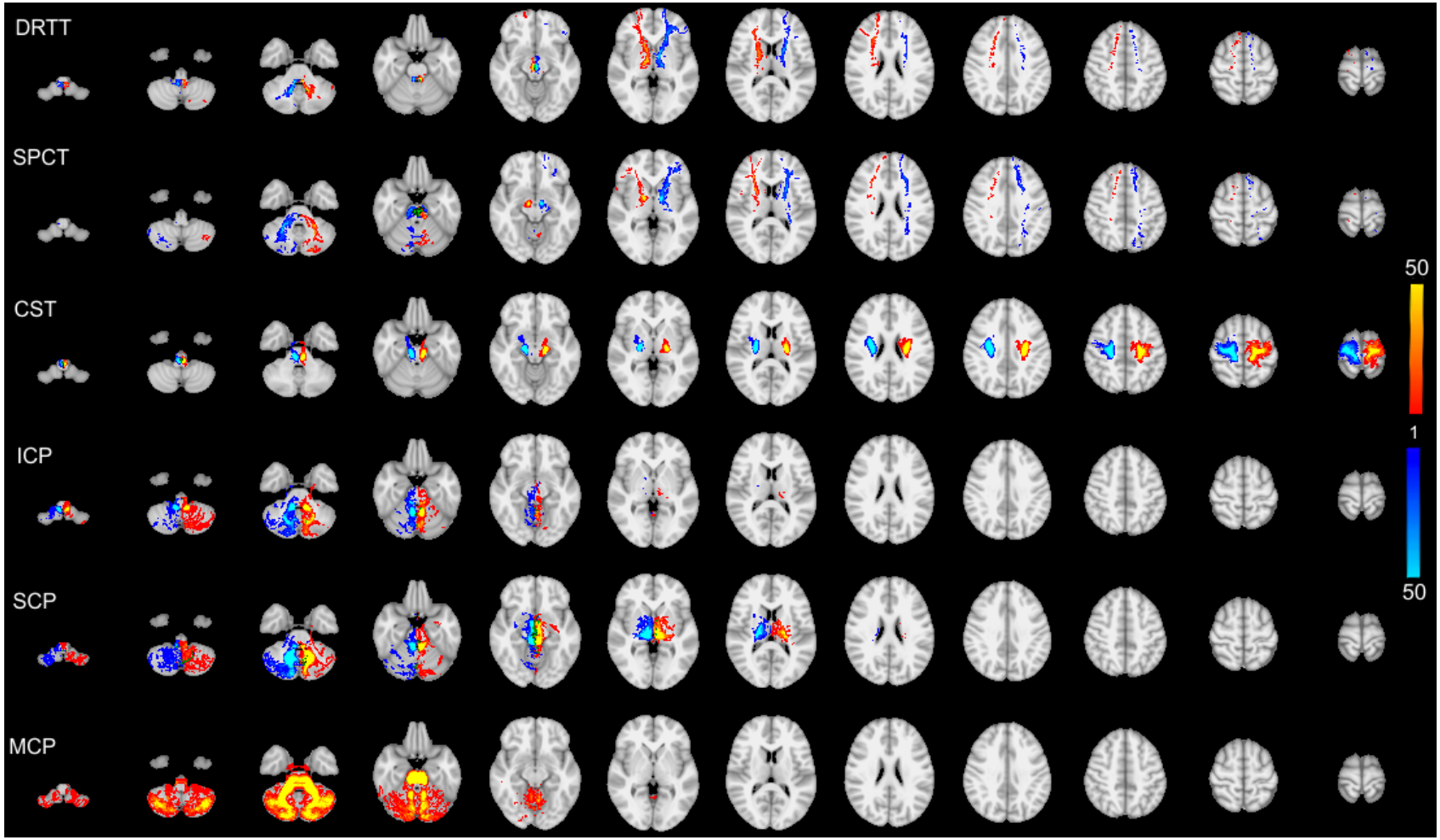

Figure 4.5 The probability maps in axial slices, showing the probability (in percent) of the DRTT, SPCT, CST, ICP, SCP and MCP tracts in the YHC group. The range is from 1-50, hence areas of the brain showing yellow and light blue colours have at least 50% of participants' tracts passing through those voxels.

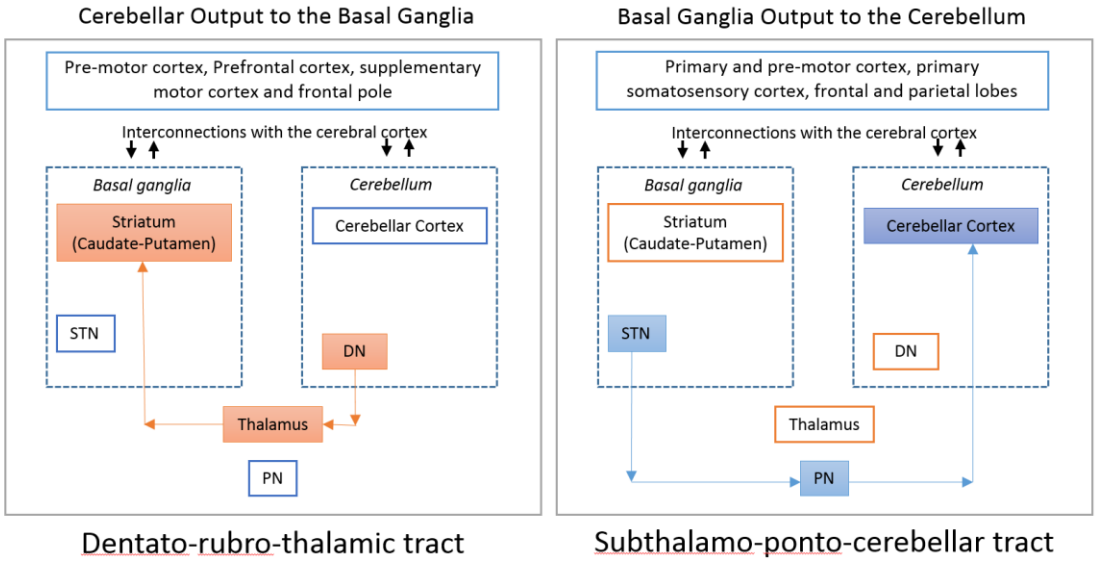

Figure 4.6 Circuits interconnecting the cerebellum and the basal ganglia including the cerebral cortex connections.

Based on findings from the current tractography reconstructions and probability maps in the YHC group [adapted and modified from (Bostan and Strick 2010)]. STN - Subthalamic nucleus, PN – Pontine nucleus and DN – Dentate nucleus

4.5.2 Spatial overlap between tracts

The spatial overlap between tracts (as percent of each of the tracts' voxels occupying voxels of the DRTT or the SPCT) are shown in Table 4.2 and the results from the spatial overlap among all the tracts in both directions are depicted in the matrix plots (Figure 4.7). The DRTT predominately overlaps with and travels through the SCP, with the YHC group showing that the left SCP occupies an average 15.59% of the left DRTT and the right SCP occupies an average 16.97% of the right DRTT (see Table 4.2). While the left and right DRTT occupy less than 2.92% of the left and right SCPs across all groups [hemisphere (mean ± standard deviation) in YHC, R(2.28 ± 2.02) L(1.95 ± 1.91), in PD, R(2.62 ± 2.22) L(2.92 ± 2.58) and in MHC, R(1.37 ± 1.34) L(2.15 ± 2.10)].

The left and right SPCTs predominately overlap with the MCP, with the YHC group showing that the MCP occupies an average 32.28% of the left SPCT and occupies an average 29.61% of the right SPCT (see Table 4.2). While the left and right SPCTs occupy less than 4.93% of the MCPs across all groups [hemisphere (mean ± standard deviation) in YHC, R(1.88 ± 2.29) L(2.15 ± 1.61), in PD, R(2.82 ± 2.80) L(4.63 ± 3.46) and in MHC, R(4.30 ± 2.95) L(4.93 ± 2.78)].

Table 4.2 Spatial overlap

Dice similarity coefficient (DSC) (Mean ± SD)						
L DRTT						
	L CST	L DRTT	L ICP	MCP	L SCP	L SPCT
YHC	0.46% ± 1.34%	100%	4.91% ± 6.62%	1.60% ± 2.94%	15.59% ± 16.23%	0.57% ± 1.16%
PD	0%	100%	1.35% ±2.02%	0.66% ± 1.24%	8.25% ± 6.09%	1.16% ± 1.94%
MHC	1.42% ± 3.00%	100%	1.68% ± 3.00%	0.18% ± 0.54%	7.30% ± 6.12%	3.90% ± 9.03%
R DRTT						
	R CST	R DRTT	R ICP	MCP	R SCP	R SPCT
YHC	0.10% ± 0.28%	100%	4.22% ± 5.88%	1.28% ± 2.78%	16.97% ± 19.26%	0.77% ± 1.22%
PD	0.03% ± 0.09%	100%	1.70% ± 2.70%	0.13% ± 0.30%	9.86% ± 6.88%	0.65%± 2.31%
MHC	1.47% ± 2.84%	100%	0.80% ± 1.46%	0.17% ± 0.45%	9.06% ± 9.45%	0.70% ± 1.69%
L SPCT						
	L CST	L DRTT	L ICP	MCP	L SCP	L SPCT
YHC	1.63% ± 1.69%	0.97% ± 2.34%	0.52% ± 0.63%	32.28% ± 13.96%	0.39% ± 0.93%	100%
PD	1.02% ± 0.85%	1.05% ± 1.75%	0.57% ± 1.24%	22.87% ± 11.70%	0.17% ± 0.61%	100%
MHC	0.80% ± 0.65%	1.19% ± 1.94%	0.50% ± 0.97%	25.60% ± 10.72%	0.28% ± 0.64%	100%
R SPCT						
	R CST	R DRTT	R ICP	MCP	R SCP	R SPCT
YHC	1.78% ± 1.60%	1.31% ± 2.63%	1.70% ± 2.70%	29.61% ± 12.52%	0.58% ± 0.86%	100%
PD	1.38% ± 1.06%	0.70 % ± 2.47%	0.73% ± 1.46%	25.60% ± 10.81%	0.12% ± 0.29%	100%
MHC	1.69% ± 1.12%	0.99% ± 2.81%	0.29% ± 0.72%	27.18% ± 10.06%	0.11% ± 0.31%	100%

YHC - Young Healthy Controls, PD – Parkinson's disease, MHC – Matched Healthy Controls, SD - Standard deviation, L - Left, R - Right, DRTT – Dentato-Rubro-Thalamic Tract, SPCT – Subthalamo-Ponto-Cerebellar Tract, CST – Corticospinal tract, ICP – Inferior Cerebellar Peduncle, SCP – Superior Cerebellar Peduncle, MCP - Middle Cerebellar Peduncle

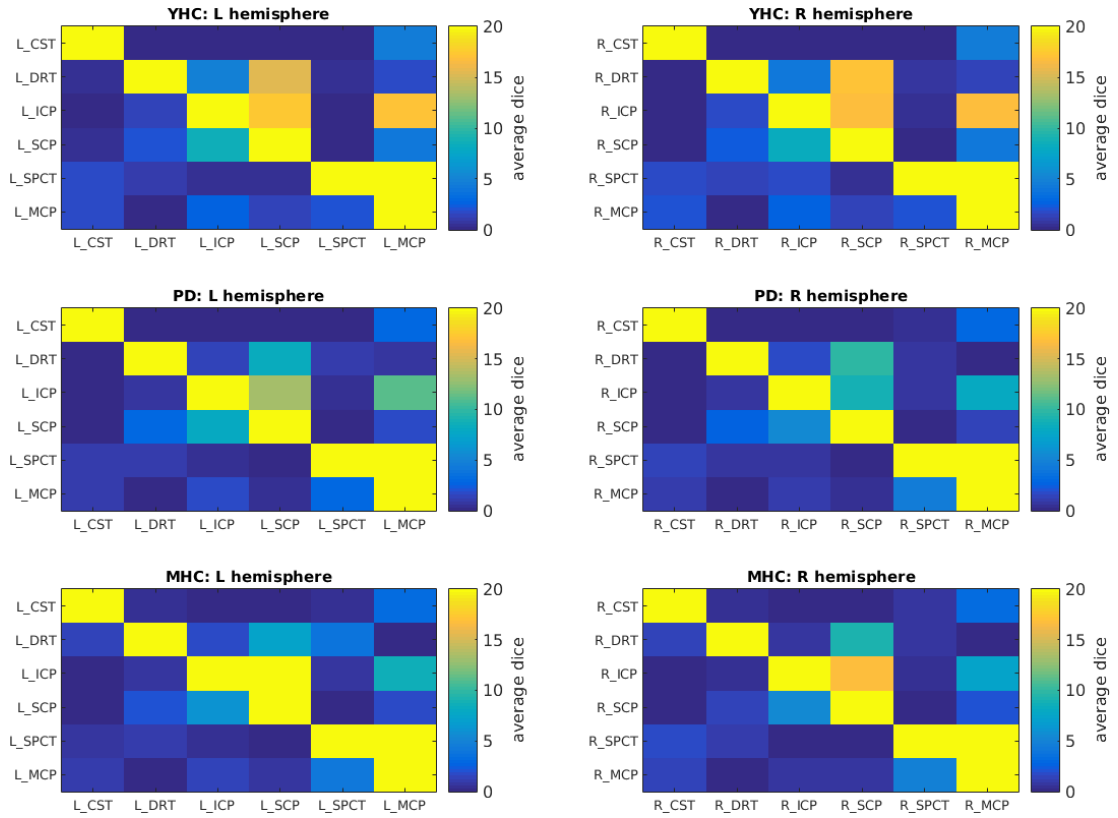

Figure 4.7 Matrix plots representing the overlaps as group-averaged dice scores between the tracts in each group.

L - Left, R - Right, DRTT – Dentato-Rubro-Thalamic Tract, SPCT – Subthalamo-Ponto-Cerebellar Tract, CST – Corticospinal tract, ICP – Inferior Cerebellar Peduncle, SCP – Superior Cerebellar Peduncle, MCP - Middle Cerebellar Peduncle

4.5.3 Inter-rater reliability of tract reconstruction

The inter-rater reliability of the reconstructed tracts was measured as the spatial agreement between the tracts reconstructed by operator 1 (JPM) and operator 2 (IL). On average the spatial agreement for all tracts was above 50% and comparable across tracts, with the exception of the MCP which showed particularly high agreement (CST: L: 64±28 (n = 15), R: 69±27 (n = 15); DRT: L: 61±25 (n = 10), R: 66±30 (n = 7); ICP: L: 58±22 (n = 15), R: 67±15 (n = 15); SCP: L: 66±15 (n = 15), R: 61±15 (n = 12); SPCT: L: 68±21 (n = 9), R: 75±25 (n = 8); MCP: 93±5 (n = 15)). Closer inspection revealed that tracts from one operator were consistently larger than tracts from the other operator, whose smaller tracts were mostly comprised within the larger ones (see Supplementary Table 4.1). However, the extracted fractional anisotropy values from the full reconstructed tracts showed high inter-class correlation across operators (PD, ICC 0.671, p=0.0286 and MHC, ICC 0.969, p=3.32e-07) (see Supplementary Table 4.3 and Supplementary Table 4.4).

4.6 Discussion

In this study, an anatomically guided tractography protocol was developed to reconstruct the DRTT (cerebellar output to the basal ganglia) and the SPCT (basal ganglia output to the cerebellum) using HARDI data (60 directions) from a group of young healthy participants. The anatomical protocol was then also used to successfully reconstruct these tracts in a dataset (30 directions) of Parkinson's disease patients and matched controls. Most importantly and for the first time the tract probability maps and spatial overlap of the reconstructed tracts have been described in humans using diffusion tractography.

4.6.1 Tract probability maps

There was evidence of cortical motor and non-motor connections for the DRTT and the SPCT and to date this is the first study to report these cerebellar-cortical connections in humans.

4.6.1.1 DRTT

The projections of the DRTT followed the previously described animal literature (Hoshi *et al.* 2005) and various studies in humans using tractography, histology and post-mortem dissection studies (Kwon *et al.* 2011; Sweet *et al.* 2014; Surova *et al.* 2015; Hana *et al.* 2016; Mollink *et al.* 2016; Fenoy *et al.* 2017). The DRTT originates in the dentate nucleus, ascending through the SCP towards the brainstem and then decussates in the mid brain at the level of the red nucleus towards the contralateral thalamus, with projections further on towards the cortical regions (Figure 4.1, Figure 4.4, Figure 4.5). One retrograde transneuronal virus tracer study has looked at the motor and non-motor cerebral cortex projections of the dentate nucleus and showed that it projects to the primary motor, premotor, prefrontal and posterior parietal areas of the cortex (Dum and Strick 2003). This is in line with the current tractography findings for the DRTT (Figure 4.4), which suggest that these projections could be a result of neuronal connections between the dentate nucleus and the cortical regions via the DRTT. The DRTT cerebellar connections are also in line with the following studies using retrograde transneuronal transport in monkeys: firstly, disynaptic projections from the dentate nucleus to the SMA and pre-SMA have been found (Akkal *et al.* 2007). Secondly, the dentate nucleus has been found to project to and receive input from the primary motor

cortex and the dorsolateral prefrontal cortex (Kelly and Strick 2003). Furthermore, the dentate nucleus provides input to the frontal eye field (Lynch *et al.* 1994) and projects to the different regions of the prefrontal cortex via the thalamus (Middleton and Strick 2001). Finally, a review has reported that cerebellar nuclei project to the subdivision of the thalamus which in turn project to neocortical regions including the premotor, prefrontal and posterior parietal areas of the cerebral cortex (Percheron *et al.* 1996). However, the inferior parietal lobule (Clower *et al.* 2001) and posterior parietal cortex (Clower *et al.* 2005) are targets for output from the dentate nucleus, but there were no similar DRTT connections to the parietal cortex in the current study.

4.6.1.2 SPCT

The connectivity of the SPCT also followed the animal literature (Bostan and Strick 2010). The SPCT originates in the subthalamic nucleus descending though the brainstem and decussating in the upper and/or middle pons (Figure 4.2), before travelling into the contralateral cerebellar hemisphere. The SPCTs that were reconstructed in the current study did not however enter the contralateral cerebellar cortex via the SCP as described by the previous study in humans (Sweet *et al.* 2014), but through the MCP. The current findings have been replicated within different healthy participant groups and in the PD patient group with findings consistently showing that the SPCT overlaps with MCP and not the SCP (Table 4.2, Figure 4.7). The finding of cortical connections of the SPCT from the current data (Figure 4.4, Figure 4.5) are in support of the classical view that cerebellum receives input from widespread neocortical areas including portions of the frontal, parietal, temporal and occipital lobes (Glickstein *et al.* 1985; Schmahmann 1996).

4.6.2 Spatial overlap

It was observed that there was overall low spatial overlap between the main tracts of interest (the DRTT and the SPCT) with the CST, MCP, SCP and the ICP (Table 4.2). This is very encouraging as spatial independence suggests that these tracts are distinct pathways and not just part of the major cerebellar pathways even if the DRTT passes through the SCP and the SPCT through the MCP.

4.6.2.1 DRTT

Of all the investigated tracts, the SCP showed highest spatial overlap with the DRTT (Table 4.2, Figure 4.7, and Supplementary Figure 4.5). This finding is in line with a recent human connectome-based tractography and microdissection study using 488 subjects which found that the DRTT runs superiorly and medially inside the SCP and verified the same using microdissection (Meola *et al.* 2016). A probabilistic tractography study in 41 healthy subjects showed that the DRTT is a part of the SCP where the SCP acts as a channel for the DRTT leaving the cerebellum (Kwon et al. 2011). Other studies showed that fibers arising from the dentate nuclei pass through ipsilateral SCP before decussating at the level of the inferior colliculi in the mesencephalic tegmentum (Parraga *et al.* 2016).

4.6.2.2 SPCT

The MCP showed the highest spatial overlap with the SPCTs (Table 4.2, Figure 4.7). The SPCT described previously in humans (Sweet *et al.* 2014) did not demonstrate a similar overlap. Here, the high overlap between SPCT and MCP is likely due to the decussation of the SPCT occurring at the level of the pons, where the MCP joins the two cerebellar hemispheres (Supplementary Figure 4.9).

4.6.3 Inter-rater reliability

Using the developed protocol a researcher new to tractography (operator 2/I.L.) was also able to reconstruct the DRTT and the SPCT using the developed protocol, as suggested by good inter-rater reliability. This was comparable to the inter-rater reliability for the more established tracts (CST, MCP, SCP and ICP). The tract with the highest inter-rater reliability was the MCP, which is a large tract and quite easy to reconstruct. It should be noted that although all the tracts were reliably reconstructed and were visually and anatomical accurate, the volume was thinner in most of the operator 2 tracts, suggesting that measures of tract size (and derived measures such as average fractional anisotropy across a tract) can depend on how an operator draws the ROIs, thereby highlighting the importance of consistent application of manual tractography protocols. Regardless of the limited spatial concordance across operators, the reliability of the obtained semi-quantitative measure of fractional anisotropy for each tract was good, which is an important prerequisite for any study looking at inter-

individual or group (e.g., patients vs. controls) differences (Supplementary Table 4.3 and Supplementary Table 4.4).

4.6.4 Consistent reconstruction across data sets

Although previous tractography papers have obtained the full DRTT including the cortical projections, the current study is the first to follow the cortical projections and verify its course in a larger participant sample, including different age groups, patients, and different acquisition protocols. Moreover, the tracts reconstructed in three different datasets were qualitatively comparable across groups (see tract probability maps in Figure 4.4, Figure 4.5, Supplementary Figure 4.3, Supplementary Figure 4.4).

4.6.5 Limitations

It was not possible to reconstruct the DRTT and the SPCT in all participants. This may be in part caused by their anatomical nature; for instance, they are smaller, longer and have more curvature than more well-established tracts (e.g. CST, MCP). Even though the data were correction for participant motion, eddy current and echo planar imaging distortion, residual noise and signal artefacts from free water and air tissue interfaces may have contributed to this. The choice of the imaging parameters, the image quality, the tracking algorithms and pre-processing pipelines are also known to affect the quality, precision and reliability of tractography results and contribute to false positive and false negative findings (Jbabdi and Johansen-Berg 2011). It has to be noted that not all tracts that could potentially overlap with the cortical connections of the DRTT and SPCT have been reconstructed in this study (e.g. the anterior thalamic radiation) as the focus was on looking at overlap with the main cerebellar tracts and the CST.

4.7 Conclusion

The current study is the first to describe and develop anatomical protocols for the cerebellar output (DRTT) and cerebellar input (SPCT) connections that have been previously described in non-human primates in healthy young adults, older participants and PD patients. Also for the first time their cortical connections and spatial overlap with the major cerebellar pathways (MCP, ICP, SCP) and the CST are described.

These findings are in support of previous studies suggesting that there are distinct and direct anatomical connections between the basal ganglia and the cerebellum (Hoshi *et al.* 2005; Bostan and Strick 2010). These findings also challenge the classical view that the cerebellum receives input from neocortical areas but then funnels this information back to only the primary motor cortex through the thalamus (Allen and Tsukahara 1974), as there was distinct cerebral connections with various cortical regions in both DRTT and SPCT.

Using the developed anatomical protocol one can now reconstruct the DRTT and the SPCT from data that is routinely obtained in clinical research studies. Clinical and research applications include anatomical localisation for deep brain stimulation (Sweet *et al.* 2014; Coenen *et al.* 2015; Hana *et al.* 2016; Fenoy *et al.* 2017) and identification of changes in these tracts in neurodegenerative and movement disorders (Jeong *et al.* 2012; Jang and Kwon 2015; Surova *et al.* 2015).

Chapter 5 Investigating microstructural differences in the white matter of the main cerebellar and basal ganglia-cerebellar pathways in Parkinson's disease

5.1 Abstract

Objective

To compare microstructural differences in a cohort of Parkinson's disease (PD) patients and their matched healthy controls (MHC), in the three main cerebellar pathways (the middle, inferior and superior cerebellar peduncles) and in the two basal ganglia-cerebellar connections (dentato-rubro-thalamic tract and subthalamo-ponto-cerebellar tract).

Methods

Diffusion weighted imaging data of 24 PD patients and 25 MHCs were analysed and deterministic tractography was performed using the spherical deconvolution-based damped Richardson-Lucy algorithm. Diffusion metrics reflecting the underlying white matter microstructure (fractional anisotropy (FA), mean, axial and radial diffusivity; (MD, AD, RD) and hindrance modulated orientational anisotropy (HMOA)) were extracted from the tracts of the interest and statistical analysis were performed.

Results

PD patients had higher FA in the right superior cerebellar peduncle, the right inferior cerebellar and significantly increased HMOA in the right superior cerebellar peduncle compared to MHCs.

Conclusion

This is the first study to explore the microstructural differences in the main cerebellar pathways and the two basal-ganglia cerebellar connections in PD. I found higher FA, and HMOA of the selected cerebellar tracts in patients compared to controls. Current results suggest that the microstructural characteristics of cerebellar input and output connections are altered in PD, however future studies are required to delineate the specific compensatory, pathological and/or disease progression contributions of these pathways to PD.

Key points

1. In the PD cohort, there was significantly increased FA in the right superior cerebellar peduncle and the right inferior cerebellar peduncle.

2. In the PD cohort, there was significantly increased hindrance modulated orientational anisotropy in the right superior cerebellar peduncle.

3. These results suggest that microstructural characteristics of cerebellar input and output pathways are altered in PD. Future studies are required to delineate the specific compensatory, pathological and/or disease progression contributions of these pathways in PD.

5.2 Background and Rationale

Research in PD has mostly targeted the basal ganglia ever since the finding of reduced dopamine levels in the striatum in the 1960s (Hornykiewicz 2006). Accumulating evidence from anatomical studies in animals and functional studies in humans show the influence of the cerebellum in parkinsonian motor symptoms such as akinesia/rigidity, tremor, dyskinesia, gait disturbances and some non-motor symptoms such as cognition and olfaction (Wu and Hallett 2013). Although the cerebellum is known to be involved in voluntary movement, gait, posture and motor functions, (Ghez and W Thomas 2000) research into the role of the cerebellum in PD has been very limited.

For instance, a post-mortem study revealed reduced dopamine receptors in the cerebellum of PD patients compared to healthy participants highlighting its role in the symptoms of the disease (Hurley *et al.* 2003). In the rat brain, the cerebellum receives dopaminergic projections from the substantia nigra pars compacta and the ventral tegmental area which lies close to the substantia nigra and the red nucleus (Ikai *et al.* 1992; Panagopoulos *et al.* 1991). One study showed that degeneration of nigrostriatal dopaminergic neurons caused decrease in neural activity in thalamo-cortical neurons receiving input from substantia nigra and cerebellum in primate models of PD; thereby suggesting both basal ganglia-thalamic and cerebellar-thalamic pathways are involved in PD symptoms (Rolland *et al.* 2007).

The middle cerebellar peduncle (MCP) connects the two cerebellar hemispheres to the pons, the superior cerebellar peduncle (SCP) is the main output pathway from the cerebellum connecting it to the midbrain, and the inferior cerebellar peduncle (ICP) carries inputs from the spinal cord and the medulla oblongata into the cerebellum (Nieuwenhuys *et al.* 2008). Previous studies have found that the MCP and the SCP in addition to the basal ganglia contributed to differentiating PD from multiple system atrophy (MSA-P) and progressive supranuclear palsy (PSP) (Nair *et al.* 2013; Nicoletti *et al.* 2008; Nicoletti *et al.* 2006; Quattrone *et al.* 2008; Nicoletti *et al.* 2013).

Moreover, recent animal tracing studies have found reciprocal interconnections between the cerebellum and the basal ganglia (Bostan and Strick 2010; Hoshi *et al.* 2005), while previously the basal ganglia and the cerebellum were assumed to interact only at the level of the cerebral cortex (Percheron *et al.* 1996). In Chapter 4, I

successfully developed an anatomical protocol and reconstructed these basal ganglia-cerebellar interconnections namely, the DRTT and SPCT.

Despite the increasing evidence that the interplay between the basal ganglia and cerebellum plays an important role in mediating cognitive and motor functions in PD, no published studies to date have explored the role of the main cerebellar white matter tracts (MCP, SCP and ICP) and basal ganglia-cerebellar white matter connections (DRTT and SPCT) in PD. Hence, deterministic tractography using the spherical deconvolution based damped Richardson-Lucy (dRL) algorithm (Dell'acqua *et al.* 2010), detailed in Chapter 2, was employed to reconstruct the main cerebellar pathways and basal ganglia-cerebellar white matter pathways and to characterize the average microstructural properties of these tracts.

In addition to the standard diffusion metrics, hindrance modulated orientational anisotropy (HMOA), a novel tract-specific index of white matter microstructural organisation was implemented in the current study. The HMOA is defined as the absolute amplitude of the fibre orientation distribution and it provides a fibre population specific index of the diffusion properties along the reconstructed fibres (Dell'Acqua *et al.* 2013). So far only eight papers were present on PubMed central search using the criteria "Hindrance modulated orientational anisotropy" and/or "HMOA" on 24th September 2017, and this metric has not been used in PD. One paper reported that lower HMOA values of the fornix predicted brain structure and function suggesting that recognition memory performance may be influenced by underlying neuroanatomical alterations in very preterm born individuals (Tseng *et al.* 2017). Another study found that individual HMOA variation in post-commissural, but not pre-commissural, fibres of the fornix correlated positively with visual recall performance (Christiansen *et al.* 2016). A study showed increased HMOA values in the superior longitudinal fasiculus (SLF) with abnormal lateralisation of occipito-frontal and parito-frontal pathways in developmental dyslexia (Zhao *et al.* 2016). Another recent paper that looked at human visuospatial attention found increased HMOA in the SLF (Cazzoli and Chechlacz 2017) and advised caution in interpreting increased HMOA as a surrogate for higher connectivity. A study that investigated perinatal brain injury (PBI) found significantly reduced HMOA in the dorsal cingulum of the PBI group compared with controls, but reported increased HMOA in the SLF and suggested that this increase could be due to the possibility of lateral neuroanatomical compensation for medial structural deficits in

the PBI group (Froudist-Walsh *et al.* 2015). In a study that looked at visuospatial attention, individual differences in visual short-term memory (VSTM) were linked to variability in the HMOA of the inferior fronto-occipital fasciculus (IFOF) the SLF II and the SLF III (Chechlacz et al. 2015). From these studies, HMOA metric has been shown to be sensitive to individual variation in white matter microstructural organization (Chechlacz et al. 2015). It has been proposed to be more sensitive to changes in diffusion than conventional diffusion metrics (Dell'Acqua et al. 2013; Christiansen et al. 2016).

5.3 Aims

The aim of this study was to explore the microstructural metrics in a cohort of PD patients and matched healthy controls, in the three main cerebellar pathways (the MCP, SCP and ICP) and in the two basal-ganglia cerebellar tracts (DRTT and SPCT). In addition, I investigated how the potential microstructural differences may be correlated with clinical and behavioural measures in the PD patient group.

5.4 Materials and Methods

5.4.1 Data cohorts, MR acquisition and processing

Full details of the MR data acquisition, diffusion MR pre-processing and the deterministic tractography algorithms used can be found in Chapter 2. The final participant sample in this chapter was comprised of contained 24 PD patients and 25 MHCs as one participant from the MHC group did not have diffusion data that covered the cerebellum (Table 5.1).

Table 5.1 Demographics of the participants for the cerebellar analyses

	PD (n=24)	MHC (n=25)	Analyses
Age	63.42 ± 10.82	64.84 ± 8.22	P = 0.6065, Two sample t-test
Sex (M:F)	22:2	16:9	P = 0.0203, Chi squared test
H & Y Stage	1.75 ± 0.47	NA	-
MOCA	26.54 ± 2.01	NA	-
LEDD (mg)	537.64 ± 340.69	NA	-

Abbreviations: MOCA –The Montreal Cognitive Assessment; H & Y - Hoehn & Yahr Stage; LEDD – Levodopa Equivalent Daily Dose; PD - Parkinson's disease patients; MHC – Matched Healthy Controls; M - Male; F - Female; R – Right; L - Left

5.4.2 Reconstruction of the major cerebellar pathways

5.4.2.1 Middle cerebellar peduncle (MCP)

For the reconstruction of the MCP, AND regions were drawn around the pons on a coronal slice on both hemispheres as shown in (Figure 5.1, A). Appropriate NOT regions were drawn to eliminate any erroneous fibres. The MCP of a representative participant on axial and sagittal slices of a T1 anatomical image is shown in (Figure 5.1, B and C), respectively. The anatomical accuracy of the MCP was checked by making sure that the tract connected the two cerebellar hemispheres and did not have tract projections towards the cortex or the lower part of the brainstem.

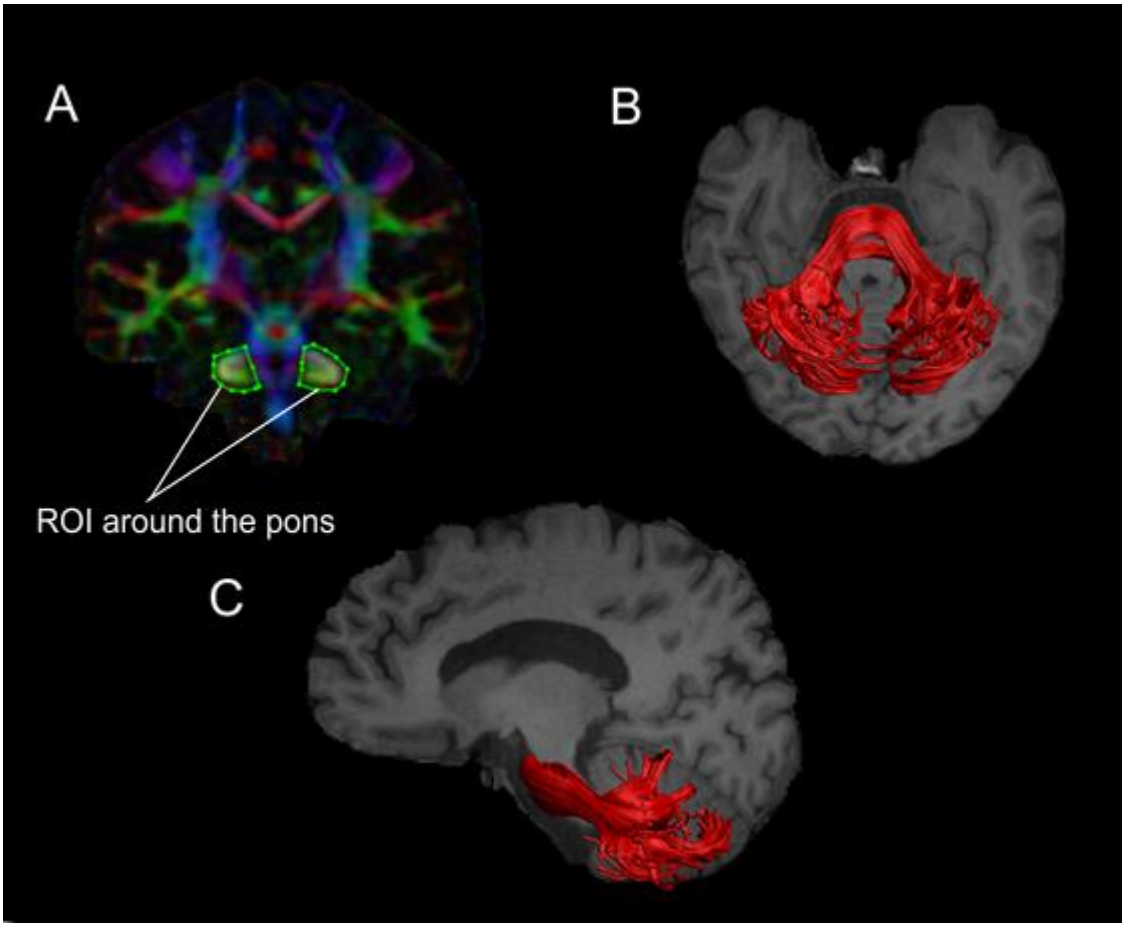

Figure 5.1 Reconstruction of the Middle Cerebellar Peduncle (MCP).

The figure shows the AND region around the pons in green in a colour-coded fibre orientation image (A) of a representative participant for reconstruction of the MCP. The MCP on a T1 image of a representative participant is shown in axial (B) and sagittal (C) views, respectively.

5.4.2.2 Superior cerebellar peduncle (SCP)

The SCP was identified in the coronal plane of a colour-coded fibre orientation image, the AND region was drawn around the SCP (visible as a small light blue structure) as shown in (Figure 5.2, A). Additionally, two large NOT regions were drawn above (Figure 5.2, Red ROI 1) and in front of the fornix (Figure 5.2, Red ROI 2), to remove tracts going to the frontal and cortical regions. Two more NOT regions were drawn, one NOT region at longitudinal fissure to cut fibres that cross into the other hemisphere (Figure 5.2, Red ROI 3) and another to cut fibres that go into the brain stem (Figure 5.2, Red ROI 4). This procedure was repeated for both hemispheres separately. The SCP of a representative participant in sagittal and coronal views is shown in (Figure 5.2, A and B), respectively.

The anatomical accuracy for the reconstruction of the SCP was checked by making sure the ROIs were placed as described above in each hemisphere and that the resulting tract did not have any unwanted fibres going towards the cortex or the brain stem.

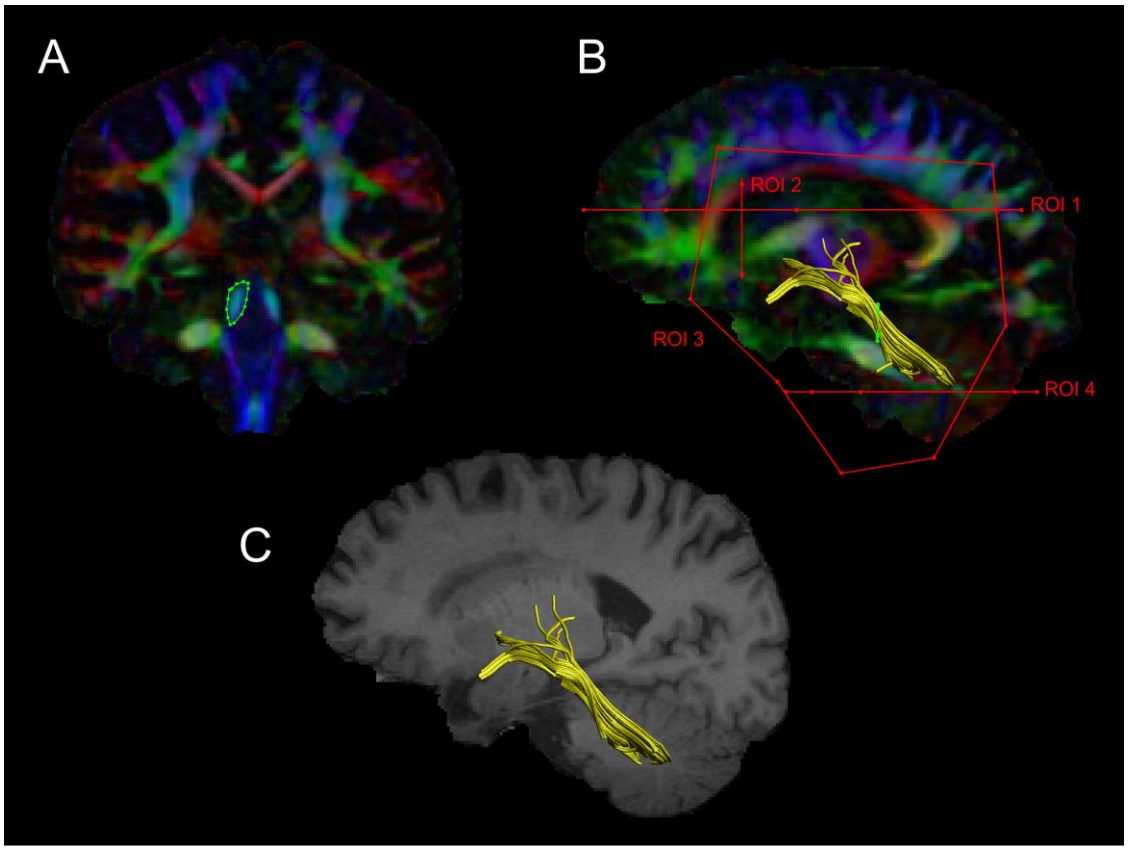

Figure 5.2 Reconstruction of the Superior Cerebellar Peduncle (SCP).

The figure shows the AND region in green (A) and the NOT regions along with the reconstructed SCP in the colour-coded fibre orientation image (B) and the reconstructed SCP on a T1 image (C) of a representative participant. Red NOT regions, ROI 1 and ROI 2 were drawn above and in front of the fornix, ROI 3 at the longitudinal fissure and ROI 4 to cut fibres towards the brainstem.

5.4.2.3 Inferior cerebellar peduncle (ICP)

For the reconstruction of the ICP, the large NOT region (Red ROI 1, ROI 2 and ROI 3) from the SCP reconstruction were retained. In a colour-coded fibre orientation image, an AND region was drawn in the axial slice around the ICP (visible as the small light blue structure) located by moving up slices from the bottom of the brain where the medial lemniscus and cerebellar peduncle is visible (Figure 5.3, A). Another AND gate was drawn around the region (visible as the light green structure) located at approximately five slices above the first AND gate (Figure 5.3, B). The ICP ROI placement used here was previously described in (Catani *et al.* 2008). The ICP of a representative participant in sagittal views of a colour-coded fibre orientation image

and a T1 image are shown in (Figure 5.3, C and D), respectively. Anatomical accuracy for reconstruction of the ICP was checked by making sure the ROI were placed correctly in each hemisphere as described above and that the tract did not have any unwanted fibres towards the other hemisphere or the cortical regions.

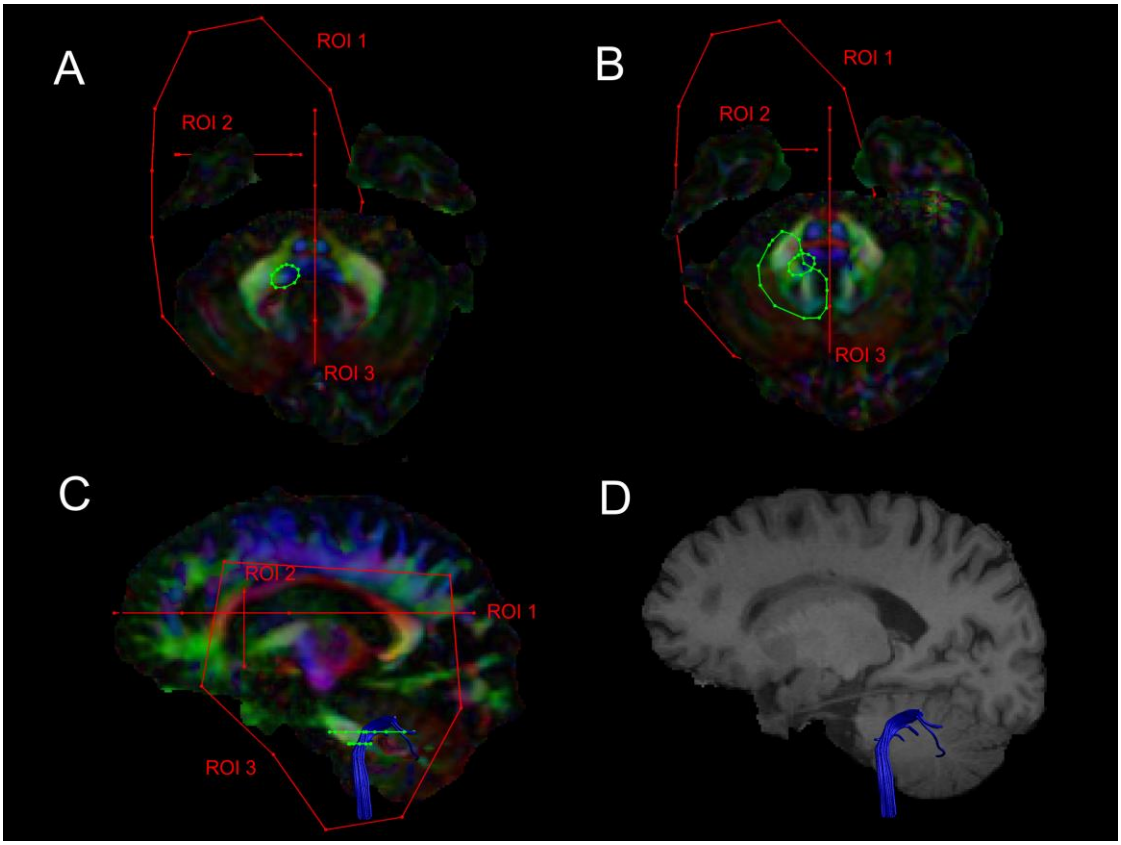

Figure 5.3 Reconstruction of the Inferior Cerebellar Peduncle (ICP).

The figure shows the first AND region (A), second AND region (B), the three retained NOT regions along with a reconstructed ICP tract in a colour-coded fibre orientation image (C) and the reconstructed ICP in a T1 anatomical image (D) of a representative participant. Red NOT regions, ROI 1 and ROI 2 were drawn above and in front of the fornix and final ROI 3 at the longitudinal fissure.

Each reconstructed tract was visually inspected and any obvious outlier streamlines that were not consistent with their known anatomy were excluded by drawing "NOT" regions and the entire reconstruction procedure was performed separately in the left and right hemispheres for the left and right SCP and ICP, respectively.

5.4.2.4 DRTT and SPCT

The full protocol for reconstruction of the DRTT and the SPCT is described in Chapter 4. The reconstructed DRTT and SPCT also included their cortical projections and here they were then segmented using the Splitter tracts tool within ExploreDTI4.8.3. The splitter tracts tool is used to segment portions of a reconstructed tract by drawing SEED

and AND ROIs to specify the location of segmentation. This was used here to include only the portion of the DRTT between the dentate nucleus and the thalamus, and portion of the SPCT from the subthalamic nucleus to the cerebellum for extracting the diffusion metrics from these tracts. The number of DRTTs and SPCTs successfully reconstructed in the PD and MHC groups are shown in Chapter 4 (Table 4.1). A representative segmented DRTT and SPCT with the ROIs are shown in Figure 5.4.

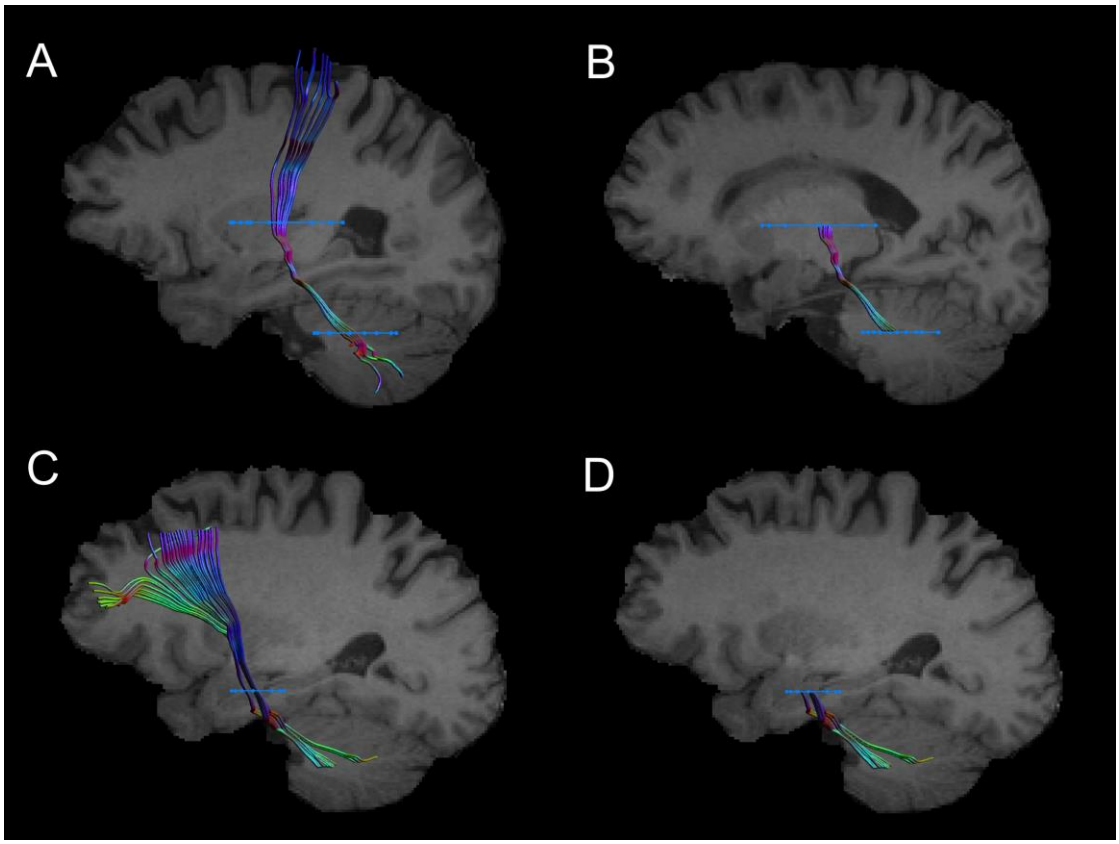

Figure 5.4 Reconstructed full and segmented DRTT and SPCT.

The reconstructed DRTT with its cortical projections is shown in A and the segmented DRTT is shown in B along with the ROIs at the level of the thalamus and the dentate nucleus. The fully reconstructed SPCT with its cortical connections is shown in C and the segmented SPCT is shown in D along with the ROI at the level of the sub-thalamic nucleus.

5.4.3 Statistical Analysis

All statistical analyses were carried out in the R statistical software v3.0.0 (R Core Team 2014). Before data analysis, all variables were checked for Gaussian distribution using the Shapiro-Wilk test ($p < 0.05$) and visually assessed using the histogram function and appropriate transformations were performed as required. The data was checked for outliers and homogeneity of variance using the Levene's test within R statistical software's car package (R Core Team 2014).

To assess the microstructural differences, multivariate covariate analyses of variance (MANCOVAs) were performed for the major cerebellar tracts (MCP, left SCP, right SCP, right ICP, left ICP) with FA, MD, AD, RD and HMOA as dependent variables and group (PD and MHC) as independent variable, along with age and gender as covariates. All significant results ($p<0.05$) were further analysed using post-hoc univariate ANOVAs corrected for multiple comparisons using FDR correction.

Separate MANCOVAs were also performed for the basal ganglia – cerebellar tracts (left DRTT, right DRTT, left SPCT, right SPCT) and all significant results ($p<0.05$) were further analysed using post-hoc univariate ANOVAs corrected for multiple comparisons using FDR correction.

Post-hoc correlations were also performed in the PD group between the metrics and the tracts that showed significant group differences and the following clinical and behavioural measures: off medication baseline Unified Parkinson's Disease Rating Scale (UPDRS) scores, duration since diagnosis (in months), scores from a standard finger tapping task and a four button finger sequence task measuring the correct number of responses and reaction time.

Additionally, I performed analysis to investigate the macrostructural differences (the average tract volumes) in the main cerebellar tracts between PD patients and the MHCs (See Chapter 5 supplementary material for full details)

5.5 Results

5.5.1 Microstructural differences

Results from the MANCOVAs (Table 5.2) showed significant group effects for the right SCP ($F(5,41) = 3.24$, Pillai's trace = 0.28, $p = 0.0147$), the right ICP ($F(5,41) = 4.22$, Pillai's trace = 0.34, $p = 0.0034$) and the left ICP ($F(5,41) = 2.72$, Pillai's trace = 0.25, $p = 0.032$).

Table 5.2 Results from the MANCOVAs for the main cerebellar tracts

Tract		MHC (n=25) vs PD (n=24)		
		F statistic	Pillai's trace	p-value
Middle Cerebellar Peduncle				
	Group	F(5,41)=1.32	0.14	0.27523
	Age	F(5,41)=2.26	0.22	0.06598
	Gender	F(5,41)=0.83	0.09	0.53914
Left Superior Cerebellar Peduncle				
	Group	F(5,41)=1.47	0.15	0.2223
	Age	F(5,41)=1.58	0.16	0.1876
	Gender	F(5,41)=1.03	0.11	0.4126
Right Superior Cerebellar Peduncle				
	Group	F(5,41)=3.24	0.28	0.014787
	Age	F(5,41)=5.56	0.40	0.000535
	Gender	F(5,41)=1.29	0.14	0.288652
Left Inferior Cerebellar Peduncle				
	Group	F(5,41)=2.72	0.25	0.03274
	Age	F(5,41)=1.30	0.14	0.28192
	Gender	F(5,41)=1.19	0.13	0.33141
Right Inferior Cerebellar Peduncle				
	Group	F(5,41)=4.22	0.34	0.003465
	Age	F(5,41)=2.06	0.20	0.090584
	Gender	F(5,41)=0.65	0.07	0.661444

MHC – Matched healthy controls, PD - Parkinson's disease patients

Results from the post-hoc ANCOVAs (Table 5.3) of these three tracts showed significantly increased FA in the PD patients compared to MHCs in the right SCP (0.44 ± 0.020 [MHC, mean±SD], 0.46 ± 0.029 [PD, mean±sd], $F(3,45) = 10.89$, FDR corrected p-value = 0.014), right ICP (0.43 ± 0.030 [MHC, mean±sd], 0.45 ± 0.027

[PD, mean±sd], F(1,47) = 8.23, FDR corrected p-value = 0.031) and significantly increased HMOA in the PD patients compared to MHCs in the right SCP (0.17 ± 0.013 [MHC, mean±sd], 0.19 ± 0.019 [PD, mean±sd], F(3,45) = 11.03, FDR corrected p-value = 0.014).

Table 5.3 Post-hoc ANCOVAs for the main cerebellar tracts

Tract		**MHC (n=25) vs Session 1 PD (n=24)**	
		F statistic	Uncorrected p-value
Left Superior Cerebellar Peduncle			
FA	Group	2.236	0.14181
	Age	3.8201	0.05687
	Gender	3.1594	0.08225
MD	Group	1.5827	0.21486
	Age	3.2599	0.07768
	Gender	0.1308	0.71935
RD	Group	3.8497	0.05596
	Age	0.588	0.44721
	Gender	1.0659	0.30739
AD	Group	0.0456	0.83185
	Age	5.754	0.02066
	Gender	0.1733	0.67915
HMOA	Group	6.4048	0.01495
	Age	0.1551	0.69557
	Gender	1.6853	0.20084
Right Superior Cerebellar Peduncle			
FA	Group	10.899	0.001889
	Age	11.1258	0.001713
	Gender	4.2952	0.043979
MD	Group	0.0725	0.789
	Age	2.3568	0.1317
	Gender	0.6415	0.4274
RD	Group	2.4664	0.1233
	Age	0.0044	0.9475
	Gender	1.8768	0.1775
AD	Group	2.4923	0.121409
	Age	10.5162	0.002232
	Gender	0.0216	0.883797
HMOA	Group	11.031	0.001785
	Age	0.6467	0.425515

	Gender	3.3324	0.07457
Right Inferior Cerebellar Peduncle			
FA	Group	8.2384	0.006229
	Age	1.0264	0.316422
	Gender	0.3943	0.533245
MD	Group	1.3385	0.2534
	Age	0.3654	0.5486
	Gender	1.3473	0.2519
RD	Group	6.2952	0.01578
	Age	0.2136	0.64616
	Gender	2.0705	0.15709
AD	Group	0.0806	0.7778
	Age	0.4236	0.5185
	Gender	0.5333	0.469
HMOA	Group	5.6614	0.02164
	Age	0.0786	0.78055
	Gender	0.4186	0.52094

MHC – Matched healthy controls, PD - Parkinson's disease patients, FA – Fractional anisotropy, MD – Mean diffusivity, RD – Radial diffusivity, AD – Axial diffusivity, HMOA – Hindrance Modulated orientational anisotropy

The correlation analyses and the separate MANCOVAs for the DRTT and SPCT tracts did not show any significant results (see supplementary table 5.3 and supplementary table 5.4).

5.6 Discussion

Patients with early stage PD relative to matched healthy controls showed increased FA in the right superior and right inferior cerebellar peduncles and increased HMOA in the right superior cerebellar peduncles. However, there were no significant differences in the basal ganglia-cerebellar connections of the dentato-rubro-thalamic tracts and the subthalamo-ponto-cerebellar tracts between the PD patients and their matched controls. Additionally, there were no significant correlations between any of the diffusion metrics in the cerebellar tracts and the clinical and behavioural measures in the PD group.

5.6.1 Increased FA in the Right SCP and Right ICP

The current increased FA findings are consistent with our previous finding of increased FA in the motor tracts i.e., the bilateral corticospinal tract (right; corrected $p = 0.0003$, left; corrected $p = 0.03$), bilateral thalamus-motor cortex tract (right; corrected $p = 0.02$, left; corrected $p = 0.004$) and the right supplementary area-putamen tract (corrected $p = 0.001$) compared to non-motor tracts in PD patients as demonstrated in Chapter 3. This could be due to potential compensatory and/or selective neurodegenerative mechanisms in the motor pathways that occur at pre-symptomatic stages of the disease (Mole *et al.* 2016). The current findings of increased FA in the right SCP and the right ICP oppose the several findings from previous studies. One study reported decreased FA in the entire white matter of the cerebellar hemispheres in PD patients suggesting damaged white matter microstructure (Mormina *et al.* 2015). Another study found decreased FA and increased MD in PD cerebellum and a positive correlation with the decrease in FA and thresholds of olfactory identification (K. Zhang *et al.* 2011); however, there were no measures of olfaction available within the current PD cohort to explore similar correlations. Previous studies have also reported no significant FA alterations in the SCP and the MCP (Nicoletti *et al.* 2006; Nicoletti *et al.* 2008; Wang *et al.* 2011; Rizzo *et al.* 2008; Blain *et al.* 2006; Nicoletti *et al.* 2013).

Interpreting the results in the literature in context of our current results is challenging due to the various differences in methodology, processing and analysis of the diffusion data. In addition all the aforementioned studies used whole brain voxel based or region of interest based analysis rather than a priori selection of individual tracts. Taking all this into context with the current results, the specific increase in FA in just the input

and output from the cerebellum (ICP and SCP) might be either be related to compensatory mechanisms that help mask the disease during the pre-symptomatic stages but eventually fail as the pathological damage becomes severe (Jankovic 2005) or selective neurodegenerative processes that affect the different regions of the brain at different stages. Functional studies have showed task specific hyperactivation in the cerebellum during performance of finger sequence tasks and motor learning (Sen *et al.* 2010; Yu *et al.* 2007b). Previous functional MRI studies have demonstrated increased activation of the cerebellum in PD and interpreted this as early compensatory mechanism that seems to decrease as the disease progresses possibly due to cerebellar degeneration process (Yu *et al.* 2007a; Wu and Hallett 2013; Jankovic and Kapadia 2001). It was suggested that the cerebellar involvement might vary according to the various clinical stages of the disease. Therefore, in the preclinical stage, the cerebellum might be fully compensating for the loss in basal ganglia function, and later cerebellar compensation may reduce as the severity of the PD symptoms accumulates (Wu and Hallett 2013). One functional MRI study showed hyperactivation of the ipsilateral cerebellum in PD as a compensatory mechanism for defective basal ganglia motor controls signals (Yu *et al.* 2007a). There was also increased recruitment of the cerebello-thalamo-cortical circuit as the disease progresses suggesting its involvement in compensatory effects (Sen *et al.* 2010). The right lateralised effect in the current results may be due to the ipsilateral control of body movements in the cerebellum and its compensatory effects in PD as our PD cohort was predominately right-handed (Table 3.1). However, there were no FA differences between the affected vs unaffected hemisphere in the motor tracts and cerebellar tracts (See Table 3.6, Supplementary Table 3.2 and Supplementary Table 5.2).

5.6.2 Increased HMOA in the right SCP

There was significantly increased HMOA in the right SCP, left and right ICP, the MCP, the DRTTs, and the SPCTs. whereas in the current study there were no correlations between HMOA and PD patients' clinical and behavioural data. This in context with the current results could also suggest similar lateralised neuroanatomical compensation as there was statistically significant increase in the PD group's HMOA metric only in the right SCP but not in the other main cerebellar tracts or the basal ganglia-cerebellar pathways.

It has been shown that HMOA decreases with increasing radial diffusivity and axonal radius; thus, it is likely that increased myelination decreases HMOA (Tournier *et al.* 2004; Dell'Acqua *et al.* 2013). This could suggest that the current increased HMOA could be due to decreases in myelination in the right SCP which is the main output pathway from the cerebellum to the mid brain and also through which the DRTT leaves the cerebellum. While the HMOA index characterises microstructural properties of the specific white matter tract, it still depends on several white matter properties (as with FA). Therefore, despite the sensitivity of HMOA, it is influenced by myelination, axon density, axon diameter, and fibre dispersion, and is problematic to interpret it in way that a higher HMOA index explicitly means stronger connectivity (Dell'Acqua *et al.* 2013; Jones *et al.* 2013; Beaulieu 2002). Nevertheless, as HMOA is specific to the direction followed by tractography, this index measures how much water is diffusing in the tractography reconstruction direction independently of other directions and is therefore a true tract specific index, being less influenced by crossing fibres and partial volume effects (Dell'Acqua *et al.* 2013). Based on the results from the current data, I speculate that a higher HMOA index combined together with the higher FA in the same tract represents white matter microstructural alterations associated with compensatory mechanisms, rather than pathological or neurodegenerative processes in the PD cohort. Nevertheless no substantial conclusions can be drawn due to lack of HMOA correlations with clinical and behavioural measures in this cohort.

A direct comparison between the FA index from DTI tractography and the HMOA index from SD tractography models was performed to verify that SD provides unique and additive information especially in regions of crossing fibres (Vanderauwera *et al.* 2015). The FA model was more confounded by crossing fibres than the SD model, however there did not seem to be a direct influence of crossing fibres on the metrics as both the FA and HMOA were highly correlated. Nevertheless, the HMOA index seems to provide an advantage for the quantitative study of white matter changes over FA, as confirmed by simulation and inter-individual variability studies (Dell'Acqua *et al.* 2013; Christiansen *et al.* 2016; Chechlacz *et al.* 2015).

5.6.3 DRTT and SPCT

The microstructural measures from the DRTT and SPCT did not show any significant differences (Supplementary table 5.4) even though various studies have shown the

influence of cerebello-cortical circuits to have impact on PD (Sweet *et al.* 2014; Martinu and Monchi 2013). Both the basal ganglia and the cerebellum are known to influence activity in the cerebral cortices via the thalamus with their recurrent circuitry, known to affect motor, cognitive and affective behaviour (Alexander *et al.* 1986; Middleton and Strick 2000; Lewis *et al.* 2013). Outputs from basal ganglia and the cerebellum project to the ventro anterior and ventro lateral thalamic nuclei respectively with differential involvement in external and internal guided tasks (Middleton and Strick 2000; MacMillan *et al.* 2004; Vaillancourt *et al.* 2003).

Since the motor symptoms in PD only occur after 50% of dopaminergic nigral cells and 60-80% of striatal dopamine levels are depleted (Fearnley and Lees 1991; Lee *et al.* 2000) and the lack of observed motor symptoms despite this cell loss indicates redundant and compensatory mechanisms that may be preserving optimal level of motor function (Zigmond *et al.* 1990; Bezard *et al.* 2001). One possible compensatory mechanism for the generation of movement in PD has been suggested as the recruitment of cortico-cerebellar networks (Martinu and Monchi 2013; Rascol *et al.* 1997; Palmer *et al.* 2009).

In a study that explored the neurofunctional basis of externally and internally guided movements in PD patients, there was increased signal in the cerebellum, putamen, supplementary motor area and the thalamus during the externally guided task (Cerasa *et al.* 2006). Another study showed that increased cerebello-thalamo-cortical activity could reflect compensation for breakdown of the striato-thalamo-cortical pathway to successfully perform internally guided task (Sen *et al.* 2010). They could not definitively delineate between compensatory and/or pathological processes so they suggested that this could be due to disease progression in PD as the patients transitioned from unilateral to bilateral symptoms therefore (Sen *et al.* 2010). From these previous studies it is clear that the cerebellum plays a role in compensation and symptomology in PD.

The DRTT has been shown to play an important role in the PD symptoms as placing a Deep Brain Stimulation (DBS) contact at close proximity to the DRTT has been shown to be efficient in relieving symptoms especially the tremor (Sweet *et al.* 2014). This suggests that the tract may be a more suitable target to be stimulated by DBS and may hence lead to better therapeutic outcomes in PD. Differences in cerebellar activity may

be considered a pathological mechanism related to basal ganglia dysfunction, or a compensatory mechanism. The nature of the cerebellar involvement is complex and is likely influenced by dopamine, patient subtypes, and the particular symptom or function assessed. Lastly, given that PD is largely heterogeneous in nature, a combined approach would help clarify whether particular symptoms of PD are mediated by particular white matter pathways. Ultimately, this could lead to stronger conclusions regarding whether the cerebellum plays a pathological role driven by striatal dysfunction or a compensatory role to overcome striatal dysfunction.

5.6.4 Limitations and future directions

There were no significant correlations between the diffusion metrics and the clinical and behavioural data from the clinical PD data. This is very likely due to the limited sample size which could also be why we do not see any significant correlations in our sample of 24 PD patients and 25 healthy controls as well. This is based on previous studies that report smaller sample sizes as limitations for correlational analyses in PD (Mischley *et al.* 2017; Heinzel *et al.* 2016). Any results observed from such correlations should be interpreted with caution and further validation assessments would still be needed (Mokkink *et al.* 2010).

The current results also show asymmetry and right lateralised significant effects in HMOA and FA which are in line with previous studies showing that the asymmetry of white matter pathways varies across different diffusion MRI derived measures (De Santis *et al.* 2014). One study found that the HMOA and the tract volume differentially contributed to the anatomical lateralization of frontoparietal attention networks and individual differences in attention, but did not find any correlations (Chechlacz *et al.* 2015). They attributed this to large number of right-handed participants which may also be the case for our current PD cohort (Table 3.1).

It should be noted that the HMOA is estimated based on several white matter characteristics, including myelination, axon density, axon diameter, and fibre dispersion with each factor contributing differentially to HMOA (Dell'Acqua *et al.* 2013). Therefore, interpreting that higher HMOA is equivalent to higher connectivity should be avoided (Beaulieu 2002; Jones *et al.* 2013; Dell'Acqua *et al.* 2013).

The current knowledge of the role of cerebellum in PD is limited. Future studies that can ascertain the specific degenerative and/or compensatory effects in cerebellum are

required to better understand its contribution to the disease and also to inform better treatments and interventions. Furthermore, investigation of the white matter connections between the basal ganglia and the cerebellum in a larger sample of PD data is warranted.

5.7 Conclusion

In summary, this is the first study to explore the microstructural differences in the main cerebellar pathways and the two basal-ganglia cerebellar connections between PD patients and matched healthy controls. I found increased FA in the superior and inferior cerebellar peduncles and increased HMOA in the superior cerebellar peduncle. This shows that the cerebellar input and output connections are altered in PD, however future studies that explicitly probe the functions of the cerebellum would help to shed light onto the specific contributions of the white matter connections in PD.

Chapter 6 General discussion

6.1 Summary of findings

The work described in this thesis utilised diffusion tractography methods to explore selected white matter connections of the basal ganglia circuitry to increase our understanding of the underlying pathophysiology in PD.

As PD is clinically classified as a motor disorder affecting the basal ganglia circuitry, it was of particular interest to explore the basal ganglia white matter motor connections in PD. Therefore in Chapter 3, I investigated for the first time the differences in diffusion metrics in selected motor tracts of the basal ganglia circuitry; Corticospinal tract (CST), and the white matter connections between the supplementary motor area-putamen (SMA-PUT) and the thalamus-motor cortex (THAL-MC), and selected non-motor tracts; uncinate fasiculus (UNF), supero-lateral medial forebrain bundle (slMFB) in PD. Increased FA was found in all the basal ganglia motor tracts while there was decreased FA in the UNF and no differences in the slMFB. Additionally, I also investigated differences in subcortical volumes between PD patients and MHCs and found no such volumes differences.

Furthermore, it was found that the basal ganglia and the cerebellum have direct anatomical connections between them via the denato-rubto-thalamic tract (DRTT) and the subthalamo-ponto-cerebellar tract (SPCT) and these connections had not been anatomically well defined in humans. Therefore in Chapter 4, I developed an anatomically guided tractography protocol to reconstruct the DRTT and the SPCT and demonstrated feasibility of transferring this protocol to reconstruct these tracts in a cohort of PD patients. And for the first time, I also assess the spatial independence and map the cortical connections of these tracts in humans.

Recent evidence show the involvement of the cerebellum in PD, and that the non-motor symptoms of the disease in most cases precede the motor symptoms. This in addition to the reconstructed basal ganglia-cerebellar connections from Chapter 4 provided the opportunity and rationale for investigation of these tracts and the main cerebellar pathways (the middle, inferior and superior cerebellar peduncles) in PD. Hence in Chapter 5, I investigated the differences in diffusion metrics in the main cerebellar pathways and the two basal ganglia-cerebellar connections and found increased FA in the superior and inferior cerebellar peduncles and increased HMOA in the superior cerebellar peduncle.

Overall, the results of increased FA in the motor and cerebellar tracts in PD suggest that the basal ganglia motor pathways and the cerebellar input and output connections are altered in PD. These alterations may suggest selective neurodegeneration due to consequences of the disease or compensation along these pathways due to extended and adaptive neuroplasticity. Using the developed anatomical protocol, one can now reconstruct and study the DRTT and the SPCT from data that is routinely obtained in clinical research studies.

Together, the findings highlight the importance of white matter connections of the basal ganglia circuitry and their connections with the cerebellum in PD. The novel findings support the involvement of structures such as the putamen, thalamus, SMA, dentate nucleus, subthalamic nucleus and the motor cortex through their white matter interconnections. Although there were no significant results from the correlational analyses within this thesis, one can still see that the tracts of interest showed marked changes in the diffusion metrics indicating their involvement in compensatory and neurodegenerative process within the disease. This suggests that a better understanding of PD at the level of brain circuitry can be derived by not just studying the individual grey matter structures but also studying the interconnections among them in brain imaging studies but also in post-mortem brains, cellular models and mechanistic models of the disease.

The individual white matter connections investigated here offer patient/participant specific, brain region specific as well as symptom specific results that show motor symptoms in PD may progress differently compared to non-motor symptoms and their involved structures may also undergo very specific changes, respectively. The study methodology to delineate the white matter connections of interest manually is also very important for instance in deep brain simulation surgery for PD. The method used within this thesis for detecting individual differences in brain specific areas is also important for instance in stroke patients. This also shows that group average and automated atlas based studies may limit detecting true differences due to averaging of voxels across participants. Replicating the findings from this thesis in these white matter connections in larger databases with more clinical and behavioural information can help unravel the exact aetiology of PD and thereby enable the research community to get a step closer to finding therapeutic interventions that delay disease progression.

Results from this thesis now provide the background and foundation for future studies in PD that explicitly probe the functions of these specific white matter connections, their correlation with clinical and behavioural measures as well as their functions in healthy and diseased states. Moreover, the developed anatomical protocol for delineation of the DRTT and SPCT not only suggests the importance of studying grey matter structures such as the cerebellum and the basal ganglia as a whole but also the importance of their sub-structures such as the dentate nucleus, the putamen and the thalamus as well as the exploration of their white matter interconnections in PD.

6.2 Limitations and future research in PD

Several methodological considerations were needed to be taken to avoid misinterpretation of results. Diffusion metrics though sensitive to underlying changes in white matter microstructure are not specific to change in any particular component of white matter microstructure or specific biological mechanism. Both the FA and the HMOA metrics are estimated based on several white matter characteristics, including myelination, axon density, axon diameter, and fibre dispersion with each factor contributing differentially to FA and HMOA (Dell'Acqua *et al.* 2013). Therefore, interpreting higher FA and higher HMOA as higher connectivity or stronger/healthier white matter connections should be avoided (Beaulieu 2002; Jones *et al.* 2013; Dell'Acqua *et al.* 2013). To better understand and delineate the specific contributions of axonal microstructural changes and myelination changes in the white matter architecture in PD, future studies could apply complex diffusion microstructural models such as Composite Hindered and Restricted Model of Diffusion (CHARMED) or AxCaliber (Assaf 2008; Assaf and Basser 2005). Myelin water fraction mapping and quantitative magnetization transfer techniques could also be used in future studies to better quantify myelination (Levesque *et al.* 2010).

There were no significant correlations between the diffusion metrics and the clinical and behavioural data from the clinical PD data, making it very difficult to interpret the increased FA results in the PD cohort. This is very likely due to the limited sample size of 24 PD patients. Therefore, it would also be of particular interest to investigate the connections between the basal ganglia and the cerebellum in a larger sample of PD data, as current data may have been under sampled to detect any significant differences in these pathways.

Future studies that explicitly probe the functions of the cerebellum and the cerebellar pathways would help to shed light into the specific contribution of cerebellar white matter in PD. Tractography analysis should be incorporated in future longitudinal imaging studies in PD to evaluate the specific role of white matter changes in neurodegenerative and neuroplastic processes as the disease progresses. I propose to do by this investigating these connections from a larger dataset of PD and healthy controls from the Parkinson's Progression Marker's Initiative (PPMI) database (PPMI 2011). This study would be performed in an attempt to replicate the current findings in this thesis. This would not only give us more power to detect differences but also look at longitudinal data that may help provide further information.

Although PD is clinically diagnosed based on the presence of motor signs, it is now recognised that this is preceded by significant neurodegeneration and compensatory neuroplasticity within and outside the basal ganglia (Bezard *et al.* 2003) which is also reflected in alterations in white matter connections in early PD as reported in this thesis (Mole *et al.* 2016). The prodromal phase of PD may be present for over a decade before clinical diagnosis. Although symptomatic treatment exists, clinical studies mainly depend on motor clinical markers and there is of lack disease modifying or curative therapies for PD. Therefore identifying markers during prodromal PD could identify patients earlier and enable the development of high impact interventions and prophylactic treatments that help prevent clinical PD. I propose to evaluate imaging biomarkers of disease progression in patients with REM-sleep behaviour disorder (RBD). RBD is the strongest clinical marker for prodromal PD (Postuma and Berg 2016) and over 80% of patients with RBD develop neurodegenerative disease within 10 years (PD, Dementia with Lewy bodies or Multiple System Atrophy) (Boeve *et al.* 2013). This also constitutes a potential for longitudinal studies of disease progression as RBD to PD conversion is ~10% per year hence the number of PD identified from a cohort of 50 patients with RBDs followed up for five years would further the understanding of transition from prodromal to the clinical motor phase.

Future studies should also attempt to delineate the compensatory changes and the disease pathology related changes in PD. For instance, one could use behavioural tests that require patients to perform tasks that are challenging for them or tasks that increase in difficulty. The assumption is that there would be no change or improvement in the performance of the task if it is disease pathology related but if the performance is

maintain and/or improved this could be due to compensatory mechanisms that are in place.

Further advances in the development of higher order diffusion models as well as of techniques that can target specific microstructural properties could help to further increase the understanding of the contribution that white matter microstructure plays in PD. However, the advanced and higher order diffusion models will have to be researched in healthy developing and healthy aging brain to provide better interpretation of the extracted metrics in diseased states.

6.3 Wider clinical relevance of investigated BG white matter connections

The investigated tracts within this thesis have clinical importance and relevance in a wide range of disorders and in understanding healthy developing and aging human brain (Zhao *et al.* 2016; Callaghan *et al.* 2014; Metzler-Baddeley *et al.* 2011; Inuggi *et al.* 2011; Christiansen *et al.* 2016). Detailed knowledge of the anatomy of the basal ganglia circuitry in humans would not only be important in understanding the pathophysiology of neurological and neurodegenerative disorders such as Parkinson's disease, Huntington's disease, Progressive supranuclear palsy, Wilson's disease, Fahr's disease and Gilles de la Tourette's syndrome (Worbe *et al.* 2015; van Wassenaer-van Hall *et al.* 1995; Phillips *et al.* 2014; DeLong 1990; Surova *et al.* 2015; Nicoletti *et al.* 2013) but also identification of changes in these tracts in neurodegenerative and movement disorders (Jeong *et al.* 2012; Jang and Kwon 2015; Surova *et al.* 2015).

The basal ganglia circuitry is also involved in neuropsychiatric disorders such as Schizophrenia, Bipolar disorder, Obsessive-compulsive disorder, depression and addiction (Ring 2002; Middleton and Strick 2000; Dirnberger and Jahanshahi 2013; Obeso, Rodríguez-Oroz, *et al.* 2008). The basal ganglia circuitry is thus not only involved in motor functions and implicated in their impairment but also in different levels of non-motor and cognitive impairment as well as varying degrees of non-motor signs and symptoms. Clinical and research applications include anatomical localisation for deep brain stimulation (Sweet *et al.* 2014; Coenen *et al.* 2015; Hana *et al.* 2016; Fenoy *et al.* 2017; Anthofer *et al.* 2017; Hacker *et al.* 2015; Torres *et al.* 2014; Rodriguez *et al.* 1998; Calabrese *et al.* 2015) and tractography guided surgery (Torres *et al.* 2014; Parraga *et al.* 2016; Papagno *et al.* 2011; Linhares and Tasker 2000; Coenen *et al.* 2011; Feigl *et al.* 2014).

6.4 Conclusion

In conclusion, this thesis demonstrates that white matter connections of the basal ganglia motor system and the cerebellar system are involved in Parkinson's disease. The microstructural differences observed could be due to compensation and/or disease pathology related. This warrants the need for future cross-sectional and longitudinal imaging studies with tractography analysis that explicitly probe the functions of the basal ganglia and cerebellum in PD.

Furthermore, future studies that study the specific motor and non-motor white matter connections in Parkinson's as well as the connections between the basal ganglia and the cerebellum need to be investigated at a much higher resolution using novel diffusion and brain imaging techniques. This would shed light into the specific role of white matter changes in the neurodegenerative and neuroplastic processes.

Studying the underlying structural connections of the basal ganglia with the cortex in humans within the context of the basal ganglia circuitry and the connections between the basal ganglia and the cerebellum and exploring their functions in relation to heath and disease would better our understanding of a wide range of disorders.

This thesis not only demonstrates the importance and novelty of studying individual white matter connections in PD within the basal ganglia circuitry in order to understand the underlying pathophysiology but also the importance of these individual connections for surgical procedures such as DBS and therefore their contribution to effective and timely treatment strategies and novel therapies for rehabilitation.

Chapter 7 References

Abbott, R.D., Ross, G.W., Petrovitch, H., Tanner, C.M., Davis, D.G., Masaki, K.H., Launer, L.J., *et al.* (2007). Bowel movement frequency in late-life and incidental lewy bodies. *Movement Disorders* **22**:1581–1586.

Abdo, W.F., van de Warrenburg, B.P.C., Burn, D.J., Quinn, N.P. and Bloem, B.R. (2010). The clinical approach to movement disorders. *Nature Reviews Neurology* **6**:29–37.

Akkal, D., Dum, R.P. and Strick, P.L. (2007). Supplementary motor area and presupplementary motor area: targets of basal ganglia and cerebellar output. *J Neurosci* **27**:10659–10673.

Albin, R.L., Young, A.B. and Penney, J.B. (1989). The functional anatomy of basal ganglia disorders. *Trends in Neurosciences* **12**:366–375.

Alexander, D.C. (2013). An Introduction to Computational Diffusion MRI: The Diffusion Tensor and Beyond. In: *Visualization and Processing of Tensor Fields*. pp. 83–106.

Alexander, G.E. (1987). Selective neuronal discharge in monkey putamen reflects intended direction of planned limb movements. *Exp Brain Res* **67**:623–634.

Alexander, G.E. and Crutcher, M.D. (1990). Functional architecture of basal ganglia circuits: neural substrates of parallel processing. *Trends in Neurosciences* **13**:266–71.

Alexander, G.E. and DeLong, M.R. (1985). Microstimulation of the primate neostriatum. II. Somatotopic organization of striatal microexcitable zones and their relation to neuronal response properties. *J Neurophysiol* **53**:1417–1430.

Alexander, G.E., DeLong, M.R. and Delong, R. (1985). Microstimulation of the primate neostriatum. I. Physiological properties of striatal microexcitable zones. *J Neurophysiol* **53**:1401–1416.

Alexander, G.E., DeLong, M.R. and Strick, P.L. (1986). Parallel organization of functionally segregated circuits linking basal ganglia and cortex. *Annu Rev Neurosci* **9**:357–381.

Allen, G.I. and Tsukahara, N. (1974). Cerebrocerebellar communication systems. *Physiol Rev* **54**:957–1006.

Andalib, S., Vafaee, M.S. and Gjedde, A. (2014). Parkinson's disease and mitochondrial gene variations: A review. *J Neurol Sci* **346**:11–19.

Anderson, A.W. (2005). Measurement of fiber orientation distributions using high angular resolution diffusion imaging. *Magnetic resonance in medicine* **54**:1194–1206.

Andersson, J.L.R., Jenkinson, M. and Smith, S.M. (2010). Non-linear registration, aka spatial normalisation: FMRIB technical report TR07JA2.

Andrews, C.J., Burke, D. and Lance, J.W. (1972). The response to muscle stretch and shortening in parkinsonian rigidity. *Brain* **95**:795–812.

Anthofer, J.M., Steib, K., Lange, M., Rothenfusser, E., Fellner, C., Brawanski, A. and Schlaier, J. (2017). Distance between Active Electrode Contacts and Dentatorubrothalamic Tract in Patients with Habituation of Stimulation Effect of Deep Brain Stimulation in Essential Tremor. *J Neurol Surg A Cent Eur Neurosurg* **78**:350–357.

Arkadir, D., Bergman, H. and Fahn, S. (2014). Redundant dopaminergic activity may enable compensatory axonal sprouting in Parkinson disease. *Neurology* **82**:1093–1098.

Assaf, Y. (2008). Can we use diffusion MRI as a bio-marker of neurodegenerative processes? *Bioessays* **30**:1235–1245.

Assaf, Y. and Basser, P.J. (2005). Composite hindered and restricted model of diffusion (CHARMED) MR imaging of the human brain. *NeuroImage* **27**:48–58.

Assaf, Y. and Pasternak, O. (2008). Diffusion Tensor Imaging (DTI)-based White Matter Mapping in Brain Research: A Review. *Journal of Molecular Neuroscience* **34**:51–61.

Balsters, J.H., Laird, A.R., Fox, P.T. and Eickhoff, S.B. (2014). Bridging the gap between functional and anatomical features of cortico-cerebellar circuits using meta-analytic connectivity modeling. *Human brain mapping* **35**:3152–3169.

Balsters, J.H. and Ramnani, N. (2011). Cerebellar plasticity and the automation of first-order rules. *The Journal of neuroscience : the official journal of the Society for Neuroscience* **31**:2305–2312.

Basser, P.J., Mattiello, J. and LeBihan, D. (1994). Estimation of the effective self-diffusion tensor from the NMR spin echo. *J Magn Reson B* **103**:247–254.

Basser, P.J., Pajevic, S., Pierpaoli, C., Duda, J. and Aldroubi, A. (2000). In vivo fiber tractography using DT-MRI data. *Magn Reson Med* **44**:625–632.

Beach, T.G., Adler, C.H., Lue, L.F., Sue, L.I., Bachalakuri, J., Henry-Watson, J., Sasse, J., *et al.* (2009). Unified staging system for Lewy body disorders: Correlation with nigrostriatal degeneration, cognitive impairment and motor dysfunction. *Acta Neuropathologica* **117**:613–34.

Beach, T.G., White, C.L., Hladik, C.L., Sabbagh, M.N., Connor, D.J., Shill, H.A., Sue, L.I., *et al.* (2009). Olfactory bulb α-synucleinopathy has high specificity and sensitivity for Lewy body disorders. *Acta Neuropathologica* **117**:169–174.

Beaulieu, C. (2002). The basis of anisotropic water diffusion in the nervous system – a technical review. *NMR in Biomedicine* **15**:435–455.

Behrens, T.E., Woolrich, M.W., Jenkinson, M., Johansen-Berg, H., Nunes, R.G., Clare, S., Matthews, P.M., *et al.* (2003). Characterization and propagation of uncertainty in diffusion-weighted MR imaging. *Magn Reson Med* **50**:1077–1088.

Benamer, H.T.S., Patterson, J., Wyper, D.J., Hadley, D.M., Macphee, G.J.A. and Grosset, D.G. (2000). Correlation of Parkinson's disease severity and duration with 123I-FP-CIT SPECT striatal uptake. *Movement Disorders* **15**:692–698.

Benninger, D.H., Thees, S., Kollias, S.S., Bassetti, C.L. and Waldvogel, D. (2009). Morphological differences in Parkinson's disease with and without rest tremor. *Journal of neurology* **256**:256–263.

Bergman, H., Wichmann, T. and DeLong, M. (1990). Reversal of experimental parkinsonism by lesions of the subthalamic nucleus. *Science* **249**:1436–1438.

Bernheimer, H., Birkmayer, W., Hornykiewicz, O., Jellinger, K. and Seitelberger, F. (1973). Brain dopamine and the syndromes of Parkinson and Huntington Clinical, morphological and neurochemical correlations. *Journal of the Neurological Sciences* **20**:415–455.

Bevan, M.D., Magill, P.J., Terman, D., Bolam, J.P. and Wilson, C.J. (2002). Move to the rhythm: Oscillations in the subthalamic nucleus-external globus pallidus network. *Trends in Neurosciences* **25**:525–531.

Bezard, E., Crossman, A.R., Gross, C.E. and Brotchie, J.M. (2001). Structures outside the

basal ganglia may compensate for dopamine loss in the presymptomatic stages of Parkinson's disease. *FASEB journal : official publication of the Federation of American Societies for Experimental Biology* **15**:1092–1094.

Bezard, E., Gross, C.E. and Brotchie, J.M. (2003). Presymptomatic compensation in Parkinson's disease is not dopamine-mediated. *Trends Neurosci* **26**:215–221.

Biber, M.P., Kneisley, L.W. and LaVail, J.H. (1978). Cortical neurons projecting to the cervical and lumbar enlargements of the spinal cord in young and adult rhesus monkeys. *Experimental Neurology* **59**:492–508.

Le Bihan, D., Breton, E., Lallemand, D., Grenier, P., Cabanis, E. and Laval-Jeantet, M. (1986). MR imaging of intravoxel incoherent motions: application to diffusion and perfusion in neurologic disorders. *Radiology* **161**:401–407.

Le Bihan, D. and Johansen-Berg, H. (2012). Diffusion MRI at 25: exploring brain tissue structure and function. *Neuroimage* [Online] **61**:324–341. Available at: http://www.ncbi.nlm.nih.gov/pubmed/22120012.

Le Bihan, D., Mangin, J.F., Poupon, C., Clark, C.A., Pappata, S., Molko, N. and Chabriat, H. (2001). Diffusion tensor imaging: concepts and applications. *J Magn Reson Imaging* **13**:534–546.

Blain, C.R. V, Barker, G.J., Jarosz, J.M., Coyle, N.A., Landau, S., Brown, R.G., Chaudhuri, K.R., *et al.* (2006). Measuring brain stem and cerebellar damage in parkinsonian syndromes using diffusion tensor MRI. *Neurology* **67**:2199–2205.

Bloch, A., Probst, A., Bissig, H., Adams, H. and Tolnay, M. (2006). α-Synuclein pathology of the spinal and peripheral autonomic nervous system in neurologically unimpaired elderly subjects. *Neuropathology and Applied Neurobiology* **32**:284–295.

Blumenfeld, H. (2010). *Neuroanatomy through Clinical Cases*. 1st ed.

Boeve, B.F., Silber, M.H., Ferman, T.J., Lin, S.C., Benarroch, E.E., Schmeichel, A.M., Ahlskog, J.E., *et al.* (2013). Clinicopathologic correlations in 172 cases of rapid eye movement sleep behavior disorder with or without a coexisting neurologic disorder. *Sleep Medicine* [Online] **14**:754–762. Available at: http://www.sciencedirect.com/science/article/pii/S1389945712003875.

Boraud, T., Bezard, E., Bioulac, B. and Gross, C.E. (2000). Ratio of inhibited-to-activated pallidal neurons decreases dramatically during passive limb movement in the MPTP-treated monkey. *Journal of neurophysiology* **83**:1760–1763.

Borghammer, P., Ostergaard, K., Cumming, P., Gjedde, A., Rodell, A., Hall, N. and Chakravarty, M.M. (2009). A deformation-based morphometry study of patients with early-stage Parkinson's disease. *Eur J Neurol*.

Borghammer, P., Ostergaard, K., Cumming, P., Gjedde, A., Rodell, A., Hall, N. and Chakravarty, M.M. (2010). A deformation-based morphometry study of patients with early-stage Parkinson's disease. *European journal of neurology* **17**:314–320.

Bostan, A.C., Dum, R.P. and Strick, P.L. (2013). Cerebellar networks with the cerebral cortex and basal ganglia. *Trends in cognitive sciences* **17**:241–254.

Bostan, A.C., Dum, R.P. and Strick, P.L. (2010). The basal ganglia communicate with the cerebellum. *Proc Natl Acad Sci U S A* **107**:8452–8456.

Bostan, A.C. and Strick, P.L. (2010). The cerebellum and basal ganglia are interconnected. *Neuropsychol Rev* **20**:261–270.

Braak, H., Bohl, J.R., Muller, C.M., Rub, U., de Vos, R.A. and Del Tredici, K. (2006). Stanley Fahn Lecture 2005: The staging procedure for the inclusion body pathology associated with sporadic Parkinson's disease reconsidered. *Mov Disord* **21**:2042–2051.

Braak, H., Rub, U., Jansen Steur, E.N.H., Del Tredici, K. and de Vos, R.A.I. (2005). Cognitive status correlates with neuropathologic stage in Parkinson disease. *Neurology* **64**:1404–1410.

Braak, H., Rub, U. and Del Tredici, K. (2006). Cognitive decline correlates with neuropathological stage in Parkinson's disease. *Journal of the neurological sciences* **248**:255–258.

Braak, H., Del Tredici, K., Rüb, U., De Vos, R.A.I., Jansen Steur, E.N.H. and Braak, E. (2003). Staging of brain pathology related to sporadic Parkinson's disease. *Neurobiology of Aging* **24**:197–211.

Braak, H., De Vos, R.A.I., Bohl, J. and Del Tredici, K. (2006). Gastric α-synuclein immunoreactive inclusions in Meissner's and Auerbach's plexuses in cases staged for

Parkinson's disease-related brain pathology. *Neuroscience Letters* **396**:67–72.

Bracht, T., Jones, D.K., Muller, T.J., Wiest, R. and Walther, S. (2015). Limbic white matter microstructure plasticity reflects recovery from depression. *J Affect Disord* **170**:143–149.

Brinkman, C. and Porter, R. (1979). Supplementary motor area in the monkey: activity of neurons during performance of a learned motor task. *Journal of neurophysiology* **42**:681–709.

Brown, R.G. and Pluck, G. (2000). Negative symptoms: the 'pathology' of motivation and goal-directed behaviour. *Trends in neurosciences* **23**:412–417.

Buckner, R.L., Krienen, F.M. and Yeo, B.T.T. (2013). Opportunities and limitations of intrinsic functional connectivity MRI. *Nat Neurosci* [Online] **16**:832–837. Available at: http://dx.doi.org/10.1038/nn.3423.

Budde, M.D., Janes, L., Gold, E., Turtzo, L.C. and Frank, J.A. (2011). The contribution of gliosis to diffusion tensor anisotropy and tractography following traumatic brain injury: validation in the rat using Fourier analysis of stained tissue sections. *Brain* **134**:2248–2260.

Calabrese, E., Hickey, P., Hulette, C., Zhang, J., Parente, B., Lad, S.P. and Johnson, G.A. (2015). Postmortem diffusion MRI of the human brainstem and thalamus for deep brain stimulator electrode localization. *Hum Brain Mapp* **36**:3167–3178.

Callaghan, M.F., Freund, P., Draganski, B., Anderson, E., Cappelletti, M., Chowdhury, R., Diedrichsen, J., *et al.* (2014). Widespread age-related differences in the human brain microstructure revealed by quantitative magnetic resonance imaging(). *Neurobiol Aging* [Online] **35**:1862–1872. Available at: http://www.ncbi.nlm.nih.gov/pmc/articles/PMC4024196/.

Camicioli, R., Gee, M., Bouchard, T.P., Fisher, N.J., Hanstock, C.C., Emery, D.J. and Martin, W.R.W. (2009). Voxel-based morphometry reveals extra-nigral atrophy patterns associated with dopamine refractory cognitive and motor impairment in parkinsonism. *Parkinsonism & related disorders* **15**:187–195.

Catani, M., Howard, R.J., Pajevic, S. and Jones, D.K. (2002). Virtual in Vivo Interactive Dissection of White Matter Fasciculi in the Human Brain. *NeuroImage* **17**:77–94.

Catani, M., Jones, D.K., Daly, E., Embiricos, N., Deeley, Q., Pugliese, L., Curran, S., *et al.*

(2008). Altered cerebellar feedback projections in Asperger syndrome. *Neuroimage* **41**:1184–1191.

Cazzoli, D. and Chechlacz, M. (2017). A matter of hand: Causal links between hand dominance, structural organization of fronto-parietal attention networks, and variability in behavioural responses to transcranial magnetic stimulation. *Cortex* **86**:230–246.

Cerasa, A., Hagberg, G.E., Peppe, A., Bianciardi, M., Gioia, M.C., Costa, A., Castriota-Scanderbeg, A., *et al.* (2006). Functional changes in the activity of cerebellum and frontostriatal regions during externally and internally timed movement in Parkinson's disease. *Brain Research Bulletin* **71**:259–269.

Chaudhuri, K.R., Healy, D.G. and Schapira, A.H. V (2006). Non-motor symptoms of Parkinson's disease: diagnosis and management. *The Lancet. Neurology* **5**:235–245.

Chechlacz, M., Gillebert, C.R., Vangkilde, S.A., Petersen, A. and Humphreys, G.W. (2015). Structural Variability within Frontoparietal Networks and Individual Differences in Attentional Functions: An Approach Using the Theory of Visual Attention. *The Journal of Neuroscience* **35**:10647–10658.

Christiansen, K., Aggleton, J.P., Parker, G.D., O'Sullivan, M.J., Vann, S.D. and Metzler-Baddeley, C. (2016). The status of the precommissural and postcommissural fornix in normal ageing and mild cognitive impairment: An MRI tractography study. *Neuroimage* **130**:35–47.

Chung, H.W., Chou, M.C. and Chen, C.Y. (2011). Principles and limitations of computational algorithms in clinical diffusion tensor MR tractography. *AJNR Am J Neuroradiol* **32**:3–13.

Ciccarelli, O., Catani, M., Johansen-Berg, H., Clark, C. and Thompson, A. (2008). Diffusion-based tractography in neurological disorders: concepts, applications, and future developments. *Lancet Neurol* **7**:715–727.

Clower, D.M., Dum, R.P. and Strick, P.L. (2005). Basal ganglia and cerebellar inputs to 'AIP'. *Cereb Cortex* **15**:913–920.

Clower, D.M., West, R.A., Lynch, J.C. and Strick, P.L. (2001). The inferior parietal lobule is the target of output from the superior colliculus, hippocampus, and cerebellum. *J Neurosci* **21**:6283–6291.

Coenen, V.A., Kieselbach, K., Mader, I. and Reinacher, P.C. (2015). Diffusion tensor magnetic resonance imaging (DTI) tractography-guided deep brain stimulation in neuropathic pain. *Acta Neurochir (Wien)* **157**:739–741.

Coenen, V.A., Mädler, B., Schiffbauer, H., Urbach, H. and Allert, N. (2011). Individual Fiber Anatomy of the Subthalamic Region Revealed With Diffusion Tensor ImagingA Concept to Identify the Deep Brain Stimulation Target for Tremor Suppression. *Neurosurgery* **68**:1069–1076.

Coenen, V.A., Panksepp, J., Hurwitz, T.A., Urbach, H. and Madler, B. (2012). Human medial forebrain bundle (MFB) and anterior thalamic radiation (ATR): imaging of two major subcortical pathways and the dynamic balance of opposite affects in understanding depression. *J Neuropsychiatry Clin Neurosci* **24**:223–236.

Concha, L., Gross, D.W., Wheatley, B.M. and Beaulieu, C. (2006). Diffusion tensor imaging of time-dependent axonal and myelin degradation after corpus callosotomy in epilepsy patients. *Neuroimage* **32**:1090–1099.

Cox, R.W. (1996). AFNI: software for analysis and visualization of functional magnetic resonance neuroimages. *Comput Biomed Res* **29**:162–173.

Crutcher, M.D. and DeLong, M.R. (1984). Single cell studies of the primate putamen. *Experimental Brain Research* **53**:233–243.

Dell'acqua, F., Scifo, P., Rizzo, G., Catani, M., Simmons, A., Scotti, G. and Fazio, F. (2010). A modified damped Richardson-Lucy algorithm to reduce isotropic background effects in spherical deconvolution. *Neuroimage* **49**:1446–1458.

Dell'Acqua, F., Simmons, A., Williams, S.C.R. and Catani, M. (2013). Can spherical deconvolution provide more information than fiber orientations? Hindrance modulated orientational anisotropy, a true-tract specific index to characterize white matter diffusion. *Hum Brain Mapp* **34**:2464–2483.

DeLong, M.R. (1971). Activity of pallidal neurons during movement. *J Neurophysiol* **34**:414–427.

DeLong, M.R. (1990). Primate models of movement disorders of basal ganglia origin. *Trends in Neurosciences*.

DeLong, M.R., Alexander, G.E., Georgopoulos, A.P., Crutcher, M.D., Mitchell, S.J. and Richardson, R.T. (1984). Role of basal ganglia in limb movements. *Human neurobiology* **2**:235–44.

DeLong, M.R., Crutcher, M.D. and Georgopoulos, A.P. (1985). Primate globus pallidus and subthalamic nucleus: functional organization. *Journal of Neurophysiology* **53**:530–543.

DeLong, M.R., Crutcher, M.D. and Georgopoulos, A.P. (1983). Relations between movement and single cell discharge in the substantia nigra of the behaving monkey. *J Neurosci.* **3**:1599–1606.

Dijkhuizen, R.M., van der Marel, K., Otte, W.M., Hoff, E.I., van der Zijden, J.P., van der Toorn, A. and van Meer, M.P. (2012). Functional MRI and diffusion tensor imaging of brain reorganization after experimental stroke. *Transl Stroke Res* [Online] **3**:36–43. Available at: http://www.ncbi.nlm.nih.gov/pubmed/22408692.

Dirkx, M.F., den Ouden, H., Aarts, E., Timmer, M., Bloem, B.R., Toni, I. and Helmich, R.C. (2016). The Cerebral Network of Parkinson's Tremor: An Effective Connectivity fMRI Study. *The Journal of neuroscience : the official journal of the Society for Neuroscience* **36**:5362–5372.

Dirnberger, G. and Jahanshahi, M. (2013). Executive dysfunction in Parkinson's disease: a review. *J Neuropsychol* [Online] **7**:193–224. Available at: http://www.ncbi.nlm.nih.gov/pubmed/24007368.

Disbrow, E.A., Carmichael, O., He, J., Lanni, K.E., Dressler, E.M., Zhang, L., Malhado-Chang, N., *et al.* (2014). Resting state functional connectivity is associated with cognitive dysfunction in non-demented people with Parkinson's disease. *Journal of Parkinson's disease* **4**:453–465.

Doty, R.L. (2012). Olfaction in Parkinson's disease and related disorders. *Neurobiology of Disease* **46**:527–52.

Dovzhenok, A. and Rubchinsky, L.L. (2012). On the origin of tremor in Parkinson's disease. *PLoS One* [Online] **7**:e41598. Available at: http://www.ncbi.nlm.nih.gov/pmc/articles/PMC3407214/pdf/pone.0041598.pdf.

Doya, K. (2000). Complementary roles of basal ganglia and cerebellum in learning and motor

control. *Curr Opin Neurobiol* **10**:732–739.

Drolet, R.E., Cannon, J.R., Montero, L. and Greenamyre, J.T. (2009). Chronic rotenone exposure reproduces Parkinson's disease gastrointestinal neuropathology. *Neurobiology of Disease* **36**:96–102.

Dum, R.P. and Strick, P.L. (2003). An unfolded map of the cerebellar dentate nucleus and its projections to the cerebral cortex. *J Neurophysiol* **89**:634–639.

Elgh, E., Domellöf, M., Linder, J., Edström, M., Stenlund, H. and Forsgren, L. (2009). Cognitive function in early Parkinson's disease: A population-based study. *European Journal of Neurology* **16**:1278–1284.

Escola, L., Michelet, T., Macia, F., Guehl, D., Bioulac, B. and Burbaud, P. (2003). Disruption of information processing in the supplementary motor area of the MPTP-treated monkey: A clue to the pathophysiology of akinesia? *Brain* **126**:95–114.

Fahn, S. (2015). The medical treatment of Parkinson disease from James Parkinson to George Cotzias. *Movement Disorders* **30**:4–18.

Fearnley, J.M. and Lees, A.J. (1991). Ageing and Parkinson's disease: substantia nigra regional selectivity. *Brain* **114**:2283–2301.

Feigl, G.C., Hiergeist, W., Fellner, C., Schebesch, K.M., Doenitz, C., Finkenzeller, T., Brawanski, A., *et al.* (2014). Magnetic resonance imaging diffusion tensor tractography: evaluation of anatomic accuracy of different fiber tracking software packages. *World Neurosurg* [Online] **81**:144–150. Available at: http://ac.els-cdn.com/S1878875013000119/1-s2.0-S1878875013000119-main.pdf?_tid=6052a182-25de-11e7-b0b1-00000aab0f6b&acdnat=1492702448_82b06177b50adba2a0e2f0d061210726.

Fenoy, A.J., McHenry, M.A. and Schiess, M.C. (2017). Speech changes induced by deep brain stimulation of the subthalamic nucleus in Parkinson disease: involvement of the dentatorubrothalamic tract. *J Neurosurg* **126**:2017–2027.

Fernandez, H.H. (2012). Updates in the medical management of Parkinson disease. *Cleveland Clinic Journal of Medicine* **79**:28–35.

Foltynie, T., Brayne, C.E.G., Robbins, T.W. and Barker, R.A. (2004). The cognitive ability of an incident cohort of Parkinson's patients in the UK. The CamPaIGN study. *Brain* **127**:550–

560.

Froudist-Walsh, S., Karolis, V., Caldinelli, C., Brittain, P.J., Kroll, J., Rodriguez-Toscano, E., Tesse, M., *et al.* (2015). Very Early Brain Damage Leads to Remodeling of the Working Memory System in Adulthood: A Combined fMRI/Tractography Study. *Journal of Neuroscience* **35**:15787–15799.

Fuchs, J., Tichopad, A., Golub, Y., Munz, M., Schweitzer, K.J., Wolf, B., Berg, D., *et al.* (2008). Genetic variability in the SNCA gene influences α-synuclein levels in the blood and brain. *The FASEB journal* **22**:1327–34.

Gao, L., Zhang, J., Hou, Y., Hallett, M., Chan, P. and Wu, T. (2017). The cerebellum in dual-task performance in Parkinson's disease. *Scientific Reports* **7**:45662.

Geng, D.Y., Li, Y.X. and Zee, C.S. (2006). Magnetic resonance imaging-based volumetric analysis of basal ganglia nuclei and substantia nigra in patients with Parkinson's disease. *Neurosurgery* **58**:256–262.

Gerrits, N.J.H.M., Van Loenhoud, A.C., Van Den Berg, S.F., Berendse, H.W., Foncke, E.M.J., Klein, M., Stoffers, D., *et al.* (2016). Cortical thickness, surface area and subcortical volume differentially contribute to cognitive heterogeneity in Parkinson's disease. *PLoS ONE* **11**.

Ghez, C. and W Thomas, T. (2000). The Cerebellum. In: *Principles of Neural Science*. pp. 832–851.

Gibb, W.R. and Lees, A.J. (1988). A comparison of clinical and pathological features of young- and old-onset Parkinson's disease. *Neurology* **38**:1402–1406.

Glickstein, M., May 3rd, J.G. and Mercier, B.E. (1985). Corticopontine projection in the macaque: the distribution of labelled cortical cells after large injections of horseradish peroxidase in the pontine nuclei. *J Comp Neurol* **235**:343–359.

Goetz, C.G. (2011). The history of Parkinson's disease: Early clinical descriptions and neurological therapies. *Cold Spring Harbor Perspectives in Medicine* **1**.

Goetz, C.G., Tilley, B.C., Shaftman, S.R., Stebbins, G.T., Fahn, S., Martinez-Martin, P., Poewe, W., *et al.* (2008). Movement Disorder Society-Sponsored Revision of the Unified Parkinson's Disease Rating Scale (MDS-UPDRS): Scale presentation and clinimetric testing

results. *Movement Disorders* **23**:2129–2170.

Goldberg, J.A., Boraud, T., Maraton, S., Haber, S.N., Vaadia, E. and Bergman, H. (2002). Enhanced synchrony among primary motor cortex neurons in the 1-methyl-4-phenyl-1,2,3,6-tetrahydropyridine primate model of Parkinson's disease. *Journal of Neuroscience* **22**:4639–4653.

Goldman, J.G. and Postuma, R. (2014). Premotor and non-motor features of Parkinson's disease. *Current opinion in neurology* **27**:434–441.

Greffard, S., Verny, M., Bonnet, A.-M., Beinis, J.-Y., Gallinari, C., Meaume, S., Piette, F., *et al.* (2006). Motor score of the Unified Parkinson Disease Rating Scale as a good predictor of Lewy body-associated neuronal loss in the substantia nigra. *Archives of neurology* **63**:584–588.

Hacker, M.L., Tonascia, J., Turchan, M., Currie, A., Heusinkveld, L., Konrad, P.E., Davis, T.L., *et al.* (2015). Deep brain stimulation may reduce the relative risk of clinically important worsening in early stage Parkinson's disease. *Parkinsonism and Related Disorders* **21**:1177–1183.

Von Dem Hagen, E.A.H. and Henkelman, R.M. (2002). Orientational diffusion reflects fiber structure within a voxel. *Magnetic Resonance in Medicine* **48**:454–9.

Hagmann, P., Jonasson, L., Maeder, P., Thiran, J.P., Wedeen, V.J. and Meuli, R. (2006). Understanding diffusion MR imaging techniques: from scalar diffusion-weighted imaging to diffusion tensor imaging and beyond. *Radiographics* **26 Suppl 1**:S205-23.

Hallett, P.J., McLean, J.R., Kartunen, A., Langston, J.W. and Isacson, O. (2012). Alpha-synuclein overexpressing transgenic mice show internal organ pathology and autonomic deficits. *Neurobiology of Disease* **47**:258–267.

Halliday, G., Hely, M., Reid, W. and Morris, J. (2008). The progression of pathology in longitudinally followed patients with Parkinson's disease. *Acta Neuropathologica* **115**:409–415.

Halliday, G., Lees, A. and Stern, M. (2011). Milestones in Parkinson's disease-Clinical and pathologic features. *Movement Disorders* **26**:1015–1021.

Hamani, C., Saint-Cyr, J.A., Fraser, J., Kaplitt, M. and Lozano, A.M. (2004). The

subthalamic nucleus in the context of movement disorders. *Brain* **127**:4–20.

Hana, A., Hana, A., Dooms, G., Boecher-Schwarz, H. and Hertel, F. (2016). Depiction of dentatorubrothalamic tract fibers in patients with Parkinson's disease and multiple sclerosis in deep brain stimulation. *BMC Res Notes* **9**:345.

Von Der Heide, R.J., Skipper, L.M., Klobusicky, E. and Olson, I.R. (2013). Dissecting the uncinate fasciculus: disorders, controversies and a hypothesis. *Brain* **136**:1692–1707.

Heinzel, S., Roeben, B., Ben-Shlomo, Y., Lerche, S., Alves, G., Barone, P., Behnke, S., *et al.* (2016). Prodromal Markers in Parkinson's Disease: Limitations in Longitudinal Studies and Lessons Learned. *Frontiers in Aging Neuroscience* [Online] **8**:147. Available at: http://www.ncbi.nlm.nih.gov/pmc/articles/PMC4916171/.

Helmich, R.C., Hallett, M., Deuschl, G., Toni, I. and Bloem, B.R. (2012). Cerebral causes and consequences of parkinsonian resting tremor: A tale of two circuits? *Brain* **135**:3206–3226.

Hely, M.A., Reid, W.G.J., Adena, M.A., Halliday, G.M. and Morris, J.G.L. (2008). The Sydney Multicenter Study of Parkinson's disease: The inevitability of dementia at 20 years. *Movement Disorders* **23**:837–844.

Herz, D.M., Haagensen, B.N., Christensen, M.S., Madsen, K.H., Rowe, J.B., Løkkegaard, A. and Siebner, H.R. (2015). Abnormal dopaminergic modulation of striato-cortical networks underlies levodopa-induced dyskinesias in humans. *Brain* **138**:1658–1666.

Highley, J.R., Walker, M.A., Esiri, M.M., Crow, T.J. and Harrison, P.J. (2002). Asymmetry of the uncinate fasciculus: a post-mortem study of normal subjects and patients with schizophrenia. *Cereb Cortex* [Online] **12**:1218–1224. Available at: http://cercor.oxfordjournals.org/content/12/11/1218.full.pdf.

Hoover, J.E. and Strick, P.L. (1999). The organization of cerebellar and basal ganglia outputs to primary motor cortex as revealed by retrograde transneuronal transport of herpes simplex virus type 1. *The Journal of neuroscience : the official journal of the Society for Neuroscience* **19**:1446–1463.

Hornykiewicz, O. (2006). The discovery of dopamine deficiency in the parkinsonian brain. *Journal of neural transmission. Supplementum*:9–15.

Hoshi, E., Tremblay, L., Feger, J., Carras, P.L. and Strick, P.L. (2005). The cerebellum communicates with the basal ganglia. *Nat Neurosci* **8**:1491–1493.

Hsiao, I.-T., Weng, Y.-H., Hsieh, C.-J., Lin, W.-Y., Wey, S.-P., Kung, M.-P., Yen, T.-C., *et al.* (2014). Correlation of Parkinson disease severity and 18F-DTBZ positron emission tomography. *JAMA neurology* **71**:758–66.

Hubbard, P.S., Esiri, M.M., Reading, M., McShane, R. and Nagy, Z. (2007). Alpha-synuclein pathology in the olfactory pathways of dementia patients. *Journal of Anatomy* **211**:117–124.

Huisman, T.A.G.M. (2010). Diffusion-weighted and diffusion tensor imaging of the brain, made easy. *Cancer Imaging* **10**:S163-71.

Hurley, M.J., Mash, D.C. and Jenner, P. (2003). Markers for dopaminergic neurotransmission in the cerebellum in normal individuals and patients with Parkinson's disease examined by RT-PCR. *Eur J Neurosci* **18**:2668–2672.

Ikai, Y., Takada, M., Shinonaga, Y. and Mizuno, N. (1992). Dopaminergic and non-dopaminergic neurons in the ventral tegmental area of the rat project, respectively, to the cerebellar cortex and deep cerebellar nuclei. *Neuroscience* **51**:719–728.

Inuggi, A., Amato, N., Magnani, G., González-Rosa, J.J., Chieffo, R., Comi, G. and Leocani, L. (2011). Cortical control of unilateral simple movement in healthy aging. *Neurobiology of Aging* **32**:524–538.

Irfanoglu, M.O., Walker, L., Sarlls, J., Marenco, S. and Pierpaoli, C. (2012). Effects of image distortions originating from susceptibility variations and concomitant fields on diffusion MRI tractography results. *Neuroimage* **61**:275–288.

Jahanshahi, M., Jones, C.R.G., Dirnberger, G. and Frith, C.D. (2006). The substantia nigra pars compacta and temporal processing. *Journal of Neuroscience* **26**:12266–12273.

Jahanshahi, M., Jones, C.R.G., Zijlmans, J., Katzenschlager, R., Lee, L., Quinn, N., Frith, C.D., *et al.* (2010). Dopaminergic modulation of striato-frontal connectivity during motor timing in Parkinson's disease. *Brain* **133**:727–745.

Jang, S.H. (2014). The corticospinal tract from the viewpoint of brain rehabilitation. *Journal of Rehabilitation Medicine* **46**:193–199.

Jang, S.H. and Kwon, H.G. (2015). Injury of the dentato-rubro-thalamic tract in a patient with mild traumatic brain injury. *Brain Inj* **29**:1725–1728.

Jankovic, J. (2008). Parkinson's disease: clinical features and diagnosis. *J Neurol Neurosurg Psychiatry* **79**:368–376.

Jankovic, J. (2005). Progression of Parkinson disease: are we making progress in charting the course? *Arch Neurol* **62**:351–352.

Jankovic, J. and Kapadia, A.S. (2001). Functional Decline in Parkinson Disease. *Archives of neurology* **58**:1611–5.

Jansons, K.M. and Alexander, D.C. (2003). Persistent Angular Structure: new insights from diffusion MRI data. Dummy version. *Information processing in medical imaging : proceedings of the ... conference* **18**:672–683.

Jbabdi, S. and Johansen-Berg, H. (2011). Tractography: where do we go from here? *Brain Connect* **1**:169–183.

Jellinger, K.A. (2008). A critical reappraisal of current staging of Lewy-related pathology in human brain. *Acta Neuropathologica* **116**:1–16.

Jellinger, K. a (2004). Lewy body-related alpha-synucleinopathy in the aged human brain. *Journal of neural transmission (Vienna, Austria : 1996)* **111**:1219–35.

Jellison, B.J., Field, A.S., Medow, J., Lazar, M., Salamat, M.S. and Alexander, A.L. (2004). Diffusion tensor imaging of cerebral white matter: a pictorial review of physics, fiber tract anatomy, and tumor imaging patterns. *AJNR Am J Neuroradiol* **25**:356–369.

Jenkinson, M., Beckmann, C.F., Behrens, T.E., Woolrich, M.W. and Smith, S.M. (2012). FSL. *Neuroimage* **62**:782–790.

Jeong, J.-W., Chugani, D.C., Behen, M.E., Tiwari, V.N. and Chugani, H.T. (2012). Altered White Matter Structure of the Dentatorubrothalamic Pathway in Children with Autistic Spectrum Disorders. *The Cerebellum* **11**:957–971.

Jeurissen, B., Leemans, A., Tournier, J.D., Jones, D.K. and Sijbers, J. (2013). Investigating the prevalence of complex fiber configurations in white matter tissue with diffusion magnetic resonance imaging. *Hum Brain Mapp* **34**:2747–2766.

Jezzard, P., Barnett, A.S. and Pierpaoli, C. (1998). Characterization of and correction for eddy current artifacts in echo planar diffusion imaging. *Magn Reson Med* **39**:801–812.

Jones, D.K. (2010). *Diffusion MRI Theory, Methods, and Applications*.

Jones, D.K. (2004). The effect of gradient sampling schemes on measures derived from diffusion tensor MRI: a Monte Carlo study. *Magnetic resonance in medicine* **51**:807–815.

Jones, D.K., Horsfield, M.A. and Simmons, A. (1999). Optimal strategies for measuring diffusion in anisotropic systems by magnetic resonance imaging. *Magn Reson Med* **42**:515–525.

Jones, D.K., Knosche, T.R. and Turner, R. (2013). White matter integrity, fiber count, and other fallacies: the do's and don'ts of diffusion MRI. *Neuroimage* **73**:239–254.

Jones, D.K. and Pierpaoli, C. (2005). Confidence mapping in diffusion tensor magnetic resonance imaging tractography using a bootstrap approach. *Magn Reson Med* **53**:1143–1149.

Jones, D.K., Simmons, A., Williams, S.C.R. and Horsfield, M.A. (1999). Non-invasive assessment of axonal fiber connectivity in the human brain via diffusion tensor MRI. *Magnetic Resonance in Medicine* **42**:37–41.

Jones, D.K., Williams, S.C.R., Gasston, D., Horsfield, M.A., Simmons, A. and Howard, R. (2002). Isotropic resolution diffusion tensor imaging with whole brain acquisition in a clinically acceptable time. *Human brain mapping* **15**:216–230.

Jones, E.G., Coulter, J.D., Burton, H. and Porter, R. (1977). Cells of origin and terminal distrubution of corticostriatal fibers arising in the sensory-motor cortex of monkeys. *Journal of Comparative Neurology* **173**:53–80.

Kalaitzakis, M.E., Graeber, M.B., Gentleman, S.M. and Pearce, R.K.B. (2009). Evidence against a reliable staging system of α-synuclein pathology in Parkinson's disease. *Neuropathology and Applied Neurobiology* **35**:125–126.

Kapitan, M., Ferrando, R., Dieguez, E., de Medina, O., Aljanati, R., Ventura, R., Amorin, I., *et al.* (2009). [Regional cerebral blood flow changes in Parkinson's disease: correlation with disease duration]. *Rev Esp Med Nucl* **28**:114–120.

Karachi, C., Yelnik, J., Tande, D., Tremblay, L., Hirsch, E.C. and Francois, C. (2005). The pallidosubthalamic projection: an anatomical substrate for nonmotor functions of the subthalamic nucleus in primates. *Movement disorders : official journal of the Movement Disorder Society* **20**:172–180.

Kelly, L.P., Carvey, P.M., Keshavarzian, A., Shannon, K.M., Shaikh, M., Bakay, R.A.E. and Kordower, J.H. (2014). Progression of intestinal permeability changes and alpha-synuclein expression in a mouse model of Parkinson's disease. *Movement Disorders* **29**:999–1009.

Kelly, R.M. and Strick, P.L. (2003). Cerebellar loops with motor cortex and prefrontal cortex of a nonhuman primate. *J Neurosci* **23**:8432–8444.

Kita, H. (2005). Balance of Monosynaptic Excitatory and Disynaptic Inhibitory Responses of the Globus Pallidus Induced after Stimulation of the Subthalamic Nucleus in the Monkey. *Journal of Neuroscience* **25**:8611–8619.

Kleiner-Fisman, G., Herzog, J., Fisman, D.N., Tamma, F., Lyons, K.E., Pahwa, R., Lang, A.E., *et al.* (2006). Subthalamic nucleus deep brain stimulation: summary and meta-analysis of outcomes. *Movement Disorders* **21**:290–304.

Koch, G., Brusa, L., Carrillo, F., Lo Gerfo, E., Torriero, S., Oliveri, M., Mir, P., *et al.* (2009). Cerebellar magnetic stimulation decreases levodopa-induced dyskinesias in Parkinson disease. *Neurology* **73**:113–119.

Koziol, L.F., Budding, D., Andreasen, N., D'Arrigo, S., Bulgheroni, S., Imamizu, H., Ito, M., *et al.* (2014). Consensus paper: the cerebellum's role in movement and cognition. *Cerebellum (London, England)* **13**:151–177.

Kunig, G., Leenders, K.L., Martin-Solch, C., Missimer, J., Magyar, S. and Schultz, W. (2000). Reduced reward processing in the brains of Parkinsonian patients. *Neuroreport* **11**:3681–3687.

Kunzle, H. (1977). Projections from the primary somatosensory cortex to basal ganglia and thalamus in the monkey. *Exp.Brain Res.* **30**:481–492.

Künzle, H. (1975). Bilateral projections from precentral motor cortex to the putamen and other parts of the basal ganglia. An autoradiographic study in Macaca fascicularis. *Brain Research* **88**:195–209.

Kwon, H.G., Hong, J.H., Hong, C.P., Lee, D.H., Ahn, S.H. and Jang, S.H. (2011). Dentatorubrothalamic tract in human brain: diffusion tensor tractography study. *Neuroradiology* **53**:787–791.

Lebel, C., Walker, L., Leemans, A., Phillips, L. and Beaulieu, C. (2008). Microstructural maturation of the human brain from childhood to adulthood. *Neuroimage* **40**:1044–1055.

Lee, A. and Gilbert, R.M. (2016). Epidemiology of Parkinson Disease. *Neurologic Clinics* **34**:955–965.

Lee, C.S., Samii, A., Sossi, V., Ruth, T.J., Schulzer, M., Holden, J.E., Wudel, J., *et al.* (2000). In vivo positron emission tomographic evidence for compensatory changes in presynaptic dopaminergic nerve terminals in Parkinson's disease. *Annals of Neurology* **47**:493–503.

Lee, S.H., Kim, S.S., Tae, W.S., Lee, S.Y., Choi, J.W., Koh, S.B. and Kwon, D.Y. (2011). Regional volume analysis of the Parkinson disease brain in early disease stage: Gray matter, white matter, striatum, and thalamus. *American Journal of Neuroradiology* **32**:682–687.

Leemans, A., Jeurissen, B., Siibers, J. and Jones, D.K. (2009). ExploreDTI: A graphical tool box for processing, analyzing, and visualizing diffusion MR data. *17th Anuual Meeting of the International Society of Magnetic Resonnance in Medicine*.

Leemans, A., Jeurissen, B., Sijbers, J. and Jones, D.K. (2009). ExploreDTI: A graphical toolbox for processing, analyzing and visualizing diffusion MR data. . In: *Proceedings of the International Society for Magnetic Resonance in Medicine 17th Annual Meeting*. Honolulu, Hawaii, 3536.

Leemans, A. and Jones, D.K. (2009). The B-matrix must be rotated when correcting for subject motion in DTI data. *Magn Reson Med* **61**:1336–1349.

Lefaucheur, J.P. (2005). Motor cortex dysfunction revealed by cortical excitability studies in Parkinson's disease: Influence of antiparkinsonian treatment and cortical stimulation. *Clinical Neurophysiology* **116**:244–253.

Leitner, Y., Travis, K.E., Ben-Shachar, M., Yeom, K.W. and Feldman, H.M. (2015). Tract Profiles of the Cerebellar White Matter Pathways in Children and Adolescents. *Cerebellum* **14**:613–623.

Levesque, I.R., Giacomini, P.S., Narayanan, S., Ribeiro, L.T., Sled, J.G., Arnold, D.L. and Pike, G.B. (2010). Quantitative magnetization transfer and myelin water imaging of the evolution of acute multiple sclerosis lesions. *Magn Reson Med* **63**:633–640.

Lewis, M.M., Galley, S., Johnson, S., Stevenson, J., Huang, X. and McKeown, M.J. (2013). The role of the cerebellum in the pathophysiology of Parkinson's disease. *Can J Neurol Sci* **40**:299–306.

Liles, S.L. (1985). Activity of neurons in putamen during active and passive movements of wrist. *Journal of neurophysiology* **53**:217–236.

Lindenbach, D. and Bishop, C. (2013). Critical involvement of the motor cortex in the pathophysiology and treatment of Parkinson's disease. *Neurosci Biobehav Rev* **37**:2737–2750.

Linder, J., Birgander, R., Olsson, I., Riklund, K., Larsson, A.K., Edström, M., Stenlund, H., *et al.* (2009). Degenerative changes were common in brain magnetic resonance imaging in patients with newly diagnosed Parkinson's disease in a population-based cohort. *Journal of Neurology*.

Linhares, M.N. and Tasker, R.R. (2000). Microelectrode-guided thalamotomy for Parkinson's disease. *Neurosurgery* **46**:390–398.

Lisanby, S.H., McDonald, W.M., Massey, E.W., Doraiswamy, P.M., Rozear, M., Boyko, O.B., Krishnan, K.R., *et al.* (1993). Diminished subcortical nuclei volumes in Parkinson's disease by MR imaging. *J Neural Transm Suppl* **40**:13–21.

Lozano, A.M. and Lang, A.E. (1998). Pallidotomy for Parkinson's disease. *Neurosurg Clin N Am* **9**:325–36.

Lynch, J.C., Hoover, J.E. and Strick, P.L. (1994). Input to the primate frontal eye field from the substantia nigra, superior colliculus, and dentate nucleus demonstrated by transneuronal transport. *Exp Brain Res* **100**:181–186.

MacMillan, M.L., Dostrovsky, J.O., Lozano, a M. and Hutchison, W.D. (2004). Involvement of human thalamic neurons in internally and externally generated movements. *Journal of neurophysiology* **91**:1085–90.

Macpherson, J.M., Marangoz, C., Miles, T.S. and Wiesendanger, M. (1982).

Microstimulation of the supplementary motor area (SMA) in the awake monkey. *Experimental Brain Research* **45**:410–416.

Magrinelli, F., Picelli, A., Tocco, P., Federico, A., Roncari, L., Smania, N., Zanette, G., *et al.* (2016). Pathophysiology of Motor Dysfunction in Parkinson's Disease as the Rationale for Drug Treatment and Rehabilitation. *Parkinson's Disease* **2016**.

Makris, N., Schlerf, J.E., Hodge, S.M., Haselgrove, C., Albaugh, M.D., Seidman, L.J., Rauch, S.L., *et al.* (2005). MRI-based surface-assisted parcellation of human cerebellar cortex: An anatomically specified method with estimate of reliability. *NeuroImage* **25**:1146–1160.

Martinu, K. and Monchi, O. (2013). Cortico-basal ganglia and cortico-cerebellar circuits in Parkinson's disease: pathophysiology or compensation? *Behavioral neuroscience* **127**:222–236.

Meck, W.H. (2006). Neuroanatomical localization of an internal clock: A functional link between mesolimbic, nigrostriatal, and mesocortical dopaminergic systems. *Brain Research* **1109**:93–107.

Meijer, F.J., Bloem, B.R., Mahlknecht, P., Seppi, K. and Goraj, B. (2013). Update on diffusion MRI in Parkinson's disease and atypical parkinsonism. *J Neurol Sci* **332**:21–29.

Menke, R.A.L., Szewczyk-Krolikowski, K., Jbabdi, S., Jenkinson, M., Talbot, K., Mackay, C.E. and Hu, M. (2014). Comprehensive morphometry of subcortical grey matter structures in early-stage Parkinson's disease. *Human Brain Mapping* **35**:1681–1690.

Meola, A., Comert, A., Yeh, F.C., Sivakanthan, S. and Fernandez-Miranda, J.C. (2016). The nondecussating pathway of the dentatorubrothalamic tract in humans: human connectome-based tractographic study and microdissection validation. *J Neurosurg* **124**:1406–1412.

Messina, D., Cerasa, A., Condino, F., Arabia, G., Novellino, F., Nicoletti, G., Salsone, M., *et al.* (2011). Patterns of brain atrophy in Parkinson's disease, progressive supranuclear palsy and multiple system atrophy. *Parkinsonism Relat. Disord.*

Metzler-Baddeley, C., Caeyenberghs, K., Foley, S. and Jones, D.K. (2016). Task complexity and location specific changes of cortical thickness in executive and salience networks after working memory training. *Neuroimage* **130**:48–62.

Metzler-Baddeley, C., Foley, S., de Santis, S., Charron, C., Hampshire, A., Caeyenberghs, K. and Jones, D.K. (2017). Dynamics of White Matter Plasticity Underlying Working Memory Training: Multimodal Evidence from Diffusion MRI and Relaxometry. *Journal of cognitive neuroscience* **29**:1509–1520.

Metzler-Baddeley, C., Jones, D.K., Belaroussi, B., Aggleton, J.P. and O'Sullivan, M.J. (2011). Frontotemporal connections in episodic memory and aging: a diffusion MRI tractography study. *J Neurosci* **31**:13236–13245.

Metzler-Baddeley, C., O'Sullivan, M.J., Bells, S., Pasternak, O. and Jones, D.K. (2012). How and how not to correct for CSF-contamination in diffusion MRI. *Neuroimage* **59**:1394–1403.

Middleton, F.A. and Strick, P.L. (2000). Basal ganglia and cerebellar loops: motor and cognitive circuits. *Brain Research Reviews* **31**:236–250.

Middleton, F.A. and Strick, P.L. (2001). Cerebellar projections to the prefrontal cortex of the primate. *J Neurosci* **21**:700–712.

Mink, J.W. (1996). The basal ganglia: focused selection and inhibition of competing motor programs. *Prog Neurobiol* **50**:381–425.

Mink, J.W. and Thach, W.T. (1991). Basal ganglia motor control. II. Late pallidal timing relative to movement onset and inconsistent pallidal coding of movement parameters. *J Neurophysiol* **65**:301–29.

Mir, P., Matsunaga, K., Gilio, F., Quinn, N.P., Siebner, H.R. and Rothwell, J.C. (2005). Dopaminergic drugs restore facilitatory premotor-motor interactions in Parkinson disease. *Neurology* **64**:1906–1912.

Mirdamadi, J.L. (2016). Cerebellar Role in Parkinson's Disease. *Journal of neurophysiology* **116**:917–9.

Mischley, L.K., Lau, R.C. and Weiss, N.S. (2017). Use of a self-rating scale of the nature and severity of symptoms in Parkinson's Disease (PRO-PD): Correlation with quality of life and existing scales of disease severity. *NPJ Parkinson's Disease* [Online] **3**:20. Available at: http://www.ncbi.nlm.nih.gov/pmc/articles/PMC5473828/.

Mokkink, L.B., Terwee, C.B., Patrick, D.L., Alonso, J., Stratford, P.W., Knol, D.L., Bouter, L.M., *et al.* (2010). The COSMIN checklist for assessing the methodological quality of

studies on measurement properties of health status measurement instruments: an international Delphi study. *Quality of life research : an international journal of quality of life aspects of treatment, care and rehabilitation* **19**:539–549.

Mole, J.P., Subramanian, L., Bracht, T., Morris, H., Metzler-Baddeley, C. and Linden, D.E.J. (2016). Increased fractional anisotropy in the motor tracts of Parkinson's disease suggests compensatory neuroplasticity or selective neurodegeneration. *European Radiology* **26**:3327–3335.

Mollink, J., van Baarsen, K.M., Dederen, P.J., Foxley, S., Miller, K.L., Jbabdi, S., Slump, C.H., *et al.* (2016). Dentatorubrothalamic tract localization with postmortem MR diffusion tractography compared to histological 3D reconstruction. *Brain Struct Funct* **221**:3487–3501.

Montgomery, E.B.J., Baker, K.B., Lyons, K. and Koller, W.C. (1999). Abnormal performance on the PD test battery by asymptomatic first-degree relatives. *Neurology* **52**:757–762.

Mori, S., Crain, B.J., Chacko, V.P. and van Zijl, P.C. (1999). Three-dimensional tracking of axonal projections in the brain by magnetic resonance imaging. *Ann Neurol* **45**:265–269.

Mormina, E., Arrigo, A., Calamuneri, A., Granata, F., Quartarone, A., Ghilardi, M.F., Inglese, M., *et al.* (2015). Diffusion tensor imaging parameters' changes of cerebellar hemispheres in Parkinson's disease. *Neuroradiology* **57**:327–334.

Muakkassa, K.F. and Strick, P.L. (1979). Frontal lobe inputs to primate motor cortex: evidence for four somatotopically organized 'premotor' areas. *Brain Research* **177**:176–182.

Murray, E.A. and Coulter, J.D. (1981). Organization of corticospinal neurons in the monkey. *Journal of Comparative Neurology* **195**:339–365.

Muslimović, D., Post, B., Speelman, J.D. and Schmand, B. (2005). Cognitive profile of patients with newly diagnosed Parkinson disease. *Neurology* **13**:1239–45.

Nair, S.R., Tan, L.K., Mohd Ramli, N., Lim, S.Y., Rahmat, K. and Mohd Nor, H. (2013). A decision tree for differentiating multiple system atrophy from Parkinson's disease using 3-T MR imaging. *European Radiology* **23**:1459–1466.

Nambu, A., Takada, M., Inase, M. and Tokuno, H. (1996). Dual somatotopical representations in the primate subthalamic nucleus: evidence for ordered but reversed body-

map transformations from the primary motor cortex and the supplementary motor area. *The Journal of neuroscience : the official journal of the Society for Neuroscience* **16**:2671–2683.

Nambu, A., Tokuno, H., Hamada, I., Kita, H., Imanishi, M., Akazawa, T., Ikeuchi, Y., *et al.* (1998). Excitatory cortical inputs to pallidal neurons via the subthalamic nucleus. *Neuroscience Research* **31**:S175.

Natale, G., Kastsiushenka, O., Fulceri, F., Ruggieri, S., Paparelli, A. and Fornai, F. (2010). MPTP-induced parkinsonism extends to a subclass of TH-positive neurons in the gut. *Brain Research* **1355**:195–206.

Nemmi, F., Sabatini, U., Rascol, O. and Péran, P. (2015). Parkinson's disease and local atrophy in subcortical nuclei: Insight from shape analysis. *Neurobiology of Aging* **36**:424–433.

Nicoletti, G., Lodi, R., Condino, F., Tonon, C., Fera, F., Malucelli, E., Manners, D., *et al.* (2006). Apparent diffusion coefficient measurements of the middle cerebellar peduncle differentiate the Parkinson variant of MSA from Parkinson's disease and progressive supranuclear palsy. *Brain* **129**:2679–2687.

Nicoletti, G., Rizzo, G., Barbagallo, G., Tonon, C., Condino, F., Manners, D., Messina, D., *et al.* (2013). Diffusivity of cerebellar hemispheres enables discrimination of cerebellar or parkinsonian multiple system atrophy from progressive supranuclear palsy-Richardson syndrome and Parkinson disease. *Radiology* **267**:843–850.

Nicoletti, G., Tonon, C., Lodi, R., Condino, F., Manners, D., Malucelli, E., Morelli, M., *et al.* (2008). Apparent diffusion coefficient of the superior cerebellar peduncle differentiates progressive supranuclear palsy from Parkinson's disease. *Movement Disorders* **23**:2370–2376.

Nieuwenhuys, R., Voogd, J. and van Huijzen, C. (2008). *The Human Central Nervous System*.

Nishio, Y., Hirayama, K., Takeda, A., Hosokai, Y., Ishioka, T., Suzuki, K., Itoyama, Y., *et al.* (2010). Corticolimbic gray matter loss in Parkinson's disease without dementia. *European journal of neurology* **17**:1090–1097.

O'Callaghan, C., Hornberger, M., Balsters, J.H., Halliday, G.M., Lewis, S.J.G. and Shine,

J.M. (2016). Cerebellar atrophy in Parkinson's disease and its implication for network connectivity. *Brain : a journal of neurology* **139**:845–855.

O'Reilly, J.X., Beckmann, C.F., Tomassini, V., Ramnani, N. and Johansen-Berg, H. (2010). Distinct and overlapping functional zones in the cerebellum defined by resting state functional connectivity. *Cerebral cortex (New York, N.Y. : 1991)* **20**:953–965.

Obeso, J.A., Marin, C., Rodriguez-Oroz, C., Blesa, J., Benitez-Temiño, B., Mena-Segovia, J., Rodríguez, M., *et al.* (2008). The basal ganglia in Parkinson's disease: Current concepts and unexplained observations. *Annals of Neurology* **64**:S30-46.

Obeso, J.A., Rodríguez-Oroz, M.C., Benitez-Temino, B., Blesa, F.J., Guridi, J., Marin, C. and Rodriguez, M. (2008). Functional organization of the basal ganglia: Therapeutic implications for Parkinson's disease. *Movement Disorders* **23**:S548–S559.

Oishi, K., Faria, A. V, van Zijl, P.C.M. and Mori, S. (2011). *MRI Atlas of Human White Matter* . 2nd Editio. Elsevier.

Oppenheim, C., Rodrigo, S., Poupon, C., Dumas de la Roque, A., Naggara, O., Meder, J.F. and Frédy, D. (2004). Diffusion tensor MR imaging of the brain. Clinical applications. *Journal de radiologie* **85**:287–296.

Palmer, C., Schmidt, E.M. and McIntosh, J.S. (1981). Corticospinal and corticorubral projections from the supplementary motor area in the monkey. *Brain Research* **209**:305–314.

Palmer, S.J., Ng, B., Abugharbieh, R., Eigenraam, L. and McKeown, M.J. (2009). Motor reserve and novel area recruitment: Amplitude and spatial characteristics of compensation in Parkinson's disease. *European Journal of Neuroscience* **29**:2187–2196.

Panagopoulos, N.T., Papadopoulos, G.C. and Matsokis, N.A. (1991). Dopaminergic innervation and binding in the rat cerebellum. *Neuroscience Letters* **130**:208–12.

Papagno, C., Miracapillo, C., Casarotti, A., Romero Lauro, L.J., Castellano, A., Falini, A., Casaceli, G., *et al.* (2011). What is the role of the uncinate fasciculus? Surgical removal and proper name retrieval. *Brain* [Online] **134**:405–414. Available at: http://brain.oxfordjournals.org/content/134/2/405.full.pdf.

Parraga, R.G., Possatti, L.L., Alves, R. V, Ribas, G.C., Ture, U. and de Oliveira, E. (2016). Microsurgical anatomy and internal architecture of the brainstem in 3D images: surgical

considerations. *J Neurosurg* **124**:1377–1395.

Pasternak, O., Sochen, N., Gur, Y., Intrator, N. and Assaf, Y. (2009). Free water elimination and mapping from diffusion MRI. *Magn Reson Med* **62**:717–730.

Patenaude, B., Smith, S.M., Kennedy, D.N. and Jenkinson, M. (2011). A Bayesian model of shape and appearance for subcortical brain segmentation. *Neuroimage* **56**:907–922.

Percheron, G., Francois, C., Talbi, B., Yelnik, J. and Fenelon, G. (1996). The primate motor thalamus. *Brain Res Brain Res Rev* **22**:93–181.

Pereira, J.B., Junque, C., Marti, M.J., Ramirez-Ruiz, B., Bartres-Faz, D. and Tolosa, E. (2009). Structural brain correlates of verbal fluency in Parkinson's disease. *Neuroreport* **20**:741–744.

Phillips, O., Squitieri, F., Sanchez-Castaneda, C., Elifani, F., Griguoli, A., Maglione, V., Caltagirone, C., *et al.* (2014). The Corticospinal Tract in Huntington's Disease. *Cereb Cortex* **25**:2670–2682.

Picard, N. and Strick, P.L. (2003). Activation of the supplementary motor area (SMA) during performance of visually guided movements. *Cerebral Cortex* **13**:977–986.

Pierpaoli, C. and Basser, P.J. (1996). Toward a quantitative assessment of diffusion anisotropy. *Magnetic Resonance in Medicine* **36**:893–906.

Pierpaoli, C., Jezzard, P., Basser, P.J., Barnett, A. and Di Chiro, G. (1996). Diffusion tensor MR imaging of the human brain. *Radiology* **201**:637–648.

Postuma, R.B. and Berg, D. (2016). Advances in markers of prodromal Parkinson disease. *Nat Rev Neurol* [Online] **12**:622–634. Available at: http://dx.doi.org/10.1038/nrneurol.2016.152.

PPMI (2011). The Parkinson Progression Marker Initiative (PPMI). *Prog Neurobiol* [Online] **95**:629–635. Available at: http://ac.els-cdn.com/S0301008211001651/1-s2.0-S0301008211001651-main.pdf?_tid=70fa83c4-41fe-11e7-8983-00000aacb35e&acdnat=1495794853_d302f326e8815e5bf0cc51994079a63d.

Prodoehl, J., Burciu, R.G. and Vaillancourt, D.E. (2014). Resting state functional magnetic resonance imaging in Parkinson's disease. *Current neurology and neuroscience reports*

14:448.

Quattrone, A., Nicoletti, G., Messina, D., Fera, F., Condino, F., Pugliese, P., Lanza, P., *et al.* (2008). MR imaging index for differentiation of progressive supranuclear palsy from Parkinson disease and the Parkinson variant of multiple system atrophy. *Radiology* **246**:214–221.

Rabey, J.M. and Hefti, F. (1990). Neuromelanin synthesis in rat and human substantia nigra. *Journal of Neural Transmission - Parkinson's Disease and Dementia Section* **2**:1–14.

R Core Team (2014). R: A Language and Environment for Statistical Computing. *R Foundation for Statistical Computing*.

Rae, C.L., Correia, M.M., Altena, E., Hughes, L.E., Barker, R.A. and Rowe, J.B. (2012). White matter pathology in Parkinson's disease: the effect of imaging protocol differences and relevance to executive function. *Neuroimage* **62**:1675–1684.

Ramnani, N. (2012). Frontal lobe and posterior parietal contributions to the cortico-cerebellar system. *Cerebellum* **11**:366–383.

Ramnani, N. (2006). The primate cortico-cerebellar system: anatomy and function. *Nature Reviews Neuroscience* **7**:511–522.

Ramnani, N. and Owen, A.M. (2004). Anterior prefrontal cortex: insights into function from anatomy and neuroimaging. *Nature Reviews Neuroscience* **5**:184–194.

Rascol, O., Sabatini, U., Fabre, N., Brefel, C., Loubinoux, I., Celsis, P., Senard, J.M., *et al.* (1997). The ipsilateral cerebellar hemisphere is overactive during hand movements in akinetic parkinsonian patients. *Brain* **120**:103–110.

Redgrave, P., Prescott, T.J. and Gurney, K. (1999). The basal ganglia: A vertebrate solution to the selection problem? *Neuroscience* **89**:1009–1023.

Rietdijk, C.D., Perez-Pardo, P., Garssen, J., van Wezel, R.J.A. and Kraneveld, A.D. (2017). Exploring Braak's hypothesis of parkinson's disease. *Frontiers in Neurology* **8**.

Ring, H.A. (2002). Neuropsychiatry of the basal ganglia. *Journal of Neurology, Neurosurgery & Psychiatry* **72**:12–21.

Rizzo, G., Martinelli, P., Manners, D., Scaglione, C., Tonon, C., Cortelli, P., Malucelli, E., *et*

al. (2008). Diffusion-weighted brain imaging study of patients with clinical diagnosis of corticobasal degeneration, progressive supranuclear palsy and Parkinson's disease. *Brain* **131**:2690–2700.

Robbins, T.W. and Everitt, B.J. (1996). Neurobehavioural mechanisms of reward and motivation. *Current opinion in neurobiology* **6**:228–236.

Rodriguez-Mena, R., Piquer-Belloch, J., Llacer-Ortega, J.L., Riesgo-Suarez, P. and Rovira-Lillo, V. (2017). [3D anatomy of cerebellar peduncles based on fibre microdissection and a demonstration with tractography]. *Neurocirugia (Astur)* **28**:111–123.

Rodriguez-Oroz, M.C., Jahanshahi, M., Krack, P., Litvan, I., Macias, R., Bezard, E. and Obeso, J.A. (2009). Initial clinical manifestations of Parkinson's disease: features and pathophysiological mechanisms. *Lancet Neurol* **8**:1128–1139.

Rodriguez, M.C., Guridi, O.J., Alvarez, L., Mewes, K., Macias, R., Vitek, J., DeLong, M.R., *et al.* (1998). The subthalamic nucleus and tremor in Parkinson's disease. *Movement disorders : official journal of the Movement Disorder Society* **13**:111–118.

Roland, P.E., Larsen, B., Lassen, N.A. and Skinhoj, E. (1980). Supplementary motor area and other cortical areas in organization of voluntary movements in man. *J Neurophysiol* **43**:118–136.

Rolland, A.S., Herrero, M.T., Garcia-Martinez, V., Ruberg, M., Hirsch, E.C. and Francois, C. (2007). Metabolic activity of cerebellar and basal ganglia-thalamic neurons is reduced in parkinsonism. *Brain* **130**:265–275.

Romanelli, P., Esposito, V., Schaal, D.W. and Heit, G. (2005). Somatotopy in the basal ganglia: Experimental and clinical evidence for segregated sensorimotor channels. *Brain Research Reviews* **48**:112–128.

van Rooden, S.M., Visser, M., Verbaan, D., Marinus, J. and van Hilten, J.J. (2009). Patterns of motor and non-motor features in Parkinson's disease. *Journal of Neurology, Neurosurgery, and Psychiatry* **80**:846–850.

Roostaei, T., Nazeri, A., Sahraian, M. and Minagar, A. (2016). *The Human Cerebellum: A Review of Physiologic Neuroanatomy*.

Rosenberg-Katz, K., Herman, T., Jacob, Y., Kliper, E., Giladi, N. and Hausdorff, J.M.

(2016). Subcortical Volumes Differ in Parkinson's Disease Motor Subtypes: New Insights into the Pathophysiology of Disparate Symptoms. *Frontiers in Human Neuroscience* **10**.

Ross, G.W., Petrovitch, H., Abbott, R.D., Tanner, C.M., Popper, J., Masaki, K., Launer, L., *et al.* (2008a). Association of olfactory dysfunction with risk for future Parkinson's disease. *Annals of Neurology* **63**:167–173.

Ross, G.W., Petrovitch, H., Abbott, R.D., Tanner, C.M., Popper, J., Masaki, K., Launer, L., *et al.* (2008b). Association of olfactory dysfunction with risk for future Parkinson's disease. *Annals of Neurology*.

Rye, D.B. (2004). The two faces of Eve: dopamine's modulation of wakefulness and sleep. *Neurology* **63**:S2-7.

Sakai, S.T., Inase, M. and Tanji, J. (1996). Comparison of cerebellothalamic and pallidothalamic projections in the monkey (Macaca fuscata): a double anterograde labeling study. *J Comp Neurol* **368**:215–228.

Sako, W., Murakami, N., Miyazaki, Y., Abe, T., Harada, M., Izumi, Y. and Kaji, R. (2015). The effect of tremor onset on middle cerebellar peduncle of Parkinson's disease. *Journal of the Neurological Sciences* **358**:172–177.

Samuel, M., Ceballos-Baumann, A.O., Boecker, H. and Brooks, D.J. (2001). Motor imagery in normal subjects and Parkinson's disease patients: an H215O PET study. *Neuroreport* **12**:821–8.

De Santis, S., Drakesmith, M., Bells, S., Assaf, Y. and Jones, D.K. (2014). Why diffusion tensor MRI does well only some of the time: Variance and covariance of white matter tissue microstructure attributes in the living human brain. *NeuroImage* **89**:35–44.

Saper, C.B., Chou, T.C. and Scammell, T.E. (2001). The sleep switch: hypothalamic control of sleep and wakefulness. *Trends in neurosciences* **24**:726–731.

Schell, G.R. and Strick, P.L. (1984). The origin of thalamic inputs to the arcuate premotor and supplementary motor areas. *The Journal of neuroscience : the official journal of the Society for Neuroscience* **4**:539–560.

Schmahmann, J.D. (1996). From movement to thought: anatomic substrates of the cerebellar contribution to cognitive processing. *Hum Brain Mapp* **4**:174–198.

Schonberg, T., Pianka, P., Hendler, T., Pasternak, O. and Assaf, Y. (2006). Characterization of displaced white matter by brain tumors using combined DTI and fMRI. *NeuroImage* **30**:1100–11.

Schwarz, S.T., Abaei, M., Gontu, V., Morgan, P.S., Bajaj, N. and Auer, D.P. (2013). Diffusion tensor imaging of nigral degeneration in Parkinson's disease: A region-of-interest and voxel-based study at 3 T and systematic review with meta-analysis. *Neuroimage Clin* **3**:481–488.

Schweder, P.M., Hansen, P.C., Green, A.L., Quaghebeur, G., Stein, J. and Aziz, T.Z. (2010). Connectivity of the pedunculopontine nucleus in parkinsonian freezing of gait. *NeuroReport* **21**:914–916.

Selemon, L.D. and Goldman-Rakic, P.S. (1985). Longitudinal topography and interdigitation of corticostriatal projections in the rhesus monkey. *The Journal of Neuroscience* **5**:776–794.

Sen, S., Kawaguchi, A., Truong, Y., Lewis, M.M. and Huang, X. (2010). Dynamic changes in cerebello-thalamo-cortical motor circuitry during progression of Parkinson's disease. *Neuroscience* **166**:712–719.

Shannon, K.M., Keshavarzian, A., Mutlu, E., Dodiya, H.B., Daian, D., Jaglin, J.A. and Kordower, J.H. (2012). Alpha-synuclein in colonic submucosa in early untreated Parkinson's disease. *Movement Disorders* **27**:709–715.

Smith, S.M., Jenkinson, M., Johansen-Berg, H., Rueckert, D., Nichols, T.E., Mackay, C.E., Watkins, K.E., *et al.* (2006). Tract-based spatial statistics: Voxelwise analysis of multi-subject diffusion data. *NeuroImage* **31**:1487–1505.

Smith, S.M., Jenkinson, M., Woolrich, M.W., Beckmann, C.F., Behrens, T.E., Johansen-Berg, H., Bannister, P.R., *et al.* (2004). Advances in functional and structural MR image analysis and implementation as FSL. *Neuroimage* **23 Suppl 1**:S208-19.

Smith, S.M. and Nichols, T.E. (2009). Threshold-free cluster enhancement: Addressing problems of smoothing, threshold dependence and localisation in cluster inference. *NeuroImage* **44**:83–98.

Smith, Y., Bevan, M.D., Shink, E. and Bolam, J.P. (1998). Microcircuitry of the direct and indirect pathways of the basal ganglia. *Neuroscience* **86**:353–387.

Solano, S.M., Miller, D.W., Augood, S.J., Young, A.B. and Penney Jr., J.B. (2000). Expression of alpha-synuclein, parkin, and ubiquitin carboxy-terminal hydrolase L1 mRNA in human brain: genes associated with familial Parkinson's disease. *Annals of Neurology* **47**:201–10.

Song, S.K., Sun, S.W., Ramsbottom, M.J., Chang, C., Russell, J. and Cross, A.H. (2002). Dysmyelination revealed through MRI as increased radial (but unchanged axial) diffusion of water. *Neuroimage* **17**:1429–1436.

Stieltjes, B., Kaufmann, W.E., van Zijl, P.C., Fredericksen, K., Pearlson, G.D., Solaiyappan, M. and Mori, S. (2001). Diffusion tensor imaging and axonal tracking in the human brainstem. *Neuroimage* **14**:723–735.

Stoodley, C.J. and Schmahmann, J.D. (2009). Functional topography in the human cerebellum: a meta-analysis of neuroimaging studies. *Neuroimage* **44**:489–501.

Subramanian, L., Hindle, J. V, Johnston, S., Roberts, M. V, Husain, M., Goebel, R. and Linden, D. (2011). Real-time functional magnetic resonance imaging neurofeedback for treatment of Parkinson's disease. *J Neurosci* **31**:16309–16317.

Subramanian, L., Morris, M.B., Brosnan, M., Turner, D.L., Morris, H.R. and Linden, D.E.J. (2016). Functional Magnetic Resonance Imaging Neurofeedback-guided Motor Imagery Training and Motor Training for Parkinson's Disease: Randomized Trial. *Frontiers in Behavioral Neuroscience* **10**.

Surova, Y., Nilsson, M., Lätt, J., Lampinen, B., Lindberg, O., Hall, S., Widner, H., *et al.* (2015). Disease-specific structural changes in thalamus and dentatorubrothalamic tract in progressive supranuclear palsy. *Neuroradiology* **57**:1079–1091.

Sweet, J.A., Walter, B.L., Gunalan, K., Chaturvedi, A., McIntyre, C.C. and Miller, J.P. (2014). Fiber tractography of the axonal pathways linking the basal ganglia and cerebellum in Parkinson disease: implications for targeting in deep brain stimulation. *J Neurosurg* **120**:988–996.

Takada, M., Tokuno, H., Hamada, I., Inase, M., Ito, Y., Imanishi, M., Hasegawa, N., *et al.* (2001). Organization of inputs from cingulate motor areas to basal ganglia in macaque monkey. *European Journal of Neuroscience* **14**:1633–1650.

Takada, M., Tokuno, H., Nambu, A. and Inase, M. (1998). Corticostriatal projections from the somatic motor areas of the frontal cortex in the macaque monkey: Segregation versus overlap of input zones from the primary motor cortex, the supplementary motor area, and the premotor cortex. *Experimental Brain Research* **120**:114–128.

Takahashi, M., Ono, J., Harada, K., Maeda, M. and Hackney, D.B. (2000). Diffusional anisotropy in cranial nerves with maturation: quantitative evaluation with diffusion MR imaging in rats. *Radiology* **216**:881–885.

Takeda, S., Yamazaki, K., Miyakawa, T. and Arai, H. (1993). Parkinson's disease with involvement of the parasympathetic ganglia. *Acta Neuropathol (Berl)* **86**:397–398.

Tamas Kincses, Z., Johansen-Berg, H., Tomassini, V., Bosnell, R., Matthews, P.M. and Beckmann, C.F. (2008). Model-free characterization of brain functional networks for motor sequence learning using fMRI. *Neuroimage* **39**:1950–1958.

Tanji, J. and Kurata, K. (1979). Neuronal activity in the cortical supplementary motor area related with distal and proximal forelimb movements. *Neuroscience Letters* **12**:201–206.

Tanji, J., Taniguchi, K. and Saga, T. (1980). Supplementary motor area: neuronal response to motor instructions. *Journal of neurophysiology* **43**:60–68.

Tessitore, A., Amboni, M., Esposito, F., Russo, A., Picillo, M., Marcuccio, L., Pellecchia, M.T., *et al.* (2012). Resting-state brain connectivity in patients with Parkinson's disease and freezing of gait. *Parkinsonism Relat Disord* [Online] **18**:781–787. Available at: http://www.ncbi.nlm.nih.gov/pubmed/22510204.

Tessitore, A., Esposito, F., Vitale, C., Santangelo, G., Amboni, M., Russo, A., Corbo, D., *et al.* (2012). Default-mode network connectivity in cognitively unimpaired patients with Parkinson disease. *Neurology* **79**:2226–2232.

Torres, C. V, Manzanares, R. and Sola, R.G. (2014). Integrating diffusion tensor imaging-based tractography into deep brain stimulation surgery: a review of the literature. *Stereotactic & Functional Neurosurgery* **92**:282–90.

Tournier, J.D., Calamante, F., Gadian, D.G. and Connelly, A. (2004). Direct estimation of the fiber orientation density function from diffusion-weighted MRI data using spherical deconvolution. *Neuroimage* **23**:1176–85.

Del Tredici, K. and Braak, H. (2008). A not entirely benign procedure: progression of Parkinson's disease. *Acta Neuropathologica* **115**:379–384.

Tredici, K. Del, Hawkes, C.H., Ghebremedhin, E. and Braak, H. (2010). Lewy pathology in the submandibular gland of individuals with incidental Lewy body disease and sporadic parkinson's disease. *Acta Neuropathologica* **119**:703–713.

Del Tredici, K., Rüb, U., de Vos, R.A.I., Bohl, J.R.E. and Braak, H. (2002). Where Does Parkinson Disease Pathology Begin in the Brain? *Journal of Neuropathology & Experimental Neurology* **61**:413–426.

Tseng, C.E.J., Froudist-Walsh, S., Brittain, P.J., Karolis, V., Caldinelli, C., Kroll, J., Counsell, S.J., *et al.* (2017). A multimodal imaging study of recognition memory in very preterm born adults. *Human Brain Mapping* **38**:644–655.

Tuch, D.S. (2004). Q-ball imaging. *Magnetic Resonance in Medicine*.

Tuch, D.S., Reese, T.G., Wiegell, M.R., Makris, N., Belliveau, J.W. and Van Wedeen, J. (2002). High angular resolution diffusion imaging reveals intravoxel white matter fiber heterogeneity. *Magnetic Resonance in Medicine* **48**:577–582.

Ulmer, J.L., Klein, A.P., Mueller, W.M., DeYoe, E.A. and Mark, L.P. (2014). Preoperative diffusion tensor imaging: Improving neurosurgical outcomes in brain tumor patients. *Neuroimaging Clinics of North America* **24**:599–617.

Vaillancourt, D.E., Thulborn, K.R. and Corcos, D.M. (2003). Neural Basis for the Processes that Underlie Visually-Guided and Internally-Guided Force Control in Humans. *J Neurophysiol* **90**:3330–3340.

Vanderauwera, J., Vandermosten, M., Dell'Acqua, F., Wouters, J. and Ghesquière, P. (2015). Disentangling the relation between left temporoparietal white matter and reading: A spherical deconvolution tractography study. *Human Brain Mapping* **36**:3273–3287.

Vergani, F., Lacerda, L., Martino, J., Attems, J., Morris, C., Mitchell, P., Thiebaut de Schotten, M., *et al.* (2014). White matter connections of the supplementary motor area in humans. *J Neurol Neurosurg Psychiatry* **85**:1377–1385.

Vitek, J.L., Ashe, J., DeLong, M.R. and Alexander, G.E. (1994). Physiologic properties and somatotopic organization of the primate motor thalamus. *Journal of neurophysiology*

71:1498–1513.

Vos, S.B., Jones, D.K., Viergever, M.A. and Leemans, A. (2011). Partial volume effect as a hidden covariate in DTI analyses. *Neuroimage* **55**:1566–1576.

Wakabayashi, K., Takahashi, H., Takeda, S., Ohama, E. and Ikuta, F. (1988). Parkinson's disease: the presence of Lewy bodies in Auerbach's and Meissner's plexuses. *Acta Neuropathologica* **76**:217–221.

Wang, L., Magen, I., Yuan, P.Q., Subramaniam, S.R., Richter, F., Chesselet, M.F. and Taché, Y. (2012). Mice overexpressing wild-type human alpha-synuclein display alterations in colonic myenteric ganglia and defecation. *Neurogastroenterology and Motility* **24**:e425–e436.

Wang, P.S., Wu, H.M., Lin, C.P. and Soong, B.W. (2011). Use of diffusion tensor imaging to identify similarities and differences between cerebellar and Parkinsonism forms of multiple system atrophy. *Neuroradiology* **53**:471–81.

van Wassenaer-van Hall, H.N., van den Heuvel, A.G., Jansen, G.H., Hoogenraad, T.U. and Mali, W.P. (1995). Cranial MR in Wilson disease: abnormal white matter in extrapyramidal and pyramidal tracts. *American Journal of Neuroradiology* [Online] **16**:2021–2027. Available at: http://www.ajnr.org/content/ajnr/16/10/2021.full.pdf.

Wedeen, V.J., Hagmann, P., Tseng, W.Y.I., Reese, T.G. and Weisskoff, R.M. (2005). Mapping complex tissue architecture with diffusion spectrum magnetic resonance imaging. *Magnetic Resonance in Medicine* **54**:1377–86.

Westerlund, M., Belin, A.C., Anvret, A., Håkansson, A., Nissbrandt, H., Lind, C., Sydow, O., *et al.* (2008). Cerebellar alpha-synuclein levels are decreased in Parkinson's disease and do not correlate with SNCA polymorphisms associated with disease in a Swedish material. *The FASEB journal : official publication of the Federation of American Societies for Experimental Biology* **22**:3509–14.

Wichmann, T., Bergman, H. and DeLong, M.R. (1994). The primate subthalamic nucleus. I. Functional properties in intact animals. *Journal of Neurophysiology* **72**:494–506.

Wichmann, T. and Dostrovsky, J.O. (2011). Pathological basal ganglia activity in movement disorders. *Neuroscience* **198**:232–244.

Williams, Z.M. (2015). Good vibrations with deep brain stimulation. *Nature Neuroscience* **18**:618–619.

Winston, G.P. (2012a). The physical and biological basis of quantitative parameters derived from diffusion MRI. *Quantitative imaging in medicine and surgery* **2**:254–265.

Winston, G.P. (2012b). The physical and biological basis of quantitative parameters derived from diffusion MRI. *Quant Imaging Med Surg* **2**:254–265.

Worbe, Y., Marrakchi-Kacem, L., Lecomte, S., Valabregue, R., Poupon, F., Guevara, P., Tucholka, A., *et al.* (2015). Altered structural connectivity of cortico-striato-pallido-thalamic networks in Gilles de la Tourette syndrome. *Brain* [Online] **138**:472–482. Available at: http://brain.oxfordjournals.org/content/brain/138/2/472.full.pdf.

Wu, T. and Hallett, M. (2013). The cerebellum in Parkinson's disease. *Brain* **136**:696–709.

Wu, T., Long, X., Zang, Y., Wang, L., Hallett, M., Li, K. and Chan, P. (2009). Regional homogeneity changes in patients with Parkinson's disease. *Human brain mapping* **30**:1502–1510.

Yoo, K., Chung, S.J., Kim, H.S., Choung, O.-H., Lee, Y.-B., Kim, M.-J., You, S., *et al.* (2015). Neural substrates of motor and non-motor symptoms in Parkinson's disease: a resting FMRI study. *PloS one* **10**:e0125455.

Yu, H., Sternad, D., Corcos, D.M. and Vaillancourt, D.E. (2007a). Role of hyperactive cerebellum and motor cortex in Parkinson's disease. *NeuroImage* **35**:222–33.

Yu, H., Sternad, D., Corcos, D.M. and Vaillancourt, D.E. (2007b). Role of hyperactive cerebellum and motor cortex in Parkinson's disease. *NeuroImage*.

Zhang, K., Yu, C., Zhang, Y., Wu, X., Zhu, C., Chan, P. and Li, K. (2011). Voxel-based analysis of diffusion tensor indices in the brain in patients with Parkinson's disease. *Eur J Radiol* **77**:269–273.

Zhang, K.Y., Yu, C.S., Zhang, Y.J., Wu, X.L., Zhu, C.Z., Chan, P. and Li, K.C. (2011). Voxel-based analysis of diffusion tensor indices in the brain in patients with Parkinson's disease. *European Journal of Radiology*.

Zhao, J., Thiebaut de Schotten, M., Altarelli, I., Dubois, J. and Ramus, F. (2016). Altered

hemispheric lateralization of white matter pathways in developmental dyslexia: Evidence from spherical deconvolution tractography. *Cortex* **76**:51–62.

Zigmond, M.J., Abercrombie, E.D., Berger, T.W., Grace, A.A. and Stricker, E.M. (1990). Compensations after lesions of central dopaminergic neurons: some clinical and basic implications. *Trends in Neurosciences* **13**:290–6.

Zijdenbos, A.P., Dawant, B.M., Margolin, R.A. and Palmer, A.C. (1994). Morphometric analysis of white matter lesions in MR images: method and validation. *IEEE Trans Med Imaging* **13**:716–724.

Chapter 8 Supplementary material

8.1 Chapter 3 Supplementary material

Supplementary Table 3.1 Affected versus unaffected hemisphere analysis

PD Tracts	FA in affected hemisphere (mean ± SD)	FA in unaffected hemisphere (mean ± SD)	t-value	df	p-value
CST	0.5687 ± 0.033	0.5705 ± 0.024	-0.2861	21	0.7776
SMA-PUT	0.4612 ± 0.032	0.4701 ± 0.034	-1.3333	21	0.1967
THAL-MC	0.5200 ± 0.033	0.5137 ± 0.041	0.9283	21	0.3638
UNF	0.4037 ± 0.023	0.4045 ± 0.020	-0.1787	21	0.8599
MFB	0.4480 ± 0.028	0.4488 ± 0.031	-0.1251	21	0.9016

Supplementary Table 3.1 shows paired-t-tests between the FA values of the affected and unaffected hemispheres of the PD patients. The affected hemisphere calculation was done from the motor scale of the pre intervention off medication UPDRS scores. Of the 24 PD patients, 10 were affected on the left hemisphere and 12 were affected on the right hemisphere while two were affected bilaterally. The results show no differences in FA.

Supplementary Table 3.2 Additional tractography measures

ADDITIONAL TRACTOGRAPHY MEASURES	26 HC mean ± sd	24 PD mean ± sd	Uncorrected p value	Bonferroni corrected p value
Number of reconstructed streamlines				
L-CST	226.08 ± 114.02	388.4583 ± 144.21	7.00E-05	0.00448128
R-CST	150.8 ± 74.59	301.38 ± 154.31	0.0001313	0.0084032
L-UNF	122.6538 ± 77.41	319.375 ± 120.81	4.32E-08	2.77E-06
R-UNF	127.3077 ± 89.29	245.4167 ± 115.81	0.000233	0.014912
L-THAL-MC	511.7692 ± 213.29	861.6667 ± 286.66	1.62E-05	0.00103936
R-THAL-MC	482.5 ± 206.54	845.5 ± 342.39	6.60E-05	0.00422464
L-SMA-PUT	309.1538 ± 304.34	387.125 ± 243.01	0.3202	1
R-SMA-PUT	412.2692 ± 258.92	305.4583 ± 226.61	0.1265	1
Number of voxels occupied				
L-CST	55144.92 ± 31355.74	101776 ± 39556.99	3.66E-05	0.0023392
R-CST	36720.04 ± 19048.19	76711.96 ± 39201.36	7.48E-05	0.004784
L-UNF	21796.31 ± 14363.91	51676.46 ± 22440.19	2.20E-06	0.00014099
R-UNF	20803 ± 15147.96	36972.25 ± 19556.66715	0.002251	0.144064
L-THAL-MC	70840.92 ± 31314.81	123591.33 ± 45097.07	2.41E-05	0.00154112
R-THAL-MC	65971.58 ± 30102.2	118596.58 ± 51327.33	9.70E-05	0.00620608
L-SMA-PUT	41776.5 ± 41788.07	51178.96 ± 33445.52	0.3825	1
R-SMA-PUT	52861.46 ± 32879.99	40739.88 ± 2281.64	0.1856	1
Tract volume				
L-CST	4062.192 ± 1331.57	5679.39 ± 1631.49	0.000409	0.026176
R-CST	3225.038 ± 1069.84	4783.381 ± 1848.04	0.0009185	0.058784

L-UNF	2321.385 ± 1199.01	4917.796 ± 1725.59	2.92E-07	2.92E-07
R-UNF	2626.654 ± 1399.54	4269.982 ± 1709.79	0.0005878	0.0376192
L-THAL-MC	4523.423 ± 1634.04	6965.428 ± 1962.54	2.04E-05	0.00130624
R-THAL-MC	4435.346 ± 1600.88	7031.932 ± 2365.56	5.59E-05	0.00357888
L-SMA-PUT	3699.692 ± 2806.51	4029.246 ± 1979.24	0.6317	1
R-SMA-PUT	4900.962 ± 2281.64	3600.541 ± 1877.41	0.03217	1
Tract length				
L-CST	118.0652 ± 11.45	129.1263 ± 9.52	0.0005202	0.0332928
R-CST	119.9535 ± 12.09	125.7192 ± 10.24	0.07447	1
L-UNF	89.70457 ± 10.08	78.89722 ± 8.42	0.000148	0.009472
R-UNF	80.14056 ± 14.32	72.86341 ± 8.34	0.03234	1
L-THAL-MC	68.47292 ± 5.42	70.43006 ± 4.68	0.1771	1
R-THAL-MC	67.47677 ± 5.63	68.82386 ± 6.28	0.43	1
L-SMA-PUT	63.44871 ± 7.12	64.1478 ± 6.95	0.727	1
R-SMA-PUT	63.05385 ± 5.71	65.63078 ± 7.25	0.1636	1

Supplementary Table 3.2 shows the two-samples t-tests between PD and controls for each extracted additional tractography measure. PD-Parkinson's disease patients, HC-Healthy Controls. CST - Corticospinal tract, SMA-PUT - Supplementary motor area-putamen tract, THAL-MC - Thalamus-motor cortex tract, UNF - Uncinate Fasiculus. L-Left, R-Right. Bonferroni corrected $p < 0.05$ (0.05/32=0.00156), SD - Standard deviation.

Supplementary Table 3.3 Correlation analysis results

Tract and metrics	**R-CST-FA**		**L-CST-FA**		**R-SMA-PUT-FA**	
	t	p-value	t	p-value	t	p-value
Finger sequence task - Reaction time	0.6677	0.5116	0.8498	0.405	-1.0423	0.3091
Finger sequence task - Correct number of taps	-1.2174	0.2392	-1.4636	0.1605	-1.4333	0.1689
Duration since diagnosis (in months)	-0.9167	0.3697	-1.1495	0.2633	-1.0893	0.2884
Pre intervention off medication UPDRS scores	1.6902	0.1051	1.4594	0.1586	0.8887	0.3838
Finger tapping on dominant hand	0.8135	0.4247	0.6358	0.5315	0.6302	0.5351
Finger tapping on non-dominant hand	-1.4504	0.1611	-0.457	0.6521	-1.0759	0.2936
Finger tapping on both hands	-0.325	0.7483	0.1245	0.9021	-0.2344	0.8169

R-CST-FA – Right corticospinal tract fractional anisotropy, L-CST-FA – left corticospinal tract fractional anisotropy, R-SMA-PUT-FA, Right supplementary motor area-putamen fractional anisotropy

Supplementary table 3.4 Correlation analyses results

Tract and metrics	R-THAL-MC-FA		L-THAL-MC-FA		R-UNF-FA	
	t	p-value	t	p-value	t	p-value
Finger sequence task - Reaction time	0.5087	0.6162	-0.0388	0.9694	2.2022	0.03896
Finger sequence task - Correct number of taps	-0.7364	0.471	-1.4031	0.1776	0.3975	0.6956
Duration since diagnosis (in months)	-1.4269	0.1683	-1.5508	0.1359	1.9158	0.0691
Pre intervention off medication UPDRS scores	1.8738	0.07431	1.5235	0.1419	0.7046	0.4884
Finger tapping on dominant hand	-0.1591	0.8751	0.8458	0.4067	1.1152	0.2768
Finger tapping on non-dominant hand	-0.9068	0.3743	-1.1512	0.262	0.9712	0.342
Finger tapping on both hands	-0.6383	0.5298	-0.1448	0.8862	1.2986	0.2075

R-THAL-MC-FA – Right thalamus-motor cortex fractional anisotropy, L-THAL-MC-FA – Left thalamus-motor cortex fractional anisotropy, R-UNF-FA – Right uncinated fasciculus fractional anisotropy.

TBSS analysis

The FSL tool "TBSS" (Tract-based spatial statistics) (Jenkinson *et al.* 2012; Smith *et al.* 2006) was used to compare diffusion measures between PD patients and controls. Subjects' individual FA images were first registered to a common template. As PD is a neurodegenerative disease, some degree of atrophy is often present, which can result in enlarged ventricles. With normal ageing, there can also be atrophy and enlargement of the ventricles. Registration to a study-specific image was chosen with the aim of more accurate alignment of the centre of tracts across subjects. Subjects' FA images were therefore registered to the FA image of the most "representative" subject, which is automatically detected by TBSS according to which image requires the least transformation to the FA images of all other subjects. After subjects' individual FA images were registered to this initial template, they were registered to MNI152 space for convenience of display and reporting. The mean FA skeleton, a representation of the centre of the white matter tracts common to all subjects, was created and with a threshold FA > 0.2. Subjects' MNI152-registered FA images were projected onto the skeleton before statistics were performed on each skeleton voxel using permutations testing with the FSL tool "Randomise".

A design matrix was generated using the FSL tool "Glm", in which images were categorised according to subject group (PD patient or control). The repeated measures element of the design

was specified using the "group" option in the Glm tool. Age and gender were added as covariates and were demeaned within options of the Randomise tool.

This design matrix was used to analyse subjects' FA images using the FSL tool randomise, with 500 permutations. The randomise option threshold-free cluster enhancement (TFCE) was applied (Smith and Nichols 2009). All statistic images were corrected for multiple comparisons, FWE (family-wise error) with threshold of $p<0.05$. Any regions on the skeleton showing significant clusters were localised using the "John Hopkins University ICBM-DTI-81 White Matter Labels" and "John Hopkins University White Matter Tractography" atlases in FSL.

TBSS results

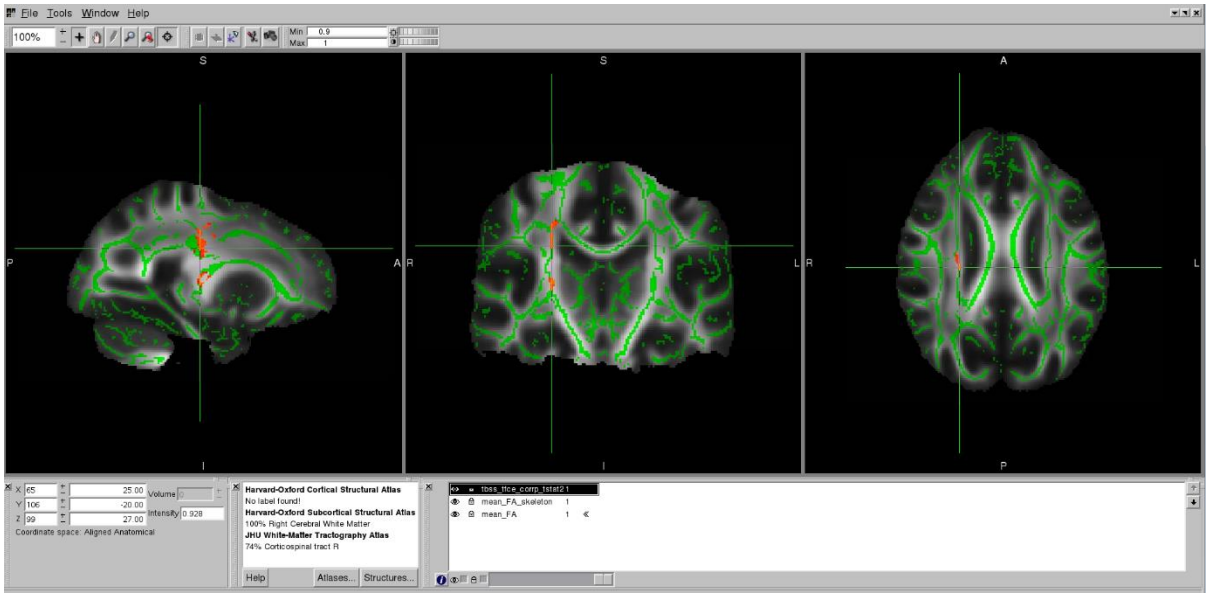

Supplementary Figure 3.1 shows FA values in PD>Controls. There was higher FA in the right corticospinal tract compared to healthy controls ($p<0.05$, FWE) and there was also higher FA in the right thalamus, right putamen and right cortex regions however this did not reach significance ($p<0.07$, FWE).

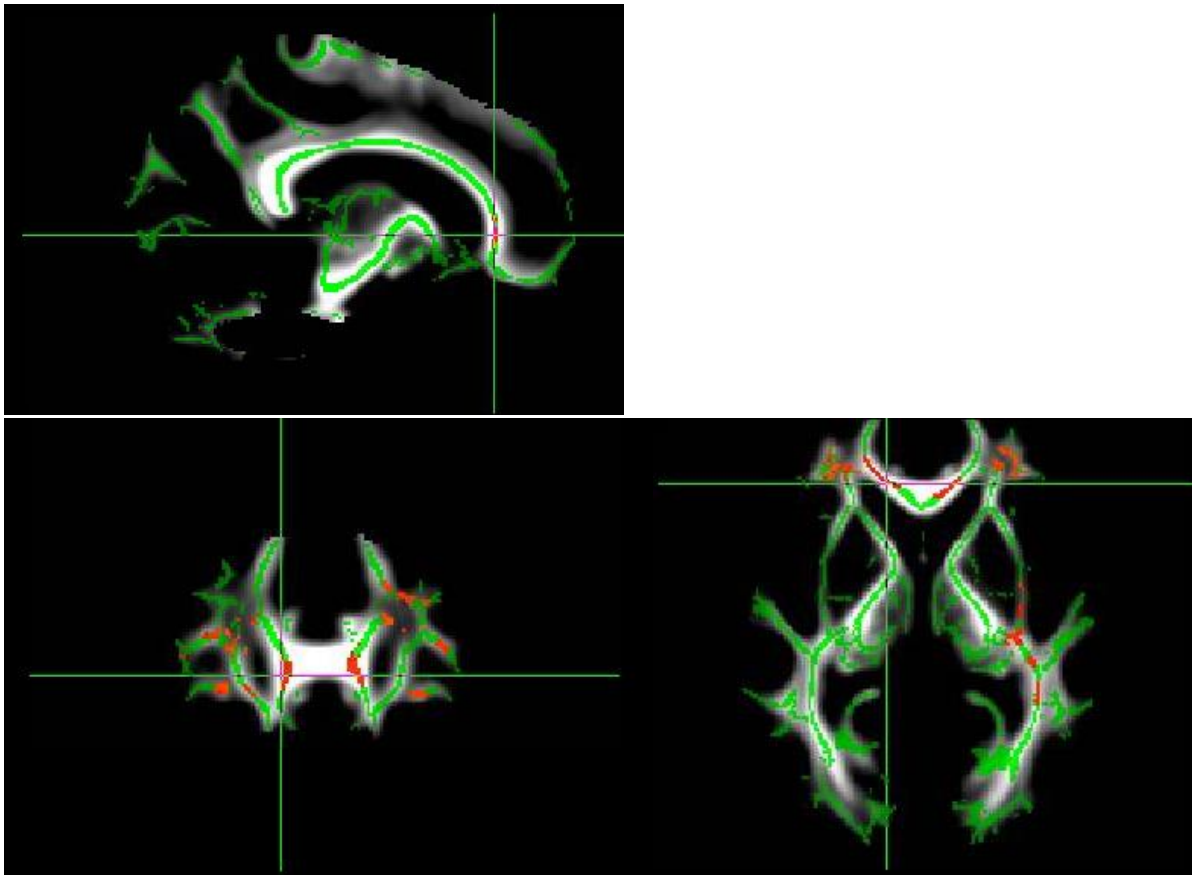

Supplementary Figure 3.2 shows TBSS results for FA values in Controls > PD, $p<0.05$ Family wise error corrected. In controls, there was higher FA in the left and right Uncinate fasiculus, , left and right superior longitudinal fasiculus, left and right inferior occipital fasiculus, Forceps minor and major, and anterior thalamic radiation.

8.2 Chapter 4 Supplementary material

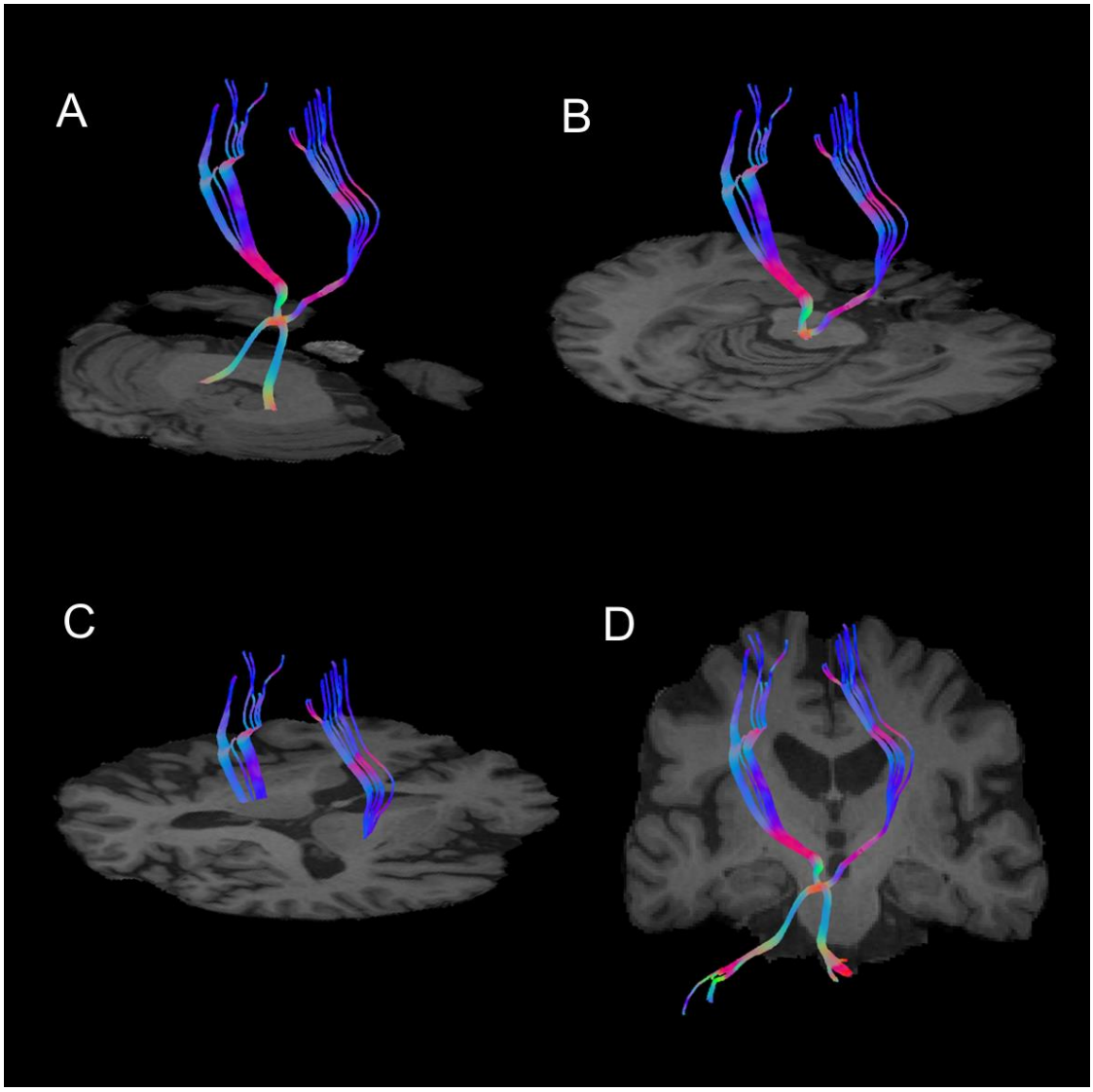

Supplementary Figure 4.1 The left and right DRTT on axial and coronal views in T1 anatomical scan of representative subject. A shows the tracts passing though the dentate nucleus on left and right side, B shows the decussation of the tracts to the contralateral hemispheres, C shows the tracts passing through the thalamus and in this example passing on to the supplementary motor area and the primary motor cortex. D shows the two tracts in the coronal view.

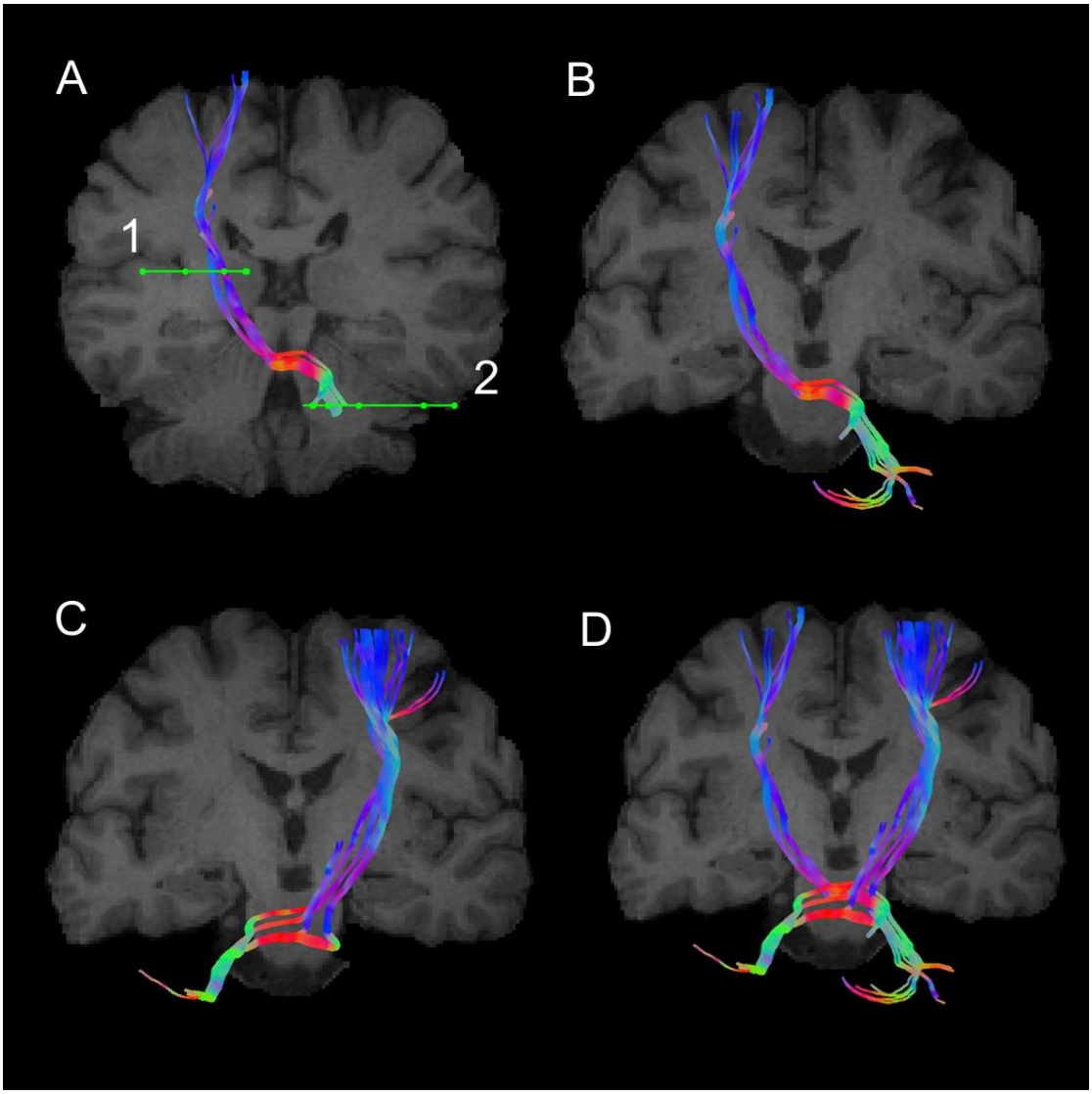

Supplementary Figure 4.2 The reconstructed SPCT in an axial view of a representative subject, A shows the left SPCT with the alternative ROIs 1 and 2, B shows the left SPCT, C shows the right SPCT, and D shows both the right and the left SPCTs.

Probability maps

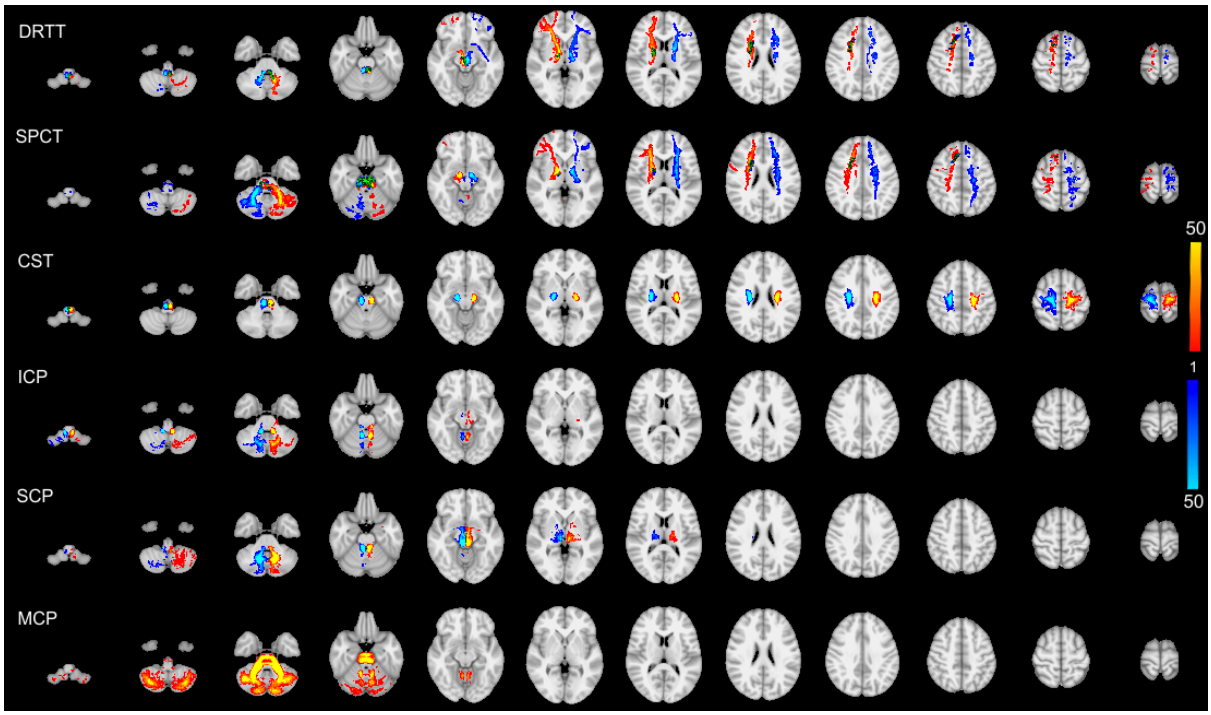

Supplementary Figure 4.3 The probability maps in axial slices, showing the probability (in percent) of projections of the DRTT, SPCT, CST, ICP, SCP and MCP tracts in the PD group. The range is from 1-50, hence areas of the brain showing yellow have at least 50% of participants' tracts passing through those voxels.

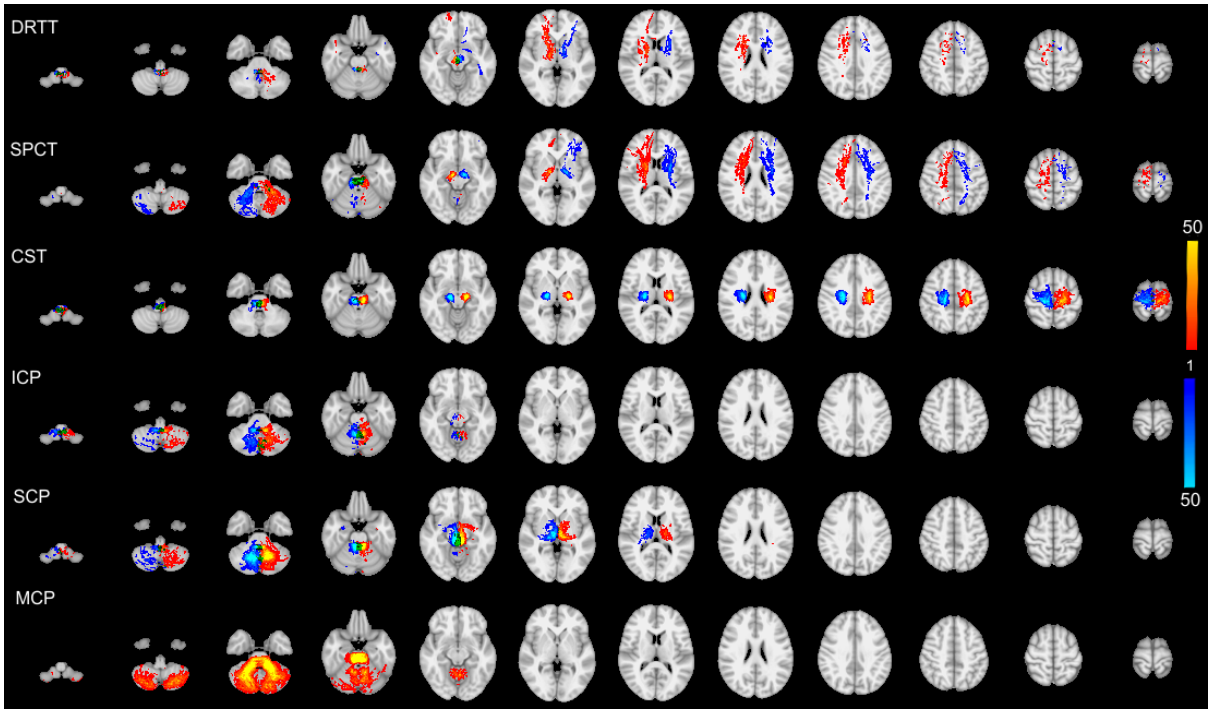

Supplementary Figure 4.4 The probability maps in axial slices, showing the probability (in percent) of projections of the DRTT, SPCT, CST, ICP, SCP and MCP tracts in the MHC group. The range is from 1-50, hence areas of the brain showing yellow have at least 50% of participants' tracts passing through those voxels.

Spatial overlap

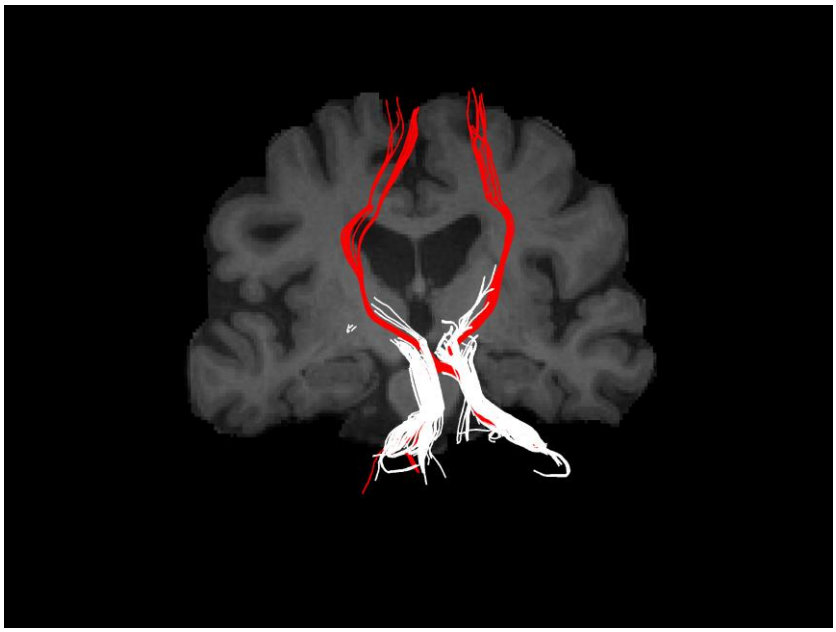

Supplementary Figure 4.5 DRTT (red) and SCP (white) overlap

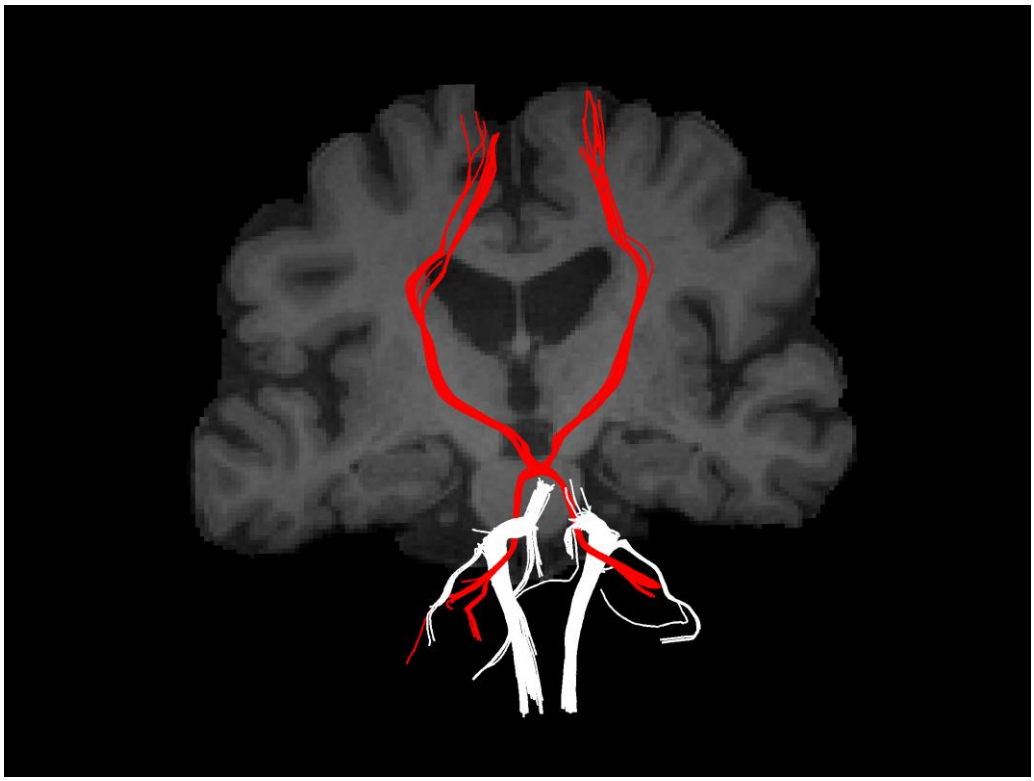

Supplementary Figure 4.6 DRTT (red) and ICP (white)

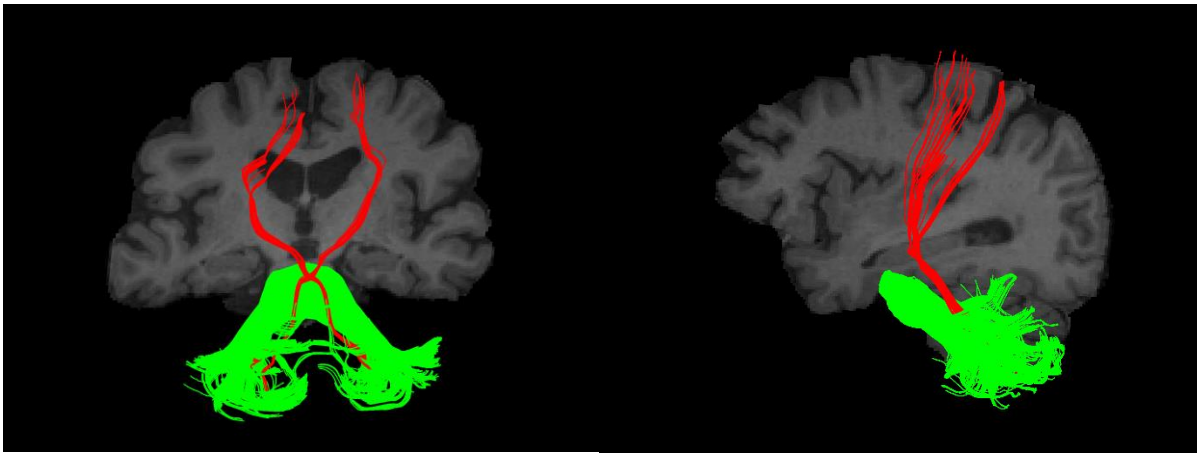

Supplementary Figure 4.7 DRTT (red) and MCP (green)

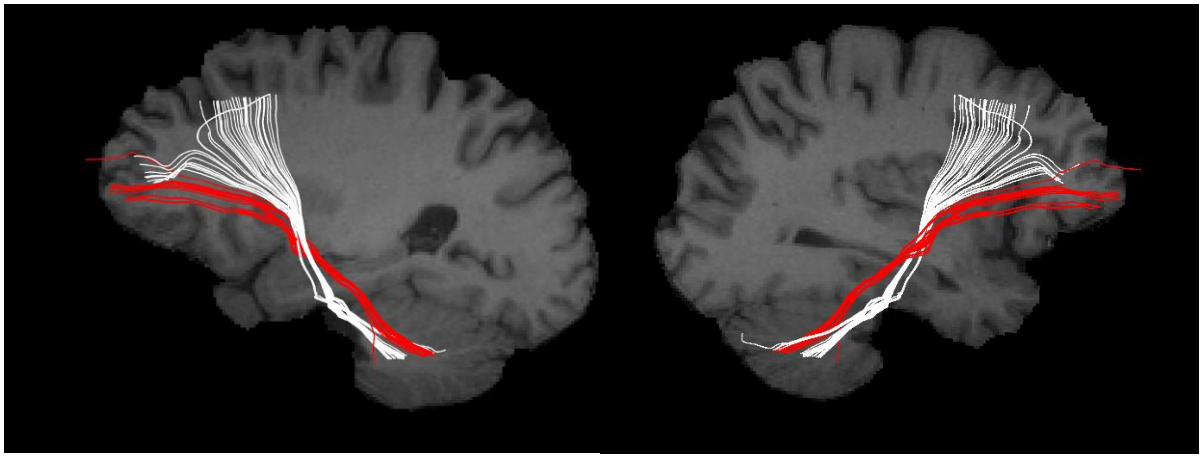

Supplementary Figure 4.8 DRTT (red) and SPCT (white)

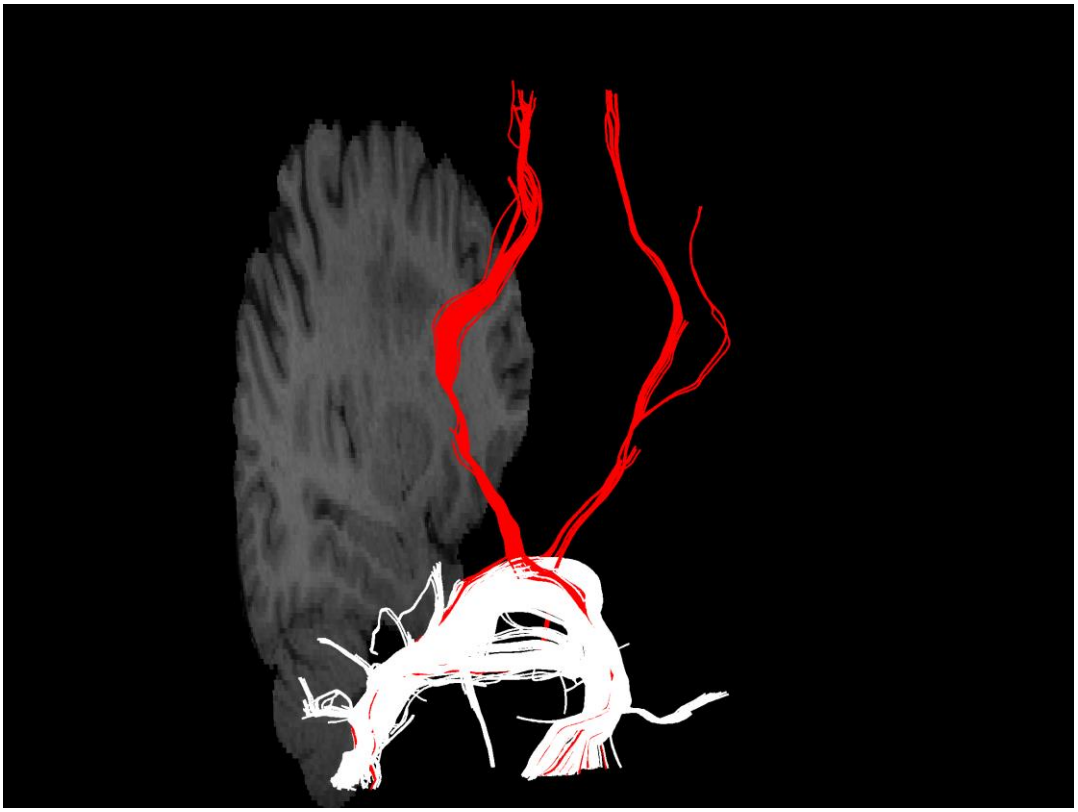

Supplementary Figure 4.9 SPCT (red) and MCP (white) overlap

Supplementary Table 4.1 Inter-rater reliability of reconstructions for individual fiber tracts

Tract	Group	Min. Dice score	Max. Dice score	Dice score mean ± SD	Percent of ILs tract voxels in JMs tract	Percent of JMs tract voxels in ILs tract
L DRTT	YHC	50	62	58 ± 7	92 ± 14	42 ± 4
	MHC	52	100	72 ± 22	93 ± 14	62 ± 28
	PD	1	72	48 ± 41	58 ± 47	45 ± 40
R DRTT	YHC	27	96	50 ± 40	100	41 ± 44
	MHC	58	100	79 ± 30	100	70 ± 42
	PD	64	86	75 ± 16	100	62 ± 21
L SPCT	YHC	90	90	90	100	82
	MHC	77	79	78 ± 1	84 ± 17	77 ± 20
	PD	30	91	58 ± 24	84 ± 30	56 ± 29
R SPCT	YHC	50	100	83 ± 22	96 ± 8	78 ± 32
	MHC	68	72	70 ± 3	89 ± 2	58 ± 4
	PD	30	100	65 ± 49	100	59 ± 58
L CST	YHC	18	66	44 ± 20	69 ± 21	36 ± 18
	MHC	13	95	70 ± 34	74 ± 30	68 ± 35
	PD	37	95	76 ± 25	75 ± 30	89 ± 18
R CST	YHC	4	95	54 ± 39	62 ± 40	50 ± 38
	MHC	40	84	63 ± 16	72 ± 17	63 ± 25
	PD	86	94	89 ± 3	92 ± 8	88 ± 9
L ICP	YHC	28	72	51 ± 18	82 ± 21	38 ± 17
	MHC	69	95	80 ± 10	74 ± 16	88 ± 3
	PD	19	56	42 ± 18	48 ± 28	40 ± 19
R ICP	YHC	46	70	56 ± 10	89 ± 9	42 ± 11
	MHC	55	78	73 ± 12	76 ± 15	71 ± 13
	PD	44	86	70 ± 17	76 ± 11	69 ± 24
L SCP	YHC	47	70	59 ± 11	76 ± 14	50 ± 13
	MHC	31	82	65 ± 24	78 ± 6	62 ± 32
	PD	65	79	73 ± 5	81 ± 13	70 ± 16
R SCP	YHC	52	75	64 ± 11	81 ± 10	55 ± 14
	MHC	43	69	54 ± 18	80 ± 14	45 ± 23
	PD	62	76	70 ± 7	77 ± 23	68 ± 11
MCP	YHC	85	97	90 ± 4	89 ± 7	91 ± 8
	MHC	88	99	85 ± 5	99 ± 1	92 ± 8
	PD	89	98	95 ± 4	98 ± 2	93 ± 8

YHC - Young Healthy Controls, PD – Parkinson's disease, MHC – Matched Healthy Controls, SD - Standard deviation, L - Left, R - Right, DRTT – Dentato-Rubro-Thalamic Tract, SPCT – Subthalamo-Ponto-Cerebellar Tract, CST – Corticospinal tract, ICP – Inferior Cerebellar Peduncle, SCP – Superior Cerebellar Peduncle, MCP - Middle Cerebellar Peduncle

Supplementary Table 4.2 Spatial tractography measures

Tract	Group	Number of streamlines (Mean ± SD)	Number of points (from all tracts) (Mean ± SD)	Mean tract length (in mm) (Mean ± SD)	Approximate tract volume (in mm^3) (Mean ± SD)
L DRTT	YHC	13.38 ± 9.85	3245 ± 2473.25	119.60 ± 19.18	862.89 ± 567.37
	PD	21.29 ± 17.18	5088.88 ± 4020.24	122.98 ± 23.73	1107.89 ± 681.18
	MHC	17.28 ± 17.89	4386.5 ± 4641.52	125.89 ± 18.89	1005.06 ± 692.56
R DRTT	YHC	21.27 ± 20.45	4967.73 ± 5563.26	107.22 ± 23.63	1091.12 ± 888.57
	PD	18.63 ± 16.99	3906.75 ± 3370.91	115.18 ± 26.46	996.62 ± 688.91
	MHC	11.07 ± 10.59	2718.14 ± 2716.34	122.44 ± 19.52	708 ± 545.68
L SPCT	YHC	17.09 ± 20.45	4310.46 ± 5138.32	139.75 ± 33.27	1037.53 ± 856.37
	PD	21.84 ± 18.40	6473.68 ± 5916.88	142.23 ± 20.83	1409.86 ± 983.63
	MHC	30.36 ± 28.29	8863.36 ± 8710.77	144.55 ± 17.59	1859.95 ± 1257.85
R SPCT	YHC	22.31 ± 24.19	6304.31 ± 6914.50	148.13 ± 31.74	1411.99 ± 1148.62
	PD	33.37 ± 36.28	10566.74 ± 12412.98	149.84 ± 27.72	1893.36 ± 1458.36
	MHC	29.83 ± 31.69	9236.91 ± 9887.11	148.45 ± 20.15	1798.74 ± 1378.39

YHC - Young Healthy Controls, PD – Parkinson's disease, MHC – Matched Healthy Controls, SD - Standard deviation, L - Left, R - Right, DRTT – Dentato-Rubro-Thalamic Tract, SPCT – Subthalamo-Ponto-Cerebellar Tract

Supplementary Table 4.3 Inter-rater reliability test for extracted FA from the full DRTT and SPCT

PD FA values	Rater 1 (JPM)	Rater 2 (IL)	MHC FA values	Rater 1 (JPM)	Rater 2 (IL)
L DRTT			**L DRTT**		
	0.46701	0.48657		0.4628	0.46276
	0.50817	0.51433		0.425	0.42318
	0.50261	0.54599		0.50532	0.50532
R DRTT				0.48335	0.48897
	0.47127	0.48777	**R DRTT**		
	0.47694	0.46683		0.46072	0.4628
	0.49164	0.50797		0.43552	0.45284
L SPCT			**L SPCT**		
	0.52505	0.48587		0.46237	0.45837
	0.52096	0.52219		0.5047	0.51392
	0.50294	0.50508		0.49435	0.48482
	0.47266	0.47492	**R SPCT**		
	0.51444	0.48728		0.49614	0.5191
R SPCT				0.49458	0.50101
	0.48003	0.50411		0.49741	0.49261
	0.47408	0.47408			
ICC	0.786		**ICC**	0.969	
p-value	p = 0.00487		**p-value**	p = 3.32e-07	

Supplementary Table 4.3 shows the IRR for the full DRTTs and the SPCTs and to check if variation in the FA values were due to inclusion of the cortical connections of these tracts, the tracts were chopped to include only the portion of the DRTT between the dentate nucleus and the thalamus and the portion of the SPCT from the sub-thalamic nucleus to the cerebellum. And the IRR extracted values from the chopped tracts are shown in Supplementary Table 4.4.

Supplementary Table 4.4 Inter-rater reliability for the extracted FA from the chopped DRTT and SPCT

PD FA values	Rater 1 (JPM)	Rater 2 (IL)	MHC FA values	Rater 1 (JPM)	Rater 2 (IL)
L DRTT			**L DRTT**		
	0.49178	0.49629		0.51106	0.48851
	0.59715	0.5865		0.40573	0.40192
	0.5561	0.57004		0.50816	0.51649
R DRTT				0.54704	0.55294
	0.53295	0.51123	**R DRTT**		
	0.47694	0.45537		0.48622	0.48988
	0.49164	0.53783		0.4873	0.4859
L SPCT			**L SPCT**		
	0.42577	0.41867		0.52649	0.45062
	0.48934	0.4992		0.48441	0.48093
	0.46495	0.48166		0.48624	0.48636
	0.45142	0.42771	**R SPCT**		
	0.51444	0.51069		0.46921	0.47054
R SPCT				0.46355	0.46963
	0.48003	0.4919		0.50987	0.47652
	0.46635	0.46677			
ICC	0.96		**ICC**	0.861	
p-value	p = 5.58e-07		**p-value**	p = 0.000973	

8.3 Chapter 5 supplementary material

Macrostructural differences

Additionally, previous studies have found that the MCP and the SCP in addition to the basal ganglia contributed to the differentiating PD from multiple system atrophy (MSA-P) and progressive supranuclear palsy (PSP) (Nair *et al.* 2013; Nicoletti *et al.* 2008; Nicoletti *et al.* 2006; Quattrone *et al.* 2008; Nicoletti *et al.* 2013) while another recent study found that the disease duration correlated negatively with MCP width in PD without tremor onset (Sako *et al.* 2015) suggesting progressive degeneration of cerebellar pathways. As these previous studies have found differences in the macrostructure of the main cerebellar tracts (eg: MCP width) in PD, the average tract volume which denotes the space occupied by the tract, calculated as the number of voxels occupied by the reconstructed streamlines was also derived from the main cerebellar tracts. To assess the macrostructural differences, the tract volumes of the MCP, ICP and SCP between PD and MHCs were also compared using two-sample t-tests.

Results

I found volume differences with higher volumes in the PD group for the MCP (mean ± standard deviation PD , MHC (12323.65 ± 4112.48, 9009.08 ± 2115.72) t = 3.5259, df = 34.065, p-value = 0.001228), left ICP ((1918.65 ± 569.03,1291.28 ± 639.25) t = 3.632, df = 46.741, p-value = 0.0006965) and the right ICP ((1792.57 ± 710.93, 1187.2 ± 485.63) t = 3.4667, df = 40.444, p-value = 0.001263) but not for the left and right SCP (p=0.21 and p=0.049, respectively) (Supplementary Table 5.1).

Supplementary Table 5.1 Macrostructural differences between the PD and MHC groups

Tract	Group	Number of streamlines	Mean tract length (in mm)	Approximate tract volume (in mm^3)
MCP	PD	610.54 ± 273.35	125.21 ± 11.62	12323.65 ± 4112.48
	MHC	397.84 ± 118.72	121.57 ± 7.44	9009.08 ± 2115.72
L ICP	PD	126.04 ± 46.26	45.85 ± 7.85	1918.65 ± 569.03
	MHC	83.4 ± 46.08	40.17 ± 9.59	1291.28 ± 639.25
R ICP	PD	121.13 ± 47.94	45.1 ± 8.84	1792.57 ± 710.93
	MHC	79.92 ± 36.78	39.65 ± 7.99	1187.2 ± 485.63
L SCP	PD	170.67 ± 81.86	56.68 ± 9.20	3112.5 ± 1058.16
	MHC	196.4 ± 52.12	54.79 ± 6.98	3458.36 ± 866.23
R SCP	PD	136.34 ± 58.04	55.84 ± 6.06	2795.95 ± 871.76
	MHC	164.16 ± 58.44	52.46 ± 6.60	3287.84 ± 830.84

L DRTT	PD	17.53 ± 12.14	46.41 ± 8.92	234.35 ± 117.75
	MHC	15.22 ± 17.70	57.11 ± 7.76	282.56 ± 168.47
R DRTT	PD	15.25 ± 13.27	50.2 ± 14	254.5 ± 168.67
	MHC	8.43 ± 8.98	57.16 ± 6.17	194.71 ± 110.91
L SPCT	PD	23.2 ± 19.72	75.4 ± 17.93	591.6 ± 399.35
	MHC	29.45 ± 27.40	75.86 ± 12.37	763.27 ± 473.16
R SPCT	PD	38.67 ± 45.91	80.75 ± 16.89	832.94 ± 609.21
	MHC	28.22 ± 29.79	75.17 ± 13.36	643 ± 439.80
L DRTT	PD	17.53 ± 12.14	46.41 ± 8.92	234.35 ± 117.75
	MHC	15.22 ± 17.70	57.11 ± 7.76	282.56 ± 168.47

R- Right, L- Left, MCP – Middle cerebellar peduncle, SCP – Superior cerebellar peduncle, ICP – Inferior cerebellar peduncle, DRTT – Dentato-rubro-thalamic tract, SPCT – Subthalamo-ponto-cerebellar tract

Discussion

Increased volume of the MCPs and the ICPs

The results demonstrated larger tract volumes in the middle cerebellar peduncle and both the inferior peduncles of the PD patients compared to healthy controls. Even though there was increased volume in the MCP, left and right ICPs, there was no correlation between the significant increased FA in the right ICPs with the ICP volumes in the PD group (t=-1.72,d.f=22,p-value=0.1002). There is inconsistency regarding the direction of cerebellar changes in PD across imaging studies (Borghammer *et al.* 2009) (Linder *et al.* 2009; Messina *et al.* 2011). Some studies have found differences in the MCP width and correlation with disease duration (Sako *et al.* 2015), while others showed that width of the MCP and SCP to be useful for differential diagnosis of PD from multiple system atrophy and Progressive supranuclear palsy (Nair *et al.* 2013; Nicoletti *et al.* 2013; Quattrone *et al.* 2008), however here there were no significant correlations as these previous studies. Although the tract volume is a tract specific average measure of the space occupied by a tract, its relationship to axonal number, axonal diameter, and density has yet to be established (Beaulieu 2002).

A study that investigated perinatal brain injury (PBI) found significantly reduced volume and HMOA of the dorsal cingulum PBI group compared with controls, but reported increased HMOA in the ventral component of the superior longitudinal fasiculus (SLF III) and suggested that this increase could be due to the possibility of lateral neuroanatomical compensation for medial structural deficits in the PBI group (Froudist-Walsh et al. 2015). This in context with the current results could also suggest similar lateralised neuroanatomical compensation as there was statistically significant

increase in the PD group's HMOA metric in the right SCP but not in the left SCP or both the ICPs or even the MCP which connects the cerebellar hemispheres.

HMOA and FA represent a markers of tissue microstructure (Dell'Acqua *et al.* 2013) while the tract volume, representing the space occupied by the tract (macrostructure) (Beaulieu 2002). One study found that the HMOA and the tract volume differentially contributed to the anatomical lateralization of frontoparietal attentional networks and individual differences in attention (Chechlacz *et al.* 2015). Their findings agree with previous studies showing that the asymmetry of white matter pathways varies across different diffusion MRI derived measures (De Santis *et al.* 2014). The current results also show asymmetry and right lateralised significant effects in HMOA and FA but not the tract volumes. Additional correlations between the significant HMOA metrics and the FA values in the PD group with the corresponding tract volumes were also performed as previous studies reported tract volume correlations with age especially in the SCP and ICP (Nair *et al.* 2013; Nicoletti *et al.* 2008), but there were no significant differences. This is in line with the attention study (Chechlacz *et al.* 2015) which also did not get any correlations and attributed this to large number of right-handed participants, which is also the case for the current PD cohort (Table 3.1).

Affected vs Unaffected hemisphere analysis

Supplementary Table 5.2 Affected vs Unaffected hemisphere analysis

PD Tracts	FA in affected hemisphere (mean ± sd)	FA in unaffected hemisphere (mean ± sd)	t-value	df	p-value
SCP	0.459 ± 0.032	0.452 ± 0.024	0.8496	21	0.4051
ICP	0.449 ± 0.027	0.444 ± 0.025	0.7284	21	0.4744

Correlation analysis results

Supplementary table 5.3 Correlation analysis results

Tract and metrics	R-SCP-FA		R-ICP-FA		R-SCP-HMOA	
	t	p-value	t	p-value	t	p-value
Finger sequence task - Reaction time	2.1123	0.04681	1.8926	0.07228	1.8137	0.08404

Finger sequence task - Correct number of taps	0.5462	0.5916	-0.1704	0.8666	0.4602	0.6509
Duration since diagnosis (in months)	-0.1083	0.9148	0.2438	0.8098	0.0587	0.9537
Pre intervention off medication UPDRS scores	-0.48	0.636	0.3944	0.6971	-0.4893	0.6295
Finger tapping on dominant hand	1.1073	0.2801	0.2378	0.8143	0.8227	0.4195
Finger tapping on non-dominant hand	1.4516	0.1607	1.4656	0.1569	1.5598	0.1331
Finger tapping on both hands	1.592	0.1257	1.0085	0.3242	1.4613	0.1581

R-SCP-FA – Right superior cerebellar peduncle fractional anisotropy, R-ICP-FA – Right inferior cerebellar peduncle fractional anisotropy, R-SCP-HMOA – Right superior cerebellar peduncle hindrance modulated orientational anisotropy

Supplementary Table 5.4 Results from the MANCOVAs for the BG-cerebellar tracts

Tract		**MHC (n=25) vs PD (n=24)**		
		F statistic	Pillai's trace	p-value
L DRTT				
	Group	F(5,27)=2.58	0.32	0.04935
	Age	F(5,27)=0.61	0.10	0.68922
	Gender	F(5,27)=0.07	0.01	0.99532
R DRTT				
	Group	F(5,27)=3.20	0.42	0.025222
	Age	F(5,27)=4.94	0.52	0.003505
	Gender	F(5,27)=0.96	0.18	0.458007
L SPCT				
	Group	F(5,27)=1.51	0.18	0.2110
	Age	F(5,27)=1.06	0.13	0.3997
	Gender	F(5,27)=0.88	0.11	0.5013
R SPCT				
	Group	F(5,27)=0.77	0.10	0.5743
	Age	F(5,27)=1.32	0.16	0.2774
	Gender	F(5,27)=1.48	0.18	0.2209

MHC – Matched healthy controls, PD - Parkinson's disease patients, L – Left, R- Right, DRTT – Dentato-rubro-thalamic tract, SPCT – Subthalamo-ponto-cerebellar tract